

AGAINST THE CURRENT:

THE MOJAVE RIVER FROM SINK TO SOURCE



The 2018 Desert Symposium Field Guide and Proceedings
David M. Miller, editor

April 2018

Against the current

The Mojave River from sink to source

David M. Miller, editor



2018 Desert Symposium Field Guide and Proceedings
April 2018

Front cover: The Mojave River in flood near East Cronese Lake (playa), May, 1978. In the background, Cat Dune is visible as light-colored sand mantling the dark intrusive rocks. This flood channel is managed by a system of levees near the mouth of Afton Canyon to divert waters away from vulnerable railroad tracks. R. E. Reynolds photograph.

Back cover: This view from near the dam that held back Lake Manix, northwestward across the former lake toward Alvord Mtn., shows the excavated flood route from failure of the dam, modern Afton Canyon. In the nearground is Miocene rock that is sheared in the Manix fault zone, and across the canyon is Pliocene alluvial fan gravel on Jurassic intrusive rocks. Upstream, the fan gravel continues, and in some places is overlain by a layer of gray gravel derived from the south as well as a thin cap of Lake Manix deposits. Enhanced vegetation in the canyon floor takes advantage of shallow water in the streambed. Gregor Losson photograph.

Title page: Goat surveying flood damage on the Mojave River bed, downstream from Camp Cady. March 27, 2005. D. M. Miller photograph.

Road Log maps prepared by Thomas Schweich.

© 2018 Desert Symposium, Inc., a 501(c)3. Terms of Use: copies may be made for academic purposes only.

The Desert Symposium is a gathering of scientists and lay people interested in the natural and cultural history of arid lands. The meeting comprises scientific presentations followed by a field trip. The Desert Symposium and its field trip take place annually, usually in April. The Desert Symposium publishes a volume of papers and a field trip road log. Safety, courtesy, desert awareness and self-reliance are expected of all participants.

A color version of this volume and past volumes may be viewed at: <http://www.desertsymposium.org/About.html>

Table of contents

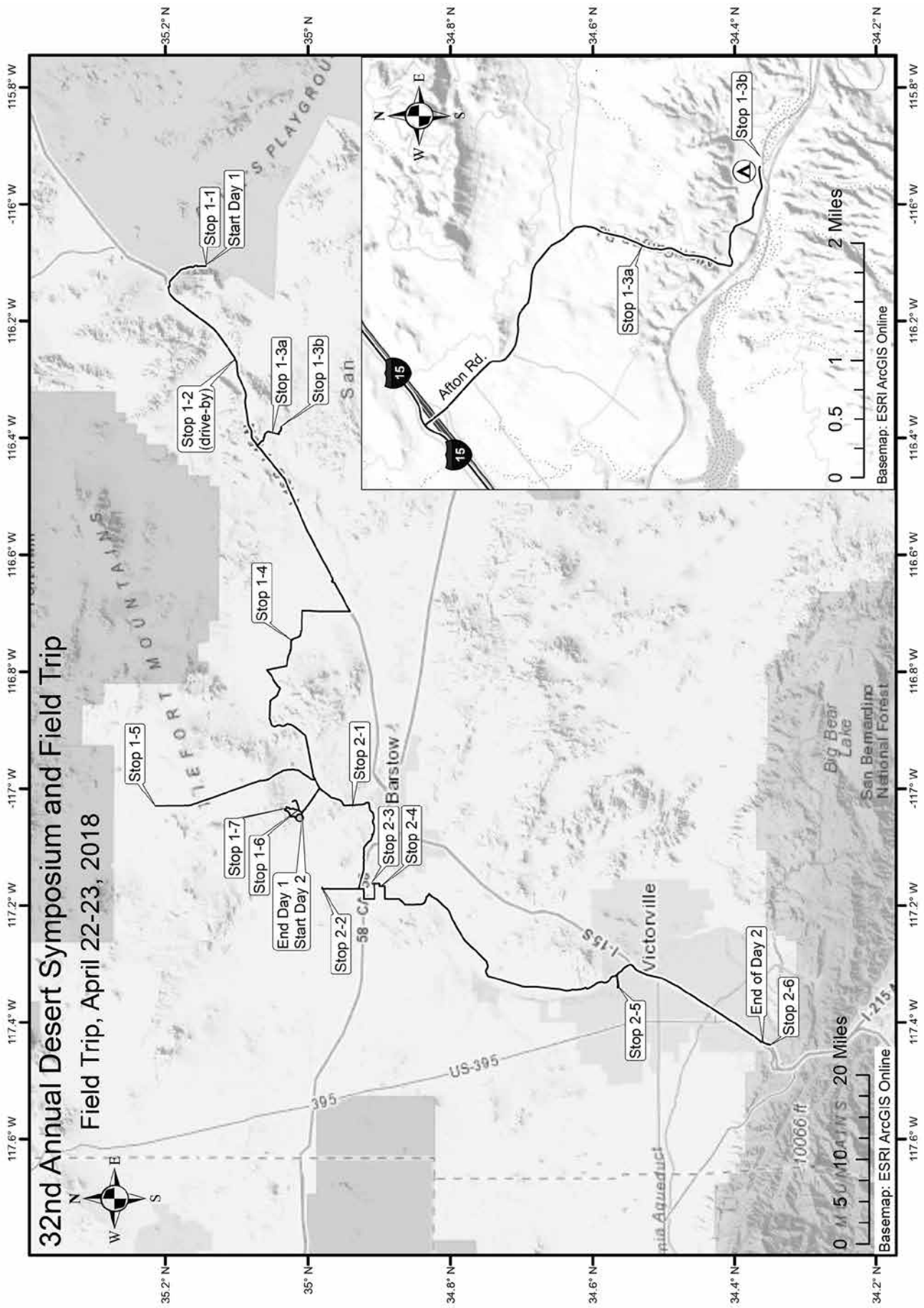
Against the current—The Mojave River from sink to source: The 2018 Desert Symposium field trip road log	7
<i>D.M. Miller, R.E. Reynolds, K. D. Groover, D.C. Buesch, H.J. Brown, G.A. Cromwell, J. Densmore, A.L. Garcia, D. Hughson, J.R. Knott, and J. Lovich</i>	
Guide to an informal field trip to the southeast part of the Central Mojave Metamorphic Core Complex, April 24, 2018	35
<i>Ernie Anderson and Nate Onderdonk, trip leaders</i>	
Broken River — Mojave River	44
<i>Walter Feller</i>	
Fishing for fossils along the course of the Mojave River	48
<i>Robert E. Reynolds</i>	
Initiation and rate of slip on the Lockhart and Mt. General faults in southern Hinkley Valley, California	56
<i>Elizabeth K. Haddon, David M. Miller, Victoria E. Langenheim, Tanzhuo Liu, Laura C. Walkup, Elmira Wan</i>	
Middle Pleistocene infill of Hinkley Valley by Mojave River sediment and associated lake sediment: Depositional architecture and deformation by strike-slip faults	58
<i>D.M. Miller, E.K. Haddon, V.E. Langenheim, A. J. Cyr, E. Wan, L.C. Walkup and S.W. Starratt</i>	
Cajon Pass: a classic geologic textbook	66
<i>Robert E. Reynolds and Michael O. Woodburne</i>	
Fault structure and biogenic soil calcite near Ivanpah Spring, Clark Mountain, San Bernardino County, California	71
<i>David K. Lynch, Paul M. Adams, and David S. P. Dearborn</i>	
Earthwatch expedition: wildlife of the Mongolian steppe	78
<i>Hal Beesley</i>	
Eastern Joshua tree (<i>Yucca jaegeriana</i>) growth rates and survivability on Cima Dome, Mojave National Preserve	84
<i>James W. Cornett</i>	
Rare ant populations in the headwaters of Mojave drainages: new records for <i>Temnothorax paiute</i> in the Clark and San Gabriel Mountains	88
<i>James Des Lauriers and Mark Ikeda</i>	
Recognition of a <i>Glaucomys</i> subspecies population isolated at the headwaters of the Mojave River	89
<i>Tom Howe and Peggy Howe</i>	
Review of Amphicyonidae (Mammalia, Carnivora) from the Barstow Formation of California	91
<i>Donald Lofgren, Maya Fassler, and Stephanie Aldaz</i>	
New records of <i>Miomustela</i> from the Barstow and Crowder formations of California	102
<i>Donald Lofgren and Will Abersek</i>	
A notable canid baculum from the Miocene Barstow formation, Mud Hills, California	106
<i>Robert E. Reynolds</i>	
Size variation in <i>Cynarctus galushai</i> (Canidae) dentition from the Barstow Fauna, Mud Hills, California	108
<i>Robert E. Reynolds</i>	

A small invertebrate fauna from the middle Miocene Monterey Formation, including a possible new species of bivalve, in southern Orange County, California	111
<i>N. Scott Rugh</i>	
A diverse freshwater molluscan fauna from the latest Pleistocene deposits from Salt Creek, Menifee, California	115
<i>N. Scott Rugh and Mark A. Roeder</i>	
A glance to the east: Lake Ivanpah— an isolated southern Great Basin paleolake	121
<i>W. Geoffrey Spaulding and Douglas B. Sims</i>	
An overview of stamp mills of the California Desert	132
<i>Larry M. Vredenburg and Charlie Cornell</i>	
Geology of the Old Mojave Road and surrounding areas, San Bernardino County, California and Clark County, Nevada: a field guide	135
<i>Gregg Wilkerson</i>	
Abstracts from proceedings: the 2018 Desert Symposium	150
<i>David M. Miller, compiler</i>	
Early Miocene extension in the central Mojave; where do we go from here?	150
<i>Ernie Anderson</i>	
Mammal diversity and tectonic history of the Basin and Range	152
<i>Catherine Badgley and Tara M. Smiley</i>	
Silver production from the Silver King Vein, Calico, California: A forensic geology estimate	152
<i>Joy Berry</i>	
Incision and reoccupation of a Miocene paleovalley in the northern Marble Mountains, California	153
<i>David C. Buesch</i>	
~3.7 Ma Black Mountains basalt flows geochemically correlated to boreholes in Superior Basin, western Fort Irwin, California	154
<i>David C. Buesch</i>	
Integrating geologic and geophysical data into a geologic framework model of two groundwater basins at Fort Irwin National Training Center in the Mojave Desert, California	154
<i>Geoff Cromwell, Lyndsay Ball, David Buesch, David Miller, and Jill Densmore-Judy</i>	
Biodiversity of amphibians and reptiles at the Camp Cady Wildlife Area, Mojave Desert, California and comparisons with other desert locations	154
<i>Kristy L. Cummings, Shellie R. Puffer, Jeffrey E. Lovich, and Kathie Meyer-Wilkins</i>	
Quaternary record of Mojave River discharge determined from detrital ¹⁰Be pebble exposure ages	155
<i>Andrew J. Cyr and David M. Miller</i>	
The Cerutti Mastodon site: evidence for hominins in southern California 130,000 years ago.	156
<i>Thomas A Deméré and Steven R. Holen</i>	
Evaluating groundwater discharge and water quality at springs, Fort Irwin National Training Center, San Bernardino County, California	156
<i>Jill N. Densmore</i>	
Trace element concentrations in alluvium of the Mojave River floodplain	156
<i>Krishangi Groover and John Izbicki</i>	
Modeling land-surface deformation with UAV photogrammetry in Bicycle and Red Pass Basins, Fort Irwin National Training Center, California	157
<i>Elizabeth K. Haddon, Jill N. Densmore, Josip D. Adams, J. Luke Blair, and David M. Miller</i>	
Fire frequency and C₄ vegetation expansion in the Barstow Formation	157
<i>Anna Harkness, Katharine Loughney, and Catherine Badgley</i>	
Comparison of heteromyid rodents from the Sespe Formation of Orange County with Mojave Desert local faunas	158
<i>Jared R. Heuck and James F. Parham</i>	
Use of a summative scale for decision-making at a Cr(VI) contamination site	158
<i>John A. Izbicki and Krishangi Groover</i>	

Motion camera surveillance for Mohave ground squirrel on mitigation parcels in the west Mojave Desert <i>Edward L. LaRue, Jr., M.S.</i>	159
High school student research at the Raymond Alf Museum of Paleontology: Filling the gap in alpha level paleontology for the Barstow Formation <i>Don Lofgren, Andrew Farke, and Gabe Santos</i>	159
Reconstructing environmental change in the Barstow Formation, Mojave Desert, California, through the Middle Miocene Climatic Optimum <i>Katharine M. Loughney, Michael T. Hren, and Selena Y. Smith</i>	160
The southwestern pond turtle (<i>Actinemys pallida</i>) in the Mojave River of California: past, present and future <i>Jeffrey E. Lovich, Robert Fisher, Shellie R. Puffer, Kristy Cummings, Sarah Greely and Morgan Ford</i>	160
Geologic framework of groundwater basins of western Fort Irwin, California <i>D.M. Miller, D.C Buesch, V.E. Langenheim, L.B. Ball, P.A. Bedrosian, and G. Cromwell</i>	160
First report of fossil plants from the Box Springs Mountains, Riverside, CA <i>Jess Miller-Camp, Andy Sanders, Lido Delgadillo, and Jeremiah George</i>	161
How long can desert tortoises, <i>Gopherus agassizii</i>, hide in their burrows from climate change? <i>Jenna L. Norris, Jeffrey E. Lovich, Rafael A. Lara ResÉndiz and Shellie R. Puffer</i>	162
Preliminary geologic map of the Mesquite Springs Fault Zone <i>G. Phelps</i>	162
Birds not in flight: using camera traps at desert tortoise (<i>Gopherus agassizii</i>) burrows to study avian behavior at a wind farm <i>Shellie R. Puffer, Laura A. Tennant, Mickey Agha, David Delaney, Jeffrey E. Lovich, Leo J. Fleckenstein, Jessica Briggs, Terence R. Arundel, Amanda L. Smith, Andrew Walde, Joshua R. Ennen</i>	163
Pleistocene lakes and paleohydrologic environments of the Tecopa Basin: constraints on the drainage integration of the Amargosa River <i>Marith Reheis, John Caskey, and Jordon Bright</i>	164
The Island of California: is there a scientific explanation for the 17th-century myth? <i>Jenny E. Ross</i>	164
Pre-development water-levels in the Centro area of the Mojave River groundwater basin <i>Whitney A. Seymour and John A. Izbicki</i>	165
Initial report of fossil wood from the Alverson formation, Anza-Borrego Desert State Park, California <i>Tom Spinks</i>	165
The Las Vegas Formation <i>Kathleen B. Springer, Jeffrey S. Pigati, Craig R. Manker, and Shannon A. Mahan</i>	166
Ecological diversity of mammalian faunas of the Mojave Desert and the Great Plains, in relation to landscape history <i>Bian Wang, Catherine Badgley</i>	166

32nd Annual Desert Symposium and Field Trip

Field Trip, April 22-23, 2018



Against the current—

The Mojave River from sink to source:

The 2018 Desert Symposium field trip road log

D.M. Miller, R.E. Reynolds, K. D. Groover, D.C. Buesch, H.J. Brown, G.A. Cromwell, J. Densmore, A.L. Garcia, D. Hughson, J.R. Knott, and J. Lovich

The Mojave River evolved over the past few million years by “fill and spill” from upper basins near its source in the Transverse Ranges to lower basins in the Mojave Desert. Each newly “spilled into” basin sustained a long-lived lake but gradually filled with Mojave River sediment, leading to spill to a yet lower elevation basin. The Mojave River currently terminates at Silver Lake, near Baker, CA, but previously has overflowed this terminus onward to Death Valley during the last glacial period. The river’s origin and evolution are intricately interwoven with tectonic, climatic, and geomorphic processes through time, beginning with San Andreas fault interactions that during the Pliocene created a mountain range across a former externally draining river. We will see and discuss the Mojave River’s predecessor streams and basins, its evolution as it lengthened to reach the central Mojave Desert, local and regional tectonic controls, groundwater flow, flood history, and support of isolated perennial stream reaches that host endemic species. In association with these subjects are supporting studies such as paleoclimate records, location and timing for groundwater and wetlands in the central Mojave Desert, and effects of modern water usage. The trip introduces new data for the groundwater basin of Hinkley Valley where an ongoing remediation project has yielded a wealth of information on past and present river flow and its associated groundwater system. The trip also includes an overview of some of the groundwater basins in the Fort Irwin area that evolved independently of the Mojave River system.

This year’s two-day field trip begins at the sink for the Mojave River, near Zzyzx, and proceeds to its source, where it issues near Cajon Pass. The trip will highlight several new multidisciplinary studies along the river course and integrate new work with earlier studies, themselves previously highlighted on past Desert Symposium field trips. We will camp overnight. Those who can carpool and return to Zzyzx for your car are highly encouraged to do so. For others, we will use local carpooling each day to minimize logistics for some stops. The trip does not require 4WD but skill in driving on dirt roads is important. Make sure your spare tire is in good shape and carry a shovel and water.

Following the two-day trip will be an informal one-day trip to examine structural controls on the Mojave River in the vicinity of Barstow. Locations are provided in the accompanying overview map. Important turns and

locations are identified with locations in the projection: UTM, zone 11; datum NAD 83: e.g., [578530 E 3917335 N].

Day 1

Convene at the Desert Studies Center with a full tank of gas, water, snacks, and protection from sun and wind. **Fire Drill Carpooling will be necessary on Day 1 and 2.** Plan “Jump In” carpool arrangements in advance. Day 1 is about 125 miles in length. No gas will be available at the overnight area, but there will be a chance to fill gas tanks the morning of Day 2 if needed. Day 2 will be about 85 miles in length.

WHAT WE WILL SEE: Day 1 will traverse the lower Mojave River and its watershed, from Soda Lake to Barstow. We will climb through two major lake basins of the system: Lake Mojave and Lake Manix. Past stream flow and lake history will be compared with historical records, and the importance of perennial stream reaches to wildlife and human history will be emphasized. We will end with a visit to groundwater basins of Fort Irwin, where several years of study are yielding information on the origin of these basins that are largely separated from the Mojave River watershed.

STOP 1-1. [581793 3889260] Walk onto the flats of Soda Lake next to the Desert Studies Consortium facilities. Two sets of springs can be distinguished on the basis of water chemistry. The following is contributed by Jeff Honke, USGS Denver CO:

Soda Lake, Zzyzx Springs and the Mojave River

See Google Earth images of Soda lake- especially June 2010 and July 2016

Zzyzx Springs water source- Not the Mojave River

Barthel (2008) utilized physical and geochemical methods to demonstrate that the water from the springs was not likely from the sub-surface water found under the playa. This study concludes that the likely source of spring water was from Soda Mountain bedrock, with fractures acting as conduits.

Elevation models also do not support shallow aquifer sources. Satellite imagery shows the spring’s discharge flowing towards the playa center, at the driest times

of the year. The constriction of the distal Soda Lake playa, as it flows under I-15 (~282 masl) does not exhibit ground water discharge (GWD) morphology, despite being lower in elevation than the springs at Zzyzx (~284 masl). The constriction is bedrock controlled and formed the 'neck' in pluvial Lake Mojave (Wells et al., 2003).

Imagery from the last decade suggests that the eastern part of Soda Lake is the area where sub-surface water is closest to the surface, however perennial springs do not appear.

The springs at Zzyzx have been historically perennial, despite local and regional droughts, some multi-season and intense. This suggests that the Zzyzx springs are not related to short-term, local precipitation.

The Zzyzx springs occur in almost linear fashion above the suspected location of the Soda-Avawatz fault zone (Langenheim and Miller, 2017).

The intersection of alluvial fans and playa margins are often the site of GWD, as subsurface flow is forced to the surface as it intersects finer-grained material. Several of the large springs at Zzyzx occur at the playa / bedrock interface, suggesting the discharge is not a result of sub-surface water in the alluvial fans themselves.

The bedrock exposure of the Soda Mountains, and its interface with surface sediments, from Razor Rd. to Soda Lake, and from I-15 to the Mojave River floodplain, does not have any known spring discharge areas other than those at Zzyzx.

Springs occur along other fault strikes, releasing deep aquifer water, at other locations in the region. Saratoga Springs in the SE corner of Death Valley National Park occurs at a bedrock / floodplain interface, and has shown no connection to the river hydrology. The springs at Ash Meadows NWR have also demonstrated high volume discharge not related to its surface or near surface hydrology (Winograd and Thordarson, 1975; Dekker and Hughson, 2014). All of this does not preclude the Soda Mountains as being the source of the water, or at least part of the source. But this data does suggest that the water is likely from a source deeper than the Mojave River sub-surface water, and likely expresses on the surface here as a result of fault control.

Soda Lake- The discharging playa

The Mojave River discharge infiltrates into Quaternary sediments down-gradient (east) of Afton Canyon, resulting in sub-surface flow, with occasional flashy surface episodes.

Lake Mojave (~ 25 to 10 cal kyrBP) sediments are clay rich, and likely act as an aquitard to vertical water flow through the Quaternary sediments at the mouth of Afton Canyon. The top of the lacustrine sediments is roughly 5 m below the current ground surface near Zzyzx, and deeper, ~10 m below ground surface, near

the playa center (Muessig et al. 1957). This dramatically limits the potential size of aquifer storage of the basin.

Wet surfaces on the playa appear dark brown to gray. As the sediments dry, the efflorescent salts turn the surface white. After further drying—mid to late summer—the salts degrade and the resulting surface is much firmer and buff colored.

The salts contain halite (NaCl), thenardite (Na_2SO_4), calcite (CaCO_3) and anhydrite (CaSO_4). These data are from just a handful of samples.

The soft surface, even when dry, is a result of the shrink-swell process, and the efflorescent salts.

The eastern playa margin seems to be wetter than other areas. However, the surface channels of the 'flashy' streams are spread across the playa surface. This is further evidence of a disconnect between the surface and sub-surface hydrology.

Floods from snowmelt infrequently reach Soda Lake. After several years of no floods, what is the source of the sub-surface flow? Local precipitation events? Deeper aquifer discharge into the sediments? How can we determine the current sources?

Soda Lake is inundated by Mojave River flood waters every few years, but it is a flow-through playa (Rosen, 1994), because it slopes northward and water passes downstream to Silver Lake. Floodwaters ultimately pond farther north, at Silver Lake playa.

Return to vehicles. Leave the Desert Studies Center (DSC) at Zzyzx and proceed north along the edge of Soda Lake.

0.0 (0.0) Drive north on Zzyzx Road from DSC to Zzyzx Overpass, passing several springs with interesting Holocene histories (Miller et al., 2017).

0.1 (0.1) Cross young, light colored alluvial fan deposits incised into older, darker varnished fan deposits.

0.4 (0.3) SLOW through curves

1.3 (0.9) Road bears eastward around a lobe of alluvial fan gravel.

1.3 (0.4) Note the presence of springs along the playa margin. Soda Lake is underlain by a sedimentary basin, as much as ~1 km deep as estimated by Langenheim and Miller (2017) using gravity data. The margins of the basin project toward a strand of the Soda-Avawatz fault to the northwest and a strand of the Bristol Mountains fault to the southeast, suggesting that the basin formed within a releasing step between the two faults.

1.4 (0.1) SLOW through curves.

1.6 (0.2) Cross young, light-colored fan deposits incised into older, darker fans with stronger desert varnish. These fans end abruptly at the playa margin.

1.8 (0.2) SLOW through curves.

2.3 (0.5) Proceed north to I-15.

4.2 (1.9) Road bears left (west).

4.6 (0.4) Road bears right (north).

4.7 (0.1) TURN LEFT (south) and enter I-15 toward Barstow and Los Angeles. The geology of the Soda Mountains in view to our north was recently described (Miller and others, 2017).

10.5 (5.8) Pass Rasor Road exit.

11.0 (0.5) View of Cave Mountain, named for the caves in Cave Canyon (later renamed Afton Canyon) near the mountain's south base that were cut into Miocene and Pliocene conglomerate by piping and overflow of Lake Manix (Meek, 1990).

12.0 (1.0) View at 2 o'clock of Cat Mountain with a cat-shaped dune. Wind from the west captures sand from the Mojave River fluvial plain and Coyote Lake. "Climbing" dunes form on windward slopes when sand is forced up a ridge; "falling" dunes form on the leeward side of ridges, when wind carries sand over the ridge top.

13.5 (1.5) View north of Soda Mountains fault, which cuts diagonally up the west face of the Soda Mountains, crossing over to the north near Red Pass Lake.

15.4 (1.9) Pass Basin Road exit.

STOP 1-2. [566970 3884660] This is a drive-by stop. DO NOT EXIT. East Cronese Lake, a dry playa most of the time, lies on our right (north). It has interesting hydrology and archeology. It is about 35 m (105 ft) higher in elevation than Soda Lake, yet receives flow from the Mojave River, which can arc widely downstream of Afton Canyon. East Cronese may have deposited lake sediment if the broad clastic wedge below Afton Canyon was built above the level of the playa while perennial lakes were still being formed. This hypothesis is supported by cores acquired by Steve Wells and others, who provided unpublished material on lake sediments in the cores taken from East Cronese Lake showing they overlapped ages for the youngest lake sediment in Silver Lake.

East Cronese Lake receives water from Mojave River flow, whereas its sibling West Cronese Lake that is out of view to the north, receives flow from a major stream leading from the Bitter Spring area of Fort Irwin, well to the north. Shallow water in these playas is well known by 4WD travelers; many months of the year they can be driven on with extreme caution.

In the recent past, travelers used resources of Cronese Lake as they passed, leaving scattered piles of shells and charcoal. Shorelines associated with those middens and dating of the *Anodonta* shells and charcoal have shown that paleoIndians used the site (Schneider, 1994; Warren and Schneider, 2000) during the last thousand

years along the trade route from the Pacific Coast to the Colorado Plateau (Hull and Fayek, 2013). The most recent inundation with *Anodonta* was the Little Ice Age, about 1650 A.D. (Miller et al., 2010).

17.7 (2.3) Continue past the north side of Cave Mountain, where spectacularly steep fans lie below cliffs of granite and several potential faults and landslides are visible. Large boulders on the fan were in part deposited by debris flows but may also represent landslide runouts. The Cave Mountain fault lies along the north face of the mountain, which is an enormous popup (block between two faults elevated by compression) in the fault system.

20.1 (2.4) At the crest of the hill we can see a sand-sheet-draped valley to the south with two prominent dunes near the skyline. Each of these dunes lies on or near the Cave Mountain fault, but the north facing escarpments we see are probably the sides of the dunes, not fault scarps. These longitudinal dunes connect Cave Mountain on the east with low hills farther west.

23.6 (3.5) The road cut on the left (south) exhibits stratified early Pliocene gravel and sand cut by several small faults. This unit is named informally the Cave Mountain gravel (Miller et al., 2017). The gray sand makes up much of the deposit in this exposure, with gravel layers standing out in relief because of their coarse grain size and also strong calcite cementation. An ash bed found west of Cave Mountain in this unit is correlated with ~4-5 Ma ashes of the Alturas volcanic system of northern California (E. Wan, written commun. 2018).

24.2 (0.6) EXIT at Afton Road.

24.5 (0.3) STOP. TURN RIGHT (N) into cleared area and initiate "Jump In" carpooling. We will return in about 1.5 hours.

24.6 (0.1) Retrace south to Afton Road overpass.

24.8 (0.2) Cross over I-15 freeway and continue south on the graded dirt of Afton Road (AC9614).

24.9 (0.1) We are driving on the crest of the Afton beach bar (543 m; 1780 ft elevation), a flat-pebble gravel ridge developed by wave action on the east side of Lake Manix, a position of maximum wave energy from westerly winds. A lagoon once lay east of the beach bar (Meek, 1990; Reheis et al., 2007, 2012).

25.3 (0.4) At the south end of the beach bar, the deposit is faulted against a hill of coarse Cave Mountain gravel (Meek, 1990). This beach was formed ~24.5 ka (Reheis et al., 2012), so the last rupture on this fault (the main strand of the Cave Mountain fault) was latest Pleistocene or Holocene. The fault can be traced west through Lake Manix muds and onward to the west, to the south side of an unnamed small mountain about three miles west of here, on the north side of I-15. Afton Road bears right.

25.2 (0.2) The graded road bears left (east) as it passes a right turn for County Road 20882.

25.6 (0.4) Afton Road bears left (east).

26.1 (0.5) Cross under the powerline. BLM road AC9641 runs west; BLM route AC 9624 runs east. Continue on Afton Road.

26.2 (0.1) Optional Side trip to visit North Afton Beach Ridge.

TURN LEFT onto BLM road AC9622; proceed easterly 1.3 miles to a "Y" intersection. TURN RIGHT (SW) towards beach bar. PARK vehicles east of beach bar. Walk SW to top of the 2-km-long north Afton beach ridge (Meek, 1990; Reheis et al., 2007) formed by wave energy during three episodes of Lake Manix. Fossils, including cormorant bills found here and flamingo remains from the lake, suggest that this water body was a relatively permanent feature on bird migratory paths during the late Pleistocene. Cuts on both sides of the beach ridge display interlayered fan gravels and lacustrine sediments, illustrating the three lake cycles of the Afton arm of Lake Manix. The youngest lake is approximately 24.5 cal kyrBP based on the most recently dated Anodonta (Reheis et al., 2012).

26.2 (0.1) pass BLM road AC9622. Continue downslope across alternating alluvial gravel wedges and lake sediments that illustrate alternating deep and shallow lakes.

26.7 (0.5) **STOP 1-3A.** [555500 3878750] Pull to the shoulder of the road to avoid blocking traffic. We are perched above the inner gorge of the Mojave River, where it cut below the bottom of Lake Manix after Afton Canyon was cut. We will discuss the history of the Afton arm of Lake Manix, Afton Canyon and the draining of Lake Manix, and tectonics that contributed to the formation of this arm of Lake Manix. We also will discuss studies of bedload transport in the ancestral Mojave River.

Continue south toward Afton Canyon Campground.

27.3 (0.6) TURN SHARP LEFT as you pass BLM AC9609 road junction. Pass group camp on right (S).

27.6 (0.3) SLOW. Use caution as you go down slope. Watch for oncoming traffic.

28.0 (0.4) TURN LEFT into BLM Afton Canyon Campground. **STOP 1-3B.** [556550 3877435].

The western pond turtle, formerly considered a single species, is now recognized as two: the northwestern (*Actinemys marmorata*) and southwestern (*A. pallida*) pond turtles. They are one of the few freshwater turtles in the United States to have a Pacific-coastal distribution. Only one other species, the painted turtle

(*Chrysemys picta*), has a distribution that includes part of the west coast. Both pond turtles are typically found in streams and rivers draining into the Pacific Ocean from Washington State to Baja California, Mexico. There are a few isolated populations found in interior-draining stream systems in the Great Basin and Mojave deserts. The southwestern pond turtle is found in the coastal ranges from south of San Francisco into southern California and northwestern Mexico. A relict population occupies the Mojave River from near its headwaters in the San Bernardino Mountains to Afton Canyon. Pond turtles in the Mojave River were "marooned" along isolated reaches of the river as range contraction occurred when the climate became warmer and dryer after the Pleistocene as evidenced by fossils of that age or older at various locations in and around the river.

In the late 1990s, small populations of pond turtles were studied at Camp Cady Wildlife Area (about 15 miles upstream) and at Afton Canyon. Fewer than 50 individual turtles remained at both locations (Lovich and Meyer, 2002), but turtles were relatively easy to trap for research. Radio-transmittered turtles only left the water to bask or to nest in the case of females. Concerted efforts to reassess the status of pond turtles in the Mojave River in 2015-17 yielded mixed results. The population at Camp Cady was extirpated and the last turtles were observed in 2014. Only two turtles were observed at Afton Canyon despite significant trapping efforts: an adult female and a hatchling (Lovich et al., 2018). A seemingly robust population appears to survive in the upper Mojave River. Reasons for their decline in the lower river may include the recent drought and effects of floods that alter habitat making it less suitable for turtles. The disappearance of turtles at Camp Cady may be due to increased predation during the recent epic drought, or the fact that the population was already too small to persist for long in the late 1990s. Efforts to keep pond turtles as part of the fauna of the lower Mojave River may require more intensive habitat management and protection, and possibly population augmentation by breeding turtles in accredited



Figure 1: Pond turtle 2017. Photograph J. Lovich.

captive facilities for later release of juveniles.

Regularly seen are tiny northern Baja California treefrogs (*Pseudacris hypochondriaca*). Large, introduced American bullfrogs (*Lithobates catesbeianus*) are often heard. Two species of toads are possible; the western toad (*Anaxyrus boreas*) is documented, while the red-spotted toad (*Anaxyrus punctatus*) occurs in many desert watering spots. Jeff Lovich and colleagues have a manuscript that is currently in review describing the biodiversity of amphibians and reptiles at the nearby Camp Cady Wildlife Area; a summary is presented by Cummings (this volume). The fish at Afton Canyon are arroyo chubs (*Siphateles orcutti*). The native Mojave tui chub (*S. bicolor mohavensis*) is apparently lost from Afton Canyon but pure populations exist in several refugia, including the ponds at Zzyzx.

There are about 30 reliable records of Gila monsters (*Heloderma suspectum cinctum*) in California (Lovich and Beaman, 2007; Lovich and Haxel, 2011; Ruppert, 2010). The oldest record is from the “Mohave River” and was likely collected in 1853 or 1854 by Caleb Kennerly, the surgeon/naturalist that accompanied Lieutenant Amiel W. Whipple on Pacific Railroad Surveys along the 35th parallel. The specimen was cataloged as a partial skull and partial post cranial skeleton (presumed to be USNM 228171) in 1861 into the National Museum of Natural History (Smithsonian). Lovich and Beaman (2007) found that all other Gila monster records in California were east of about -116° longitude. The area to the east of this meridian typically receives both winter and summer precipitation. Gila monsters are conspicuously absent from areas where summer precipitation is less than 25% of annual precipitation. More specific locality details were not provided for USNM 228171, but based on the distribution of other records, it is likely that the specimen in question was collected somewhere along the lower Mojave River, somewhere east of Barstow, perhaps in or near Afton Canyon.

In mesquite thickets with mistletoe, phainopepla are very common. Birds that are rare in the Mojave, but sighted at Afton, include Virginia Rail, White-faced Ibis, Great Blue Heron, Green Heron, Least Sandpiper, Wilson’s Snipe,

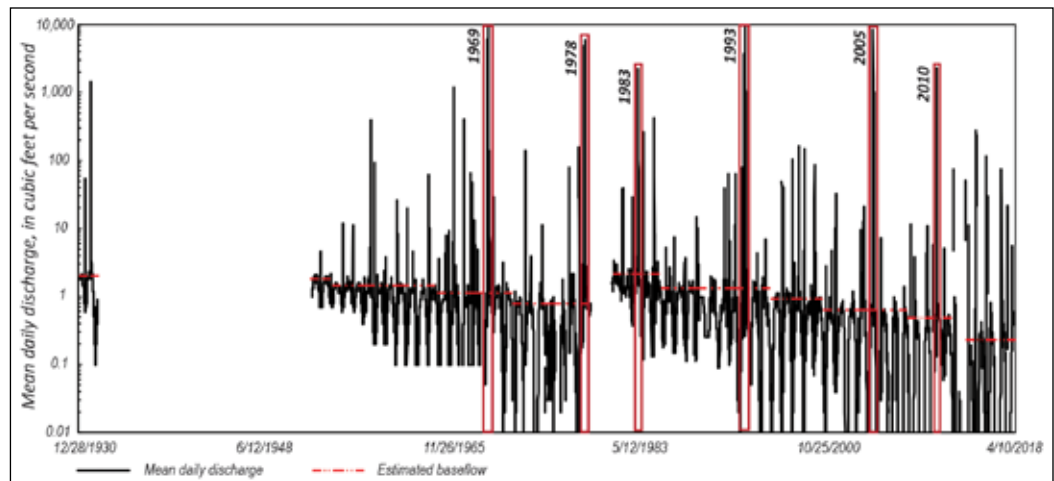


Figure 2. Mean daily discharge at USGS stream gauge 10263000, Mojave River at Afton Canyon, with estimated average baseflow and selected major storm events indicated by red boxes.

Osprey, Yellow-headed Blackbird, Greater Yellowlegs, (<https://ebird.org/hotspot/L444756>, <http://digital-desert.com/watchable-wildlife/afton-canyon.html>, https://www.blm.gov/ca/pdfs/cdd_pdfs/clemmys1.PDF).

Mammals that come to Afton for water include bighorn sheep, kit and gray foxes, coyotes, and bobcats.

Flow in the Mojave River at Afton Canyon has been measured intermittently since 1930. Base flow in Afton Canyon is sustained by groundwater in the floodplain aquifer discharging to land surface due to a bedrock constriction narrowing the floodplain, and a decrease in depth of the floodplain aquifer in the area. Occasional large storms near Cajon Pass are sufficient to cause the Mojave River to flow more than 160 km (100 mi) downstream, increasing flow in Afton Canyon for short periods of time. Pumping of groundwater in upstream reaches of the Mojave River in excess of recharge from the headwaters has contributed to gradual declines in baseflow at Afton Canyon (Lines, 1996) (Fig. 2). In addition, Lines showed that removal of dense thickets of the invasive plant species, tamarisk, with apparently increased water needs, caused baseflow rebound.

Upstream 15 miles, at Camp Cady, shallow water in the river bed supports an extensive riparian zone. This location was not only an important stop on military roads, but was also the point where the Old Spanish Trail came overland from the north to join the Mojave River. This was the first reliable water for those travelers after springs in the Death Valley area.

RETRACE NORTH along Afton Road to I-15.

28.4 (0.4) Slow through turns. Watch for fast traffic coming downhill.

29.2 (0.8) Slow through curves as you drive uphill.

31.5 (2.3) Pass road on right. Proceed under transmission lines.

32.5 (1.0) Slow as Afton Road bears right.

33.1 (0.6) Cross I-15 and retrieve parked vehicles. RETRACE southwest to I-15 onramp.

33.5 (0.4) ENTER I-15 west bound.

34.8 (1.3) To your right (N), an unnamed hill has been popped up between two strands of the Cave Mountain fault (Miller et al., 2017).

Drive uphill toward the Field Road interchange, on a ridge at an elevation of 1960 ft., approximately 180 feet higher than the Lake Manix highstand. Although late Tertiary and early Quaternary strata underlying this ridge are folded, the Lake Manix shorelines (~550 to 24.5 cal kyrBP) along the ridge do not appear to be deformed.

40.3 (5.5) Pass the Field Road off ramp.

42.5 (2.2) Cross Manix Wash. Lake Manix muds are overlapped by sand and gravel of the Mojave River fluvial plain.

44.6 (2.1) Pass under the overpass to Alvord Mountain.

47.4 (2.8) EXIT at Harvard Road.

47.6 (0.3) Stop at Harvard Road overpass. TURN RIGHT (N).

47.7 (0.1) TURN LEFT (SW) on Hacienda Road, which will soon parallel I-15.

49.5 (1.8) Pass Kathy Lane.

50.0 (0.5) Pass Mountain View Road. View NW of Lake Dolores water park, which was built on a hill of Miocene basalt. Nearby limestone of the Barstow Formation is of stratigraphically uncertain relation to the basalt. To the south, Barstow Formation limestone at Harvard Hill contains the Peach Spring Tuff (18.8 Ma) and appears to overlie basalt.

50.9 (0.9) TURN RIGHT (N) on Bragdon Road (CL8121) toward St. Anthony's Monastery.

52.3 (1.4) Cross under power lines leading northeast.

52.5 (0.2) Cross Kern River Pipeline route.

53.1 (0.6) Pass Warbonnett Road.

53.6 (0.5) Pass E-W transmission line. Agate Hill is to the NW (Byers, 1960).

54.1 (0.5) Bragdon/Coyote Lake Road (CL8121) jogs right then north.

55.0 (0.9) Turn LEFT (W) on CM7652/CL7652 prior to reaching St. Anthony's Monastery. Proceed west toward Paradise Springs Road. **Note:** Yellow signs on right (E), say "Demmill Road" and St. Karas Farm.

55.5 (0.5) Pass SW corner of St. Anthony's fence. Proceed west.

62.0 (1.9) Bear RIGHT (NW) then left (W) at fork on obvious main route.

62.5 (0.5) Turn RIGHT on CM7651 and continue NNW

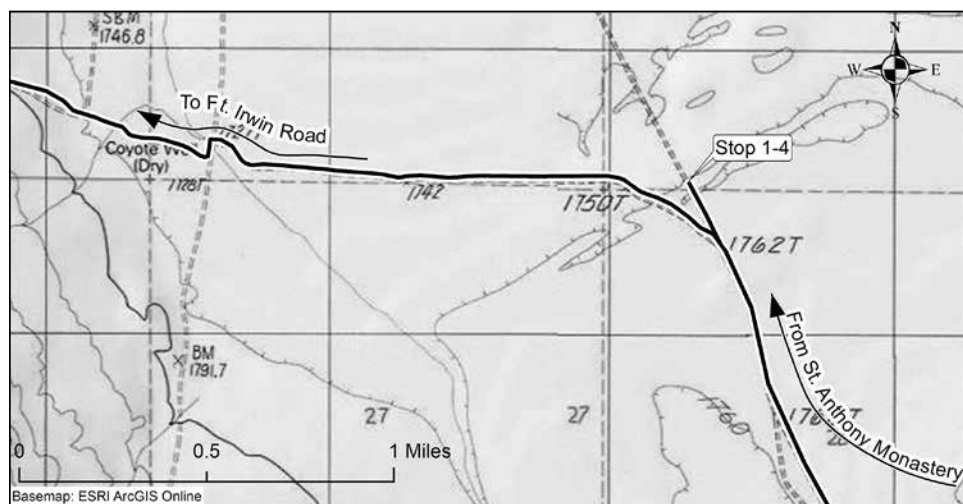
62.7 (0.2) Acute junction with Paradise Springs Road. Travel north along ridge crest that is a remnant of the Mojave River.

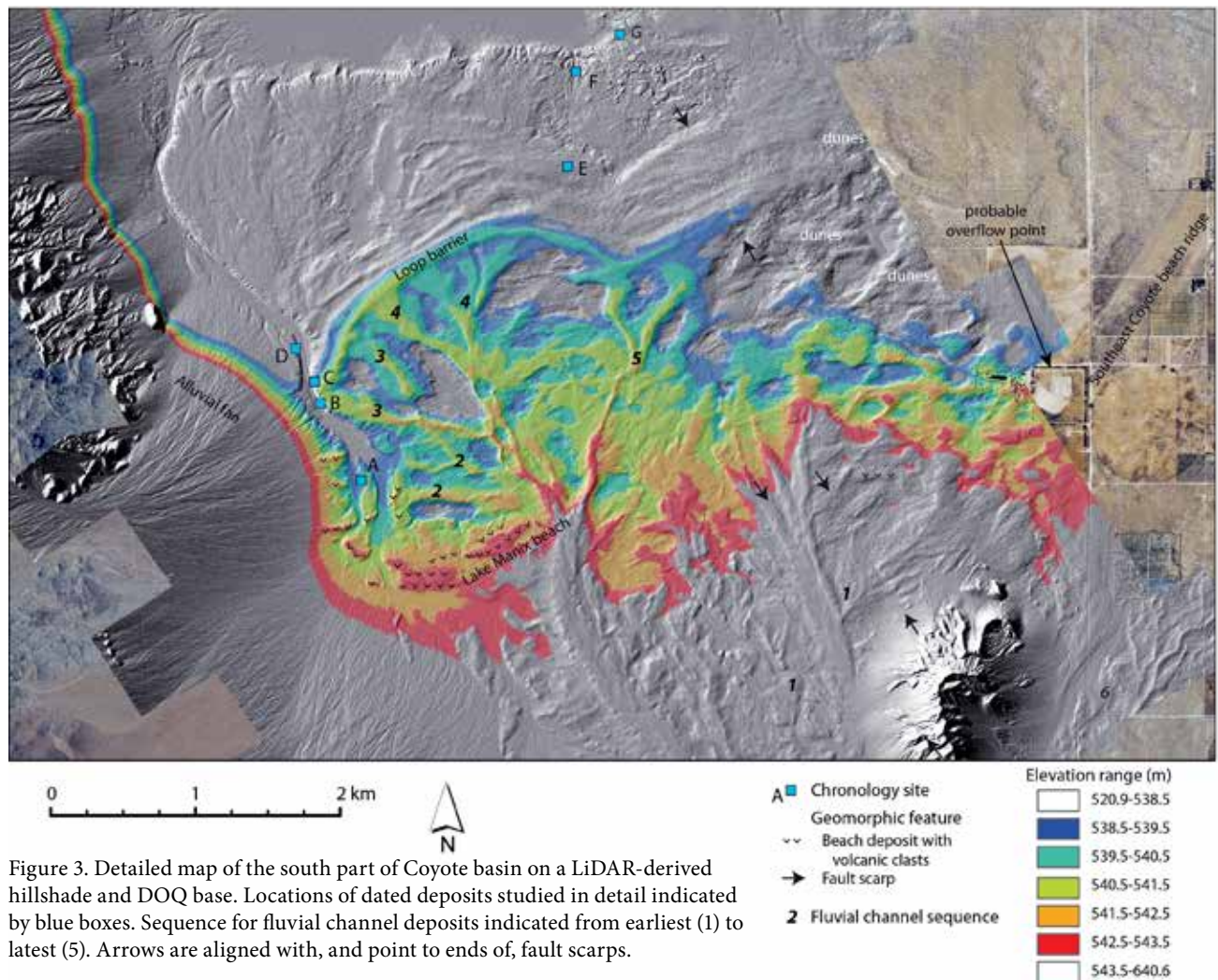
63.4 (0.7) Complex Junction with Paradise Springs Road (CM7651) and Field Road (CM7772). Follow right fork (CM7651) north.

63.5 (0.1) Continue past a faint road to the left (west). Continue 0.1 mile north and STOP when cresting low ridge. Make a hard left onto the ridge top.

63.6 (0.1) STOP 1-4 Coyote Lake: [523200 3875725]

Pleistocene Coyote Lake, which formed in one of five basins along the Mojave River course, was initially integrated with Lake Manix. After the formation of Afton Canyon and draining of Lake Manix ~24.5 cal kyrBP, Coyote was a side basin that was filled episodically for the next ~10 ka. As such, its record of lake level is an important counterpart to the record of the other terminal basin, Lake Mojave, following the Lake Manix history (Meek, 2004). Based on study of lake and fluvial deposits and their geomorphology, Miller et al., (in press) resolved the timing for five periods of recurring lakes in the Coyote basin by dating mollusks in several sediment sections. Several of these periods consist of multiple lake-rise pulses, for which specific fluvial deposits that represent





arrival of Mojave River sediment to the basin. The pulsed record of rapid lake rise and decline is interpreted as switching of the Mojave River course between Lake Coyote and Afton Canyon (and thence to Lake Mojave). A composite lake record for both basins shows nearly continuous lake maintenance by the Mojave River from 24.5 to ~14 cal kyrBP. One potential gap in the lake record at ~22 cal kyrBP, may indicate temporary routing to yet another basin or a dry climatic period. Mojave River discharge was sufficient to maintain at least one terminal lake throughout most of the last glacial maximum and deglacial period. Nuances of lake-level changes in both basins are difficult to interpret as paleoclimatic events because the current chronologic control on lake levels from nearshore deposits does not provide the necessary precision.

Mojave River avulsion leading to flow into Coyote basin may have been influenced by rupture on an oblique normal fault. Earliest post-Lake-Manix Mojave River stream deposits leading to Coyote basin are faulted and most subsequent streams were confined to the downthrown (western) fault block. The timing of fault rupture, and possible enhanced river flow to Lake Coyote

rather than Lake Mojave, is bracketed at ~20-19 cal kyrBP by shells dated in beach deposits. Later, headward erosion through the fluvial plain by the Mojave River eliminated flow to Coyote basin after ~14 cal kyrBP and completed incision of the plain after ~12 cal kyrBP (Miller et al., 2017).

Geomorphic features are subtle in this location, but Hagar (1966), Meek (1990), and Dudash (2006) came to the conclusion that deltas fed by the Mojave River interacted with temporary lakes in Coyote basin. They referred to the features as deltas, and taken broadly as landforms associated with rivers feeding standing water bodies, this is a concise and appropriate term. We have been able to use high-resolution topography to examine subtle features and establish their elevations. This study led to the recognition that successive periods of river channel flow led to progressively higher lakes that formed this composite beach ridge that we stand on. The channel landforms are shown in Fig. 3 and labeled in sequence. Successive channels are higher in elevation, with the youngest channel grading laterally to the beach ridge. Farther east, a less well-developed arcuate beach ridge is cut by two faults that are mapped most of the distance

from Agate Hill to the beach. The scarps represent evidence for the ~20-19 cal kyrBP rupture of Dolores Lake fault.

During drilling and trenching for the IPP Electrode southeast of Coyote Lake, archeological, paleontological, and geological studies were performed. Stratified faunal remains recovered from deep drill holes show that stickleback (*Gasterosteus* sp.) fossils were clustered 180 to 280 feet below the surface, while tui chub (*Siphateles* sp.) occurred throughout the stratigraphic column. This stratification indicates that waters in early Coyote Lake enabled stickleback, which requires clear, cool water and plant cover, but can tolerate saline water. Perhaps fluvial freshening of the Lake Manix phase of Coyote Basin allowed proliferation of tui chub as well as mollusk populations (Reynolds, this volume).

Groundwater levels in wells installed around the playa range between 400 ft below land surface to artesian (actively discharging above land surface). Groundwater originating from the south side of Fort Irwin, and some groundwater from the Mojave River, flows into the area

around the lake and discharges to land surface through evaporation (Stamos et al. 2002). The evaporative parts of the playa are in the northwest and south, and these puffy discharging playa areas are underlain by dry clay, leading Hagar (1966) to conclude that local subflow from alluvial fans causes the local discharge on the playa. Wells penetrating through clay and deeper deposits in the lakebed tap confined aquifers. The release of pressure resulting from the installation of the well casing allows it to actively flow above land surface, which is sometimes hundreds of feet above the actual water level in the aquifer (potentiometric pressure). Shallow, thin lenses of sand (typically 13 m [40 ft] below land surface), near the boundary between oxic and reduced clay deposits, may contain trapped (perched) groundwater from wetter climates, or may hydraulically connect to the Mojave River (Fig. 4). Pumping in the Mojave River groundwater basins has decreased the amount of water flowing into Coyote Lake from the south, resulting in land subsidence at rates of 0.4 feet per year (Brandt and Sneed, 2017).

Historical water-quality data on shallow groundwater indicates relatively high sulfide content, which may be

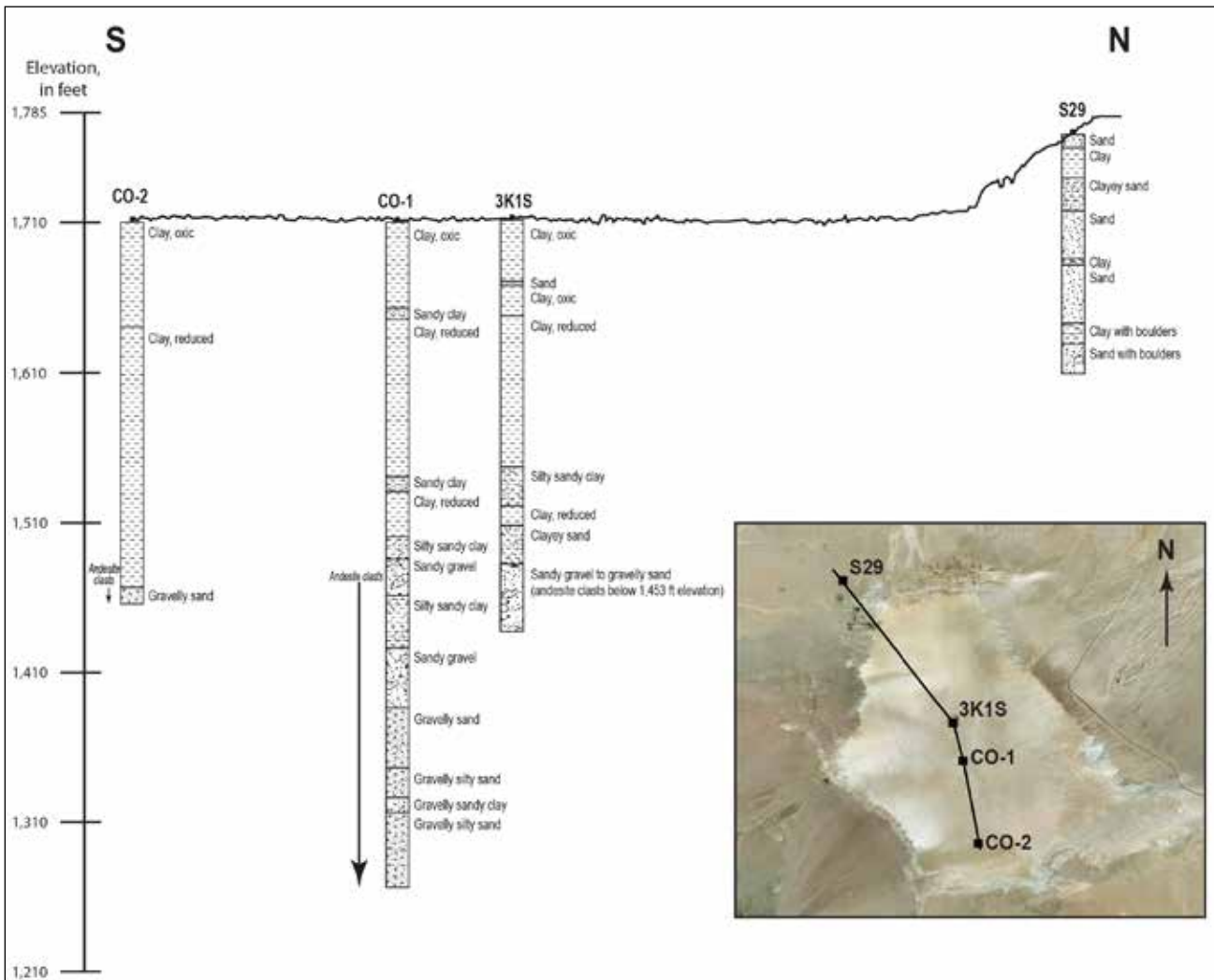


Figure 4. Simplified lithologic cross section across Coyote (dry) Lake.

related to weathering of andesite clasts in alluvium at depths below 75 m (250 ft) (Fig. 4). Stable isotopes of deuterium (^2H) and oxygen (^{18}O) in deep groundwater (greater than 130 m (400 ft) below land surface) north of Coyote Lake are similar to data from the regional groundwater aquifer, indicating a local source of groundwater that was most likely recharged thousands of years ago.

Return to vehicles. Retrace 0.1 miles south to complex junction.

63.9 (0.3) TURN SHARP RIGHT at complex junction. Proceed westerly on Field Road CM7772.

An alternative route is to continue south on this road to Interstate 15, drive west to Fort Irwin Road, and arrive at Old Fort Irwin Road. If this route is taken, note the hill at the Minneola Road interchange. The hill is uplifted along the west side of the Calico fault.

64.9 (1.0) Slow. Road bends right, then left, dropping into Coyote Wash. At the wash, Paradise Springs/Coyote Lake roads lead to the right (N). There is a large mesquite tree to the south. TURN SOUTH toward fenced well. This is Coyote Well, a source of shallow fresh water. Lake sediment in the stream banks to the east are indurated, laminated claystone overlain by soft-weathering silt and fine sand, all overlain by gravelly sand. The claystone can be traced laterally to the margin of Coyote Lake playa, where efforts to date *Anodonta* in it yielded ages at the limit for radiocarbon (>50 cal kyr). *Anodonta* collected from overlying silt and sand has yielded ages that are younger than Lake Manix (<24 cal kyr) and therefore represent times that the Mojave River led directly to the Coyote Basin. The coarsening upward sequence indicates an overall trend of delta encroachment.

65.1 (0.2) TURN LEFT (S), then RIGHT (W) at the fenced well. Proceed west on CM7770. AVOID faint right turn (N) on Starbright Road. Careful: dips lie ahead.

65.6 (0.6) Field Road CM7770 winds left around rock outcrops. Note: this road originally led to gold and lead prospects to the west-southwest. Proceed west.

66.2 (0.6) Hill to the right (N) contains sericite (fine-grained muscovite) schist.

66.5(0.3) TURN RIGHT (N) off CM7770 onto pole line Road CM7643. Caution: dips lie ahead. Proceed downhill to the north.

68.5 (2.0) TURN SHARP LEFT (SW) on Road CM8102.

69.9 (1.4) Pass the Wolly wollastonite deposit (calcium silicate in marble) and Road CM8111. Significant wollastonite deposits on the north side of the Calico Mts. are present in the mixed carbonate/hornfels sequence. The 250 feet thick wollastonite sequence is repeated several times by folding and extends for over 1 mile on strike. The

Wolly wollastonite quarry at the north end of the deposit contains fine to very coarse crystals of white wollastonite interbedded with diopside and quartz. Individual layers of pure wollastonite are up to 10 feet thick. The wollastonite rock sequence, with about 15-20% interbedded wollastonite, amounts to a very large (>50 million tons) resource (Brown, 2016a, b; Brown et al., 2016).

70.1 (0.2) Pass Road CM7660 on left (S) leading to an unnamed nickel deposit (MRDS ID #10237669) containing millerite (nickel sulfide), niccolite (nickel arsenide), anabergite (nickel arsenate), and uvarovite (chromium) garnet in an E-W dike that cuts wollastonite marble (Southern Pacific Co. 1964). This interesting deposit does not conform to the typical nickel deposit rock associations (Brown, 2016a, b; Brown et al., 2016).

70.7 (0.6) Pass a road on the left to Puertas Negras mine (MRDS ID #10140810), prospected along a major fault between footwall quartzite and hanging wall graphitic schist. Carbonaceous graphite acts as a reductant, causing deposition of gold and arsenopyrite in the shear zone. Other workings to west are "gold prospects" with arsenopyrite. These prospects are within a different rock sequence than the Puertas Negras. The prospects occur on fault zones within rusty black iron-impregnated quartzite (Brown, 2016a, b; Brown et al., 2016).

70.8 (0.1) TURN RIGHT onto powerline road CM8040. Paleozoic to early Mesozoic metasedimentary rocks on the north slope of the Calico Mountains include impure carbonate rocks, calc-silicate hornfels, thick turbidites, quartzite sequences, and a thick metavolcanic sequence. The rocks were highly deformed by multiphase pre-mid Jurassic folding and thrust faulting and were metamorphosed during intrusion of Mesozoic granitic plutons (Jurassic diorite and quartz monzonite, and Cretaceous granite). Numerous low and high angle faults of Miocene age place Paleozoic quartzite over intrusive Miocene andesite. Pink and tan fine-grained volcanic rocks in the road berm are largely Miocene rhyolite, dacite, and andesite derived from Early Miocene Jackhammer and Pickhandle formation plugs and domes high on the slopes of the Calico Mountains.

Pass road CM7620 that continues SW to prospects with mineralization occurring in quartzite (Brown, 2016a, b; Brown et al., 2016).

71.1 (0.3) Use caution; dips in the road.

71.5 (0.4) Stay right through junction, turning onto Madrugador Road (CM8040) that reached the Shining Dawn (American Progress) gold mine to the SSW. The Shining Dawn mine was active from the 1970s to 1980s and produced several hundred ounces of gold (Fife, 1980). Inclined shafts explored a hydrothermally mineralized low angle fault and shear zones within Paleozoic quartzite and Cretaceous granite. The Shining Dawn mineralized

fault zone places Miocene upper Jackhammer Formation volcanic rocks in the hanging wall over footwall Paleozoic quartzite. Mineralization is likely of Miocene age (Brown, 2016a, b; Brown et al., 2016).

72.3 (0.8) BEAR LEFT (W), traveling toward Fort Irwin road.

73.2 (0.9) The Lone Mountain wollastonite deposit (MRDS ID #10262370) is on the right (N) at 2:00. This prospect exposes highly metamorphosed and folded sequences of metasedimentary rocks intruded by Mesozoic plutonic rocks. The sequences here closely resemble the sequence to the southeast at the Wolly wollastonite mine, and rock units may be displaced several miles (Brown, 2016a, b; Brown et al., 2016).

73.5 (0.3) Pass an east road to Lone Mountain wollastonite deposit.

73.7 (0.2) Pass a road on the right (CM8045) to the Lone Mountain wollastonite deposit.

74.2 (0.5) STOP at Fort Irwin Road. High speed traffic comes from both directions. CAUTION! Look both ways until both lanes are clear. Prepare to TURN LEFT (SW). One at a time – vehicles cautiously enter pavement and proceed SW toward Jackhammer Gap in the northern Calico Mts.

74.8 (0.6) Pass a power line road crossing.

76.1 (1.3) Pass through Jackhammer Gap, near the type locality for the Early Miocene Jackhammer Formation (Dibblee, 1968) of dacite tuffs and basalt.

76.6 (0.5) Pass a left turn to mines containing Miocene veins of barite two feet thick in Paleozoic limestone metamorphosed to marble and tremolite (calcium, magnesium, iron silicate; Durrell, 1954).

77.5 (0.9) Pass through Pickhandle Pass, near the type locality for the Pickhandle Formation (Dibblee, 1968). The Pickhandle Formation consists of conglomerates, breccia, dacite domes, and tuffs that conformably overlie the Jackhammer Formation and are unconformably overlain by the Barstow Formation.

78.8 (1.3) Pass the left turn to Russ's Mailbox and a route to the northwestern Calico silver district (Reynolds and Miller, 2010).

79.4 (0.6) Slow. Watch traffic from behind and in front. Pull to the right lane and prepare for right turn.

79.7 (0.3) TURN RIGHT on Irwin Road. Reconvene vehicles along right shoulder. Proceed west on Irwin Road (Old Fort Irwin Road).

80.2 (0.5) Pass Old Yermo Cutoff to Copper City on right. Cross the northwest trending trace of the Calico Fault (Bortugno and Spittler, 1986). The fault is not expressed

in Quaternary sediment but is represented by folded Miocene sediments.

82.6 (2.4) Prepare for a right turn onto Copper City Road. Watch for traffic ahead and behind.

83.0 (0.4) TURN RIGHT (N) on Copper City Road, CG7171. Pull to the right. Look for traffic ahead and behind. Pull LEFT (west) across Copper City Road and PARK in cleared area. Execute jump-in carpooling. Proceed north on Copper City Road.

84.4 (1.4) Pass a left turn to a zeolite quarry in Skyline Tuff (Sheppard, and Gude, 1969).

84.9 (0.5) Pass a right turn to Gypsum Basin in the lower Barstow Formation (Reynolds and Miller, 2010).

85.3 (0.4) Pass through lower Barstow Formation marker beds (Reynolds et al., 2010) in siltstone and sandstone (Reynolds and Miller, 2010).

85.5 (0.3) Cross under powerlines.

86.2 (0.7) Drive through Pickhandle Formation volcanic rocks and pass road CM7244.

87.6 (1.4) Watch for oncoming vehicles. Ascend steep hill front underlain by Cretaceous granite. Slow through curves.

89.4 (1.8) Watch for oncoming vehicles. Pass left turn to a microwave station. Drive north downhill along the Coolgardie Plateau, here a pediment cut into Cretaceous granite. We are driving on BLM 7171 in a BLM managed Joshua Tree habitat restoration area.

90.0 (0.6) Pass a left turn on Coolgardie Road leading northwest to gold placers (Clark, 1970). Lane Mountain (4522 ft. elev.) rises to the northeast at 2:00.

90.7 (0.7) Pass signs at cluster of residences. View at 2:00 (NE) is of red-brown, somewhat conical Lane Mountain Quartz Latite extrusive flow dome of Miocene age (McCulloh, 1960; dated at 23.1 ± 0.2 Ma, Burke et al. (1982).

92.0 (1.3) Pass Via de la Rosa Road, which is closed to traffic. Continue NNW on Copper City Road.

92.1 (0.1) Posted road on left.

92.8 (0.7) Pass through a row (left and right) of yellow-brown, hills composed of Lane Mountain Quartz Latite.

93.1 (0.3) The road bends left and then right.

95.2 (2.1) Pass a turn to the right. View at 2:00 (NE) is of two red-brown hills, underlain by the Miocene Lane Mountain Quartz Latite (McCulloh, 1960; Burke et al., 1982).

95.3 (0.1). Prepare for dips ahead.

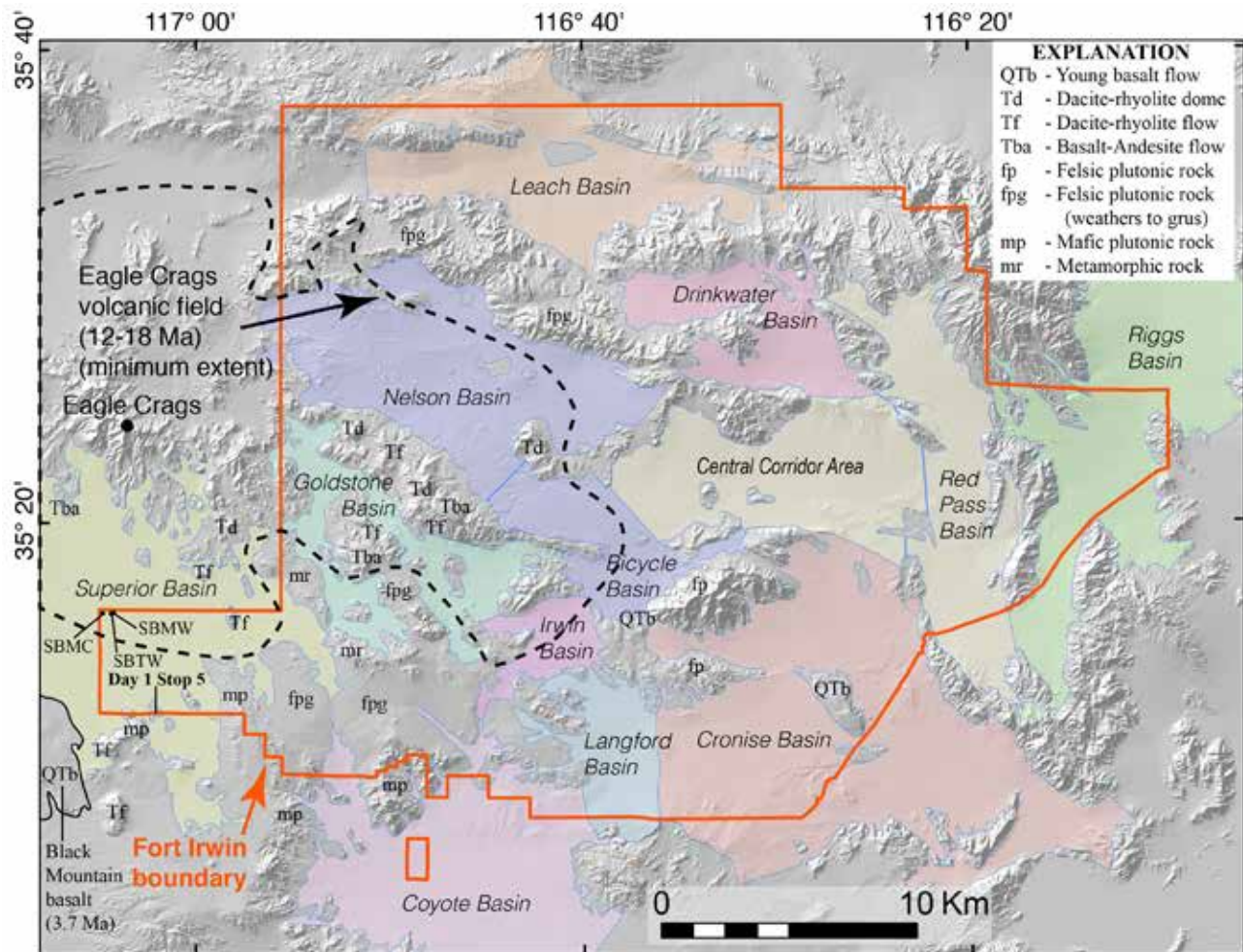


Figure 5. Location map of the Superior Basin, and other groundwater basins, in the Fort Irwin National Training Center, California. The 18-12 Ma Eagle Crags volcanic field and ~3.7 Ma Black Mountain basalt volcanic field are located, as are selected locations of plutonic, metamorphic, and volcanic rocks. Wells SBMW, SBTW, and SBMC are located in the central part of Superior Basin.

97.1 (1.8) Copper City road bears right (N).

98.4 (1.3) Pass a road on the right.

99.5 (1.1) Stop at the gate across the road at the edge of Fort Irwin. Vantage points west of here may be “superior”.

STOP 1-5. [497290 3896800] Superior Basin.

This stop is located on the edge of a small ridge, underlain by mafic plutonic rocks, that lies near the southwest boundary of Fort Irwin National Training Center (NTC), and overlooks Superior Basin. The NTC, a major desert warfare military training area since the 1940s, covers 3,050 km² (1,177 mi²). The NTC obtains all of its potable water supply from three groundwater basins; Bicycle, Irwin, and Langford Basins (Densmore et al., 2017; Fig. 5). Because of increasing water demands at the NTC, water resources are being evaluated in Superior Basin and other groundwater basins of the NTC. The NTC is in a densely-faulted and geologically-complex area bounded by the Garlock Fault to the north, and is part of the Eastern California Shear Zone and the more broadly defined

Mojave Strike-Slip Province (Dokka and Travis, 1990; Miller and Yount, 2002; Fig. 5). Typical of many parts of the Mojave Desert, the geology and landscape of the Fort Irwin area consists of rugged mountains separated by broad valleys.

Groundwater basins at the NTC are underlain by a pre-Tertiary basement complex of plutonic and metamorphic rocks. Miocene volcanic rocks comprise one type of the basin-fill deposits, predominantly in western basins, that have highly variable permeability. For instance: (1) lava flows, welded tuffs, and some sedimentary breccia are highly fractured and may yield water, (2) some volcanic sandstones and conglomerates have matrix and possibly fracture permeability, and (3) some tuffaceous sedimentary rocks have low permeability, especially where altered. The alluvial basin deposits also consist of semi-consolidated to unconsolidated Tertiary and Quaternary alluvial deposits derived from the surrounding mountains. Alluvial basin deposits, especially those of Tertiary age, are commonly interlayered with Miocene volcanic rocks. Quaternary deposits are generally

more permeable than Tertiary deposits and typically have higher water yield, where saturated. Numerous faults crossing the NTC control the lateral extent and movement of groundwater.

Superior Basin is bounded on the (1) east by a low ridge of metamorphosed Paleozoic rocks (Miller and Sutter, 1982), (2) south and west by Jurassic mafic and Cretaceous felsic plutonic rocks, and (3) north by rocks of the 18-12 Ma Eagle Crags volcanic field (ECVF) (Sabin, 1994). The ECVF consists of thick sections of andesite to rhyolite lava flows interstratified with thick sections of ignimbrites, fallout tephra deposits, tuffaceous sedimentary rocks, and some epiclastic sandstone and conglomerate. Locally, rocks from the ECVF (especially the volcanoclastic sedimentary rocks) and other Miocene volcanic and sedimentary rocks (including the Barstow Formation in the west) onlap plutonic and metamorphic rocks. Along the southwestern margin of the basin (and proximal to Stop 1-5) is the ~3.7 Ma Black Mountain basalt volcanic field.

The Superior Basin is filled with Miocene to Quaternary deposits. The Miocene sedimentary rocks (derived from the ECVF and surrounding plutonic and metamorphic rocks) overlie the plutonic rocks with an increasing number of lava flows interbedded with sedimentary rocks to the north. The Pliocene to Quaternary sediments are thickest in the middle of the basin and form a widely distributed and thin veneer on the plutonic rocks around the basin margins. Near the center of the basin (in well SBTW, Fig. 5), Quaternary to Pliocene sandstone and conglomerate are 110 m (360 ft) thick and include a 3-m (10 ft) thick basalt correlated to the Black Mountain basalt (Buesch, this volume); these rocks overlie >72 m Miocene(?) volcanoclastic sedimentary rocks (at total depth of the well). The basalt in three boreholes (wells SBTW, SBMC, and SBMW) indicates there was a basin in this area prior to 3.7 Ma and subsequently the basin has been deformed (Buesch, this volume), probably resulting in a fold associated with faulting in the Eastern California Shear Zone (Miller et al., this volume a).

In the early to mid-1900s, Superior Basin had brief periods of attempted ranching, farming, and prospecting such as between 1914-1917 when 20 wells were completed (Thompson, 1929). Currently, there are 37 pre-2009 wells of which 17 are monitored for depth to water (data can be found on the National Water Information System website; URL: <https://maps.waterdata.usgs.gov/mapper/index.html>). The deepest and most productive wells are near the center of the valley where water levels are about 30-36 m (100-120 ft) below land surface. Wells along the sides of the valley typically were dry, and many penetrated bedrock at depths as shallow as 15-45 m (50-148 ft) (Thompson, 1929). Because of limited water resources, farming efforts failed. Historical records from 1973 to 2006 indicate an average annual precipitation of 14.7 cm

(5.80 in; Western Region Climate Center, accessed in 2009, <https://wrcc.dri.edu/cgi-bin/cliMAIN.pl?ca3498>), but rainfall can vary greatly from year to year. Natural recharge occurs, primarily during winter rains or short summer thunderstorms, by precipitation runoff and infiltration along ephemeral washes and near the bases of the surrounding mountains (Densmore and Londquist, 1997). Surface runoff from storms occurs primarily in the higher topographic area of volcanic highlands adjacent to Nelson, Goldstone, and Superior Basins in the west and in local plutonic and metamorphic highlands in the central and northern parts of the base (fig. 5). Depth to groundwater and direction of groundwater flow are affected by the distribution of faults, locations and amount of recharge and discharge, and aquifer hydraulic properties. In some basins, groundwater discharges by subsurface flow through saddles and along faulted or fractured zones in the bedrock.

A three-dimensional hydrogeologic model of Superior Basin was developed from geologic and geophysical data, quantifying the subsurface extent of the volcanic and basin-fill units described above. This model allows for an evaluation of the relationships among various hydrogeologic units, and ultimately will be used to develop groundwater-flow models for studies of groundwater resources for the NTC. The models will provide tools for NTC managers to better utilize their limited water resources.

RETRACE south to return to cars parked at Old Fort Irwin Road.

102.8 (3.3) Pass a turn to the right.

107.0 (4.2) Pass Via de la Rosa Road.

107.6 (0.6) Sign posts at cluster of residences.

107.7 (0.1) Pass Beverly Road.

109.6 (1.9) Pass a right turn to a microwave station. SLOW for downhill curves. Watch for oncoming vehicles.

111.2 (1.6) Ridges underlain by volcanic rocks of the Pickhandle Formation lie on both sides of the road. Watch for cross traffic from numerous side roads.

112.5 (1.3) Ridges underlain by the Barstow Formation lie on both sides of the road.

113.6 (1.1) Pass road west.

115.0 (1.4) Retrieve vehicles at Old Fort Irwin Road (at mileage 80.6 in road log).

STOP at Pavement, look both directions for high-speed oncoming vehicles. **TURN RIGHT (SW)** onto Old Fort Irwin Road.

115.5 (0.5) Caution. Poor visibility ahead due to hill and curve. Prepare for right turn onto dirt road.

115.9 (0.4) TURN RIGHT (W) onto Fossil Bed Road and proceed west. We are paralleling the suspected trace of the Fossil Bed Road fault (Dokka, 1986).

118.8 (2.9) Stop at the entrance to Rainbow Basin Loop Road (BLM 7155). TURN LEFT and PARK in cleared area to south for jump-in carpooling procedures. Proceed north.

119.2 (0.4) Pass a right turn to Owl Canyon Camp. Rainbow Loop Road passes through sediments dating from 19 to 14 Ma, containing faunas representing the transition from the late Hemingfordian to the early Barstovian Land Mammal Age.

119.5 (0.3) **STOP 1-6.** Pull to the right and PARK before walking downhill into the wash.

The coarse, red Owl Conglomerate Member is the Red Division of the Barstow Formation, visible NW at 10 o'clock. These coarse sediments are not paleosols, but deeply weathered material possibly shed from the rising Mitchell and Waterman ranges to the south. Lithologies include the dark red rhyolite from the upper plate of the Waterman Hills Detachment Fault (WHDF; Glazner et al., 1989) and gneiss from the lower plate. The depositional sequence in this part of the Barstow Basin includes the Red Tuff (19.3 Ma) and is capped by the Rak Tuff (16.3 Ma). The Red Division Fauna of late Hemingfordian age is located near the top of the red section. Upsection, the greenish-gray sediments represent the Rak Division, contained between the Rak Tuff and the Oreodont Tuff

(15.9 Ma). The Rak Division is the lower portion of the Middle Member of the Barstow Formation in the Mud Hills, and contains the early Barstovian Rak Division Fauna. Proceed north.

119.8 (0.3) View left (NW) as we pass the transition from the red sediments of the Red Division into the greenish-gray sediments of the Rak Division. The transition occurred at 16 Ma.

120.1 (0.3) The Loop Road bears right, then left.

120.4 (0.1) Leave the greenish-gray Rak Division and enter the resistant hills of the upper part of the middle member (16 Ma to 15 Ma) of the Barstow Formation. This member contains the Green Hills Fauna which dates between 15.9 and 15.4 Ma (Woodburne et al., 1990). The Green Hills Fauna is replaced upward by the Second Division Fauna dating from 15.4 to 14.8 Ma (Woodburne and others, 1990).

120.5 (0.1) Loop Road bears left and then right.

120.6 (0.1) Road bears sharply left (W). Slow through curves ahead. The cliff to the north contains the Skyline Tuff on the south limb of the Barstow Syncline.

120.7 (0.1) Bear right, then left, and pass marker limestone (Dibblee, 1968).

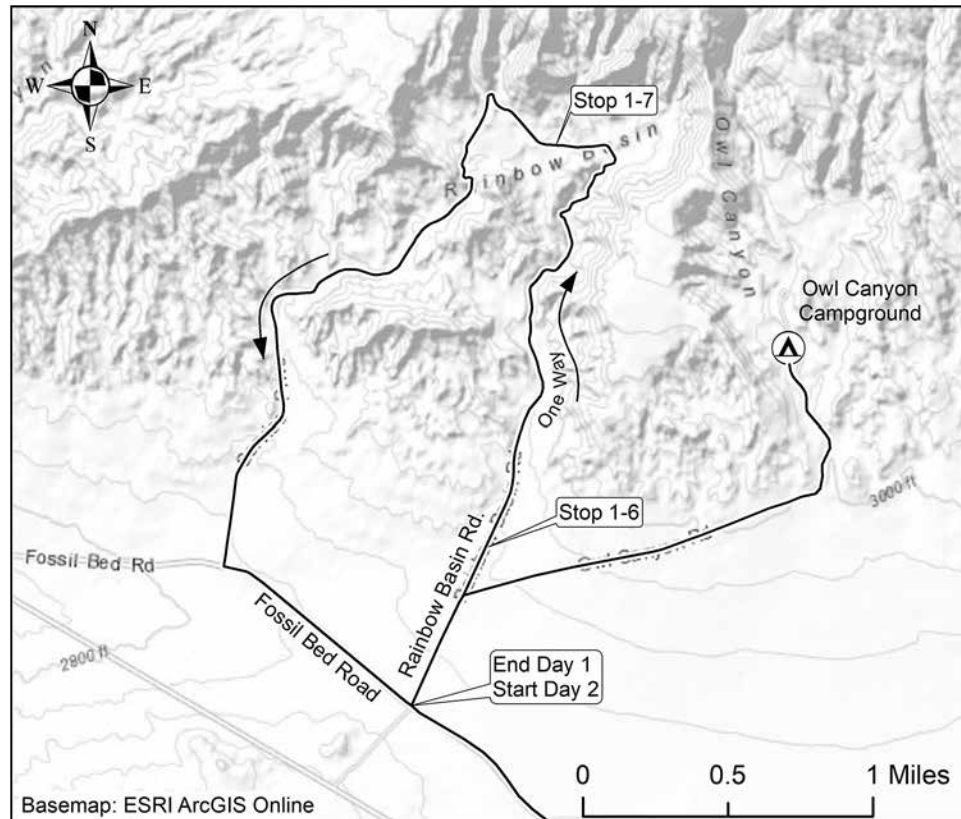
120.8 (0.1) Pass white blocky Skyline Tuff underlying the Dated Tuff (14.8). The Loop road bears right (NE).

120.9 (0.1) The Loop Road bears left (W). We have entered

chocolate and brown colored siltstone, and the red Barstow Syncline is on our right (NE). The brown siltstones may be playa deposits.

130.0 (0.1) Pull right and park in scenic view area.

STOP 1-7. Park in Rainbow Loop turn out. View east is toward the brown and red sediments in the axis of the Barstow Syncline. Look west and east to see strike-slip faults and associated drag folds. An angular unconformity separates the steeply-dipping Miocene sediments from the overlying nearly horizontal beds of Pleistocene arkosic sand. The Quaternary beds are considered to be about 160-190 kyr in age based on soils (Amoroso



and Miller, 2012). These beds, consisting of grus derived from Coolgardie Plateau, are cut by a strike slip fault with a reverse component, creating a tall fault scarp on the piedmont overlying Barstow rocks.

The Skyline Tuff and nearby overlying Dated Tuff (14.8 Ma) can be seen on the skyline to the north and southwest, and are included within the Second Division, ranging in age from about 15-14.6 Ma. This division contains the Second Division Fauna (15.4 to 14.8 Ma; (Woodburne et al., 1990). Zircons from the Skyline Tuff dated by U-Pb methods are 15.0 Ma (D.M. Miller unpubl. data).

The Upper Division lies above the white Skyline Tuff and much of it is missing from this area in the axis of the syncline.

130.1 (0.1) Continue westerly and south westerly on Rainbow Loop Road, BLM 7155.

130.3 (0.2) Rainbow Loop Road bears sharply left (S). To the right, the north limb of the syncline exposes the Skyline Tuff.

130.5 (0.2) Slow through curves. Pass the chocolate colored Dated Tuff (14.8 Ma) and the white, 4-foot-thick, porcelainous Skyline Tuff.

130.8 (0.3) The Oreodont Tuff (15.9 Ma) is exposed in the gully on the right (NW). The middle member of the Barstow Formation produces the Rak Division Fauna from sediments similar to those in the hill of gray shale on the left (S). The Green Hills Fauna comes from sediment similar to the steep sandstone cliffs on the right (N).

131.0 (0.2) Loop Road bears right (W).

131.3 (0.3) Bear left (S) past Cal Uranium Prospect Canyon and the vicinity of Alf's Barstow Flora and the Rainbow Loop Flora (Alf, 1970; Reynolds and Schweich, 2013, 2015).

131.4 (0.1) Enter the red and yellow coarse grained sediments (on the right) of the Owl Conglomerate in the Red Division.

131.7 (0.3) On the left, pass the last red outcrop of Owl Conglomerate marking the Red Division. Cross the Coon Canyon Fault that truncates the Barstow Formation on the south side of the Mud Hills.

132.1 (0.4) **STOP** at Fossil Bed Road, Watch for traffic. **TURN LEFT (E).**

132.8 (0.7) Stop at the junction with Rainbow Loop Road and retrieve vehicles. Proceed north on Rainbow Loop Road.

133.1 (0.3) Turn right (E) on Owl Canyon Road.

134.1 (1.0) **SLOW.** Road bears sharply left (N) toward campground. Pass the entrance to the group campground on the right.

134.4 (0.3) Proceed to camp sites in Owl Canyon BLM campground.

End of Day 1

Day 2

WHAT WE WILL SEE: Day 2 we will traverse the upper tracts of the Mojave River watershed, visiting Hinkley Valley to discuss the groundwater system and the history of Mojave River sediments there. We then continue upstream to the Victorville basin, where the ancestral Mojave River is known for its earliest lakes and river sediment during the early Pleistocene. We will continue upstream to Cajon Summit to discuss the source of the Mojave River in the San Bernardino Mountains as well as sediment and water sourced from the San Gabriel Mountains flowing into part of the Mojave River watershed.

Drive southwest from Owl Canyon Campground to Fossil Bed Road.

0.0 (0.0) **Convene vehicles** at the junction of Rainbow Loop and Fossil Bed Road. Drive southeast on Fossil Bed Road to Irwin Road (Old Fort Irwin Road).

1.8 (1.8) Pass transmission line road.

2.9 (1.1) Stop at Old Fort Irwin Road. Look both directions for cross traffic. **TURN RIGHT** (southwest) toward the northern Mitchell Range.

4.3 (1.4) Road bears left.

4.5 (0.2) Pass a right turn to the microwave facility. Drive through the Mitchell Range, passing from upper plate rocks (mainly Pickhandle Formation, Glazner, et al., 1989)

4.8 (0.3) Cross through the upper plate rocks of the Waterman Hills detachment fault, visible as red andesite on hill tops above greenish mylonite of lower plate metamorphic rocks and granite. This is a classic exposure of the Central Mojave Metamorphic Core Complex (CMMCC), named and described by a series of papers led by A.F. Glazner, R.K. Dokka, J.D. Walker, and J.M. Fletcher, and summarized by Glazner et al. (2002). Miocene granite intruded and was mylonitized along the upper footwall as Miocene and older rocks were faulted down and to the northeast, apparently translated several tens of km on this low-angle normal fault. A recent critique of this model (Anderson, 2017; this volume) will be expanded and discussed tomorrow on an informal third day field trip for those who wish to learn more.

5.3 (0.5) **SLOW** – use caution through curves.

6.0 (0.7) Curve left and pass a right turn to the Waterman mine as we exit the Mitchell Range. We are crossing the buried trace of the Harper Lake fault. The Harper Lake fault (also called the Waterman fault in some older reports) consists of multiple strands where it crosses the Mojave River (Densmore et al. 1997). Deeper groundwater in the regional aquifer is forced upward into the floodplain aquifer on the upgradient side of the fault. Water levels in both the floodplain and regional aquifers are generally close to land surface on the upgradient side of the fault (shallow enough to maintain riparian vegetation), and lower on the downgradient side of the fault (Densmore et al. 1997). Historic flow in the river in this area persisted at least until the 1950s (Lines, 1996), until groundwater pumping lowered water levels in the floodplain aquifer. Currently, the river only flows at the Harper Lake fault after large storm events in Cajon Pass, sufficient to cause the Mojave River to flow past Barstow to Afton Canyon. After these large storms, the river continues to flow at barrier faults like the Harper Lake fault for days or weeks after flow ceases in other parts of the river. Other faults crossing the river, such as the Calico fault or the Lockhart fault, may have similar effects on flow. Continue south toward Barstow on Irwin Road.

7.0 (1.0) **Drive-by STOP 2-1.** Mojave River Narrows at Barstow [497435 3866115]: A long piedmont leads down to the Mojave River to the south. Ribs in the piedmont consist of alluvial fan gravels that are mantled by strongly developed soils (Bt and calcic horizons). The ribs progressively rise downslope above the inset channels, departing by as much as 10-15 m from the modern stream channels that grade to the Mojave River. Correlative high ribs with similar soils can be found on the south side of the river, indicating that older fan deposits previously closed the Mojave River valley. We (D.M. Miller and K. Maher) have estimated the age of the alluvial fan by U-series dating of opal in the calcic horizons that mantle the ribs. The age represents a minimum for the time of sediment deposition, by about 190 kyr. Because the alluvial fans grade to well above the modern Mojave River, the narrows through Barstow had not been cut by this time, and the delivery of Mojave River sediment to downstream Lake Manix likely was not possible. The Mojave River may have been diverted to another upstream basin at this time allowing the alluvial fans to aggrade into the former Mojave River channel. We will compare this timing with that for sedimentary infill of the Hinkley Valley at the following three stops.

7.9 (0.9) Thick red paleosols in alluvial fan gravels in the cut on the right include calcic horizons with opal.

8.5 (0.6) Stop sign at old Route 58. Proceed south and prepare for a right turn.

8.6 (0.1) Stop sign. TURN RIGHT on old Route 58. Drive west along the linear front of the Waterman Hills,

composed of footwall mylonites and metamorphic rocks of the Miocene core complex. The linear front here probably resulted from Mojave River erosion, but farther to the northwest it was caused by the active Mt. General Fault. Glazner et al. (2002) noted that dikes of Miocene age cut the mylonites, themselves formed in Miocene granite, in the Waterman Hills, and therefore the diking took place in a structural position above the brittle-ductile transition. All are cut by the WHDF.

9.5 (0.9) Foundations of the Waterman mill site are ahead, roughly south of the Waterman gold mine in the Waterman Hills to the north. The Atlantic and Pacific Railroad reached the site of Waterman in 1882, (Myrick, 1963). Robert Whitney Waterman (b. 1826) developed prosperous mines in this area in 1880. A Republican, he was elected Lt. Governor of California in 1886 and became governor a few months later with the death of Democratic Governor Washington Bartlett. Waterman died in 1891 (Bancroft, 2002). We are passing through greenish-gray outcrops of mylonitic Waterman Gneiss.

12.1 (2.6) Pass left turn toward Community Boulevard. Proceed northwest, then west on Old Hwy. 58.

Best Rock Quarry produces dolomite from a marble roof pendant on right.

13.7 (1.6) Mt. General is to the northeast at 2:00. Mt. General is underlain by Miocene lava flows and domes that lie in the upper plate of the WHDF. The lower plate here consists of Miocene granite and dikes with abundant screens of metamorphosed early Paleozoic rocks. Fremont Peak is in the distance at 1:30.

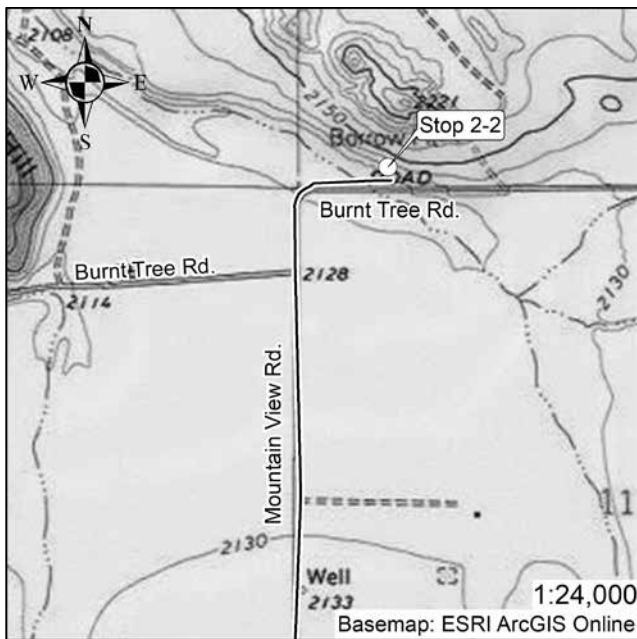
14.5 (0.8) Lenwood Road and access to Hwy 58. Continue west on Santa Fe Road. We are driving along a flat area that acts as a drainage divide (el. 2177') between the Mojave River on the south and the Hinkley and Harper valleys to the north. At this point, less than 3 m (10 ft) of relief separate our position from the surface of the Mojave River channel a mile to the south and the Mojave River has repeatedly flooded to this playa-like area. We will drive north to follow a channel down from this playa and comment more on it at Stop 2-2.

15.6 (1.1) Santa Fe Ave bears right (west-northwest) adjacent to the railroad tracks.

16.6 (1.0) Pass Summerset Road.

17.6 (1.0) TURN RIGHT on Mountain View Road and drive north along the floor of Hinkley Valley. Note that only gentle knolls break the generally flat floor of the valley. The sediments beneath us are all derived from Mojave River sources.

17.8 (0.2) Pass white hills of Paleozoic marble on the left (west) and, farther ahead, on the right. In this area of the Hinkley Valley and westward, wells have encountered



bedrock at shallow depths. Much of the sediment of this valley is derived from Mojave River flow north into Harper Basin.

20.2 (2.4) Red Hill is to the northwest.

21.0 (0.8) Pavement ends at Burnt Tree Road. Slow to 15 mph and continue north to a sharp right turn.

21.1 (0.1) TURN RIGHT.

21.2 (0.1) PARK vehicles on the far right shoulder.

STOP 2-2. [484595 3870925] Red Hill area: The hill to the north is Miocene rhyolite and dacite, as is Red Hill to the west. These stand higher than surrounding Miocene granite. Gaps between the hills are inferred to be caused by strands of the Mt. General fault (Dibblee, 1960). Recent study by Haddon et al. (this volume) using high-resolution elevation models indicates that two strands of the fault lie south of Red Hill, but a third strand north of Red Hill may be indicated by vegetation lineaments.

Walk north to examine Harper Lake sediments that contain fresh water mussels (*Anodonta californiensis*) and gastropods (Reynolds, this volume).

Lacustrine sediments (modified from Geochronology and Paleoenvironment of Pluvial Harper Lake, Mojave Desert, California, USA (Garcia et al. 2014)

Harper basin is a closed basin with elevations ranging from 615 m above mean sea level (asl) at the modern-day playa to 1397 m asl at Fremont Peak (Fig. 6). Approximately 18 km south of the present-day playa, and outside of its present drainage basin, is the west-to-east flowing Mojave River with a bed elevation of ~671 m asl. Previously, Meek (1999) provided uncalibrated radiocarbon ages ranging from 24,000 to >30,000 ¹⁴C yr BP for highstand lake deposits near 658 m elevation in Harper Lake, at our current location.

We collected samples from a hand-excavated 2.1 m (7 ft) stratigraphic section of silt and sand at ~650 m asl on Mountain View hill (informal name) and used radiocarbon and feldspar luminescence dating to infer that the age of the Harper Lake highstand was more likely ~45–40 cal kyrBP (Garcia et al., 2014; Fig. 7). Based on our inferred age for the Harper Lake highstand and the identification of paleosols in Lake Manix sediments with ages of roughly 35 ka and 40 cal kyrBP (Reheis et al., 2012), we infer that the Mojave River flowed exclusively into Harper basin at ~45–40 ka. The Mojave River was then redirected into Lake Manix and formed the lakes there at ~30–20 ka and eventually later flowed into Lake Mojave.

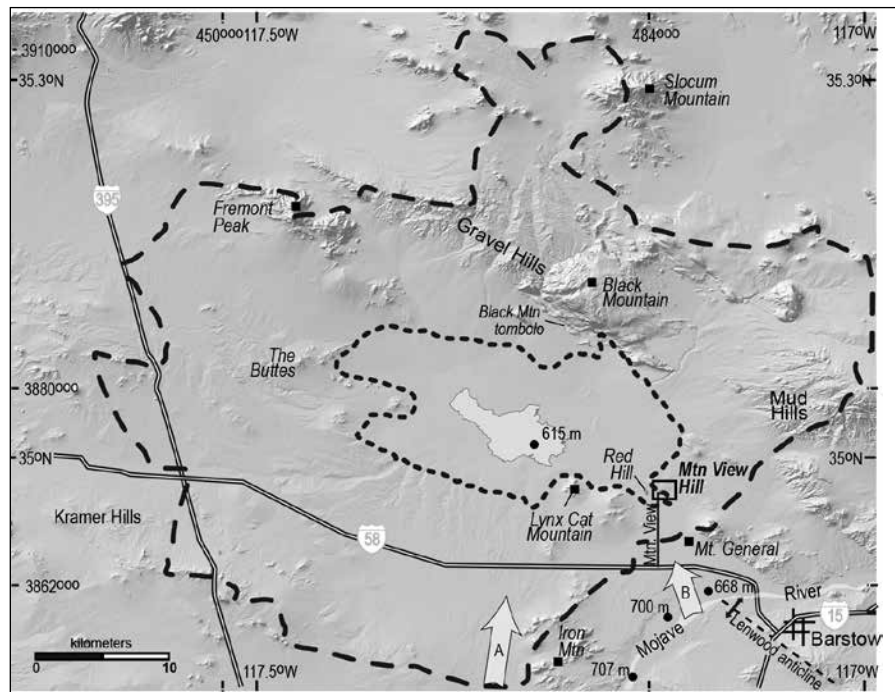


Figure 6. Shaded relief map of the Harper basin. Heavy dashed line is the present drainage basin divide. Dotted line is elevation 658 m above mean sea level, which is the approximate elevation of the Harper Lake highstand deposits mapped by Dibblee (1968). Mountain View Hill is located at the northern termination of Mountain View Road. Light colored area is the present-day Harper (dry) Lake playa; black circles indicate present day elevations. Arrows A and B are hypothesized Mojave River inflows to Harper basin (Meek, 1999; Cox et al., 2003).

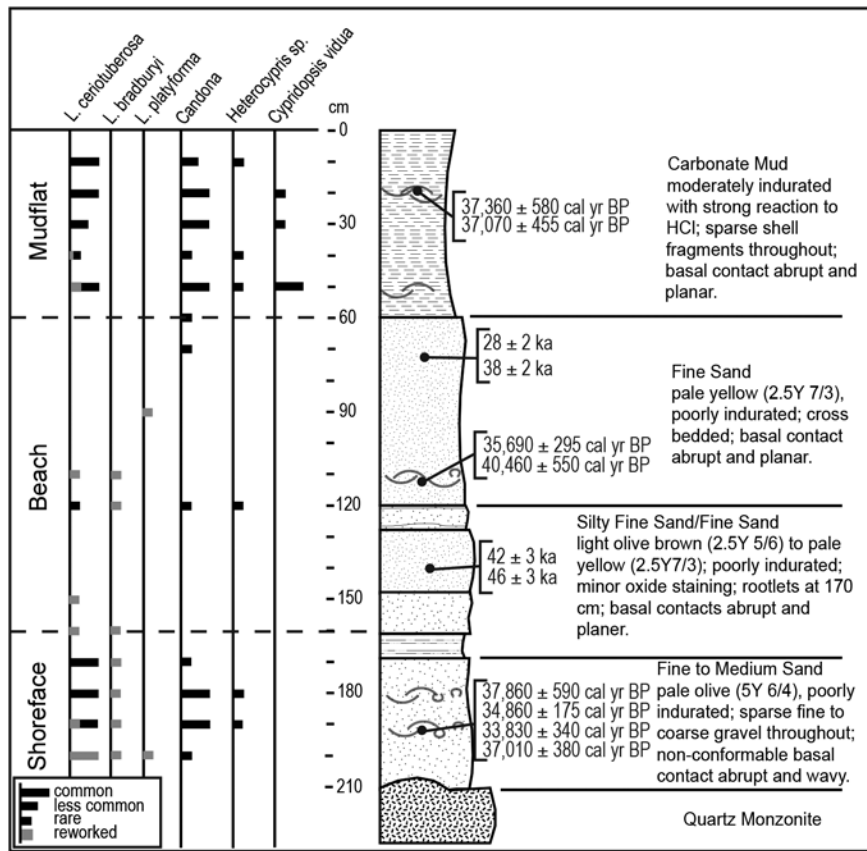


Figure 7. Measured stratigraphic section with radiocarbon (cal yr BP, plain text) and IRSL (kyr, italic) dates. Relative abundances of ostracode taxa and paleoenvironmental interpretations at left.

At Mountain View hill, located at the southeast part of Harper basin, we found that *Limnocythere ceriotuberosa* is the dominant ostracode species. *Limnocythere ceriotuberosa* and its freshwater equivalent, *Limnocythere platyforma*, prefer alkaline lakes with high seasonal inflow. Ostracodes from Harper Lake highstand sediments are consistent with an alkaline lake environment that received seasonal inflow from the Mojave River.

Our interpretation is that the Mountain View hill section is a transgressive/regressive lacustrine sequence characterized by shoreface-beach-mudflat facies (Fig. 7). The shoreface sediments, comprised of fine to medium sand with gravel, is exposed at the base of the measured section and overlain by well-sorted cross-bedded sands. This lower section represents a transgression. These sands were then buried by a carbonate mud sequence, representing mudflat deposits, as the lake receded.

Based on geologic mapping, radiocarbon and optically stimulated luminescence dating, we infer a ~45–40 ka age for this sequence of Harper Lake sediments. The inferred ~45–40 ka lake stand at Harper Lake coincides with a shallowing interval at downstream Lake Manix.

Studies of borehole core and outcrops of northern Hinkley Valley show that a sedimentary unit consisting of sand and mud, similar to the deposits we are examining, can be followed about 1 km (0.6 mi) southward in Hinkley Valley. The base of the lake deposits is at 5 to 8 m depth, and typically rests on a well-developed soil. Overlying the lake deposits is a sheet of Mojave River sand and gravel. Reynolds and Reynolds (1994b) noted that there are only 5 m (17 ft) of relief between the Mojave River drainage system to the south and Hinkley/Harper Valley system to the north. The inundation of Harper Lake could have been by river avulsion (Miller et al., this volume b), or it is possible that the Mt. General and Lockhart faults deformed the valley, elevating the base of the Mojave River locally to force it into Harper Basin (Reynolds and Kenney, 2004).

Pliocene valley configurations.

Walk up onto the hill behind the exposure of lacustrine sediments to gain a view of Harper Valley and surroundings. North of this hill are diminutive basalt outcrops, and similar basalt was encountered in boreholes in the same area. Northeast of us are low dark hills, composed of basalt flows mantled by eolian sand sheets. Beyond to the northeast is Black Mountain, capped by the basalt of Black Mountain, which was dated at ~3.7 Ma (Oskin and Iriondo, 2004). This basalt was described in Superior Lakes at Stop 1-5. Field study and geochemical analyses verify that all of the basalt flows are similar and likely derive from the Black Mountain source. Based on the overall distribution of basalt, we can infer that at late Pliocene time, the source of the Black Mountain basalt flows was at a high divide between Superior basin on the east and eastern Harper basin on the west, much as Black Mountain is today.

Farther west, studies at industrial facilities along western Harper Lake report basalt encountered in deep boreholes and have inferred continuous, thick basalt under Harper basin on the basis of a few boreholes and interpretation of aeromagnetic data. Evidently Harper basin was in existence during the Pliocene. No basalt has been found in boreholes in Hinkley Valley. From this information we can tentatively conclude that there was no connection between Hinkley and Harper valleys in the Pliocene. At a

later stop we will describe the configuration of sediment and bedrock in Hinkley Valley.

Interestingly, the Pliocene basalt flows lie on Miocene Barstow Formation rocks at Black Mountain but in the outcrops to our north, they lie on gravels of post-Barstow age, based on clast composition. Southward, those gravels pinch out against Miocene granite that was once deep in the crust. This line of pinchout passes from the hill we stand on toward the east-northeast, and must mark a boundary of rapid denudation after the early Miocene, a boundary that had topographic expression in the late Pliocene as hills to the south and lowland to the north. The basalt flowed across the lowland.

Young wetlands and flow through the Red Hill gap.

Look northwest toward Harper Lake, and note the near ground that is pale in color. This area is referred to as Water Valley because of readily available water in shallow wells a century ago (Thompson, 1929). Groundwater recharge from the Mojave River moves through unconsolidated deposits within Hinkley and Water Valleys to discharge areas near Harper (dry) Lake. During predevelopment time, extensive wetland areas were present along the margin of the dry lake as a result of discharge of groundwater. Under present-day conditions saturated deposits in the northern part of Hinkley Valley are poorly permeable. These poorly permeable deposits are overlain by coarser-grained, permeable Mojave River deposits that are now mostly unsaturated. Groundwater movement from the Mojave River through Hinkley Valley into Water Valley by way of Hinkley (Red Hill) Gap is comparatively rapid, and modern (post-nuclear era onset of high tritium values) water is present in the southern part of Water Valley.

Groundwater discharge (GWD) deposits blanket most of Water Valley, indicating that in times past there was extensive wetland development. Historical records only document wetlands near the Harper playa, and farms established on the (dry) GWD deposits demonstrate that water tables were fairly deep.

Seven miles west-northwest of this stop, along the shore of Harper playa, solar energy facilities have used recycled cooling water to keep ponds viable throughout the year. These ponds attract migratory birds, as well as being habitat for insects, reptiles and small mammals (<https://ebird.org/hotspot/L892043>). Interesting water birds seen at these ponds include: common terns, gulls, horned grebe, sandpiper, sanderling, phalarope, yellowlegs, dowitcher, canvasback, geese, tundra swan, water thrush, scaup, merganser, bufflehead, teal, Eurasian wigeon, bittern, Virginia rail, double-crested cormorant, green heron, egrets, common loon, kingfisher, and Wilson’s snipe. Other migrants include scissor-tailed flycatcher, peregrine falcon, ferruginous hawk, merlin, black-headed grosbeak, lazuli bunting, and sandhill crane.

Turn around and RETRACE route south on Mountain View Road to Santa Fe Road.

21.5 (0.3) Pavement resumes at Mountain View/Burnt Tree Road junction.

24.9 (3.4) Stop sign at Santa Fe Road. Watch for traffic and continue south across the railroad tracks.

25.4 (0.5) Stop sign. TURN RIGHT on the old Bakersfield Highway 58.

26.4 (1.0) TURN LEFT (south) on Hinkley Road.

26.7 (0.3) Stop sign. Cross the new Hwy 58, continue south.

26.9 (0.2) Stop sign at Hwy 58 access ramps. Continue south on Hinkley Road.

27.0 (0.1) Pass Pioneer Road.

27.4 (0.4) TURN LEFT (east) on Community Blvd.

28.4 (1.0) Pass Mountain View Blvd.

28.9 (0.5) Pass Fairview Road. The Pacific Gas and Electric (PG&E) compressor station is to the SE.

29.4 (0.5) TURN LEFT (north) on unpaved Summerset Road. Drive slowly past agricultural operations, noting the irrigation systems and lush green growth, which will be discussed when we stop.



STOP 2-3. PG&E remediation. NOTE: We will have permission for this trip to access PG&E routes; later use of the road log for this stop must honor locked gates and private property. Follow field trip leaders to safely traverse to an area of tanks for the remediation system that PG&E has developed.

Pacific Gas and Electric Company Hinkley Groundwater Remediation Program

PG&E has made significant progress in cleaning up the highest concentrations of chromium 6 in groundwater by implementing several interim remedies, which have been in place since 2004. As part of a long-term remedial process, PG&E evaluated numerous cleanup technologies to determine the best approach. The solution utilizes treatment-in-place systems in areas that have the highest levels of chromium, the largest in-place barrier treatment system for metals in the world, and an innovative and sustainable remediation method that treats lower levels of chromium by growing alfalfa and other fodder crops. By partnering with local farmers, PG&E's agricultural operations boost the local economy, preserves farmland and fosters working relationships toward common community goals.

In-situ Reactive Zone (IRZ)

PG&E is using in-situ treatment to achieve cleanup in areas of the plume that have the highest levels of chromium 6. The in-situ process starts by injecting a food grade material (such as ethanol) into affected groundwater to stimulate the growth of naturally occurring bacteria within the soil. The growth cycle of the bacteria creates conditions that convert chromium 6 to chromium 3, a naturally occurring substance. To date, in-situ treatment has reduced chromium concentrations across 124 acres of the plume core from over 1,000 parts per billion (ppb) to less than 10 ppb in many areas.

Agricultural Treatment

Agricultural treatment is a key component of PG&E's groundwater remediation program in Hinkley. Using drip irrigation, impacted groundwater is applied directly to the soil where crops are planted. Soil conditions surrounding the crop roots convert chromium 6 into chromium 3. Once converted, the chromium 3 leaves the groundwater and becomes part of the surrounding soil.

The post-trip route available to public is as follows (ensuing mileage uses this route):

- 28.9 (0.5) TURN LEFT (W) on Fairview Road.
- 29.4 (0.5) View right (E) of tanks at PG&E remediation facility. TURN AROUND, return south on Fairview Rd.
- 29.9 (0.5) STOP, look for traffic. Continue across Community Blvd on Fairview Road.

30.4 (0.5) TURN RIGHT (W) on Highcrest Rd.

30.7 (0.3) TURN LEFT (S) on Hervey Road. Continue south nearly ¼ mile.

30.9 (0.2) STOP along shoulder of the road. **STOP 2- 4.** [484750 3866675].

We've stopped near the site of well MW-BG-0005, a monitoring well installed upgradient of the remediation area to help evaluate background groundwater conditions. Note the rolling topography and northward gradient in slope, both different than the flatter Hinkley Valley floor to the north. We've driven part way up a clastic wedge of Mojave River sand and gravel that is sourced from the south, at the south end of Iron Mountain. This wedge led to and interfingered with lake deposits. Miller et al. (this volume b) described the facies of the valley and their general distribution. The clastic wedge and lake deposits apparently filled an internally-drained valley. The presence of the ~631 kyr Lava Creek B ash, sourced from the Yellowstone eruptive center, was verified in the lake deposits by tephrochronology study (E. Wan and L. Walkup, written commun. 2016). Thus Hinkley Valley was filled, perhaps rapidly, by sediment from the Mojave River during the time period prior to Lake Manix and after abandonment of upstream lakes that we will discuss at the next stop (Miller et al., this volume b). Borehole core made available by PG&E was instrumental in developing this history of Hinkley Valley infill.

The site of this monitoring well is on older Mojave River deposits. However, it is one of the most permeable areas in the Hinkley valley. However, water level responses to recharge from the Mojave River are damped, because groundwater movement in this area from the Mojave River is impeded by the Lockhart fault, which lies a short distance to the north (Fig. 8). Groundwater level declines from agricultural pumping in Hinkley Valley down gradient from the Lockhart fault are greater than 18 m (60 ft) and contributed to the adjudication of the Mojave River groundwater basin. Groundwater pumping has produced storage within the aquifer that can allow large quantities of surface water to infiltrate during occasional streamflows in the Mojave River.

Southeast of us, the Mojave River channel can be seen in southern Hinkley Valley. It lies well below the level of this well, and farther to the south upgradient on this clastic wedge, the river channel is inset 30 m (100 ft) below the top of the wedge. The incision of the modern channel is poorly dated here, but we may infer that it postdates the >190 kyr alluvial fans grading to positions above the Mojave River near Barstow that we saw at Stop 2-1. As we drive to our next stop we will drop into the river channel and follow the river upstream to Victorville. Along the way, at Brisbane Valley, we will pass another location where fans leading to the incised (modern) stream base have been dated. There, the ~190 kyr fans grade to the

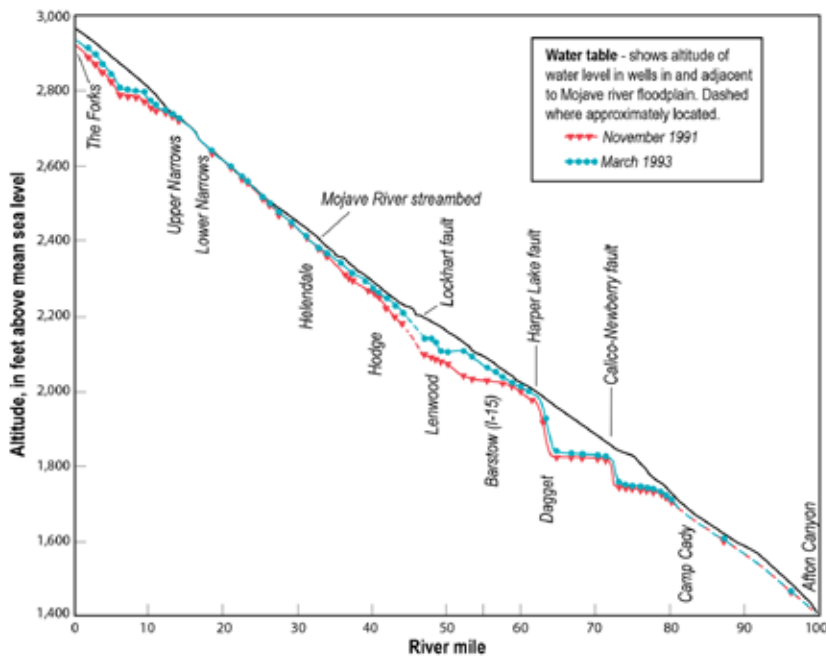


Figure 8. Water-level response to infiltration of intermittent streamflow, Mojave River, Calif., November 1991 and March 1993 (modified from Lines, 1996). Major floods during the winter of 1993 (Fig. 2) illustrate the effects of floodplain aquifer recharge compared to earlier 1991 data, which follow 8 years of little streamflow.

modern channel. These data may indicate that during the time of deposition of those ~190 kyr fans, a time period that may be several tens of thousands of years, the river cut to the modern channel level.

Proceed south on Hervey Road to Riverview Road.

31.2 (0.3) STOP, watch for traffic. TURN RIGHT (west) on Riverview Road. Cross several ridges that represent eroded Mojave River fluvial plain sand and gravel.

31.4 (0.2) Pass through intersection with Mountain View Road.

32.4 (1.0) STOP at Hinkley Road. Observe cross traffic. TURN LEFT (south) on Hinkley Road. Drive (south) upgradient along the Mojave River clastic wedge. Slow through dips and curves.

33.8 (1.4) Slow as Hinkley Road bears right (southwest).

34.6 (0.8) Slow as Hinkley Road bears left (south).

35.6 (1.0) Metamorphic rocks in Iron Mountain to the west are metamorphosed volcanic rocks of the Hodge Volcanics, thought to be correlative to the Jurassic Sidewinder Volcanics that crop out widely in mountains to the south. The southern Iron

Mountains contain the westernmost turquoise in Mojave Desert, which was also utilized by Native Americans (Murdoch and Webb, 1966).

36.2 (0.6) Hinkley Road bears left (SE). Slow, watch for traffic. Descend into the modern Mojave River channel, incised deeply into the ancient clastic wedge deposits.

36.6 (0.4) Slow for narrow bridge as we cross the Mojave River sand bed. Large flows along the Mojave River occur historically every 5 to 7 years on average in response to rain on snow events at the headwaters of the Mojave River. These weather events (sometimes referred to as pineapple express) can cause several hundred thousand acre-feet of water to discharge to the headwaters of the river. Groundwater level declines due to pumping from the floodplain aquifer attenuate these large streamflows that historically would have flowed to Afton Canyon but instead recharge the floodplain

aquifer. Particularly large stormflow events can cause the river to flow for several days or weeks due to recently recharged groundwater in the floodplain aquifer coming out of storage, especially near faults that transect the river. Similarly, pumping of groundwater in excess of recharge has decreased baseflow in perennial reaches of the Mojave River at Afton Canyon and the Victorville Narrows, due to the connection between groundwater and surface flows in the river (Fig. 9).

Prior to widespread pumping starting in the 1940s and 1950s, water in the Mojave River flowed at land surface at several reaches along the riverbed, maintaining riparian forests of cottonwood and willow. Many reaches of the

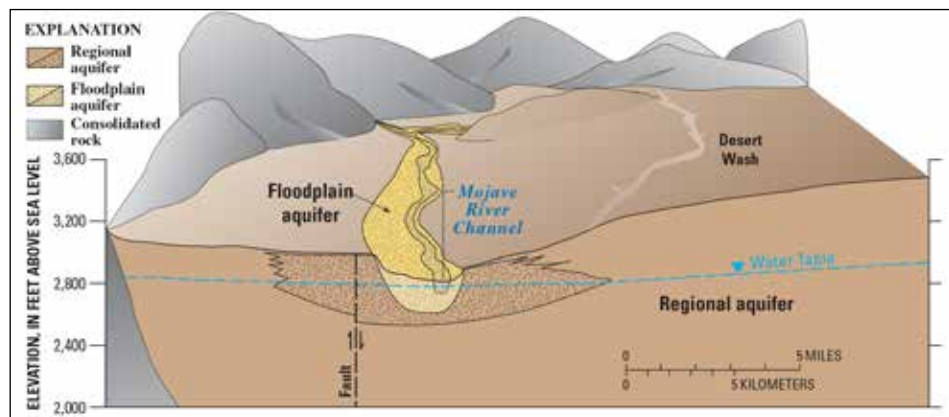


Figure 9. Simplified geologic model of the Mojave River, floodplain aquifer, and regional aquifer near a mountain front (Stamos et al., 2002).

riverbed with sustained flow were near faults crossing the floodplain, or bedrock constrictions.

37.0 (0.4) Bear right and SLOW as you cross uneven railroad tracks.

37.4 (0.4) Stop at Johnston's Corner. Watch for traffic coming from both directions. TURN RIGHT (southwest) on National Trails Highway (Rt. 66) to drive upstream along the Mojave River.

40.6 (3.2) Pass Hodge Road on the left.

44.2 (3.6) Pass right turn for Indian Trail. North of here, the Helendale Ash (Reynolds and Cox, 1999) is a Mono "W" type tephra that best correlates with a sample that is between 0.9 and 1.18 Ma. The Helendale Ash is located at the base of the Mojave River gravels (El: 762 m; 2500 ft), and overlies the fine sediments of the Victorville Basin. This sequence suggests that the river had finished filling the Victorville Basin by ~1 Ma (Reynolds and Miller, 2010).

At Brisbane Valley, south of the highway, several alluvial fan deposits are inset into ancestral Mojave River deposits. Two well-developed Pleistocene units with strong desert pavements are represented, indicating ages of ~70 to 300 ka. A varnish microlamination age of 74-85 ka from boulders in the younger deposit is consistent with ages elsewhere for correlative deposits, suggesting that the older deposit is also representative and ~160-300 ka. This is a minimum limiting age for incision of the Mojave River channel.

45.0 (0.8) Cross Bonanza Trail. We are travelling across bluffs younger than one million years (Reynolds and Cox, 1999).

46.1 (1.1) National Trails Hwy bears right (west-southwest).

46.6 (0.5) Pass a left turn for Murphey Co. Road. Road bears right: slow through downhill curves. Watch for oncoming traffic.

47.8 (1.0) Route 66 bears left (south) at railroad. Watch for oncoming traffic.

48.7 (1.1) Watch for oncoming traffic at the junction of Vista Road that runs north to Silver Lake (Reynolds and Miller, 2015; Stops 2-2 & 2-3). The Victor Valley Wastewater Reclamation Authority has discharged treated wastewater to the Mojave River since 1982. Treated water flows at the surface along the riverbed for approximately 4 miles from the discharge point, maintaining local riparian vegetation and creating braided channel morphology, before the water infiltrates into the streambed. A shallow fine-grained layer (composed of silt and clay, typically 15 m (50 ft) below land surface) in the floodplain in this area (Huff et al. 2002) prevents water discharges

from immediately infiltrating into the streambed and recharging the floodplain aquifer.

51.3 (2.6) Pass Andover Road. Route 66 bears left (south).

51.9 (0.6) Pass Turner Road.

52.4 (0.5) Pass aggregate plant on left (east).

52.9 (0.5) Cross Heritage – Bryman Road. Silver Mountain is to the left (east).

54.4 (1.5) Cross the other Bryman Road.

55.3 (0.9) National Trails Hwy. bears left (south).

56.0 (0.7) Use caution through curves and dips.

57.0 (1.0) Pass aggregate mixing plant on left. Quartzite Mountain is at 10:30. Slow for downhill curve. Watch for traffic entering roadway.

57.3 (0.3) Pass entrance to CalPortland Oro Grande Cement Plant (Fife and others, 1980) and Oro Grande Canyon Road. Caution, underpass ahead.

57.4 (0.1) SLOW while passing under the railroad trestle. Watch for vehicles entering Route 66. Route 66 bears left (southeast) through Oro Grande.

57.9 (0.5) Slow to 45 mph while entering the community of Oro Grande. Pass the Mill Street trestle. Note the bluffs on the west side of the river. These contain the stratigraphy we will discuss at the next stop. The strata indicate that Victorville basin was the first of the basins the Mojave River filled with sediment in order to fill successive downstream basins and eventually connect the route to Silver Lake.

58.2 (0.3) Stop for light at Riverside Prep School Street.

59.2 (1.0) Route 66 bears left (south-southeast).

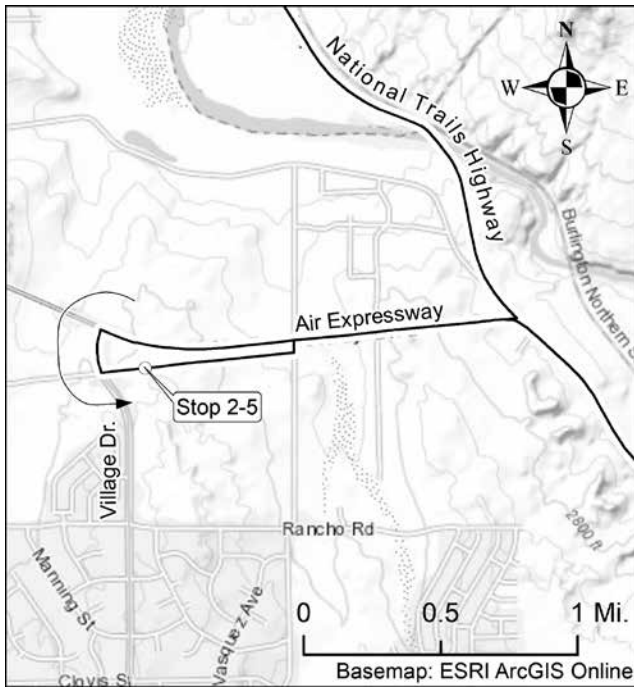
60.1 (0.9) Slow crossing the bridge over the Mojave River. Pass Rockview Nature Park at the Lower Narrows.

60.5 (0.4) Pass Turner Road on the right.

60.7 (0.2) Stop light at Air Expressway. Caution – vehicles entering from the right. TURN RIGHT (west) at the signal for Air Expressway. Move to the left lane.

61.2 (0.5) TURN LEFT on Gas Line Road. Immediately TURN RIGHT (west) on powerline road. Proceed west to hill top view of Village Drive.

61.6 (0.4) **STOP 2-5.** Victorville Stratigraphy. View west of Victorville basin sedimentary sequence in bluffs on the west side of Village Drive. View northwest toward Southern California Logistics Airport (formerly George Air Force Base). Stratigraphy described here consists of three stratigraphic units: lower, middle and upper (Reynolds and Cox, 1999; Cox and Tinsley, 1999; Sibbett, 1999; Cox et al., 1998, 2003).



The **lower unit** is a pebble–cobble arkosic sand deposited by a southward-flowing axial stream system, based on clast composition. Clasts of Jurassic and early Miocene volcanic rocks are derived from the Mojave Desert, not from the Transverse Ranges, and include rock types from the Kramer Hills and outcrops near Barstow. Borehole magnetostratigraphy indicates that the top of this unit is about 2.5 Ma (Cox et al., 2003). This would place the lower unit within the 4.1 to 1.5 Ma range of the Phelan Peak Formation on the north slope of the San Gabriel Mountains west of Cajon Pass, or within the 4 Ma range of the uppermost Crowder Formation on the northwestern slope of the San Bernardino Mountains.

The **middle unit** consists of fine sandstone, siltstone, mudstone, and groundwater discharge deposits that are interpreted as lake and wetland deposits caused by damming of the former south-flow river by rising Transverse Ranges. This middle unit is roughly 2.5-0.76 Ma, its upper part constrained by magnetostratigraphy (Cox et al., 2003).

The **upper unit** consists of arkose typical of the Mojave River bedload, mostly gravel with rounded quartzite pebbles and abundant granitic debris, all sourced from the San Bernardino Mountains. The upper unit is probably time-transgressive, becoming younger away from the Transverse Ranges as it prograded across the former Victorville basin. Mojave River sediment leading north to Harper basin and northeast to Hinkley Valley represents the escape of the Mojave River to downstream basins (Cox et al., 2003).

Proceed west toward Village Drive

61.7 (0.1) STOP at pavement. Check for oncoming traffic.

TURN RIGHT on Village Drive.

61.8 (0.1) TURN RIGHT (east) on Air Expressway.

63.1 (1.3) STOP at National Trails Highway. TURN RIGHT (south) toward Victorville.

64.2 (1.1) Slow while entering Victorville. National Trails Hwy is renamed North ‘D’ Street. The sandstone bluffs on right (Cox et al., 2003) have been dated in part by the contained fossils (Power, 1989; Reynolds and Reynolds, 1994a).

64.8 (0.6) Prepare for right turn onto I-15 south toward Cajon Pass and San Bernardino. Services on right.

65.0 (0.2) TURN RIGHT onto I-15 southbound. Watch traffic while merging.

68.0 (3.0) Pass Palmdale Road interchange

76.3 (8.3) Continue past the Joshua Street exit north to SR-395.

76.5 (0.3) Move toward the right lane after the traffic from 395 merges onto I-15. Cross under Rancho Road. Prepare to exit at Oak Hill Road.

82.8 (6.2) EXIT at Oak Hill Road.

83.1 (0.3) STOP. TURN LEFT (southeast) on Oak Hill Road. Pass services and the site of the historic Summit Inn, destroyed by the Blue Cut Fire in August 2016.



83.2 (0.1) STOP. Watch for traffic from both directions. TURN RIGHT on Mariposa Road. Proceed southeast.

83.9 (0.7) Jog sharp left, then right onto dirt track leading south.

84.2 (0.3) Pass water tanks on left and make a SHARP LEFT (E) TURN and an IMMEDIATE RIGHT TURN. PARK in roundabout.

STOP 2-6. Headwaters of the Mojave River and Cajon Pass: uplift and erosion of the San Bernardino Mountains.

The Mojave River: Movement along the San Andreas fault over the last several million years has changed the surface drainage contributing to the Mojave River and created Cajon Pass. Some alluvium within the Victorville Fan, and the present-day Sheep Creek Fan to the west, is eroded from the Pelona Schist and is naturally high in elements such as chromium. High chromium concentrations in alluvium within the two fans have resulted in high concentrations of hexavalent chromium, Cr(VI), in local groundwater. Traces of Pelona Schist, which was derived from the San Gabriel Mountains, can be found in older Mojave River deposits as far downstream as Barstow. These traces are remnants of when the source rocks in the San Gabriel Mountains containing Pelona Schist were further to the southeast along the San Andreas fault, and closer to the headwaters of the Mojave River. In the geologic past some Pelona Schist fragments may also have been transported into Mojave River deposits when Sheep Creek connected to the river through Fremont Wash. Reworked fragments of Pelona Schist may continue to be delivered to the Mojave river through Oro Grande Wash.

Precipitation near Cajon Pass is the source of groundwater recharge for much of the floodplain aquifer along the Mojave River. This precipitation falls mostly in the winter. Air masses that produce precipitation that falls within the pass condensed at warmer temperatures than precipitation that has been uplifted over the surrounding mountains and falls largely as snow at higher altitudes. The warmer low-altitude precipitation in Cajon Pass creates an “isotopically heavy” (less negative) composition in surface runoff and groundwater that can be identified throughout the floodplain aquifer as far as Afton Canyon more than 100 miles downstream (Fig. 10).

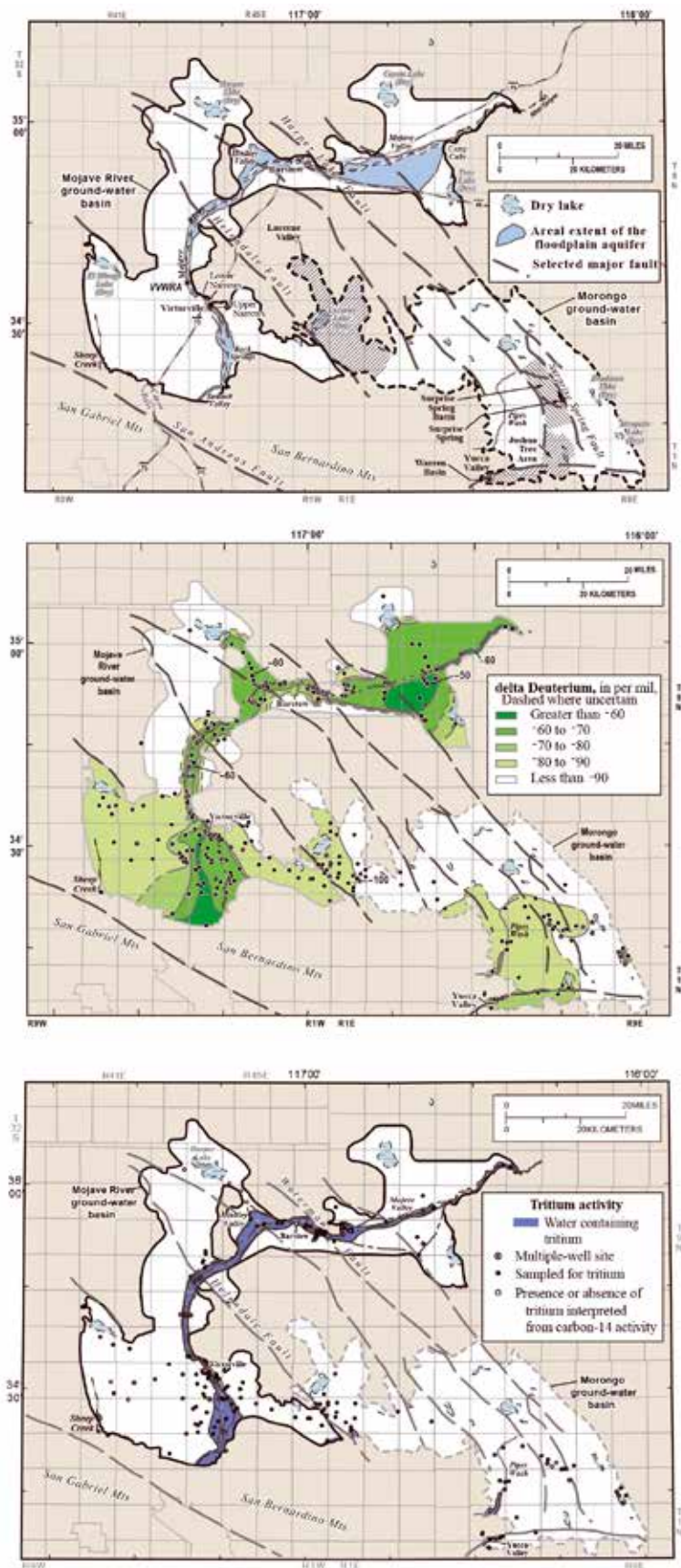


Figure 10. Source (top), movement (middle), and age (bottom) of groundwater within the Mojave River groundwater basin (modified from Izbecki, 2004; Izbecki and Michel, 2004).

Infiltration of surface flow in the Mojave River results in younger groundwater recharged to the floodplain aquifer since the atmospheric testing of nuclear weapons beginning in 1952. In contrast, recharge in adjacent basins and the surrounding and underlying regional aquifer is primarily from storms and snowmelt in the high altitudes of the San Bernardino and San Gabriel Mountains and has an “isotopically lighter” (more negative) composition. Groundwater outside of the floodplain aquifer can be up to 20,000 years old and may be isotopically lighter because of climatic changes that have occurred since the Pleistocene (Izbicki, 2004; Izbicki and Michel, 2004). Water diverted from the state water project (imported from northern California) is used to recharge the floodplain aquifer in the Victorville area at Rock Springs Rd along the Mojave River.

Biota of the river system: Mohave tui chub (*Siphateles bicolor mohavensis*) was the only fish native to the Mojave River. Its extirpation was postulated to be the result of introduction of arroyo chub (*Gila orcuttii*) in the 1930's. Hybridization and introgression between the two species was the reason stated in the Recovery Plan (1984) for the elimination of Mohave tui chub from the river by the 1960's. Most remaining chubs are not hybrids but rather *G. orcuttii* (Chen et al., 2013). Around 2007 hitch (*Lavinia exilicauda*), a minnow species from the Sacramento River, was discovered in Afton Canyon by staff from Mojave National Preserve, California Department of Fish and Wildlife, and researchers from North Dakota State University. Graduate student Sujun Henkanaththegedara assembled the following invasion timeline from surveys conducted by the National Park Service, published information, and agency records. Following the introduction of arroyo chub in the 1930's, mosquitofish (*Gambusia affinis*) were found in 1956 and three-spined stickleback (*Gasterosteus aculeatus*) in 1967.

The California Aqueduct East Branch of the State Water Project was completed to the Silverwood Reservoir in 1972. By 1980 the number of exotic fish species in the Mojave River doubled (from 6 to 12) with species commonly found in the Sacramento River, such as hitch and green sunfish (*Lepomis cyanellus*). The number of exotic species jumped again, to 19, when the aqueduct was enlarged in 1995.

The Mohave tui chub currently persists in four highly modified isolated habitats. Potential reintroduction sites with

permanent water flow have exotic species that make them unsuitable for reintroduction. Southwestern pond turtles (*Actinemys pallida*) occur in some of the headwater streams with non-native turtle species including western painted turtles (*Chrysemys picta bellii*), red-eared sliders (*Trachemys scripta elegans*) and spiny softshell turtles (*Trionyx spiniferus*).

Deeper time tectonics and sediment packages: Note that we have been travelling along and next to ridges trending northeast. These erosional features were developed after deposition from the San Gabriel Mountains ended, and during the initial phases of erosion associated with final elevation of those mountains. This may have occurred only 500,000 years ago, and before Cajon Valley drainage systems separated the San Gabriel Mts. from the Inface bluffs just to the southwest of us. Refer to Reynolds and Woodburne (this volume) who describe and discuss these major concepts:

- Junction of Pacific Oceanic Plate with North American Continental Plate
- Deposition of Cretaceous Cosy Dell Fm. and fossils
- Deposition of Oligocene Vaqueros Fm. and fossils
- Deposition of Cajon Valley Beds and fossils
- Deposition of Crowder Fm. and fossils
- Deposition of Phelan Peak Fm. & fossils
- Uplift of San Gabriel and San Bernardino Mountains
- Deposition of Shoemaker Gravels and Noble's Alluvium
- Palinspastic reconstruction of sediments and depocenters.
- Headward erosion on Cajon Creek

End of trip



Figure 11. View west of the middle Miocene (18 Ma) Cajon Valley Beds with the earliest Miocene (22 Ma) Vaqueros Formation in the hill to the right. The snow capped San Gabriel Mountains have risen to 10,000 feet in the last half-million years. Jennifer Reynolds photograph.

What we have seen:

We've traversed the entirety of the Mojave River from sink to source, examining several of the basins that river sediment filled before spilling to the next lower basin and thereby lengthening the river course. The final step, to fill Silver Lake and overflow permanently to Death Valley, has yet to be completed. Some basins, such as Harper, have apparently only held Mojave River water for short periods and have not been filled with sediment. Others, such as Hinkley Valley, are filled and yet show evidence for complex river switching points that can route floods either of two ways. The river system is still youthful, and the numerous active faults that traverse it will continue to modify the river and influence depth to groundwater. Along the river course, reaches with emergent water exist where bedrock or faults cause rise in the water table, and these locations are critical for many species, including humans (pre-historic, historic, and modern). Archeology and paleontology of lake sediments of the Mojave River system provide much information on past life, but the records are incomplete; a major challenge is to integrate the records and complete the picture of life evolving in and near the river.

The modern Mojave River has water added from Northern California, dams in the upper reaches, engineered recharge systems along the way, and multiple reaches where water use depletes the floodplain aquifer. It is very much a managed system that departs significantly from its prehistoric configuration. Learning more about that prehistoric configuration by modeling, study of isotope geochemistry, and other approaches is essential to inform on sustainable management of the river system.

We also visited small groundwater basins detached from the Mojave River, yet every bit as vital to local uses. They face similar issues in wise management. Each of these small groundwater basins has a unique geohydrologic framework that must be established, tested, and modeled for sustainable water use.

Let trip leaders know if you are departing for home. Those who are planning to go on the optional Day 3 trip should head toward Barstow and/or Owl Canyon Campground. Arrange carpooling in 4WD vehicles before tomorrow morning.

References

- Amoroso, L., and Miller, D.M., 2012, Surficial geologic map of the Cuddeback Lake 30' x 60' quadrangle, San Bernardino and Kern Counties, California: USGS Scientific Investigations Map 3107, 31 p., scale 1:100,000.
- Anderson, E., 2017, Major revisions of the timing, style, magnitude, and cause of Early Miocene extension in the Central Mojave metamorphic core complex and subsequent role of the Eastern California Shear Zone, *in* Reynolds, R.E., ed., *Revisiting the Eastern California Shear Zone*: California State University, Fullerton, Desert Studies Consortium, p. 60-70.
- Anderson, E., this volume, Early Miocene extension in the central Mojave; where do we go from [here](#)?
- Bancroft Library, 2002. California Views from the R.W. Waterman Family Papers, ca. 1865–1900. http://www.oac.cdlib.org/dynaweb/ead/calher/waterman/@Generic_BookTextView/129 (accessed 4/12/02).
- Barthel, P.S., 2008, Water Budget and Hydrogeologic Model of Spring Flow at Limestone Hill, Zzyzx Desert Studies Center: Unpublished M.S. thesis, California State University Fullerton CA, 113 p.
- Bortugno, E. J., and Spittler, T. E., 1986, Geologic map of the San Bernardino quadrangle, scale 1:250,000: Regional Geologic Map Series, Map No. 3A, California Division of Mines and Geology.
- Brandt, J., and Sneed, M., 2017, Land subsidence in the southwestern Mojave Desert, California, 1992-2009: U.S. Geological Survey Fact Sheet 2017-3053, 6 p., <https://doi.org/10.3133/fs20173053>
- Brown, H.J., 2016a, Detailed geologic maps of the northern Calico Mountains and the Lane mountain area, central Mojave Desert California: Part 1 The need for new mapping, Geological Society of America Abstracts with program v 48, No 4.
- Brown, H.J., 2016b, Detailed geologic maps of the northern Calico Mountains and the Lane Mountain area, central Mojave Desert California: Part 2 Stratigraphy and structure of Paleozoic, Mesozoic and Cenozoic rocks, Geological Society of America Abstracts with program, v,48, No 4.
- Brown, H.J., Stone, Paul, Rosario, Jose and Fitzpatrick, John, 2016, Detailed geologic map of the northern Calico Mountains and the Lane Mountain area, central Mojave Desert California: Part 3 Preliminary digital geologic map, Geological Society of America Abstracts with Program, v, 48, No 4.
- Buesch, D.C., this volume, ~3.7 Ma Black Mountains basalt flows geochemically correlated to boreholes in Superior Basin, western Fort Irwin, California
- Burke, D.B., Hillhouse, J.W., McKee, E.H., Miller, S.T., and Morton, J.L., 1982, Cenozoic rocks in the Barstow basin area of southern California - stratigraphic relations, radiometric ages, and paleomagnetism: U.S. Geological Survey, Bulletin 1529-E, scale 1:125,000.
- Byers, F. M., 1960, Geology of the Alvord Mountain Quadrangle, San Bernardino County, California: U.S. Geological Survey Bulletin 1089-A, 71 p.
- Chen Y, Parmenter S, May B. 2013. Genetic characterization and management of the endangered Mohave tui chub. *Conservation Genetics* 14: 11–20.
- Clark, W. B., 1970, Gold Districts of California: California Division of Mines and Geology: Bulletin 193, 183 p
- Cox, B. F., and J. C. Tinsley, III, 1999. Origin of the late Pliocene and Pleistocene Mojave River between Cajon Pass and Barstow, California. *San Bernardino County Museum Association Quarterly* 46(3):49-54.
- Cox, B. F., J. W. Hillhouse, A. M. Sarna -Wojcicki, and J. C. Tinsley, 1998. Pliocene-Pleistocene depositional history along the Mojave River north of Cajon Pass, California

- Regional tilting and drainage reversal during uplift of the central Transverse Ranges: Geol. Soc. Amer. Abstracts with Programs, v. 30, no. 5, p.11.
- Cox, B.F., Hillhouse, J.W., and Owen, L.A., 2003, Pliocene and Pleistocene evolution of the Mojave River, and associated tectonic development of the Transverse Ranges and Mojave Desert, based on borehole stratigraphy studies and mapping of landforms and sediments near Victorville, California: *in* Enzel, Y., Wells, S.G., and Lancaster, N., eds., Paleoenvironments and paleohydrology of the Mojave and southern Great Basin Deserts: Boulder, Colorado, Geological Society of America Special Paper 368, p. 1-42.
- Dekker, F.J., and Hughson, D.L., 2014, Drought sensitive montane spring reliability and hydrologic controls in Mojave National Preserve, CA: Geological Society of America Annual Meeting: https://gsa.confex.com/gsa/2014AM/finalprogram/abstract_250572.htm
- Densmore, J.N., Cox, B.F., and Crawford, C., 1997, Geohydrology and water quality of Marine Corps Logistics Base, Nebo and Yermo Annexes, near Barstow, California. U.S. Geological Survey Water-Resources Investigations Report 96-4301.
- Densmore, J.N., and Londquist, C.J., 1997, Ground-water hydrology and water quality of Irwin Basin at Fort Irwin National Training Center, California. U.S. Geological Survey Water-Resources Investigations Report 97-4092.
- Densmore, J.N., Dishart, J.E., Miller, D.M., Buesch, D.C., Ball, L.B., Bedrosian, P.A., Woolfenden, L.R., Cromwell, G., Burgess, M., Nawikas, J.M., O'Leary, D.R., Kjos, A.R., Sneed, and M., Brandt, J., 2017, Water-resources and land-surface deformation evaluation studies at Fort Irwin National Training Center, Mojave Desert, California, *in* 2017 Desert Symposium Field Guide and Proceedings - ECSZ does it: Revisiting the eastern California Shear Zone, Reynolds, B., ed., <http://nsm.fullerton.edu/dsc/images/DSCdocs/DSPProceedings/2017%20ECSZ%20does%20it.pdf>
- Dibblee, T. W., Jr. 1960. Geology of the Barstow quadrangle, San Bernardino County, California: U.S. Geological Survey Mineral Investigations Field Studies Map MF-233, scale 1:62,500.
- Dibblee, T. W., Jr. 1968. Geology of the Opal Mountain and Fremont Peak quadrangles, California. California Division of Mines and Geology, Bulletin 188:64p.
- Dokka, R.K., 1986, Patterns and modes of early Miocene crustal extension, central Mojave Desert: Geological Society of America Special Paper 208, p. 75-96.
- Dokka, R.K., and Travis, C.J., 1990, Role of the eastern California shear zone in accommodating Pacific-North American plate motion: Geophysical Research Letters, v. 17, p. 1323-1326.
- Dudash, S.L., 2006, Preliminary surficial geologic map of a Calico Mountains piedmont and part of Coyote Lake, Mojave Desert, San Bernardino County, California: U.S. Geological Survey Open-File Report 2006-1090, 44 p., scale 1:24,000.
- Durrell, C. 1954. Barite Deposits near Barstow, San Bernardino County, California: California Division of Mines and Geology Special Report 39: p. 8.
- Fife, D.L., 1980, Epithermal late Tertiary gold mineralization at the Shining Dawn Mine Lane Mountain Quadrangle, *in*: Geology and Mineral wealth of the California Desert, Dibblee Volume, South Coast Geological Society, p. 330-335.
- Fife, D.L., J. W. LaViolette and Mark Unruh, 1980, Oro Grande, p 543, *in*: Geology and Mineral wealth of the California Desert, Dibblee Volume, South Coast Geological Society, p. 555.
- Garcia, A. L., Knott, J. R., Bright, J., and Mahan, S. A., 2014, Geochronology And Paleoenvironment Of Pluvial Harper Lake, Mojave Desert, California: Quarternary Research, v. 81, p. 305-317.
- Glazner, A.F., J. M. Bartley, and J. D. Walker. 1989. The Waterman Hills Detachment Fault, central Mojave Desert, California. San Bernardino County Museum Association Special Publication 89, p. 52-60.
- Haddon, EK., Miller, D.M., Langenheim, V.E., Liu, Tanzhuo, Walkup, L.C., Wan, Elmira, this volume, Initiation and rate of slip on the Lockhart and Mt. General faults in southern Hinkley Valley, California.
- Hagar, D. J., 1966, Geomorphology of Coyote Valley, San Bernardino County, California: Ph.D. dissertation, University of Massachusetts, Amherst, MA, 210 pp.
- Huff, J.A., Clark, D.A., and Martin, P., 2002, Lithologic and ground-water data for monitoring sites in the Mojave River and Morongo ground-water basins, San Bernardino County, California, 1992-98. U.S. Geological Survey Open-File Report 02-354.
- Hull, Sharon, and Mostafa Fayek, 2013. Halloran Springs and pre-Columbian turquoise trade. California State University, Desert Studies Consortium, Desert Symposium Volume: p. 198 – 205.
- Izbicki, J.A, 2004, Source and movement of groundwater in the western part of the Mojave Desert, southern California, USA. U.S. Geological Survey Water-Resources Investigations Report 03-4313 <https://pubs.usgs.gov/wri/wrir034313/wrir034313.pdf>
- Izbicki, J.A., and Michel, R.L., 2004, Movement and age of groundwater in the western part of the Mojave Desert, southern California, USA. U.S. Geological Survey Water-Resources Investigations Report 03-4314 <https://pubs.usgs.gov/wri/wrir034314/wrir034314.pdf>
- Langenheim, V.E., and Miller, D.M., 2017, Connecting the Soda-Avawatz and Bristol-Granite Mountains faults with gravity and aeromagnetic data, Mojave Desert, California, *in* Reynolds, R.E., ed., Revisiting the Eastern California Shear Zone: California State University, Fullerton, Desert Studies Consortium, p. 83-92. <http://nsm.fullerton.edu/dsc/images/DSCdocs/DSPProceedings/2017%20ECSZ%20does%20it.pdf>.
- Lines G.G., 1996, Ground-water and surface-water relations along the Mojave River, southern California. Water-Resources Investigations Report 95-4189 <https://pubs.er.usgs.gov/publication/wri954189>
- Lovich, J.E., and K.R. Beaman. 2007. A history of Gila monster (*Heloderma suspectum cinctum*) records from California with comments on factors affecting their distribution. Bulletin of the Southern California Academy of Sciences 106:39-58.

- Lovich, J.E., and G.B. Haxel. 2011. A previously unreported locality record for the Gila monster. *Bulletin of the Southern California Academy of Sciences* 110:59-62.
- Lovich, J., and K. Meyer. 2002. The western pond turtle (*Clemmys marmorata*) in the Mojave River, California, USA: highly adapted survivor or tenuous relict? *Journal of Zoology*, London 256:537-545.
- Lovich, J.E., S.R. Puffer, K.L. Cummings, S. Greely. Feasibility study for re-establishing southwestern pond turtles and Mojave tui chubs to Afton Canyon ACEC. U.S. Geological Survey Cooperators Report to the Bureau of Land Management under IAA No. L16PG00229. 30 pp.
- McCulloh, T. H., 1960, Geologic map of the Lane Mountain quadrangle, California: U.S. Geological Survey Open File Report, scale 1:62,500. Meek, N., 1990, Late Quaternary geochronology and geomorphology of the Manix basin, San Bernardino County, California: Unpublished Ph.D. thesis, Los Angeles, University of California Los Angeles, 212 p.
- Meek, N., 1999, New discoveries about the Late Wisconsinan history of the Mojave River: San Bernardino County Museum Association Quarterly, 46(3), p. 113-117.
- Meek, N., 2004, Mojave River history from an upstream perspective. California State University, Desert Studies Consortium, Desert Symposium Volume 2004, p. 41-49.
- Miller, D.M., Schmidt, K.M., Mahan, S.A., McGeehin, J.P., Owen, L.A., Barron, J.A., Lehmkuhl, F., Lohrer, R., 2010, Holocene landscape response to seasonality of storms in the Mojave Desert: *Quaternary International*, v. 215, p. 45-61.
- Miller, D.M. Dudash, S.L., McGeehin J. P., (in press), Paleoclimate record for Lake Coyote, California, and the LGM and deglacial paleohydrology (25 to 14 cal ka) of the Mojave River: *Geological Society of America Special Paper*.
- Miller, D.M., and Yount, J.L., 2002, Late Cenozoic tectonic evolution of the north-central Mojave Desert inferred from fault history and physiographic evolution of the Fort Irwin area, California, in Glazner, A.F., and Walker, J.D., eds., *Geologic evolution of the Mojave Desert and southwestern Basin and Range: Geological Society of America Memoir* 195, p. 173-197.
- Miller, D. M., R.E. Reynolds, G.A. Phelps, J. Honke, A.J. Cyr, D.C. Buesch, K.M. Schmidt, G. Losson, 2017, Active tectonics of the northern Mojave Desert: the 2017 Desert Symposium field trip road log, California State University, Desert Studies Consortium, Desert Symposium Volume: p. 7-44.
- Miller, D.M., Buesch, D.C., Langenheim, V.E., Ball, L.B., Bedrosian, P.A., and Cromwell, G., this volume, a, Geologic framework of groundwater basins of western Fort Irwin, California.
- Miller, D.M., Haddon, E. K., Langenheim, V.E., Cyr, A. J., Wan, E., Walkup, L., and Starratt, S., this volume, b, Middle Pleistocene infill of Hinkley Valley by Mojave River sediment and associated lake sediment: Depositional architecture and deformation by strike-slip faults.
- Miller, E.L., and Sutter, J.S., 1982, Structural geology and $^{40}\text{Ar}/^{39}\text{Ar}$ geochronology of the Goldstone-Lane Mountain area, Mojave Desert, California: *Geological Society of America Bulletin*, v. 93, p. 1191-1207.
- Murdoch, Joseph and Webb, R.W., 1966, *Minerals of California*, Calif. Div. Mines and Geology, Bull. 189, p. 559.
- Muessig, S., White, G.N., and Byers, F.M. Jr., 1957, Core logs from Soda Lake, San Bernardino County, California: U.S. Geological Survey Bulletin 1045-C, p. 81-96.
- Myrick, D.F., 1963, *Railroads of Nevada and Eastern California*, vol 2, the southern roads. Berkeley: Howell-North Books.
- Oskin, M., and Iriondo, A., 2004, Large-magnitude transient strain accumulation on the Blackwater fault, Eastern California shear zone: *Geology*, v. 32, p. 313-316, doi: 10.1130/G20223.1.
- Power, Jeanne D., 1989, Episodic lake development in the Victorville Area, California. SBCMA, Special Publication 89:41-43.
- Reheis, M.C., Miller, D.M., and Redwine, J.L., 2007, Quaternary stratigraphy, drainage-basin development, and geomorphology of the Lake Manix basin, Mojave Desert: U.S. Geological Survey Open-File Report 2007-1281, 37 p.
- Reheis, M. C., Bright, J., Lund, S. P., Miller, D. M., Skipp, G., and Fleck, R. J., 2012, A half-million-year record of paleoclimate from the Lake Manix Core, Mojave Desert, California: *Palaeogeography, Palaeoclimatology, Palaeoecology*, v. 365-366, p. 11-37.
- Reynolds, R.E., and Reynolds, R.L., 1994a, The Victorville Fan and an occurrence of *Sigmodon*, in Off limits in the Mojave Desert, R.E. Reynolds, ed. Redlands, San Bernardino County Museum Association Special Publication, 94(1): 31-33.
- Reynolds, R.E. and R.L. Reynolds, 1994b, The isolation of Harper Lake Basin, in Off limits in the Mojave Desert, R.E. Reynolds, ed. Redlands, San Bernardino County Museum Association Special Publication, 94(1): 34-37.
- Reynolds, R.E., and Cox, B.F., 1999, Tracks along the Mojave: a field guide from Cajon Pass to the Manix Basin and Coyote Lake. San Bernardino County Museum Association Quarterly, 46(3): 1-26.
- Reynolds, R.E., and Kenney, Miles, 2004, Breaking Up! The Desert Symposium 2004 Field Trip Road Guide, p. 3-32.
- Reynolds, R.E., and Miller, D.M., 2010, Overboard in the Mojave: 20 Million years of lakes and wetlands: 2010 Desert Symposium Volume, California State University, Desert Studies Consortium, 292 p.
- Reynolds, R.E., D.M. Miller, M.O. Woodburne, and L.B. Albright, 2010. Extending the boundaries of the Barstow Formation in the central Mojave Desert; 2010 Desert Symposium Volume, California State University, Desert Studies Consortium. p.148-161.
- Reynolds, R.E., and Miller, D.M., 2015, Mojave Miocene: the field trip: Desert Symposium Volume, California State University, Desert Studies Consortium, p. 7-33.
- Reynolds, R.E., and Schweich, T.A., 2013, The Rainbow Loop Flora from the Mud Hills, Mojave Desert, California: 2013 Desert Symposium Volume, California State University, Desert Studies Consortium, p. 39-48.
- Reynolds, R.E., and Schweich, T.A., 2015, Additions to the floras of the Barstow Formation in the Mud Hills, Mojave Desert, California: Desert Symposium Volume, California State University, Desert Studies Consortium, p. 119-129.

- Reynolds, R.E., this volume, Fishing for fossils along the course of the Mojave River.
- Reynolds, R.E., and Woodburne, M.O., this volume, Cajon Pass: A classic geologic textbook.
- Rosen, M.R., 1994, The importance of groundwater in playas: A review of playa classifications and the sedimentology and hydrology of playas, in, Rosen, M.R., ed., Paleoclimate and basin evolution of playa systems: Boulder, CO., Geological Society of America Special Paper 289, p. 1-18.
- Ruppert, R.M. 2010. A recent sighting of a banded Gila monster, (*Heloderma suspectum cinctum*) in Mojave National Preserve. Mojave National Preserve Science Newsletter. April, Number 1:1-3.
- Sabin, A.E., 1994, Geology of the Eagle Crags volcanic field, northern Mojave Desert, China Lake Naval Air Weapons Station, California, [Ph.D. Thesis]: Golden, Colorado School of Mines, 209 p., <https://dspace.library.colostate.edu/handle/11124/170512>.
- Schneider, J. S., 1994, Fresh water mussels and paleoenvironment at East Cronese Lake, p 42-15 in G. D. Everson and J. S. Schneider (eds), Kelso Conference Papers on Prehistory of the Mojave Desert. Museum of Anthropology, California State University Bakersfield, Occasional Papers in Anthropology 4.
- Sheppard, R.A., and A.J. Gude, 3rd, 1969, Diagenesis of tuffs in the Barstow Formation, Mud Hills, San Bernardino County, California: U.S. Geological Survey Professional Paper 634:1-34.
- Sibbett, B. S., 1999, Pleistocene channels of the Mojave River near Victorville, California. San Bernardino County Museum Association Quarterly 46(3): p. 65-68.
- Southern Pacific Company, 1964, Minerals for industry, California Division of Mines and Geology Special report 95, 242 p.
- Stamos, C.L., Martin, P., and Predmore, S.K., 2002, Evaluation of artificial recharge in the Mojave River ground-water basin, California: U.S. Geological Survey Open-File Report 2002-430, 38 p. <https://pubs.er.usgs.gov/publication/ofr02430>
- Thompson, D.G., 1929, The Mohave Desert Region, California; a Geographic, Geologic, and Hydrologic Reconnaissance: U.S. Geological Survey Water-Supply Paper 578, 759 p.
- Warren, C. N., and J. S. Schneider, 2000, Archaeology in the Cronese Basin. California State University Desert Symposium, p. 40-41.
- Wells, S.G., Brown, W.J., Enzel, Y., Anderson, R.Y., and McFadden, L.D., 2003, Late Quaternary geology and paleohydrology of pluvial Lake Mojave, southern California, in Enzel, Y., Wells, S. G., and Lancaster, N., eds., Paleoenvironments and paleohydrology of the Mojave and southern Great Basin Deserts: Special Paper 368: Boulder, Colo., Geological Society of America, p. 79-114.
- Western Region Climate Center, 2009, *Cooperative Climatological Data Summaries*; accessed in 2009, <https://wrcc.dri.edu/cgi-bin/cliMAIN.pl?ca3498>
- Winograd, I.J., and Thordarson, W., 1975, Hydrogeologic and hydrochemical framework, south-central Great Basin, Nevada-California, with special reference to the Nevada Test Site: U.S. Geological Survey Professional Paper 712-C, 126 pp.
- Woodburne, M.O., and Reynolds, R.E., 2010, The mammalian litho- and biochronology of the Mojave Desert Province; 2010 Desert Symposium Volume, California State University, Desert Studies Consortium. p. 124-147.
- Woodburne, M.O., Tedford, R.H., and Swisher, C.C., III., 1990, Lithostratigraphy, biostratigraphy and geochronology of the Barstow Formation, Mojave Desert, southern California. Geological Society of America Bulletin, v. 102, p. 459-477.



Minneola: Mojave River flood damage at Minneola Road. March 7, 2005. View to the north. Note damaged power poles. D. M. Miller photograph.

Guide to an informal field trip to the southeast part of the Central Mojave Metamorphic Core Complex, April 24, 2018

Ernie Anderson and Nate Onderdonk, trip leaders

The trip follows the 32Nd Annual Desert Symposium and field trip, April 20-23, 2018

This trip will involve mandatory carpooling in 4WD high clearance vehicles. Please arrange carpool rides in advance. Start with a full tank of gas, water, lunch, snacks, sunscreen and extra clothes for all types of weather.

Following the DS Field Trip on Monday, April 23, Anderson will be at Owl Canyon camp ground and available for comments, questions regarding the trip.

Vehicles will convene west of Barstow, north of the new Highway 58, at the junction of Lenwood Road and Old Hwy 58/Santa Fe Road. Leave surplus vehicles in the cleared area north of Old Hwy 58 along the east side of Lenwood Road. Trip attendees coming from motels in Barstow will find the easiest route is to drive south on E. Main Street, turn right and enter I-15 southbound (W). After crossing under Barstow Road, move to the right lane and prepare to enter the turn NW onto new Hwy 58. Exit at Lenwood Road and drive north to Old Hwy 58/Santa Fe Road.

Trip attendees coming from Owl Canyon will drive south on Irwin Road (Old Ft. Irwin Road) to Old Hwy 58. After stops, turn right (W) on Old Hwy 58 and proceed west to Lenwood Road.

As traffic permits, cross and park along the east side of Lenwood Road where carpooling arrangements will be completed.

Abbreviations

BDT-Brittle-ductile transition
CMMCC-Central Mojave metamorphic core complex
WHP-Waterman Hills Pluton
WHDF-Waterman Hills detachment fault
WMS-Waterman Mine syncline
WW-Waterman window

Trip log

Set odometer to 0.0

0.0 (0.0) Intersection with Lenwood Road. Proceed west on Santa Fe Street. View of Mount General in the Hinkley Hills to the north at 3 o'clock.

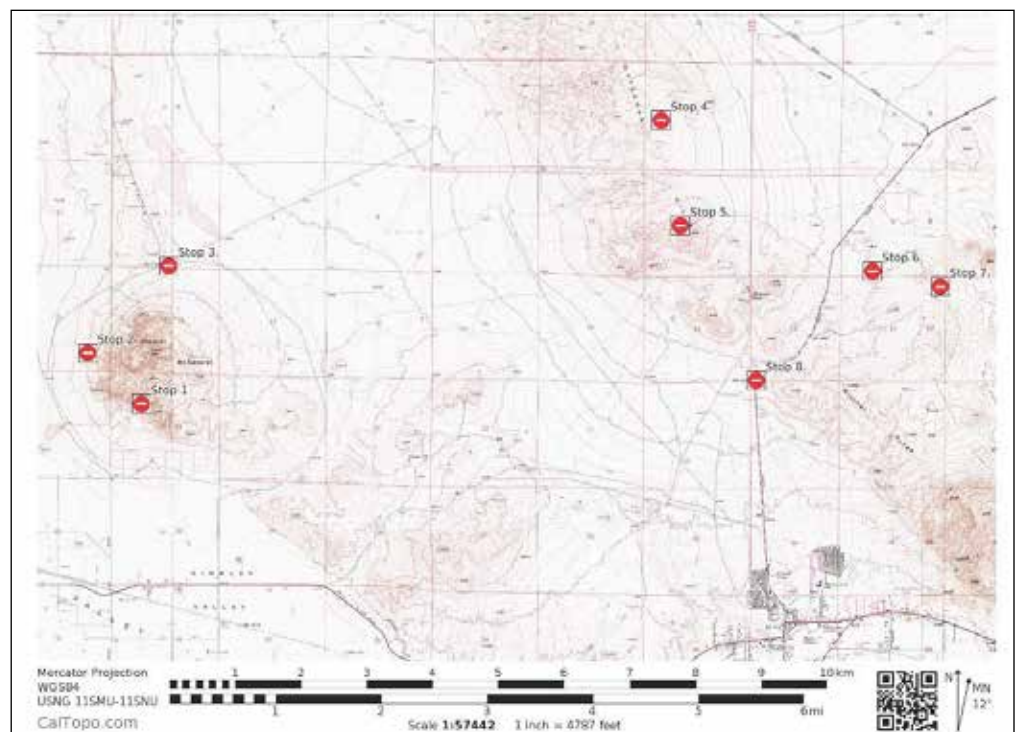
1.0 (1.0).—Directly after small grove of conifer trees, turn right (north) onto Dixie Road toward Mount General.

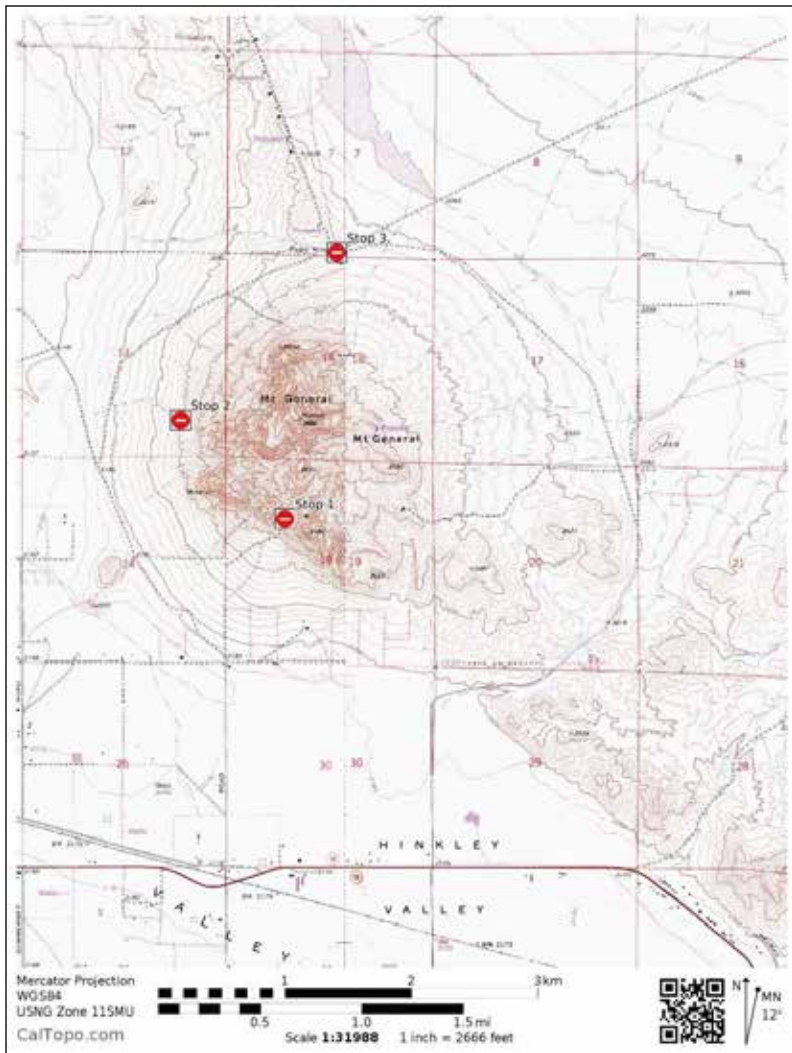
1.2 (0.2) Pass Acacia Road on left. Radio towers in Waterman Hills at 2.00 o'clock mark Stop 3-5.

2.0 (0.8) Acacia Road. Pavement ends, continue north past Coon Canyon road on left and houses on right.

2.2 (0.2) CAUTION—very big dip. Continue north on dirt road; pass branch road on left.

2.3 (0.1) TAKE THE LEFT FORK at the junction of 7146A; proceed north.





steeply tilted than in the northeast part, the opposite of dip variations predicted by models of syntectonic deposition. Stated differently, the Hinkley Hills lack evidence of syndepositional extensional tilting.

Walk up canyon about 100 m to observe a 15 m-wide conspicuously light-colored fault-bounded rhyodacite dike. Although fault-bounded here, chilled margins of this dike and other dikes in the area are common. The dikes cut the tilted Pickhandle strata at low but varied angles and mostly they dip 45°-65° to the NNE or N. If assumed to have been vertical initially, those tilts are less than those of nearby Pickhandle strata, suggesting some stratal tilting occurred before dike emplacement and some after. Several rhyodacite dikes in this area show conspicuously less alteration or internal brittle deformation than the dacite country rock, further indication of emplacement during protracted deformation. Here, the wash cuts across the dike near its southeast tip. The dike broadens northwestward to about 300 m within a distance of 800 m. This northwest broadening in the upper plate is analogous to northwest-striking rhyolite to dacite dikes in the lower plate that increase in number and width over the 8 km-long Hinkley Hills located southeast of Mt. General (Fig. 1). The lower-plate dikes comprise > 50% of the width of the Hinkley Hills where they pass northwestward

2.4 (0.1) TURN RIGHT (NE) on dirt track toward Mt. General.

2.8 (0.4) PARK at mouth of small canyon.

beneath the volcanic carapace of Mt General. This northwest-increasing abundance and width of dikes

STOP 1: Rhyodacite dike

New mapping by Onderdonk of the upper-plate rocks of Mount General reveals some of its internal structure that includes tilted early Miocene Pickhandle strata cut by dikes. The Pickhandle rocks at this stop are dark brown grungy-looking autobrecciated dacite cut by abundant fractures and small faults, locally rebrecciated and healed (or partially replaced) by ferroan carbonate, and cut by barite veins many of which are fractured or brecciated. The attitude of these rocks is not known, but nearby Pickhandle strata strike NW and have moderate to vertical dips to the SW. Actually, Pickhandle strata in this part of Mount General are more

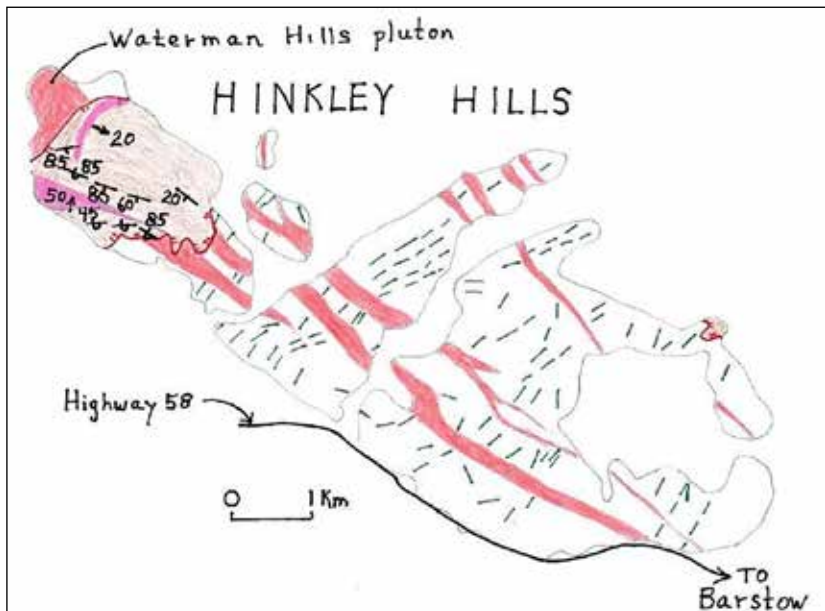


Figure 1. Hinkley Hills showing NE structural grain cut by NW dikes

reflects not only an increase in extensional spreading but also an increase in magma fertility along the length of the Hinkley Hills. If additional mapping shows that the 500+ m-thick pile of volcanic flows that make up the north part of Mt. General rest unconformably on tilted Pickhandle strata, the magma fertility argument might be extended to post Pickhandle time.

Walk up wash an additional 150 m to observe brecciated granite in the wash. The granite is overlain by a distinctive dacite flow with angular dark inclusions and, along one part of the contact, is separated from the dacite by a bed of sedimentary (?) breccia containing angular clasts of coarse grained marble. We interpret the granite as a landslide mass within the Pickhandle Formation; the area from which it was sourced is not known.

Return to vehicles. Retrace SW to Dixie Road and its junction with Thompson Road

3.1 (0.3) Dixie Road (BLM 7146A) junction with Thompson Road (BLM 7146). TURN SHARP RIGHT then LEFT and proceed west on Thompson Road. Low hill to west is an unaltered dacite flow unlike the autobreccia at Stop 1. Also, at 3:00 o'clock, is a view of contact between rhyodacite dike of Stop 1 (forms top of hill) and altered bleached overturned volcanic rocks of the Pickhandle Formation low on slope. Contact is about 1/3 the way up slope and dips about 50° into the hill. The dike is as much as 300 m wide as opposed to its 15 m width at Stop #1.

3.5 (0.4) TURN RIGHT (NW) onto Coon Canyon Road (BLM 7144).

3.6 (0.1) East-west junction. Pass a NW diagonal road.

3.7 (0.1) Pass left turn (W) toward Mountain View Road.

4.0 (0.3) Fork, bear right (NNE)

4.1 (0.1) TURN RIGHT (E) toward Mt. General.

4.6 (0.5) PARK at mouth of wash.

STOP 2: Closest exposure of the Waterman Hills Detachment Fault to the inferred breakaway of the fault

Walk up wash about 200m to observe an exposure of the WHDF. At the west base of Mt. General, this is the closest exposure of the WHDF to the previously published breakaway fault presumed as buried beneath the basin fill of the broad Hinkley Valley between here and Iron Mountain. We wish to compare the fault rocks here with those about 15 km down dip at **Stop 7**. The exposed fault here dips about 20° northeast and separates a thin layer of upper-plate conglomerate lacking volcanic clasts from a heterolithic assemblage of plutonic rocks including diorite, granite, and felsic dikes in the lower plate. The upper-plate conglomerate is overlain by an estimated 500 m of gently NE-dipping rhyodacitic and dacitic volcanic rocks of possible post-Pickhandle age. The WHDF is marked by a thin (ca 2 m) wedge of yellowish

gray breccia and microbreccia. Based on thin-section study, the rock contains domains of chloritic alteration with crenulate to cusped borders indicating invasive syn- and post-brecciation alteration. The light color results from simultaneous fracturing and fracture-controlled leaching of mafic components resulting in an end-member mottled mix of quartz, alkali feldspar, and rare pyrite. The alteration assemblage includes late-stage calcite and amorphous silica. The protoliths for the altered microbreccia were lower-plate crystalline rocks. The rock lacks an internal detachment-parallel shear fabric, but the upper-most polished surface is decorated by faint northeast-oriented striations. The lack of a shear fabric internal to the rock may suggest that, at the time of faulting, the material behaved much like slurry incapable of *shear*???? The WHDF is equally unspectacular in the east part of Mount General where, at one locality, it is marked by about 20 cm of breccia and no gouge or other rock with a shear fabric.

In the 5- to 10-meter interval directly below the WHDF here at Stop 2, blocks of pale yellowish gray felsic rock are down-set into the plutonic rocks on curved high-angle faults that result in wedging out of the blocks to the south. At first, these light-colored rocks were thought to be fault rocks related to the WHDF excised into the lower plate. If correct, they could possibly explain the unspectacular aspect of the overlying fault rocks. But study of thin sections and sawn surfaces on a 30 cm oriented billet cut from one of the blocks reveals sparse (< 1%) phenocrysts of quartz and alkali feldspar and a steeply dipping faint color layering (Fig. 2) suggesting the rocks are felsic dikes. We interpret the fault-bounded southerly wedging of these blocks as indicating a structural shoulder in the WHDF.

Return to vehicles, RETRACE west to junction and continue west to Coon Canyon Road.

5.3 (0.7) TURN RIGHT (NNW) on Coon Canyon Road (BLM 7144)

5.8 (0.5) Continue NW at a small playa.

6.1 (0.3) Cross another small playa.

6.2 (0.1) TURN RIGHT (NE) at fork.

6.4 (0.2) TURN RIGHT (E) on Mount General Road. The microwave towers of the Waterman Hills, our stop 3-5, are due east.

6.9 (0.5) View SE at 3:00 o'clock, greenish gray colors low in Mount General are chloritized lower-plate crystalline rocks and those high in slope are upper-plate hydrothermally altered volcanic rocks.

7.9 (1.0) TURN LEFT (north) at Pedry Mine. The Pedry Mine includes explorations along an amazingly long vein that extends 2.3 miles northwesterly from Mt. General. Chalcedony box work indicates that sulfides have been dissolved and precipitated down dip at the water table.

Cavities in box work are often filled with barite (Housley and Reynolds, 2002). Two roads bear north; use the westerly route. Drive north.

8.0 (0.1) STOP at mound of stones.

STOP 3: Textural variations in the Waterman Hills pluton, Pedry mine

The Pedry Mine consists of two shafts separated by about 1.6 km of a 340°-trending low topographic ridge along which there are more than 40 shallow prospect pits into a steep fault zone marked by vuggy quartz (see description below). Walk west along a shallow trench and observe compositional contrasts in mostly fine-grained and locally porphyritic and locally mylonitic plutonic rocks. Although exposures are poor, traverses across this part of the ridge show that it is formed on northwest-trending dike-like masses that are conspicuously more crystalline than the dikes that disappear under the southeast margin of Mount General. Get back into vehicles and drive along the ridge crest about 0.6 miles and stop just before the track descends into a shallow wash transverse to the ridge. Walk transverse to the ridge in both directions and note that most of the compositionally variable plutonic rocks are medium grained granitoids, conspicuously more coarsely crystalline than those at the south end of the ridge. Although these rocks were previously mapped as the WHP, our suggestion that they are genetically linked, via serial gradations from shallow to deep, to the dikes in the SE part of the Hinkley Hills reflects a new interpretation that deserves additional detailed study because temporal relations are sketchy at best. Our thesis is that 1) along the entire length of the Hinkley Hills there exists a northwest progression of increasing early Miocene plutonic fertility coupled to increasing dilatant spreading and 2) with respect to the exposed intrusive rocks, the entire structural block is slightly tilted to the SE. Dikes in the southern and central Hinkley Hills are not mylonitized whereas in the north part, some dikes are mylonitized and some are not, possibly indicating that protracted dike emplacement in the most fertile part of the plutonic system resulted in a protracted period of thermal disturbance during which mylonitization of early dikes occurred.

Previous studies (Fletcher and others, 1995) of lower-plate pre-Tertiary plutonic and metasedimentary rocks in the central part of Hinkley Hills led to a model of major uplift, southwest tilting, and extension-related shear prolongation of the brittle-ductile transition between the Hinkley Hills and Mitchel Range structural blocks. That model was mostly based on the premise that pre-Tertiary steep layering and foliation in the lower plate in the



Figure 2 Flow layered felsite

Hinkley Hills was transposed via shear into parallelism with the WHDF and that the WHDF has been removed by erosion from a former presence directly above the existing landscape. Studies by Anderson failed to corroborate the transposition part of that model (report submitted for publication).

Description of Pedry Mine, excerpted from MinDat (<https://www.mindat.org/loc-89236.html>):

A former Pb-Cu-Ag-Zn occurrence/mine operated by the Golden Witch Mining Company, California (1952). Mineralization is a vein deposit hosted in volcanic rock (aphanitic), quartz latite, granite, and granitic gneiss. The ore body strikes NW and dips 70E at a thickness of 3.05 meters and a length of 1,609.34 meters. The country rock is poorly exposed, appears to be felsite and quartz latite on the southern claim, granite and granite gneiss on the northern claim. The vein at surface is brecciated and contains fragments of wallrock and is heavily iron-stained. Local rocks include Quaternary alluvium and marine deposits. Workings include surface and underground openings with an overall depth of 82.3 meters and comprised of 2 shafts ¼ mile apart, both inclined 70SE. The N shaft is 200 feet deep with short drifts at different levels. The S shaft is 270 feet deep with 5 levels, drifts on the levels, none larger than 30 feet. A crosscut on the 100 foot level was driven W. There are also 45 prospect pits and shallow shafts between the 2 main shafts.

Drive south 0.1 mile to Mt. General Road.

8.1 (0.1) TURN LEFT onto Mt. General Road that leads straight at 060° toward the Waterman Hills.

8.3 (0.2) Radio towers at 1:00 o'clock mark location of Stop 3-5.

8.4 (0.1) Watch for dips.

8.6 (0.2) Pass a junction on the right. Cross a playa.

9.1 (0.5) Dip.

9.88 (0.7) Dip.

9.9 (0.1) Dips ahead.

10.6 (0.7) TURN RIGHT onto powerline road HL 7140.

10.8 (0.2) Powerline bears left (E) toward Waterman Hills.

11.8 (1.0) Powerline ascends Waterman Hills. Slow through curves.

12.4 (0.6) Road forks. Stay right on 7140.

13.2 (0.8) **PASS** left turn (N).

13.5 (0.3) Second road to northern crest of Waterman Hills.

TURN LEFT (N) and bear easterly around tower #1413 (SE leg). From powerline road, follow dirt track that ascends the crest of Waterman Hills.

14.5 (1.0) STOP in open area with a complex of roads.

15.0 (0.5) Road forks at Tower 1413. Take the right (S) fork.

15.18 (0.1) TURN LEFT (E) on main powerline road 7140 toward Old Irwin Road.

16.8 (1.7) Not visible from road, but one tenth mile north of powerline are exposures of folded fine-grained lacustrine beds that probably belong to the Barstow Formation. Although exposures are poor, the beds strike NE and decrease in dip from 65° to 25° in a NW to SE direction. Small SE-plunging parasitic folds trend NW-SE. This style of major folding, but opposite in sense, is present at **Stop 3-6**.

16.9 (0.1) Slow as road bears right.

17.1 (0.2) Stop at paved Old Irwin Road. Look both directions for oncoming traffic. TURN RIGHT (SW) onto paved Irwin Road.

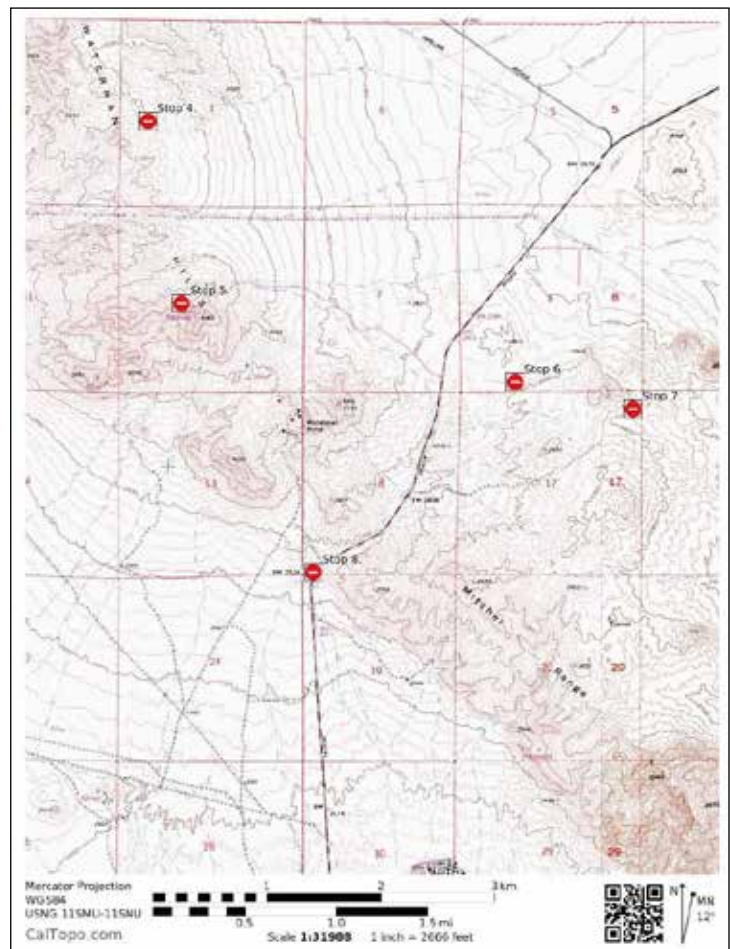
18.1 (1.0) TURN RIGHT (W) onto graded road 7166 that leads to radio towers.

18.3 (0.2) The red coloration on left (south) is formed on a breccia zone that probably marks a WNW-striking fault separating lower-plate crystalline rocks beneath the mantle on which the road is formed from dacite and rhyodacite rocks similar to those seen at Stop 1 (including widespread fracturing, brecciation, carbonate

STOP 4: Lithologic variation and dike-like accretion of the WHP

Walk to SW or NE (or both) and observe compositional and textural differences in the WHP, including mylonitic fabrics. The rocks are essentially all granitoids but range from fine to coarse crystalline and from leucocratic to melanocratic. Much like at Stop 3, the varied rock types form NW-trending dike-like bodies that record growth of the WHP by magmatic accretion, an aspect that is clearly visible on Google imagery. The dike-like aspect and the mylonitic fabrics fade along strike to the NW where the pluton is conspicuously more massive and presumably emplaced at a greater depth. The intensity of mylonitization increases to the SE toward the shallower levels in the pluton, the WHDF, and the overlying volcanic carapace on which the radio towers sit. Here, at Stop 4, mylonitic fabrics are irregularly developed. Over distances of several meters, strong dike-parallel contrasts in mylonitic development have been observed, and we have no explanation for the variations (a research opportunity?). As in the Hinkley Hills, the large-scale SE-to-NW variations suggest tilting of the pluton to the SE.

Return to vehicles and drive south to powerline road (the second powerline).



cementation, and abundant broken and disrupted barite veins). The red color marking the fault (?) results from ferroan carbonate cement in the breccia, but the zone appears to lack a shear fabric. The slopes above are pockmarked with dozens of prospect pits and Anderson's hammer is up there somewhere. The volcanic rocks are mapped as Pickhandle Formation and appear to rest depositionally on crystalline rocks. At one location, a layer of highly fractured gray limestone separates the two rocks. This may be the depositional base of a 3-km-thick section of tilted Pickhandle strata.

18.7 (0.4) Mud Hills at 3:00 o'clock.

19.0 (0.3) Dark andesite flow forms a jagged skyline on a WNW-trending ridge at 9:00 o'clock. The andesite is flanked on south and north by Pickhandle sedimentary rocks with steep to steeply overturned attitudes; all forming the steep north limb of the Waterman Mine syncline.

19.5 (0.5) Roadcuts are formed on strongly mylonitized rocks of the WHP.

19.6 (0.1) Auxiliary parking to the right.

19.7 (0.1) PARK at hilltop north of microwave stations. NOTE: Space for about seven vehicles.

STOP 5: Radio Tower Hill and the WHDF

This spectacular geomorphic feature is called the Waterman Window (WW) because erosion has cut through upper plate early Miocene rhyolite and the WHDF to expose the WHP in a lower-plate window. The following description is top down: upper plate, WHDF, and lower plate.

Upper plate

The upper plate consists of potassium metasomatized rhyolite that has been mapped as intrusive. The rhyolite is thoroughly brecciated. In the headwall of the window, the breccia is cut by steep normal faults that terminate downward at the WHDF rather than curve tangentially into it. The breccia bodies bounded by these steep faults range to several meters thick, have relatively uniform fragment size and/or color, and have shallow dipping contacts defined by a sharp decrease in clast size. The base is the WHDF. At the distant part of the headwall, note the reddish breccia is displaced downward *onto* the WHDF. Similar smaller breccia bodies are exposed in the road cut directly below the transmission towers where they are also bounded by gently dipping zones of finer breccia and cut by steep normal faults. The boundaries of the breccia bodies do not appear to be integrated into a braided shear pattern. Also, at the base of several of those breccia bodies are sag-like depressions with internal stratification of clast size and alteration products. Anderson interprets these features as dissolution seams. The relative importance

of dissolution and collapse vs. detachment-related shear in these breccias is a subject for discussion as are 1) was detachment-parallel shear restricted to the gouge zone? and 2) does the apparent absence of veining and cyclic healing and rebrecciation in these breccias serve as a major impediment to consideration of the crack/seal process as responsible for detachment faulting?

Detachment fault

The WHDF here dips south about 20° and is marked by about 20 cm of clay gouge flanked by a similar thickness of clayey breccia. Two layers of clay gouge are recognized. Analysis of clay fractions in 5 samples representing 20 cm of scaly gouge show the lower part as smectite-dominated illite-bearing and the upper part the opposite; illite-dominated smectite bearing. Delta-D and delta-¹⁸O data from the gouges suggest crystallization in equilibrium with meteoric fluids at temperatures < 100° C. Shear patterns in the gouge show N-S kinematics at 4 separate localities in the WW, an orientation that is about 45° counterclockwise of the regional extension direction. Thus, the final stage of movement on the WHDF in this area has N-S kinematics in a relatively cool and shallow setting. These observations force the question, "where is the evidence for major NE-directed tectonic transport?"

Lower plate

The lower plate here consists of mylonitized and chloritized lithologically heterogeneous porphyritic granodiorite and diorite dikes, late magmatic quartz-albite aplites and pegmatites and non-mylonitic sub-volcanic phenocrystic quartz latite. We interpret the heterogeneous assemblage as the upper part of the early Miocene WHP. As already noted, deeper non-mylonitic more coarsely crystalline and monolithic parts are exposed in the northwest part of the Waterman Hills. Two aspects of these rocks in the WW are obvious: 1) an upward lightening and 2) a light gray/dark gray streaking in the uppermost part, especially visible in the headwall area.

Upward lightening—Much of the upward lightening results from strong leaching and bleaching by fluid circulation. We documented these effects by whole-rock geochemical analysis of 5 samples from a 30 m vertical section from the west wall of the window and 2 samples from the extreme south margin. Although we could not verify a uniform original composition of these rocks, 5 of them were likely granodioritic. At both sites, the analyses reveal strong upward depletions in K₂O, CaO, Rb, and Zr, increase in Na₂O, and moderate increase in SiO₂. The percentage range for K₂O depletion is 2.55-0.47 and for CaO it is 2.09-0.31. Glazner and Bartley (1991) reported compositional changes over much larger areal dimensions, namely the 5 km length of exposures of the WHP in the Waterman Hills. They attributed the changes, which included strong silica depletion rather than increase, to gradients in the intensity of mylonitization. Their data

also indicate enrichments of some immobile elements two to six times those of non-mylonitized equivalents and they suggested the increases reflect residuals resulting from leaching. They noted that “strong silica depletion and significant mobility of normally immobile elements imply large fluid/rock ratios during mylonitization, possibly as a result of multiple-pass hydrothermal convection connecting near-surface and mid-crustal alteration regimes.”

They suggested fluid/rock ratios as high as 500 and temperatures during mylonitization of 300°- 400° C. The correlation with intensity of mylonitization is not applicable to the rocks in the WW because we detect no relationship of the compositional changes to the intensity of mylonitization and a small increase in silica, rather than a large decrease. The WHDF at the WW separates a zone of strong leaching of K from a zone of strong addition of K. We interpret the WW compositional shifts as resulting from thermally driven leaching by up-flow of fluids from the uppermost WHP and suggest the K metasomatism as well as carbonate cementation in the directly overlying rhyolite records related transposition of solutes. The up-flow likely predates formation of the clay gouge separating the zones because the gouge lacks evidence of inter-slip veining or lithification expected during extensive cross-flow of fluids. Also, clay-rich gouges typically have permeabilities on the order of a microdarcy to a nanodarcy (10^{-18} to 10^{-21}), suggesting that gouge formation and final N-S displacement post-dates the main episode of fluid movement across the fault.

Color streaking—The light- and dark-gray streaks on the steep upper 10 m below the WHDF appear, at first glance, to record detachment-parallel shear. On close inspection after removing the regolith with hand tools, the streaks mainly represent the eroded edges of the compositionally varied rocks in contact with one another by steep faults or intrusive contacts, not by detachment-parallel shear zones. The dominance of steep fractures directly beneath the WHDF is seen in areas to the east of the WW where exposures are excellent (Fig. 3). If the WHDF reflects extreme displacement, it occurred on the thin gouge. The pattern of steep fractures directly

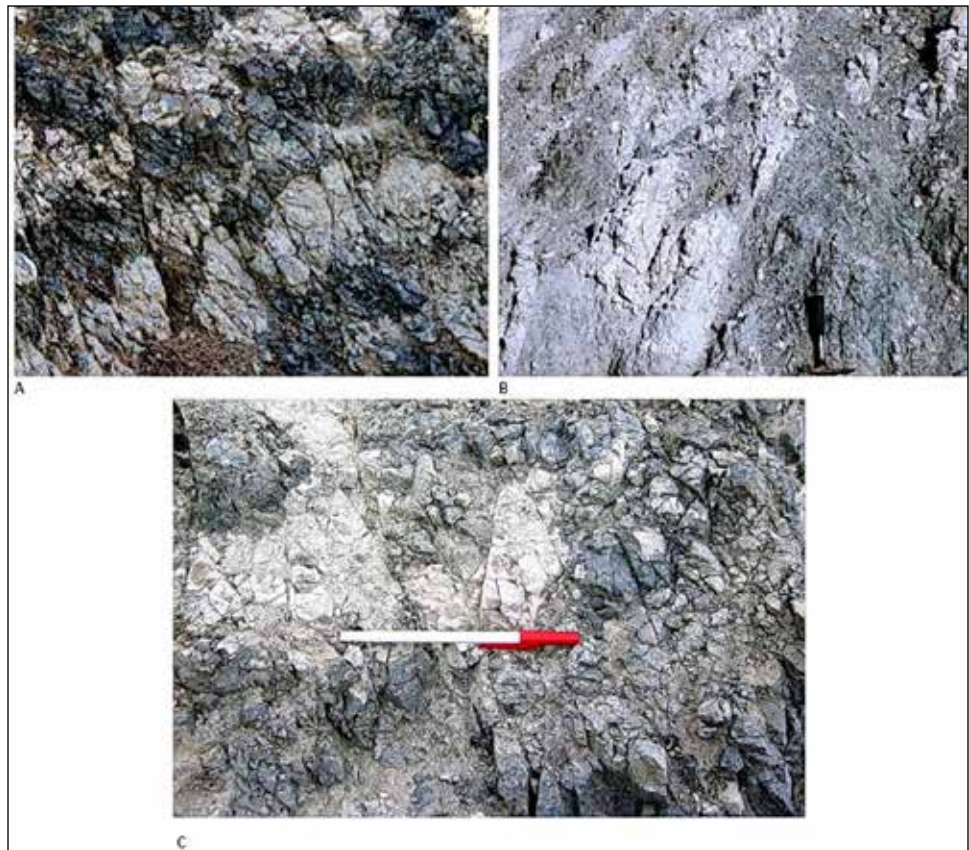


Figure 3. Steep fractures directly below WHDF.

beneath the gouge is more consistent with vertical collapse associated with extreme volume loss than with detachment-parallel shear.

Strain dilemma—L-tectonites in the SE part of the WHP are conspicuously more prominent than mylonitic foliation that, in most of the L-tectonites, is weak to undetectable. The paucity of foliation reflects a major departure from the ideal shear zone predicted by displacement of tens of kilometers on a deeply rooted detachment fault. Also, as noted by Glazner and Bartley (1991), large volume loss during mylonitization greatly complicates structural analysis of finite strain because it should result in flattening strain (foliation) rather than the non-coaxial stretching reflected in the L-tectonites. Based on compositional alterations, fault/fracture orientations, and ductile fabrics, there are major deficiencies in the large-magnitude detachment story in both ductile and brittle realms.

Return to the paved Irwin Road.

21.4 (1.7) **STOP, Look** for cross traffic. **NOTE tall berms** on east side of pavement. Use 4WD to cross berms. **Cross Irwin Road ONE VEHICLE AT A TIME!** Proceed east on dirt track (Open Route 7166) leading east toward the Mitchel Range.

21.6 (0.2) Road ascends onto cobble-strewn surface developed on exotic-clast conglomerate that

unconformably overlies fine-grained lacustrine beds that we suggest correlate with the Barstow Formation. The surface is formed on lag gravel and is mature in the sense that many of the boulder-size clasts are highly broken and disaggregated. Similar conglomerate rests on Peach Springs Tuff (18.8 Ma, PST) to the east where we suspect it is pre-Barstow (or part of the early Barstow Fm. such as Owl Conglomerate. The Barstow Fm. contains the PST at Daggett Ridge, and contains the Red Tuff – 19 Ma in the Mud Hills).

21.9 (0.3) Road passes onto pinkish surface developed on fine-grained lacustrine sediments of the Barstow Formation stratigraphically below the exotic-clast conglomerate. PARK at junction.

STOP 6: Folded Barstow Formation(?) beds, the WHDF, and young uplift of the Mitchel Range

- 1) In this area, the attitude of poorly exposed fine-grained lacustrine sedimentary rocks, possibly correlative with the Barstow Formation, has been determined by digging shallow pits. The beds dip away (NW) from the Mitchel Range, about 65° close to the range shallowing to 25° where they pass beneath the exotic-clast conglomerate noted above. This folding is similar in style but opposite in sense to that noted above at mile 1.7 following Stop 4. Folds at the two areas combine to suggest a NE-trending post-Barstow syncline along strike of the WMS, but with a shallow axis rather than a steep axis.
- 2) At this locality, a NE-oriented series of shallow prospect pits had been dug into a gently NW-dipping pyrite-bearing breccia/microbreccia layer about 20 cm thick. The layer truncates metamorphic fabrics in the range block that dip more steeply NW. Flinty microbreccia marks the WHDF at several localities on the flanks of the Mitchel Range, and we suggest its presence here represents a previously unmapped trace of the WHDF. No kinematic data were obtained from study of the breccia/microbreccia, but the NE strike is consistent with the fault serving as a right-lateral ramp in the WHDF. Although the rock lacks a shear fabric, weakly developed layering is defined by elongate clasts or trains of clasts, or by variations in clast abundance. Clasts consist of lower-plate crystalline rocks to 0.5 mm set in a microcrystalline chloritic matrix that could be either a microcataclasite or pseudotachylite.
- 3) Neither the Barstow beds nor the overlying conglomerate contain clastic debris derived from the directly adjacent Mitchel Range. The first appearance of locally derived angular clasts of chloritized mylonitic rocks is in a young range-margin debris apron. These lithostratigraphic relations indicating young range uplift are similar to those along the Harper Lake fault at the SW margin of the Mitchel Range, but there the

evidence for young range uplift is even stronger as noted at Stop 8.

Continue eastward on dirt Open Route 7166, keeping right.

22.0 (0.1) Ascend hill.

22.1 (0.1) Road crosses one of several NE-trending bands of steeply dipping white felsic porcelanite of controversial origin. These rocks have been mapped as mylonitized felsite dikes of probable Miocene age, but Anderson suspects they are Mesozoic and their NE orientation is part of the widespread steep structural fabric of the entire Mitchell Range.

22.2 (0.1) WHDF on left.

22.3 (0.1) Ridge exposed WHDF with red volcanics above.

22.4 (0.1) Prospect pit on left into recrystallized calcite (marble).

22.6 (0.2) TURN LEFT (E) off BLM 7166 onto dirt Bishop Road.

22.9 (0.3) PARK where track leads off to left just before conspicuous knob of volcanic rock.

STOP 7: The unspectacular WHDF, upper plate structure that is unresponsive of detachment faulting, and a possible new locality of exposed and anomalously extended 18.8 ma Peach Spring Tuff

- 1) Walk back to the main wash. A small patch of flinty microbreccia is exposed along the SW margin of the wash, and upper-plate rhyolite is exposed at both margins of the wash where it lacks fault-parallel shear fabric or multi-stage breccia. Faint striations are oriented NW-SE. Underlying crystalline rocks of the range core lack fault-parallel shear fabric or mylonitic lineations. Because this is the most “downstream” exposure of the WHDF (15 km from the inferred breakaway) the absence of more impressive strain features appears problematic. One could conclude that the only evidence here of a major fault is the thin microbreccia and that detachment faulting had a “thin film” attribute.
- 2) Walk about 200 m NNE and observe northwest-dipping bedding in strata of the Pickhandle Formation. The beds are cut normal to their strike by small-displacement dextral-slip faults. This pattern of strata striking toward, rather than dipping toward, the trace of the WHDF is seen along much of the NE flank of the Mitchel Range and is incompatible with strain expected in a NE-vergent extensional allochthon.
- 3) Continue walking (approx. 0.6 km) NE across varied volcanic and conglomeratic Pickhandle strata to a northwest-trending low ridge with conspicuous orange-gray color formed on tuff possibly correlative

with the 18.8 Ma Peach Spring Tuff. The tuff is repeated by SW-dipping normal faults and separated from the underlying brown volcanogenic sedimentary Pickhandle strata by a shear zone that is well exposed in an erosional undercut beneath the tuff. Note large number of striated small fault surfaces on the resistant tuff exposures showing that the tuff is internally extended. This exposure is anomalous in that 1. Unlike areas to the east, the Peach Spring tuff (?) is extended and 2. Extension is directed SW instead of NE.

- 4) The tuff here is overlain by exotic-clast conglomerate generally lacking in clasts of mylonitized rocks widely exposed in the directly adjacent Mitchel Range. Again, young range uplift is indicated. The conglomerate could correlate with the post-Barstow Formation conglomerate at Stop 6 or it could be older. It is deformed into a shallow open NW-trending fold.

Return to vehicles and retrace to stop 6 and the paved highway.

23.2 (0.3) TURN RIGHT (N) onto 7166

23.4 (0.2) Prospects with marble

23.6 (0.2) WHDF on right.

23.7 (0.1) Cross white felsic porceleanite dike.

23.9 (0.2) Pass STOP 6: FOLDED BARSTOW FORMATION with pinkish and pumpkin colored sediments

24.2 (0.3) Road descends from erosional surface developed on lacustrine sediments of the Barstow Formation.

24.4 (0.2) STOP, look both directions for cross traffic. **ONE AT A TIME** - vehicles Turn Left (S) onto Irwin Road and proceed south slowly through dangerous curves.

24.9 (0.5) SLOW, Curves ahead.

25.2 (0.3) SLOW, Irwin Road bears right (W). Look for traffic ahead and behind. We will turn right at the 2nd road ahead.

25.6 (0.4) Pass a right turn to Waterman Mine. SLOW.

25.7 (0.1) TURN RIGHT into highway maintenance area with gravel storage piles. PARK.

STOP 8: summary discussion, including young uplift of the Mitchel Range and possible young dextral-slip origin of the Waterman Mine Syncline

We will attempt to summarize the main points made by the trip leaders as well as contrasting opinions or interpretations offered by the participants.

If time permits, we will also discuss:

- 1) The age and origin of the highly anomalous, large, steep-axis Waterman Mine syncline formed in rocks

of the Pickhandle Formation in the SE part of the Waterman Hills directly NW of this stop.

- 2) Possible distributed dextral shear within the Mitchel Range, dextral bending along the Harper Lake fault at the margin of the Mitchel Range as depicted by Shelif and Oskin (2010) and elaborated on by us, and evidence for young uplift of the Mitchel Range.
- 3) The possible relationship between 1 and 2.

End of trip, return to stashed vehicles. Drive south on Irwin Road (Old Ft. Irwin Road) to Old Hwy 58. After stops, turn right (W) on Old Hwy 58 and proceed west to Lenwood Road. Hwy 58 to the south leads to Mojave and Bakersfield, and to I-15 heading south to San Bernardino and north to Las Vegas.

References cited

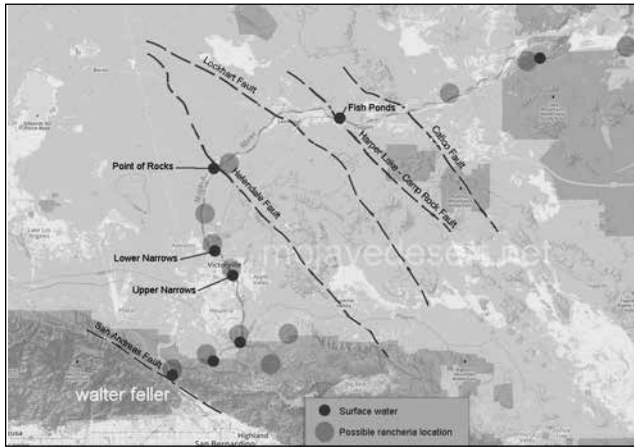
- Fletcher, J.M., Bartley, J.M., Martin, M.W., Glazner, A.F., and Walker, J.D., 1995, Large-magnitude continental extension: An example from the central Mojave metamorphic core complex: *Geological Society of America Bulletin*, v. 107, p. 1468-1483.
- Glazner, A.F., and Bartley, J.M., 1991, Volume loss, fluid flow and state of strain in extensional mylonites from the central Mojave Desert, California: *Journal of Structural Geology*, v. 13, p. 587-594.
- Housley, R.M., and Reynolds, R.E., 2002. Mineralogical survey of the Mount General area, *in* Reynolds, R.E., (ed), 2002. *Between the basins: exploring the western Mojave and southern Basin and Range Province*. California State University, Desert Studies Consortium: 61-63.
- Shelif, E., and Oskin, M., 2010, Deformation processes adjacent to active faults: Examples from eastern California: *Journal of Geophysical Research*, v. 115, B05308.

Broken River — Mojave River

Walter Feller
digital-desert.com

Rivers were made to be broken

The Piute Indians tell of a giant carrying large ollas brimming with water. He was so tall and his stride so long that his footsteps were a day apart. With each step the giant took he would rock from side to side, and each time he rocked water would generously spill into these empty footsteps becoming the oases and springs of the first trail through the desert.



The forces that created the Mojave Desert broke it separate and tilted opposite and inland from the ocean making a river that runs away from the sea and far into the desert. Water from the mountains and desert plains come together in the rocks and sand where it sinks below the surface disappearing into a broad, dry wash.



The constant shuffling of forces created faults and impermeable obstructions that dam the flow of this hidden river and bring water to the surface at points along its length resulting in perennial springs and waterholes. These verdant springs were thick with flora and fauna.

Wild game naturally wore trails from one place to another.



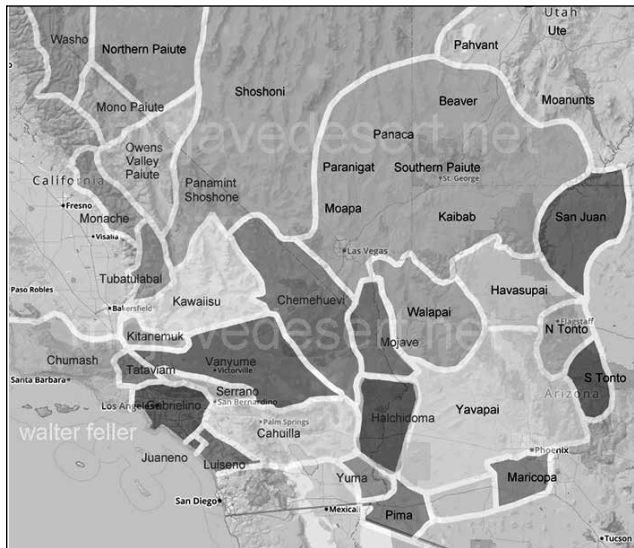
Spring near Point of Rocks

Indigenous people came and lived in small groups near these water sources. Game trails developed into subsistence loops and from these found trails leading to chains of springs bisecting the heart of the desert. Generally spaced one day's walking distance from each other these oases and seeps made it possible for man to cross the desert on foot without being overburdened by carrying water.



Mojave Indian Trail

The Mojave Indians living on the Colorado River used these trails to cross the Mojave to trade and communicate with their cousins, the Chumash, on the Pacific coast. Spring by spring they could walk across the center of the Mojave in as many days.



It was the same with trade trails to and from Utah in the northeast and connecting with the Mojave River trails. In the Indian mind these trails had always been there—they had been made by the “Old Ones,” the people who came before.



Explorers and traders (Garces 1776, and Smith 1826 & 1827) were guided along this ancient network of footpaths when coming from the Colorado River near Needles, California to Paiute Creek, to Rock Springs, Marl and



Soda Springs connecting to the Mojave River east of Afton Canyon.

Antonio Armijo and William Wolfskill had found more springs on trails between the Mojave River and north to Salt Lake in Utah. These springs were the niches where horse thieves could water hundreds, and even thousands of the Spanish horses stolen from the southern California ranchos and put on the run to New Mexico. By persistent use of the trade caravans this route became known as the Spanish Trail. Fremont and Kit Carson surveyed and mapped these mule trails in 1844. It was in 1849 when Jefferson Hunt led the first wagon train of



pioneers across the Mojave on this same trail and the Spanish Trail became the Mormon Wagon Road. It was in 1857 E.F. Beale and his Camel Corps developed the Mojave Indian Trail traversing the Mojave directly



through the center into a wagon road that we now call the Mojave Road.

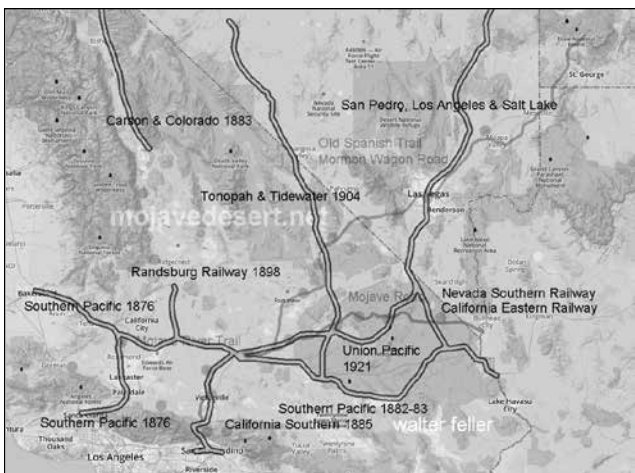
The springs were the basis for way stations, outposts and redoubts. With the increase in traffic the trails swayed and split apart joining again in a few miles or past a few valleys or ranges in order to accommodate the changing conditions of nature.

As people were moving through the west pressure was put on the desert Indians. The Indians, possibly in frustration and/or desperation began to harass travelers, steal cattle and of course, attack and kill a person or two.



Bitter Spring

Although the Indians were not always the aggressor the military moved in protecting the mail and traffic along the Mojave Road while denying water to local Indians. The main problem with the army coming in to punish the Indians for misdeeds is that the Indians had no idea why they were being punished. The local Chemehuevi and Vanyume did not live in large tribal groups but rather in extended family situations that were on the move as they hunted and gathered in their seasonal patterns. Travel on these trails turned crude roads increased and conflicts decreased as native populations disappeared. Railroads came through requiring gentle grades and sweeping curves therefore avoiding abrupt changes in elevations and adding an alternative alignment with gradual slopes. Wells, to supply water for the trains, were



dug and developed. Small communities began to appear along these water stops and road junctions. Most freight crossed the Mojave by rail. Travel by rail was preferred and elaborate depots were built to provide first class lodging and meals at key locations.



Kelso Depot

In the early 1880s the Southern Pacific built the first railway through the desert connecting Needles to the town of Mojave in a corridor south of but parallel to the Mojave Road extending due west at Barstow rather than following the river south to the Cajon Pass. However, several years later a connection was made between Barstow and a new railway that paralleled the river to the Upper Narrows then to the Cajon summit and down the pass to Colton near San Bernardino.



It was in 1905 when San Pedro, Los Angeles and Salt Lake Railroad built their Salt Lake route also to the south of the Old Spanish Trail but connecting at the same point as the Mojave Road at the eastern end of the Mojave River at Afton Canyon.

In 1913 the few roads there were were not much more than a couple ruts made from driving on the old wagon trails. Motor travel was becoming popular but the desert roads were horrible. Some parts of the roads were oiled and some parts were poorly paved, but most of it was



rough and ungraded with long, sandy stretches through wilderness. By 1920, as automobiles became affordable and commonly used the age of the horse and wagon was pretty much over. By motor it took 3 days to cross the desert from San Bernardino to Needles at the Colorado River by way of the National Old Trails Road.



was moved to a route from east of Barstow through Silver Lake following along in the same general corridor as the Old Spanish Trail. In 1925 the realigned Arrowhead Trail through Baker paved in 1932 and became U.S. Hwy 91. In 1958 the interstate highways were introduced. These freeways were built to be faster, more efficient, and less reliant on stops for water, food or fuel. Highway design became streamlined and reflective of high speed and non-stop travel. The old two lane highways along the river were nearly abandoned with the exception of local and secondary use. Through all of these changes and advancements, in 1970 two basic alignments persisted and became our streamlined I-15 (Old Spanish Trail corridor) and I-40 freeways. (1970)



In 1926, once the National Old Trails Road was paved across the Mojave, and with some variations and realignments it became designated as U.S. Route 66 across the southern corridor.

When the Silver Lake Cutoff was graded in 1922 the junction for the Arrowhead Trail north from Needles



Rather than perilous crossings demanding weeks of hardship and slow, primitive travel, moving across the Mojave Desert has become an enjoyable air-conditioned experience of only hours, passed in luxury and comfort with beautiful scenery--All born from the trails between the fractured pieces of our Broken River.

Fishing for fossils along the course of the Mojave River

Robert E. Reynolds

CSU Desert Studies Research Associate, Redlands, CA 92373, bob.reynolds220@gmail.com

Introduction

Latest Pleistocene vertebrate and molluscan taxa recovered along the Mojave River provide data on aquatic habitats and suggest the strength and course of water flow during the Wisconsinan glaciation. The Mojave River has its headwaters in the San Bernardino Mountains and flows northward and eastward into the Mojave Desert. Today, much of the flow is subsurface, but during the Pleistocene the river carried abundant water that collected in basins and formed lakes in today's Harper, Coyote Lake, Afton, Soda and Silver Lake basins. Fossils collected during paleontological and archaeological investigations offer insights into the courses and meanders of the Pleistocene Mojave River.

Habitat data for selected taxa

Ostracoda

Cyprinotus (Heterocypris) incongruens—adapted to a wide range of environmental conditions

Limnocythere ceriotuberosa—moderately alkaline lakes

Limnocythere bradburyi—shallow, turbid and warm lakes

Limnocythere platyforma—shallow, cold freshwater lakes

Limnocythere robusta—shallow, warm freshwater lakes

Pelocypris alatobulbosa—shallow small or large water bodies with moderate salinity

Ostracode summary. Ostracode genera can be very tolerant of a wide variety of temperatures and salinity. However, specific taxa require a narrow range of conditions and can be helpful with interpretation of habitat. Certain species of *Limnocythere* that prefer warm or cold lakes suggest fluctuations in regional climate (Steinmetz, 1989).

Gastropoda

Planorbidae

Helisoma (Carinifex) newberryi—well-oxygenated, cold, clear, slowly flowing water, soft substrate

Fossaria modicella—shallow ponds, streams, with vegetation

Gyraulus sp.—flowing or quiet streams or temporary ponds

Helisoma (Planorbella) ammon—well-oxygenated, slowly flowing water

Planorbella subcrenata—perennial-water supporting rooted vegetation, muddy substrate

Planorbella sp.? *P. tenuis*—freshwater aquatic pulmonate, algae grazer

Conispiral

Valvata humeralis—in vegetation of cold lakes, marshes, slow streams, mud substrates

Vorticifex effuse—cool perennial-water with rooted vegetation and muddy substrate

Physa sp.—perennial or seasonal shallow flowing or still water

Gastropod summary. Most gastropods inhabit cool, well-oxygenated fresh water (Moore and others, 1952).

Pelecypoda

Anodonta californiensis—common fresh water mussel found in lakes with moving water, slow-moving streams with sand substrates, (Moore and others, 1952; Schneider 1989, 1994).

Pisidium compressum—perennial bodies of water with current action. *P. casertanum*, found extant on the Mojave River, lives in slow moving water and patches of marsh (Taylor, 1960).

Pelecypod summary. Pelecypod taxa from the Pleistocene Mojave River inhabited fresh, moving water.

Osteichthyes

Siphateles bicolor (formerly *Gila bicolor*)—a cyprinid fish that prefers abundant fresh, cool water with some current movement (Page and Burr, 2011). Occurs today in isolated populations along the Mojave River and in Death Valley.

Gasterosteus aculeatus— threespine stickleback live in fresh, brackish, or salt water. Prefers slow-flowing water with areas of emergent vegetation. Sticklebacks are weak swimmers, and freshwater sticklebacks rarely ascend high-gradient streams (Bell, 1994; Moyle, 2002; Bell and Reynolds, 2010).

Bony fish summary. Stickleback fish can live in slow moving, brackish water. In contrast, *Siphateles* sp. prefers cool, fresh water with current.

Amphibians

Toads require temporary ponds or slow-moving streams for breeding (Stebbins, 1972). Treefrogs (*Hyla regilla*) along the Mojave River today frequent cattail marshes (Stebbins, 1972).

Anurans: (Bufonidea, Pelobatidae, Ranidae)

Scaphiopus sp.—spadefoot toad

Anaxyrus punctatus—red-spotted toad

Amphibian Summary. Toads and frogs require fresh water for breeding.

Reptiles

Actinemys pallida— the western pond turtle, formerly considered a single species (*Clemmys marmorata*), is now recognized as two: the northwestern (*Actinemys marmorata*) and southwestern (*A. pallida*) pond turtles, the latter found in isolated populations along the Mojave River and the coast of southern California. Pond turtles are associated with permanent or nearly permanent water. Turtles leave the water to bask or, in the case of females, to move overland no more than 100 m (330 ft) to find suitable sites to lay eggs (Stebbins, 1972; Nussbaum and others, 1983).

Reptile summary. Turtles can cross short distances of dry land but must stay close to water for breeding purposes.

Water birds from Pleistocene Mojave River sediments (Jefferson, 2017)

Pelecanus sp. aff. *P. erythrorhynchos*—white pelican

Phalacrocorax auritus—double-crested cormorant

P. macropus —cormorant

Phoenicopterus minutus—small flamingo

P. copei—Cope's flamingo

Gavia sp. cf. *G. pacifica*—loon

Podiceps sp. cf. *P. nigricollis*—eared grebe

Aechmophorus occidentalis—western grebe

Cygnus sp. cf. *C. columbianus*—tundra swan

Branta canadensis—Canada goose

Anas platyrhynchos —mallard

Aythya valisineria—canvasback

Anas sp. cf. *A. platyrhynchos*—mallard

A. sp. cf. *A. crecca*—teal

Aythya sp. —redhead

Mergus sp. cf. *M. merganser*— merganser

Oxyura jamaicensis—ruddy duck

Fulica sp. cf. *F. americana*—American coot

Grus sp.—crane

Ciconia maltha—La Brea stork

cf. *Actitis* sp. —sandpiper

Phalaropodinae—phalarope

Larus sp. cf. *L. oregonus*—Oregon gull

Larus sp.—gull!

Combined aquatic fauna from Pleistocene Mojave River sediments.

Cyprinotus incongruens—wide range of conditions

Limnocythere ceriotuberosa—moderately alkaline lakes

Limnocythere bradburyi —shallow, warm lakes

Limnocythere platyforma—shallow, cold freshwater lakes

Limnocythere robusta—shallow, warm freshwater lakes

Pelocypris alatobulbosa —water bodies with moderate salinity

Gyraulus sp.—still or flowing water

Physa sp. —still or flowing water

Anodonta californiensis—permanent flowing water

Pisidium sp.—permanent flowing water

Siphateles bicolor—permanent flowing water

Gasterosteus aculeatus—permanent water

Scaphiopus sp.—needs water to breed

Anaxyrus punctatus—needs water to breed

Actinemys pallida —permanent water, short travel across dry land

Pelecanus sp.—dependent on fish

Phalacrocorax sp.—dependent on small fish and crustaceans (crayfish).

Phoenicopterus sp.—ingests copepods, polychaetes, foraminifera, amphipods

Gavia sp.—eats fish, amphibians, crayfish

Podiceps sp.—depends on fish, freshwater insects, crustaceans

Aechmophorus sp.—depends on fish, freshwater insects, crustaceans

Cygnus sp.—vegetable matter, associated fish, mollusks, crustaceans, insects

Branta canadensis—eats variety of grasses and grains

Anas platyrhynchos—eats grasses, seeds, occasional insects, crustaceans

Anas crecca—eats pond grasses, grain, seeds, occasional insects, gastropods

Aythya sp.—eats pondweeds, grasses, grain, seeds

Mergus merganser—depend on fish, also amphibians, mussels, shrimp, rarely plants

Oxyura jamaicensis—filters aquatic insects, mollusks, seeds, roots from pond silts

Fulica americana —eats plant material, seeds, algae, insects, crustaceans, mollusks.

Grus sp.—eats grain, seeds, insects, small birds, reptiles, amphibians.

Ciconia maltha—eats fish, crustaceans, amphibians, and reptiles, birds, mammals

Actitis sp.—probes mud and sand for crustaceans, mollusks, insects

Phalaropodinae—pecks water for crustaceans, mollusks, insects, and small fish

Larus sp.—feeds on fish, crustaceans, polychaetes, amphipods.

Habitat Summary and Discussion

Ostracods, gastropods, and pelecypods from Pleistocene Mojave River sediments inhabit cool or warm flowing water. Selected taxa can live in brackish or moderately saline or alkaline lakes. The two taxa of fish present require permanent water. Amphibians and turtles must stay near water to breed.

Avifauna exhibit a variety of habitat constraints. Pelicans, cormorants, gulls, merganser, loons, grebes and storks eat fish from large water bodies, along with reptiles, birds, and small mammals. Geese, many ducks, coots, and cranes eat pond grasses, grain, seeds, occasional insects, and gastropods. Phalarope and sandpipers probe wet mud for crustaceans, mollusks, insects, and small fish. Flamingos and ruddy ducks filter-feed for copepods, polychaetes, foraminifera, amphipods. Flamingos rarely inhabit areas of fresh water, preferring shallow saline lagoons, salt pans, estuaries, and large saline or alkaline lakes.

Fossil localities

Pleistocene localities with fossil fauna discussed herein are located along axial valley drainages, and are presented from the northeast, north of Baker, California, through Lake Manix, Lake Coyote, Daggett and Yermo, and southwest to Harper Valley and Hawes, northeast of Victorville, California.

SALT SPRINGS is located 27 miles north of Baker, at the junction of drainages that originated in Red Pass, Kingston Wash, or possibly as overflow from the “terminal” Mojave River at Silver Lake (Wells and others, 2003; Bright and Anderson, 2007; see STOP 1-1, Miller and others, 2017). Bright and Anderson (2007) have “reinterpreted the ostracode-bearing sediment at Salt Spring as representing local groundwater-supported, high Calc/alkalic wetlands. The presence of the Mojave River in the basin is not contested, as it logically must have flowed through the basin when the sill at Silver Lake (Lake Mojave) was breached.”

In support of occasional Mojave River flow through Salt Springs basin, a semi-articulated *Actinemys* sp. was found (Jefferson, 2017; R. Reynolds, pers. obsv. 2004) within sediments that contained no associated human cultural materials. The sediments also include Pleistocene mammals (mammoth, camel; SBCM 1-67-1, 1-67-3). Focused foot surveys for fossil fauna to the west from the playa east of Red Pass (Reynolds, 1990) or Red Pass drainages, or to the east from Kingston Wash have not produced records of *Actinemys pallida* (Reynolds, pers. obsv. 1995), reinforcing the source of the pond turtle as being from the Mojave River at Silver Lake. Although pond turtles can move short distances (100 m) across dry land, it is difficult to see how this articulated specimen could have traveled 14 miles from Silver Lake to Salt Springs without following wetlands and rivulets from Silver Lake, where Pleistocene lake waters supported

Gyraulus sp., *Physa* sp., *Anodonta* sp. and *Siphateles bicolor* (Orr and Warren, 1971; Reynolds, 2004).

Fossil duck remains found at Salt Spring suggest the presence of reed-choked ponds. The presence of cormorant supports the sporadic Mojave River flow scenario (Bright and Anderson, 2007) because cormorants feed on fish living in open fresh water.

Salt Springs: SBCM 1.67.1, 1.67.3

Age: Rancholabrean, about 30 ka (Jefferson, 2017)

Aquatic taxa:

Actinemys pallida
Phalacrocorax auritus
Anas platyrhynchos
Aythya valisineria
Fulica sp. cf. *F. americana*

SILVER LAKE, nine miles north of Baker, has been proposed as a terminal lake of the Mojave River (Miller and others, 2017, p. 10, Stop 1-1). The north end of the playa has produced fossils of mollusks and fish that require permanent flowing water.

Silver Lake: SBCM, RPLI: SBCM 1-65-1, -2, -3, -4, -7, -8, -9

Age: Rancholabrean (Jefferson, 2018, _Enzel and others, 2003)

Aquatic taxa:

Limnocythere ceriotuberosa
Physa sp.
Gyraulus sp.
Anodonta californiensis
Ostracods, spp.
Siphateles bicolor

SILVER LAKE CLIMBING DUNE is 26 feet higher than the surface of Pleistocene Silver Lake Playa on hills west of the Silver Lake outlet. Perhaps because the dune was deposited by strong westerly winds, no mollusks were recovered from the site. Aquatic and terrestrial gastropods, pelecypods, and ostracods were recovered from the Silver Lake Outlet sites to the west.

The Climbing Dune site contains tui chub (*Siphateles bicolor*) and frog or toad (Anuran) remains. The area is not within the current range of the spade foot toad (*Scaphiopus* sp.) or any frogs (Ranidae, Stebbins, 1966). The range for the red-spotted toad, *Anaxyrus punctatus*, covers the area, but the described habitat “desert oases.... and floodplains of rivers” (Stebbins, 1966) suggests that it requires water. Since the dune is west of Silver Lake outlet, this suggests that transport of those specimens was westward by predators.

Silver Lake Climbing Dune: Riverside Metropolitan Museum

Age: Rancholabrean (Reynolds, 2004)

Aquatic taxa:

Siphateles bicolor
Anuran

SODA LAKE – SANDS: No aquatic species have been documented from Pleistocene sediments around Soda Lake. Pleistocene horse and mammoth occur in lacustrine and ground water discharge sediments near the southeast end of Soda Lake, near the railroad siding of Sands.

Soda Lake – Sands: SBCM 1.62.11.62.2; (Jefferson, 2017)

Age: Rancholabrean (130 ka, Froesea and others, 2017)

CRONESE BASIN is north of I-15, sixteen miles west of Baker. The fauna is Holocene (Schneider, 1989, 1994; Warren and Schneider, 2000), introduced to the Cronese basins by meanders of the Mojave River. The meandering Mojave River could have introduced a similar fauna during the latest Pleistocene, after waters of Lake Manix breached Afton Canyon.

Cronese Basin:

Age: Holocene

Aquatic taxa:

Anodonta californiensis

LAKE MANIX, NEWBERRY SPRINGS TO AFTON between Newberry Springs and Afton, was the terminal destination of snow melt water from the rising San Bernardino Mountains during the later Ice Ages. Lake Manix “sediments provide a robust record of Mojave River discharge over the last half-million years. Lake Manix persisted from Oxygen Isotope Stage (OIS) 12 through early OIS 2, including during interstadial OIS 3 and interglacials OIS 5, 7, and 9. The ostracode faunal record displays a shift from an unexpectedly warm, summer-dominated lake hydrology during OIS 12 to predominantly colder, winter-dominated conditions afterwards” (Reheis and others, 2012).

Lake Manix was fed by the Mojave River, and when blockages of that river occurred, meanders filled such basins as Harper Basin. As coarse sands of the Mojave River delta filled the Manix basin, the river was forced to meander south and north, filling the basins of Troy and Coyote. Even after the Mojave River breached Afton Canyon (24 ka, Reheis and others, 2012), *Anodonta* survived in Coyote Lake until 11,000 ka (Meek, 1999; Enzel and others, 2003).

Lake Manix was a viable lake from 550 ka to 24 ka (Meek, 1999; Jefferson, 2003; Reheis and others, 2012), and supported 21 taxa of mammalian herbivores and carnivores, 25 species of water fowl (flamingos, pelicans and cormorants), shore birds, fringillids, and raptors, fish, turtles, clams and snails, for a total of more than 53 Pleistocene species (Jefferson, 1987, 1991, 2003, Enzel and others, 2003).

Lake Manix, Newberry Springs to Afton: LACM (CIT) 540542, 582 LACM 1093, 3496, 40324039, 40544061; SBCM 528, **Stevens Lake:** SBCM 830, SBCM, RPLI 1.59.21.59.23, 1.59.30, UCMP 676, 791; UCRV 67096764, 6767, 6769, 6852, 6910069124, 70197024, 70497065, 71017115, 71297146.

Age: Latest Irvingtonian–Rancholabrean, numerous U/Th and ¹⁴C, dates, ≥350 to 19 ka.

Camp Cady Local Fauna of Manix Formation (Jefferson, 1985, 1987, 1989, 1991, 1994, 1999, 2012; Meek, 1989, 1999; Steinmetz, 1989).

Aquatic taxa:

Limnocythere platyforma

Limnocythere robusta

Limnocythere ceriotuberosa

Valvata humeralis

Fossaria modicella

Planorbella ammon

P. subcrenata

Planorbella sp.? *P. tenuis*

Carinifex newberryi

Gyraulus vermicularis

Gyraulus sp.

Vorticifex effuse

Physa sp.

Anodonta californiensis

Siphateles bicolor mojavensis

Gasterosteus aculeatus

Actinemys pallida

Gavia sp. cf. *G. pacifica*

Podiceps sp. cf. *P. nigricollis*

Aechmophorus occidentalis

Pelecanus sp. aff. *P. erythrorhynchos*

Phalacrocorax auritus

P. macropus

Ciconia maltha

Phoenicopterus minutus

P. copei

Cygnus sp. cf. *C. columbianus*

Branta canadensis

Anas sp. cf. *A. platyrhynchos*

A. sp. cf. *A. crecca*

Aythya sp.

Mergus sp. cf. *M. merganser*

Oxyura jamaicensis

Fulica americana sp. cf. *F. a. shufeldti*

Grus sp.

cf. *Actitis* sp.

Phalaropodinae

Larus sp. cf. *L. oregonus*

Larus sp.

COYOTE LAKE IPP GROUND ELECTRODES: Coyote Lake is the northern playa of the Manix Lake complex. It lies east of the Calico Mountains and north of today's Mojave River. Coyote Lake has a surface elevation above 1710 feet. The IPP Southern Ground Electrode is 2.4 miles due north of St. Antony's Monastery at the southeastern margin of Coyote Lake playa. Drilling to place electrode grounds started at a surface elevation around 1730 feet, and allowed recovery of stratified lacustrine faunal remains. Stickleback (*Gasterosteus* sp.) remains were all clustered in lacustrine sediments 120 to 280 feet below

the current surface. Gastropods and pelecypods were concentrated above 50 feet of depth, and did not coexist with stickleback at any horizon. Tui chub (*Siphateles* sp.) occurred throughout the lacustrine stratigraphic column. The stratification may suggest that Coyote Lake was initially stagnant and only habitable by stickleback. But, as the sands of the Mojave River Delta divided the Manix Basin, meanders regularly freshened the late phase of Coyote Basin allowing proliferation of tui chub and mollusk populations. *Siphateles bicolor* remains were found in the first five feet of sediment in several drill holes, indicating that Pleistocene Coyote Lake was about 20 feet higher than the current playa surface. Viable populations of *Anodonta* survived in Coyote Lake until 11,000 yr BP (Meek, 1999; Enzel and others, 2003).

Coyote Lake IPP Ground Electrodes: SBCM 1.75.7 - SBCM 1.75.15;

Age: Rancholabrean, Wisconsinan
Manix Formation, (Reynolds, 1985; Roeder, 1985; Jefferson, 1989)

Aquatic taxa:

Heterocypris incongruens
Limnocythere bradburyi
Limnocythere robusta
Limnocythere ceriotuberosa
Pelocypris alatobulbosa
Anodonta californiensis
Pisidium sp.
Physa sp.
Gyraulus sp.
Siphateles bicolor
Gasterosteus aculeatus

CALICO LAKES—YERMO: Pleistocene sediments at Calico Lakes, Yermo contain unidentified bony fish that suggest permanent water. The anuran present may only require water when depositing eggs (Reynolds and Reynolds, 1985).

Calico Lakes-Yermo SBCM 1.76.35, 1.76.35a1.76.37

Age: Late Rancholabrean–Holocene,
 ^{14}C 12,800 \pm 900, 9,050 \pm 350 ka.

Aquatic taxa:

Osteichthyes
Anuran

Daggett—Cool Water Coal Gasification Solid Waste Site. Pleistocene sediments at Daggett are 160 feet higher in elevation than the high stand of Lake Manix. The Daggett sediments yielded Ice Age fossils during construction of solar and energy sites. The presence of fish indicates permanent water; anuran specimens recovered could indicate either permanent or temporary water since frogs and toads

only require water when depositing eggs (Reynolds and Reynolds (1985).

Cool Water Coal Solid Waste Site SBCM 1.76.33

Age: Late Rancholabrean, ^{14}C 12,210 \pm 430 ka

Aquatic taxa:

Gasterosteus aculeatus
Siphateles bicolor
Scaphiopus sp.
Anuran

DAGGETT—LUZ SOLAR TROUGH/ SOLAR ONE/ DAGGETT SOLAR: (Reynolds and Reynolds, 1985). The presence of unidentified bony fish suggests permanent water. The anuran present may only require water when depositing eggs (Reynolds and Reynolds, 1985).

LUZ Solar Sites at Daggett SBCM 1.76.111.76.13, SBCM 1.76.34

Age: Latest Rancholabrean, ^{14}C 10,910 \pm 425 ka

Aquatic taxa:

Osteichthyes
Anuran

HARPER LAKE—RED HILL: Sediments contain *Anodonta* sp and tui chub along the drainage from the Mojave River to the southeast end of Harper Basin. These species require permanent freshwater (Reynolds and Reynolds, 1994; Meek, 1999; Enzel and others, 2003; Garcia and others, 2009, 2014).

“The ~ 45–40 ka high stand at Harper Lake coincides with a shallowing interval downstream at Lake Manix. Ostracodes (*Limnocythere ceriotuberosa*) from Harper Lake high stand sediments are consistent with an alkaline lake environment that received seasonal inflow from the Mojave River, thus confirming the lake was fed by the Mojave River (Garcia and others, 2014).

Harper Lake - Red Hill: SBCM 1.126.52.

Age: Rancholabrean, 45–40,000 ka

Aquatic taxa:



Solar sites along the Mojave River near Daggett, 1980s.

Limnocythere ceriotuberosa
Anodonta californiensis
Siphateles sp., cf. *bicolor*

HAWES is west of Iron Mountain, south of Highway 58, and four miles west of Hinkley Road. The cyprinid present, probably *Siphateles* sp., requires permanent water to survive, as does *Anodonta* sp. The fragile *Anodonta* shells would not survive transport by predominantly western winds from Rogers Playa. And, *Anodonta* have not been reported from Pleistocene Lake Thompson 30 miles west (Reynolds and Reynolds, 1991). The elevation of the Hawes site is 120 feet higher than the lacustrine sediments with *Anodonta* at Red Hill.

An early course of the Mojave River north from the Victorville–Oro Grande–Helendale area has been suggested (Cox and others, 1999, 2003; Reynolds and Miller, 2015, p. 25-26) as northward flowing streams leading to Harper Lake, building a broad piedmont of river gravels less than 1 million years old west of Iron Mountain. The lacustrine well-sorted, fine-grained sand in gray silt contains fresh water mussels and fish.

Hawes: SBCM 1.123.1-2

Age: RanchoLabrean, Pleistocene

Aquatic taxa:

Cyprinidae
Anodonta

Discussion

The Mojave River did not flow directly to Lake Manix during the early Pleistocene. Obstructions such as bedrock barriers, fan conglomerates from lateral drainages, and gravel-choked fans and braid plains forced the Inconstant River (Jedediah Smith, 1826 in Brooks, 1989) to meander. The river delta itself would sometimes act as a barrier and force the main stream laterally into fault bounded basins such as Harper, Coyote and Troy. Sediments along the late Pleistocene course and meanders of the Mojave River contain taxa that are restricted to moving, aerated water (*Anodonta* sp., *Pisidium* sp., *Physa* sp., *Siphateles* sp.), or from slow moving water in ponds (*Gyraulus* sp., *Gasterosteus aculeatus*) or from the perimeter of available ponds and other water sources (*Actinemys pallida*, *Scaphiopus* sp., and *Anaxyrus* sp.). Land snails (*Succinea* sp.) have not been recorded from any of the above localities with faunal concentrations.

Selected ostracode habitat data can be very helpful with interpreting the climatic sequence through the Pleistocene. However, small samples containing ostracods may not provide adequate data unless tied to a stratigraphic section. In Manix Lake and Coyote Lake, large samples of sediment were extracted from a measured stratigraphic section (Steinmetz, 1989; Reynolds, 1985) and allow development of a sequence of changing climate.

The mollusks, fish and turtles found as fossils in Mojave River sediments prefer habitat that includes cool,

moving and well-aerated streams, ponds or lakes, often with a sandy bottom and with emergent vegetation.

Supportive data about aquatic habitats is gained from preferred diet of birds present at several of the water bodies. At Salt Springs, cormorants were dependant on fish, while species of ducks fed on pond grasses, grain, seeds, gastropods and occasional insects. Lake Manix was a large water body that fluctuated in response to pluvial and interpluvial periods. Manix offered fish for pelicans, cormorants, gulls, merganser, loons, grebes and storks. Manix shorelines were dense with pond grasses, grain, seeds and occasional insects and gastropods for geese, ducks, coots and cranes. Crustaceans, mollusks and insects were captured by probes of phalarope and sandpipers.

The presence of flamingos and other filter feeders that depend on small crustaceans, copepods, polychaetes, foraminifera, and amphipods suggest that Lake Manix was warm and saline during interpluvial periods, at least until the breach of the river through Afton Canyon.

Conclusion

The presence of molluscan and vertebrate taxa that require fresh or stagnant water suggest that, during the Pleistocene, snow melt from the rising San Bernardino Mountains maintained viable, though perhaps isolated populations of mollusks along the course of the meandering Mojave River. With multiple fluvial pulses, Pleistocene faunas colonized Harper Lake, ponds at Yermo and Daggett, and the northern and southern lobes of Lake Manix: Coyote and Troy. With the breaching of Afton Canyon, aquatic faunas appeared in Silver Lake and occasionally East Cronese Basin. The presence of an articulated skeleton of *Actinemys pallida* at Salt Springs suggests that occasional overflow from Silver Lake provided a moist or riparian route for turtles to reach Salt Springs. Fossil skeletal elements of cormorant and duck suggest that the water at Salt Springs was deep, and fresh enough to support fish and a shoreline with emergent vegetation.

Acronyms

CIT—California Institute of Technology; **ky**—thousand years ago; **LACM**—Los Angeles County Museum of Natural History, Section of Vertebrate Paleontology; **Ma**—Millennium Annum, million years ago; **RMM**—Riverside Metropolitan Museum; **RPLI, SBCM**—The Regional Paleontological Locality inventory at the SBCM; **SBCM**—San Bernardino County Museum; **UCR**—University of California, Riverside; **yr BP**—years before present.

Acknowledgements

Thanks to George T. Jefferson for detailed review and comments that made this paper more comprehensive, and for his ongoing efforts compiling Pleistocene vertebrate faunal lists for the southwestern United States. Thanks to all SBCM crew and volunteers that participated in

collection, matrix washing, preparation, identification and curation of fossil specimens from localities along the inconstant meanders of the Mojave River.

References

- Bell, M.A. 1994. Paleobiology and evolution of threespine stickleback; pp. 438-471 in M. A. Bell and S. A. Foster (eds), *The Evolutionary Biology of the Threespine Stickleback*. Oxford University Press, Oxford.
- Bell, M. A., and R. E. Reynolds. 2010. Miocene and Late Pleistocene stickleback spines from the Mojave Desert, California. *Desert Symposium Volume, California State University Desert Studies Consortium*, p. 162-168.
- Bright, J. and K. C. Anderson, 2007. Re-interpretation of Pleistocene Lake Dumont, Salt Spring basin, California, based on ostracode faunal analyses, in Miller, D.M., and Valin, Z.C., editors, *Geomorphology and tectonics at the intersection of Silurian and Death Valleys, southern California: U.S. Geological Survey Open File Report 2007-1424*, p. 51-62, available at <http://pubs.usgs.gov/of/2007/1424/of2007-1424.pdf>
- Brooks, G. R. (ed). 1989. *The Southwest Expedition of Jedediah Smith: His Personal Account of the Journey to California, 1826-1827*. University of Nebraska Press, 259 p.
- Cox, B. F., and J. C. Tinsley, III. 1999. Origin of the late Pliocene and Pleistocene Mojave River between Cajon Pass and Barstow, California. *San Bernardino County Museum Association Quarterly* 46(3), p. 49-54.
- Cox, B. F., J. W. Hillhouse, L. A. Owen, 2003. Pliocene and Pleistocene evolution of the Mojave River, and associated tectonic development of the Transverse Ranges and Mojave Desert, based on borehole stratigraphy studies and mapping of landforms and sediments near Victorville, California. *Geological Society of America Special Paper 368*, Boulder, Colorado. p. 5-42.
- Enzel, Yehouda, S. G. Wells, Nicholas Lancaster, 2003. Late Pleistocene lakes along the Mojave River, southeast California, *Geological Society of America Special Paper 368*, Boulder, Colorado. p. 61-72.
- Froesea, Duane, M. Stillerb, P. D. Heintzman, A. V. Reyesa, G. D. Zazulad, A. E. R. Soaresb, M. Meyere, E. Halld, B. J. L. Jensena, L. J. Arnoldg, R. D. E. MacPheeh, and B. Shapirob. 2017. Fossil and genomic evidence constrains the timing of bison arrival in North America. *PNAS*, vol. 114 (no. 13) 3457-3462.
- Garcia, A. L., J. R. Knott, J. Bright, and S. Mahan. 2009. Geochronology and paleoenvironment of pluvial Harper Lake, Mojave Desert, California. *Desert Symposium Volume, California State University Desert Studies Consortium*, p. 202.
- Garcia, A. L., J. R. Knott, S. Mahan, and J. Bright. 2014. Geochronology and paleoenvironment of pluvial Harper Lake, Mojave Desert, California, USA. *Quaternary Research Volume 81, Issue 2*, pp. 305-317 <http://pubs.er.usgs.gov/publication/70073499>
- Jefferson, G. T. 1985. Stratigraphy and geologic history of the Pleistocene Lake Manix Formation, central Mojave Desert, California; p. 157-169 in R.E. Reynolds (ed), *Cajon Pass to Manix Lake: Geological Investigations Along Interstate 15*. San Bernardino County Museum, Redlands, California.
- Jefferson, G.T. 1987. The Camp Cady local fauna: paleoenvironment of the Lake Manix Basin. *San Bernardino County Museum Association Quarterly* 34(3&4):335.
- Jefferson, G.T. 1989. Late Pleistocene and earliest Holocene fossil localities and vertebrate taxa from the western Mojave Desert; p. 27-40. in *The Westcentral Mojave Desert: Quaternary Studies Between Kramer and Afton Canyon*, R.E. Reynolds (ed). San Bernardino County Museum Association Special Publication, Redlands, California.
- Jefferson, G.T. 1991. The Camp Cady local fauna: stratigraphy and paleontology of the Lake Manix basin; p. 93-99 in M.O. Woodburne, R. Reynolds, and D.P. Whistler (eds), *Inland Southern California: The Last 70 Million Years*. San Bernardino County Museum Association Quarterly 38(3, 4).
- Jefferson, G.T. 1994. Stratigraphy and Pliocene-Pleistocene history of the Lake Manix basin, p. 175-177 in S. F. McGill and T. M. Ross (eds), *Geological investigations of an Active Margin*. Geological Society of America Guidebook, 27th Annual Meeting, San Bernardino, California.
- Jefferson, G.T. 1999. Age and stratigraphy of Lake Manix basin, p. 109-112 in R. E. Reynolds and J. Reynolds (eds), *Tracks along the Mojave*. San Bernardino County Museum Association Quarterly, v. 46(3),
- Jefferson, G.T. 2003. Stratigraphy and Paleontology of the middle to late Pleistocene Manix Formation, and Paleoenvironments of the central Mojave River, southern California; p. 43-60, in Y. Enzel, S. G. Wells, and N. Lancaster (eds), *Paleoenvironments and Paleohydrology of the Mojave and Southern Great Basin Deserts*. Geological Society of America Special Paper 368, Boulder, Colorado.
- Jefferson, G. T. 2017. A catalogue of late Quaternary and Holocene vertebrates from Arizona. Data tables on file Colorado Desert District Stout Research Center Library archive (Revised 11 May 2017).
- Meek, N., 1989. Physiographic history of the Afton basin, revisited; p. 78-83 in Reynolds, R.E. (comp.). *The west-central Mojave Desert: Quaternary studies between Kramer and Afton Canyon*, a special publication of the San Bernardino County Museum Association, 83 p.
- Meek, N. 1999. New discoveries about the Late Wisconsinan history of the Mojave River system; p. 113-118 in R.E. Reynolds, and J. Reynolds (eds), *Tracks Along the Mojave*. San Bernardino County Museum Association Quarterly 46(3).
- Miller, D. M., R. E. Reynolds, G. A. Phelps, J. Honke, A. J. Cyr, D. C. Buesch, K. M. Schmidt, and G. Losson. 2017. Active tectonics of the northern Mojave Desert: the 2017 Desert Symposium field trip road log. *California State University Desert Symposium*: 7-44.
- Moore, R. C., C. G. Lalicker, and A. G. Fischer. 1952. *Invertebrate Fossils*. McGraw-Hill Book Company, Inc. New York, 766p.
- Moyle, P.B. 2002. *Inland Fishes of California*. Revised and Expanded. University of California Press, Berkeley, 493 p.

- Nussbaum, R. A., E. D. Brodie, Jr., and R. M. Storm. 1983. Amphibians and reptiles of the Pacific Northwest. University Press of Idaho, 332 pp.
- Page, L. M. and B. M. Burr. 2011. A field guide to freshwater fishes of North America north of Mexico. Boston: Houghton Mifflin Harcourt, 663p.
- Reheis, M.C., J. Bright, S. P. Lund, D. M. Miller, G. Skipp, and R. J. Fleck. 2012. A half-million-year record of paleoclimate from the Lake Manix core, Mojave Desert, California. *Palaeogeography, Palaeoclimatology, Palaeoecology* 365-366: 11-37.
- Reynolds, R. E. 1985. Paleontologic salvage, Intermountain Power Project, Southern Ground Electrode, Coyote Lake, San Bernardino County, California. San Bernardino County Museum, for Applied Conservation Technology, Westminster, California, p. 182.
- Reynolds, R. E. 1990. Kern River Pipeline, paleontologic resource assessment and final management plan, California portion. San Bernardino County Museum, for Dames and Moore, Report 14641-005-01. p. 64.
- Reynolds, R. E., and R. L. Reynolds. 1991. Late Pleistocene faunas of Lake Thompson. *San Bernardino County Museum Association Quarterly*, 38(3, 4):114-115.
- Reynolds, R.E., and R. L. Reynolds, 1994. The isolation of Harper Lake Basin, *in* Off limits in the Mojave Desert, R.E. Reynolds, ed. Redlands, San Bernardino County Museum Association Special Publication, 94(1): 34-37.
- Reynolds, R. E. 2004. Latest Pleistocene (Rancholabrean) fossil assemblage from the Silver Lake Climbing Dune site, northeastern Mojave Desert, California. *California State University Desert Symposium*, p. 33-38.
- Reynolds, R. E., and D. M. Miller. 2015. Mojave Miocene: the field trip. *Desert Symposium Volume*, California State University, Desert Studies Consortium, p. 7-33.
- Roeder, M. A. 1985. Late Wisconsin records of *Gasterosteus aculeatus* (threespine stickleback) and *Gila bicolor mojavensis* (Mojave tui chub) from unnamed Mojave River sediments near Daggett, San Bernardino County, California; p. 171-174 in R. E. Reynolds (ed.), *Geological Investigations along Interstate 15, Cajon Pass to Manix Lake*. San Bernardino County Museum, Redlands, California.
- Schneider, J. S. 1989. Fresh water bivalves as paleoenvironmental indicators, p. 65 in *Abstracts of Proceedings, 1989 Mojave Desert Quaternary Research Symposium*, San Bernardino County Museum Association Quarterly 37:2.
- Schneider, J. S. 1994. Fresh water mussels and paleoenvironment at East Cronese Lake, p 42-15 in G. D. Everson and J. S. Schneider (eds), *Kelso Conference Papers on Prehistory of the Mojave Desert*. Museum of Anthropology, California State University Bakersfield, Occasional Papers in Anthropology 4.
- Stebbins, R. C. 1972. *California Amphibians and Reptiles*. University of California Press, Berkeley, 152p.
- Steinmetz, J. J., 1989. Ostracoda of the late Pleistocene Manix Formation, central Mojave Desert, California. *San Bernardino County Museum Association Special Publication*, p. 70-77.
- Taylor, D. W. 1960. Late Cenozoic molluscan faunas from the high plains. U. S. Geological Survey Prof. Paper 337, pp. 1-94.
- Warren, C. N., and J. S. Schneider. 2000. Archaeology in the Cronese Basin. *California State University Desert Symposium*, p. 40-41.
- Wells, S. G., W. J. Brown, Y. Enzel, R. Y. Anderson, L. D. McFadden, 2003. Late Quaternary geology and paleohydrology of pluvial Lake Mojave, southern California, *Geological Society of America Special Paper* 368, Boulder, Colorado. p. 73-90.

Initiation and rate of slip on the Lockhart and Mt. General faults in southern Hinkley Valley, California

Elizabeth K. Haddon, David M. Miller, Victoria E. Langenheim, Tanzhuo Liu, Laura C. Walkup, Elmira Wan
U.S. Geological Survey. ehaddon@usgs.gov

An accurate picture of the evolution and dynamics of plate boundary dextral shear across the network of Eastern California shear zone (ECSZ) faults requires an inventory of distributed geologic strain over multiple timescales. The dextral Mt. General and Lockhart faults are among four primary structures in the northern central Mojave Desert portion of the ECSZ including the Helendale fault to the southwest and the Gravel Hills and Harper Lake faults to the northeast. Early mapping by Dibble (1960) described the Mt. General and Lockhart faults, which branch northwestward of the Lenwood fault (slipping at an average of ~ 1 mm/yr since the late Pleistocene) in the vicinity of Barstow (Hart et al., 1993; Oskin et al., 2007). Surface traces of the Lockhart and Mt. General faults are geometrically complex and define the contemporary margins of southern Hinkley Valley, cutting across Pliocene–Holocene surficial deposits, Miocene–Pleistocene basin fill, and Paleozoic–Miocene crystalline basement (e.g., Andrew and Walker, 2017). We leverage high-resolution Structure-from-Motion built topography (grid cell size of 18 to 23 cm), field observations, geochronology, and gravity data along these two fault systems to reconstruct the Late Pleistocene and Holocene record of fault slip based on geologic and geomorphic markers in Hinkley Valley.

Three distinct traces of the Mt. General fault deform the fan piedmont along the linear southwestern flank of Mt. General, offsetting stream channels, levees, and bedrock ridges in a predominantly dextral sense. Scarps on Holocene alluvial fans are consistently south facing and up to ~ 1.5 m in height with larger magnitude, down-on-the-west displacement of Pleistocene alluvial surfaces and Tertiary bedrock. Apparent dextral and vertical displacements of geomorphic features measured using the LADACAOZ v.2.1 Matlab analysis toolbox form clusters of dextral offset magnitude consistent with cumulative slip due to multiple surface ruptures since the late Pleistocene (e.g., Zielke et al., 2010; Haddon et al., 2016). The lowest magnitude cluster of dextral offset affecting Holocene and older deposits averages ~ 3 m, and the average vertical offset across these features is ~ 0.6 m. Regional dating of Holocene alluvium correlated with these deposits on the basis of soils, surface characteristics, and plant communities indicates deposition at ~ 8 to 13 ka (e.g., Menges and Miller, 2007) and subsequent surface rupture

during at least one Holocene earthquake on the Mt. General fault. If we assume that the duration since the last large surface rupturing event is roughly equivalent in age to these Holocene landforms, the dextral Holocene slip rate on the Mt. General fault is ~ 0.1 – 0.6 mm/yr. Summing cumulative displacements across subparallel fault traces that cut late Pleistocene surfaces likely established by ~ 160 – 170 ka suggests at least ~ 27 – 79 m of net dextral slip, although this inventory omits distributed deformation on one or more bedrock fault traces. Our longer-term slip rate estimate on the Mt. General fault is ~ 0.1 to 0.5 mm/yr, which compares well with the Holocene rate and implies somewhat constant slip on the Mt. General fault since ~ 170 ka.

Anastomosing traces of the ~ 1 – 2 km-wide Lockhart fault zone in southwestern Hinkley Valley deform a relict braid plain of middle Pleistocene fluvial sand and gravel deposited by the ancestral Mojave River. Brackets on depositional age of the fluvial deposits between ~ 200 and 550 ka rely on tephrochronologic identification of the 631 ka Lava Creek B ash in core samples collected from the lower part of the sequence and varnish microstratigraphy for overlying rockfall clasts. Apparent offsets of inverted bar and channel deposits with subtle ridge-and-swale topography show distributed right-lateral and right-reverse oblique slip with an overall down-on-the-east component. Optimum lateral offsets measured along individual fault strands range from ~ 5 to 90 m. Summing mean values for individual strands yields ~ 50 – 250 m of dextral offset across the Lockhart fault zone since aggradation and suggests a dextral slip rate of ~ 0.1 – 1.3 mm/yr. Subsequent incision of the modern Mojave River likely occurred between ~ 160 and 300 ka given age estimates for inset alluvial fans and varnish microstratigraphy for rockfall. Apparent dextral deflection of the modern channel coincides mainly with the basin-bounding strand of the Lockhart fault, which also defines the northernmost exposure of ancestral river deposits and a linear, steep gravity gradient collocated with the surface trace of the Lenwood fault. Because the amount of dextral displacement along this basin bounding strand is unknown, our estimate for slip on the Lockhart fault since the middle Pleistocene represents a minimum rate.

The Lockhart and Mt General faults dissect gravity lows likely sourced from thick early to middle Miocene Barstow Formation underlying Barstow and southern Hinkley Valley. Gravity gradients that define basin margins appear dextrally offset ~3 km by the Lockhart and Mt General faults and suggest net dextral offset of ~6 km across Hinkley Valley. Published total dextral offset estimates based on aeromagnetism and geologic markers (Carleton, 1988; Jachens et al., 2002; Andrew and Walker, 2017) agree well for the Mt General fault (3.1 km magnetic, 2.9 ± 0.5 km geologic), and are relatively low for the Lockhart fault ($\sim 1 \pm 0.7$ km magnetic) and Lenwood fault ($\sim 1 \pm 0.2$ km geologic, 2.5 km magnetic). The easternmost basin-bounding trace of the Lockhart fault apparently accounts for the majority of the ~3 km dextral slip budget on the Lockhart fault in the vicinity of the Mojave River. As the fault bends left towards Hinkley Valley, the bulk of this strain appears distributed across the dextral system. If we assume that total dextral offset accumulated uniformly on each of the Mt. General and Lockhart faults, our preliminary dextral slip rates suggest inception of strike-slip no later than ~3 Ma and as early as 15 Ma. This timing overlaps somewhat with previous studies suggesting relatively recent activation at ~1–3.8 Ma (Cox et al., 2003; Oskin et al., 2007; Andrew and Walker, 2017) and is consistent with U–Pb ages for sheared opaline silica collected from exposures of the Camp Rock and Cave Mountain faults (striking northwest and west towards southern Hinkley Valley, respectively) supporting the onset of strike-slip by ~10–11 Ma in the central Mojave Desert (Nuriel et al., 2013; Miller, 2017).

References

- Andrew, J., and Walker, D.J., 2017, Path and Amount of dextral fault slip in the Eastern California Shear Zone across the Central Mojave Desert, *GSA Bulletin*, 129 (7–8), p. 855–868.
- Cox, B.F., Hillhouse, J.W., and Owen, L.A., 2003, Pliocene and Pleistocene evolution of the Mojave River, and associated tectonic development of the Transverse Ranges and Mojave Desert, based on borehole stratigraphy studies and mapping of landforms and sediments near Victorville, California, in Enzel, Y., Wells, S.G., and Lancaster, N., eds., *Paleoenvironments and Paleohydrology of the Mojave and Southern Great Basin Deserts: Geological Society of America Special Paper 368*, p. 1–42.
- Dibblee, T.W., Jr., 1960, Geologic map of the Barstow quadrangle, San Bernardino County, California: U.S. Geological Survey Mineral Investigations Field Studies Map MF-233, scale 1:62,500.
- Haddon, E.K., Amos, C.B., Zielke, O., Jayko, A., and Burgmann, R., 2016, Surface Slip during Large Owens Valley Earthquakes, *Geochemistry, Geophysics, Geosystems* 17 (6), p. 2239–2269.
- Hart, E.W., Bryant, W.A., Treiman, J.A., 1993, Surface Faulting associated with the June 1992 Landers Earthquake, California, *California Geology*, 46 (1993), p. 10–16.
- Jachens, R.C., Langenheim, V.E., and Matti, J.C., 2002, Relationship of the 1999 Hector Mine and 1992 Landers fault ruptures to offsets on Neogene faults and distribution of late Cenozoic basins in the eastern California shear zone: *Bulletin Seismological Society America*, v. 92, p. 1592–1605.
- Menges, C.M., and Miller, D.M., 2007, Introduction, in Miller, D.M., and Valin, Z.C., eds., *Geomorphology and tectonics at the intersection of Silurian and Death Valleys, southern California—2005 Guidebook*, Pacific Cell Friends of the Pleistocene: U.S. Geological Survey Open-File Report 2007–1424, 171 p.
- Miller, D.M., 2017, The late Cenozoic eastern California shear zone after 25 years of study, *ECSZ Does It, Desert Symposium Proceedings*, California State University Desert Studies Consortium, p. 45.
- Nuriel, P., Maher, K., and Miller, D.M., 2013, U–Pb SHRIMP-RG dating of fault-related opals from the Eastern California Shear Zone, in Reynolds, R.E., ed., *Raising Questions in the Eastern Mojave Desert: The 2013 Desert Symposium Field Guide and Proceedings*, California State University Desert Studies Consortium, p. 287.
- Oskin, M.E., Le, K., Strane, M.D., 2007, Quantifying fault-zone activity in arid environments with high-resolution topography, *Geophysical Research Letters*, Volume 34, L23S05.
- Zielke, O., Arrowsmith, J.R., Ludwig, L.G. and Akçiz, S.O., 2010, Slip in the 1857 and earlier large earthquakes along the Carrizo Plain, San Andreas fault, *Science*, 327(5969), p.1119–1122.

Middle Pleistocene infill of Hinkley Valley by Mojave River sediment and associated lake sediment: Depositional architecture and deformation by strike-slip faults

D.M. Miller, E.K. Haddon, V.E. Langenheim, A. J. Cyr, E. Wan, L.C. Walkup and S.W. Starratt
U.S. Geological Survey, 345 Middlefield Road, Menlo Park CA 94025; dmiller@usgs.gov

ABSTRACT: Hinkley Valley in the Mojave Desert, near Barstow about 140 km northeast of Los Angeles and midway between Victorville Valley and the Lake Manix basin, contains a thick sedimentary sequence delivered by the Mojave River. Our study of sediment cores drilled in the valley indicates that Hinkley Valley was probably a closed playa basin with stream inflow from four directions prior to Mojave River inflow. The Mojave River deposited thick and laterally extensive clastic wedges originating from the southern valley that rapidly filled much of Hinkley Valley. Sedimentary facies representing braided stream, wetland, delta, and lacustrine depositional environments all are found in the basin fill; in some places, the sequence is greater than 74 m (245 ft) thick. The sediment is dated in part by the presence of the ~631 ka Lava Creek B ash bed low in the section, and thus represents sediment deposition after Victorville basin was overtopped by sediment and before the Manix basin began to be filled. Evidently, upstream Victorville basin filled with sediment by about 650 ka, causing the ancestral Mojave River to spill to the Harper and Hinkley basins, and later to Manix basin.

Initial river sediment overran wetland deposits in many places in southern Hinkley Valley, indicating a rapidly encroaching river system. These sediments were succeeded by a widespread lake ("blue" clay) that includes the Lava Creek B ash bed. Above the lake sediment lies a thick section of interlayered stream sediment, delta and nearshore lake sediment, mudflat and/or playa sediment, and minor lake sediment. This stratigraphic architecture is found throughout the valley, and positions of lake sediment layers indicate a successive northward progression in the closed basin. A thin overlapping sequence at the north end of the valley contains evidence for a younger late Pleistocene lake episode. This late lake episode, and bracketing braided stream deposits of the Mojave River, indicate that the river avulsed through the valley, rather than continuing toward Lake Manix, during the late Pleistocene. Two dextral strike-slip fault zones, the Lockhart and the Mt. General, fold and displace the distinctive stratigraphic units, as well as surficial late Pleistocene and Holocene deposits. The sedimentary architecture and the two fault zones provide a framework for evaluating groundwater flow in Hinkley Valley.

Introduction

The present configuration of the Mojave River was established by a series of successive basin-filling events, after each of which the river extended to another downstream basin (Cox and others, 2003). Little is known about the timing and sedimentary characteristics of deposits filling Hinkley Valley, which is one of the next basins downstream from Victorville basin (underlying Victorville deposits, Fig. 1), but a recent opportunity to study sediment core from more than 160 boreholes from the valley greatly improves our understanding of this basin. Published timing estimates for the filling of the upstream Victorville basin (~575-475 ka; Cox and others, 2003) and the initiation of the Manix basin

(~550 ka; Reheis and others, 2012) ~50 km (30 mi) downstream indicate only brief depositional histories for the intermediate Harper and Hinkley basins. However, extensive clastic wedges (green units in Fig. 1) lead to Harper and Hinkley basins (Cox and others, 2003), indicating possible long periods of river flow to the basins. Harper basin remains enigmatic but new data from extensive coring in Hinkley Valley presented herein demonstrates that thick sediments derived from the Mojave River accumulated in that basin before Lake Manix was initiated.

The present-day Hinkley Valley, bounded by Mt. General on the east and Lynx Cat and Iron mountains on the west, is a broad, nearly flat valley (Figs. 1, 2). It is

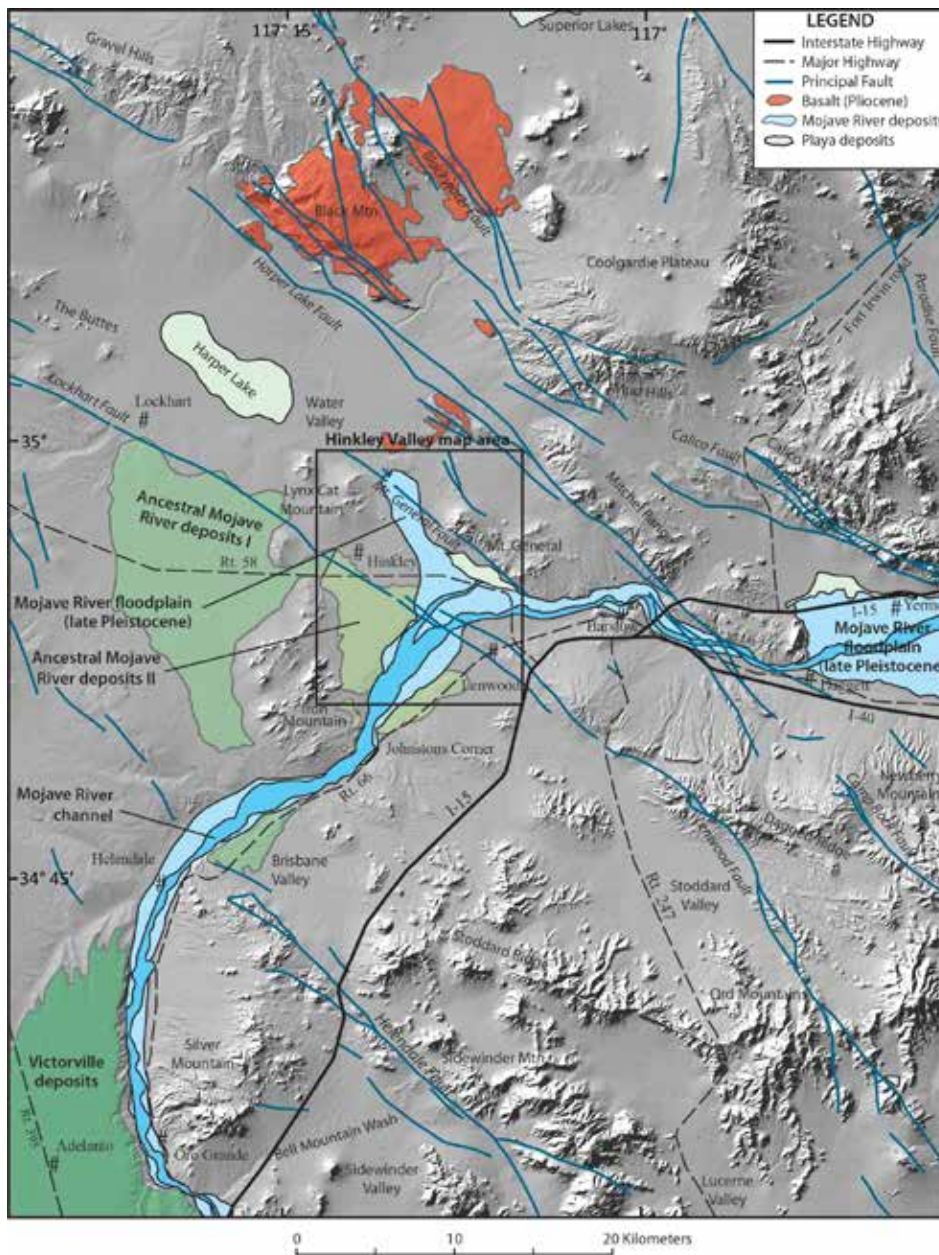


Figure 1. Location map for Hinkley Valley area (shown in black box). Mojave River-sourced deposits of several ages are shown on shaded relief. Victorville deposits (~2.5-0.7 Ma), ancestral Mojave River deposits I (0.7-0.65 Ma?), and ancestral Mojave River deposits II (0.65-0.55 Ma) are shown in greens; late Pleistocene and younger channels in blues. Note the fault zones (blue lines) cutting Hinkley Valley. Geology adapted from Dibblee (1960a, 1960b), Cox and others (2003). Lake Manix basin lies immediately east of map area. (colors refer to figures in the pdf version available online).

traversed by the Mojave River on its south side. That river channel is deeply cut (>30 m [100 ft]) in the southwest but grades nearly to the valley floor on the southeast. As a result, flood flow across Hinkley Valley changes from channelized on the west to broad and dispersed on the east, where avulsion is possible.

After a river incision event that beheaded the clastic wedge leading into southern Hinkley Valley (Fig. 1), the Mojave River primarily has been restricted to its current location, which crosses southern Hinkley Valley, passes

north of Barstow, and continues on to the east. However, a sediment package overlies the initial Mojave River package in northern Hinkley Valley (Meek, 1999) and it has been dated at ~45–40 ka (Garcia and others, 2014). Furthermore, the most recent lake in Harper basin left a distinctive shoreline deposit around much of the Harper basin, and northern Hinkley Valley (Dibblee, 1960a, 1960b). These much younger lake(s) evidently were fed by Mojave River flow north along Hinkley Valley and perhaps influenced by tectonic events (Reynolds and Reynolds, 1994). The Lockhart and Mt. General fault zones, both of which cut Holocene deposits, traverse Hinkley Valley and may be responsible for influencing river flow. The complex pattern of stratigraphic units that fill the Hinkley Valley basin and the faults that cut those units are important parts of the geologic framework that influences groundwater movement through the valley (Izbicki and Groover, 2016).

Stratigraphic units

Most bedrock fringing Hinkley Valley consists of metasedimentary rocks, intrusive rocks ranging from granite to diorite, and gneissic rocks (Dibblee, 1960a, b; Boettcher, 1990; Fletcher and others, 1995). Metamorphic and intrusive rocks have a complex Mesozoic to Miocene

history that includes detachment faulting (Fletcher and others, 1995; Glazner and others, 2002, and references therein). Miocene volcanic and sedimentary rocks are locally present. Similar rocks underlie Hinkley Valley, based on core materials we examined. Depth to basement models based on our gravity data outline a shallow, broad valley with dramatically greater depths to basement near the Mojave River course in the southeastern part of the valley (Fig. 1). In addition, the gravity models indicate

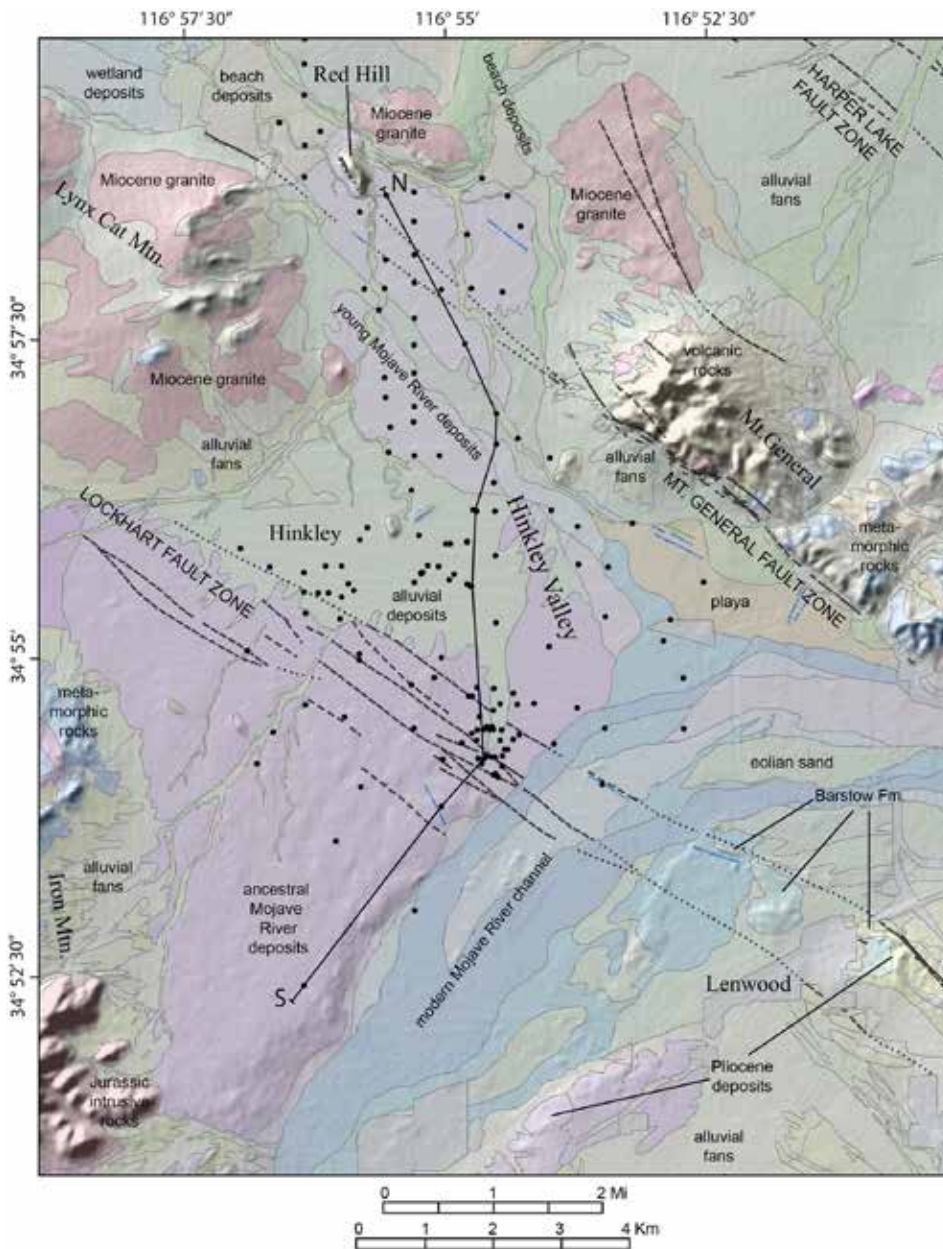


Figure 2. Geologic map of Hinkley Valley (this paper) showing our interpretation of multiple strands of the Lockhart and Mt. General fault zones based on field work and interpretation of high-resolution elevation models. Faults are dotted where concealed. Large dots are boreholes studied; line A-A' is the line of the cross section shown in Fig. 4. Major map units are labeled. Blue lines mark lineaments. Refer to Fig. 1 for location.

shallow basement at 20-37 m (70-120 ft) depth (note that some depth information is provided in feet, as used by the drilling program for the valley) in an area north and northeast of the community of Hinkley (Fig. 2).

Overlying bedrock is the Barstow Formation in the southeast, near Lenwood (Fig. 2). Elsewhere in Hinkley Valley deposits at the surface are broadly similar. Sporadically exposed gravelly sand that matches Mojave River sediment in composition and texture (arkose with rounded grains, abundant mica, and an admixture of well-rounded reddish quartzite pebbles) is widespread, and ranges in age from the active channel of the Mojave

River in the south, to deposits bearing soils that indicate Pleistocene age. These Pleistocene Mojave River deposits are exposed in cuts along the Mojave River and in a few stream banks in northern Hinkley Valley. Lacustrine sand and silt, about 45-40 ka in age (Garcia and others, 2014), are present at the north end of Hinkley Valley where they are buried by a sheet of Mojave River braided stream deposits 2-4 m (7-13 ft) thick.

Sediment core from boreholes in Hinkley Valley demonstrates that ancestral Mojave River deposits underlie the entire valley, in some places from the surface to depths greater than 74 m (245 ft). Several boreholes penetrated alluvial fan deposits below the Mojave River deposits, and these depths, along with depth to crystalline bedrock underlying the Mojave River deposits, permit the shape of Hinkley Valley prior to Mojave River incursion to be outlined (Fig. 3a). The underlying alluvial fans carry local bedrock clasts, unlike the Mojave River deposits, and clast provenance matching rock in mountains adjacent to Hinkley Valley indicates fans and streams draining from the southwest, east, and north into a valley with two low, internally drained centers that likely held playas. One borehole penetrated moderately-sorted axial stream sand and gravel (Fig. 3a) that carried clasts from piedmonts both south and west of the site, indicating flow to the northeast.

Overlying the alluvial fans and bedrock of the valley is a suite of Mojave River deposits that can be divided into deposit types that illustrate depositional environment and provenance (Table 1). In general, thin groundwater discharge deposits (GWD; e.g. Pigati and others, 2011) and stream deposits of the central Hinkley Valley are overlain by an extensive lake deposit. The GWD are carbonate-rich sand deposits bearing extensive rounded grains and

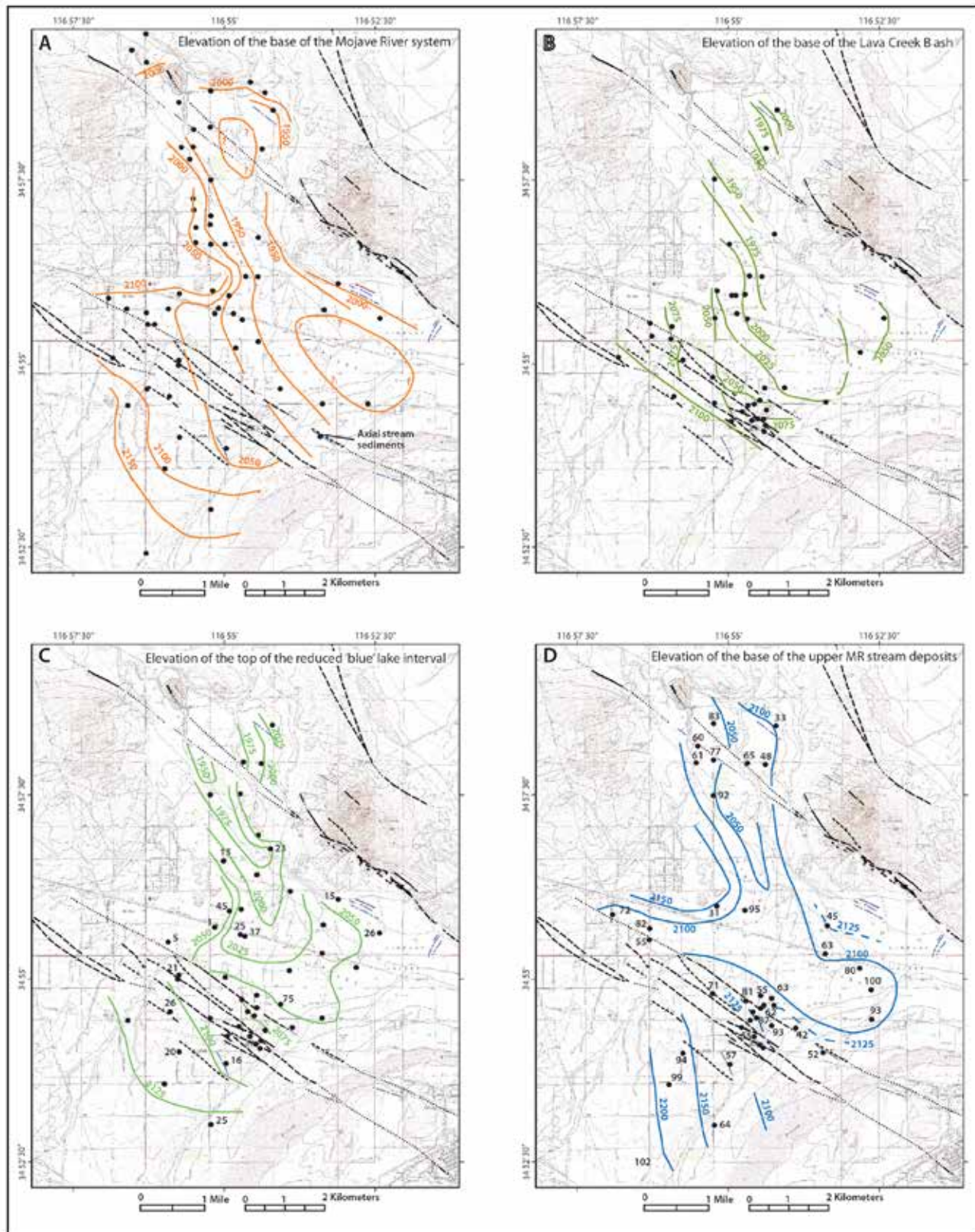


Figure 3. Maps of Hinkley Valley showing borehole locations (tiny black dots) on topography and geology. Dark black lines are the fault zones crossing Hinkley Valley. Large dots are borehole locations that constrain the feature mapped. A. Surface elevation (in ft) of the top of alluvial fan deposits and bedrock prior to the arrival of Mojave River sediment. Area outlined in blue encloses boreholes with two GWD deposits. B. Distribution and surface elevation (in ft) of the base of the Lava Creek B ash bed (~631 ka). Area of maximum thickness is indicated. C. The elevation (contour lines) of the top and the thickness (dot labels; in ft) of the reduced “blue clay” lake sediment. D. The elevation (in ft) of the base and the thickness (in ft) of the upper Mojave River stream sediment section. Note the progressive south-to-north smoothing of topography as the valley is filled.

Table 1. Interpretation of core sediment and variables used to make those assignments

Factor	Classification	Criteria
Provenance	Mojave River stream	Arkose with quartzite lithic grains; rounded- to well-rounded grains
	Local alluvial fan	Lithics similar to local bedrock; angular to subangular grains dominate
	Uncertain	Grain size is medium sand and finer; lithics and rounding not distinctive
Depositional environment	Mojave River stream system	Coarse stream channel deposits are poorly sorted, crudely bedded; lacks fossils. Color is orange to brown. Soils common in upper 2-6 m of section; less common 6-12 m; rare below
	Local alluvial fan	Poorly sorted, vaguely bedded gravel and sand of local provenance; commonly several soils within sequence; lacks fossils. Color is yellow-brown to red-brown. Sequences overlying bedrock are characterized by weathered bedrock materials interspersed with thin beds of sand; may indicate pediment deposits
	Lake margin	Moderately- to well-sorted sand and silt with sparse gravelly sand interbeds at most; thin bedded to laminated; commonly mica-rich; grain size and color vary from bed to bed; sparse fossils indicate shallow lake environment. May represent fluvial delta, beach, and nearshore lake deposits, or playa-margin deposits. Color is white to gray, tan to pale tan, and rich brown.
	Lake	Clay and silt to very fine sand, thinly bedded to laminated; commonly rippled; generally not calcareous; fossils indicate shallow lake environment. Color is gray, green, olive, tan, white, and gley; ranges to brown near base and top commonly. Commonly diatomaceous. No evidence of dropstones
	Mudflat/playa	Fine sand to silt and clay; mostly poorly sorted with admixture of coarse and very coarse sand grains; sand grains floating in mud very common. Rare mud-cracks and thin stream sheetflow beds taken to indicate playa environment. Calcareous nodules and zones of MnO ₂ stain are common; sparse fossils indicate shallow lake environment. Color is brown and orangish brown
	Groundwater discharge	Calcium-carbonate-rich sediment, typically with alluvial fan lithics and sand grains floating in a fine sand to silt composed of detrital grains and carbonate material. Very poorly sorted overall. Sand and pebble grains uniformly coated by CaCO ₃ . Color is pale gray or pale tan to white.

quartzite pebbles indicative of Mojave River derivation. In detail, two GWD are present in some boreholes south of the community of Hinkley, and in some boreholes the two are separated by alluvial fan sediment of local provenance, which indicates that the Mojave River and its sediment load entered Hinkley Valley from both north (Mojave River deposits I) and south (Mojave River deposits II) of Iron Mtn. (Fig. 1). The extensive lake deposit overlying GWD interfingers with stream and delta deposits to the south, and in this same area a thick lens of volcanic ash forms part of both deposits (Fig. 3b). Ash was collected from 41 cores for analysis and visually identified in another 9 cores on the basis of color, texture, and shard morphology. Electron microprobe analysis of glass shard samples indicates that the ash is chemically similar to the Lava Creek B ash that erupted from the Yellowstone eruptive center about 631 ka (Matthews and others, 2015). Thickness of the ash bed exceeds 2 m (7 ft) in one part of the valley, which we interpret as the location of local stream input (Fig. 3b). The ash lies above both GWD but is thickest 3 km (2 mi) southeast of Hinkley where the upper GWD is widespread, demonstrating that the Mojave River entered first from north of Iron Mtn., and then south of Iron Mtn. The contour map for the top of the overlapping lake deposits (Fig. 3c) shows progressive filling in the south lobe of the initial valley. In particular, the lobe has shifted farther north, and it is shallow, draining smoothly northward.

Overlying the lake deposits, and also interfingering with Mojave River stream deposits in the southwest, is a thick sequence of lake margin (delta, shorezone, and

nearshore lake) deposits (Table 1) that are interlayered with subordinate mudflat and stream deposits. Upward, the facies repeat several times, although there is one broad northern mass of mudflat deposits. The uppermost 8-12 m (26-40 ft) of sediment is mainly Mojave River stream sediment, the base of which is shown as a contour map in Fig. 3d. At this time the south lobe of the valley has become a gentle swale, whereas the north lobe has been replaced by a narrow valley with about 10 m (35 ft) of relief. In the northern end of the valley soils are developed on the Mojave River stream sediment, above which is the 45-40 ka lake sediment and a thin (2-3 m [6-10 ft] thick) sheet of Mojave River stream deposits. Elsewhere, soil profiles are typically present in the upper 6 m (20 ft) of the section, but are rare at greater depths. Depth and thickness of the upper Mojave River stream sediment section decreases by ~10 m (33 ft) over the Lockhart fault zone (Fig. 3d), which we interpret as syn-depositional uplift of wedges among the strands of the fault zone. As much as 30 m (100 ft) of sediment was added to the southern valley and 15-18 m (50-60 ft) to the northern valley during the deposition of the upper stream sediment section.

Stratigraphic architecture and interpretive history of basin filling

The sedimentary units described above form a fairly consistent stacking pattern throughout Hinkley Valley. For instance, Mojave River stream deposits are thickest in the southwest, and interfinger with lake, lake margin, and mudflat deposits northward (Fig. 4). This pattern indicates

have been deposited episodically over a long time period, perhaps after the Mojave River established a course to Lake Manix.

Youthful faulting

Two fault zones were extrapolated across Hinkley Valley (Dibblee, 1960a) but were only mapped in the valley in two short segments in northern Hinkley Valley. Bryant (1987) evaluated these and nearby faults, indicating that the Mt. General fault is active. Miller and others (2007) described scarps along the southwest face of Mt. General as cutting early Holocene deposits, and therefore also considered the Mt. General fault to be active. However, the precise locations of the Mt. General and Lockhart faults in Hinkley Valley have not been described. Interpreted offsets of gravity and aeromagnetic patterns (Jachens and others, 2003) indicate ~3 km of dextral offset on the Mt. General fault and ~1 km of offset on the Lockhart fault (Andrew and Walker, 2017).

Elevation models were built from high-resolution aerial photography of the Mt. General and Lockhart fault zones (Haddon and others, this volume). Geomorphic features characteristic of faulting, such as scarps, depressions, and linear features, as well as vegetation lineaments, are located near those indicated by Dibblee (1960a), and were used by Haddon and others (this volume) to develop maps of multiple fault strands in both fault zones (Fig. 2). These maps improve our knowledge of the faults, a part of the active Eastern California Shear Zone (Dokka and Travis, 1990; Andrew and Walker, 2017).

Middle Pleistocene strata logged from core study in the vicinity of the Lockhart fault zone show significant disruption, with tilted beds and significant changes in depth for key horizons (such as the Lava Creek B ash bed) in nearby boreholes. Boreholes near the Mt. General fault are too sparse to definitively identify fault-caused disruption, although the mudflat deposits could be interpreted as downdropped to the northeast (Fig. 4).

Conclusions

Hinkley Valley is underlain by a lithologically and structurally complex assembly of deposits largely of middle Pleistocene age, almost entirely sourced by the ancestral Mojave River. Initial deposits of the Mojave River are interpreted as stream and wetland deposits leading to a shallow lake. As the lake rose it overlapped stream and shore-margin deposits to occupy much of the valley. Identification of the ~631 ka Lava Creek B ash bed in this sequence of deposits shows it to be middle Pleistocene in age. The lake was succeeded by a complex of delta, near-shore, and mudflat deposits interlayered with stream sediment. Above this complex interval is a thick (locally greater than 30 m [100 ft]) sequence of predominantly stream sediment, that completed the filling of the valley. The Hinkley Valley infill period preceded river flow to downstream Lake Manix. However, as much as 6-7 m (20-23 ft) of lake and stream sediments

were deposited locally much later, about 45-40 ka, by a temporarily rerouted Mojave River that flowed northward along the valley. This stratigraphic framework, along with disruption by two youthful fault systems, have implications for the hydrologic behavior of Hinkley Valley.

Acknowledgments

We thank colleagues John Izbicki, Krishangi Groover, Chris Stamos, and Brett Cox for guidance and sharing of critical information that have greatly aided our studies. John Izbicki and Jeff Knott provided helpful reviews of an early draft of this paper. Staff associated with the drilling program at Hinkley Valley, in particular Betsy Brunswick, Chris Maxwell, Dennis Maslonkowski, and Margy Gentile, have supplied a wealth of data and made sediment cores available to us, for which we are grateful. Lastly, Norm Meek, Anna Garcia, and Jeff Knott have shared their studies in northern Hinkley Valley, which provided an early introduction to the area.

References

- Andrew, J.E., and Walker, J.D., 2017, Path and amount of dextral fault slip in the Eastern California shear zone across the central Mojave Desert: Geological Society of America Bulletin, doi: 10.1130/B31527.1.
- Boettcher, S.S., 1990, Geologic Map of Iron Mountain: Geological Society of America Digital Map and Chart Series 19, 1:12,000 scale, doi: 10.1130/1990-boettcher-ironmountain.
- Bryant, W.A., 1987, Recently active traces of the Harper, Blackwater, Lockhart, and related faults near Barstow, San Bernardino County, California: California Division of Mines and Geology Fault Evaluation Report 189, in Fault Evaluation Reports Prepared Under the Alquist-Priolo Earthquake Fault Zoning Act, Region 2 – Southern California: California Geological Survey CGS CD 2002-02 (2002).
- Cox, B.F., Hillhouse, J.W., and Owen, L.A., 2003, Pliocene and Pleistocene evolution of the Mojave River, and associated tectonic development of the Transverse Ranges and Mojave Desert, based on borehole stratigraphy studies and mapping of landforms and sediments near Victorville, California, in Enzel, Y., Wells, S.G., and Lancaster, N., eds., Paleoenvironments and paleohydrology of the Mojave and southern Great Basin Deserts: Boulder, Colorado, Geological Society of America Special Paper 368, p. 1–42.
- Dibblee, T.W., Jr., 1960a, Geologic map of the Barstow quadrangle, San Bernardino County, California: U.S. Geological Survey Mineral Investigations Field Studies Map MF-233, scale 1:62,500.
- Dibblee, T.W., Jr., 1960b, Geologic map of the Hawes quadrangle, San Bernardino County, California: U.S. Geological Survey Mineral Investigations Field Studies Map MF-226, scale 1:62,500.
- Dokka, R.K., and Travis, C.J., 1990, Late Cenozoic strike-slip faulting in the Mojave Desert, California: Tectonics, v. 9, no. 2, p. 311–340.

- Fletcher, J.M., Bartley, J.M., Martin, M.W., Glazner, A.F., and Walker, J.D., 1995, Large-magnitude continental extension; an example from the central Mojave metamorphic core complex: *Geological Society of America Bulletin*, v. 107, p. 1468–1483.
- Garcia, A.L., Knott, J.R., Bright, J., and Mahan, S.A., 2014, Geochronology and paleoenvironment of pluvial Harper Lake, Mojave Desert, California: *Quaternary Research*, v. 81, p. 305–317.
- Glazner, A.F., Walker, J.D., Bartley, J.M., and Fletcher, J.M., 2002, Cenozoic evolution of the Mojave block of southern California, *in* Glazner, A.F., Walker, J.D., Bartley, J.M., eds., *Geologic evolution of the Mojave Desert and southwestern Basin and Range: Geological Society of America Memoir 195*, p. 19–41.
- Haddon, E.K., Miller, D.M., Langenheim, V.E., Liu, Tanzhuo, Walkup, L.C., Wan, Elmira, this volume, Initiation and rate of slip on the Lockhart and Mt. General faults in southern Hinkley Valley, California.
- Izbicki, J.A., and Groover, K., 2016, A plan for study of natural and man-made hexavalent chromium, Cr(VI), in groundwater near a mapped plume, Hinkley, California: U.S. Geological Survey Open-File Report 2016-1004, 12 p.
- Jachens, R.C., Langenheim, V.E., and Matti, J.C., 2002, Relationship of the 1999 Hector Mine and 1992 Landers fault ruptures to offsets on Neogene faults and distribution of late Cenozoic basins in the eastern California shear zone: *Bulletin Seismological Society America*, v. 92, p. 1592–1605.
- Matthews, N.E., Vazquez, J.A., and Calvert A.T., 2015, Age of the Lava Creek supereruption and magma chamber assembly at Yellowstone based on $^{40}\text{Ar}/^{39}\text{Ar}$ and U-Pb dating of sanidine and zircon crystals: *Geochemistry, Geophysics, Geosystems*, v. 16, p. 2508–2528, doi:10.1002/2015GC005881
- Meek, N., 1999, New discoveries about the late Wisconsin history of the Mojave River system, *in* Reynolds, R.E., and Reynolds, J., eds., *Tracks along the Mojave: A field guide from Cajon Pass to the Calico Mountains and Coyote Lake: Redlands, California, San Bernardino County Museum Association Quarterly*, v. 46, no. 3, p. 113–117.
- Miller, D.M., Dudash, S.L., Green, H.L., Lidke, D.J., Amoroso, L., Phelps, G.A., and Schmidt, K.M., 2007, A new Quaternary view of northern Mojave Desert tectonics suggests changing fault patterns during the late Pleistocene, *in* Miller, D.M., and Valin, Z.C., editors, *Geomorphology and tectonics at the intersection of Silurian and Death Valleys, southern California: U.S. Geological Survey Open File Report 2007-1424*, p. 157–171, available at <http://pubs.usgs.gov/of/2007/1424/of2007-1424.pdf>
- Pigati, J.S., Miller, D.M., Bright, J.E., Mahan, S.A., Nekola, J.C., and Paces, J.B., 2011, Chronology, sedimentology, and microfauna of groundwater discharge deposits in the central Mojave Desert, Valley Wells, California: *Geological Society of America Bulletin*, v. 123, p. 2224–2239.
- Reheis, M.C., Bright, J., Lund, S.P., Miller, D.M., Skipp, G., and Fleck, R.J., 2012, A half-million year record of paleoclimate from the Lake Manix core, Mojave Desert, California: *Palaeogeography, Palaeoclimatology, Palaeoecology*, v. 365–366, p. 11–37.
- Reynolds, R.E., and Reynolds, R.L., 1994, The isolation of Harper Lake basin, *in* Reynolds, R.E., ed., *Off limits in the Mojave Desert: Redlands, California, San Bernardino County Museum Association Special Publication 94–1*, p. 34–37.

Cajon Pass: a classic geologic textbook

Robert E. Reynolds¹ and Michael O. Woodburne²

¹CSU Desert Studies Research Associate, Redlands, CA 92373, bob.reynolds220@gmail.com

²Department of Earth Sciences, Emeritus, University of California, CA 92521, mows@npgcable.com

ABSTRACT—In Cajon Pass, students can take a short walk across the San Andreas Fault Zone from the Pacific Oceanic Plate to the North American Continental Plate and investigate depositional environments that contain a biostratigraphic record that spans 70 million years. Fossils provide the clues.

An articulated elasmosaur verifies a late Cretaceous age for the marine Cosy Dell Formation. The younger, earliest Miocene Vaqueros Formation contains mollusks, rays, and the dolphin *Allodelphis woodburnei*. These marine strata are overlain by deposits of continental arkose derived from the central Mojave Block. Fossil plants and gastropods in the Cajon Valley Beds are associated with bones and teeth of mammals that span the early Miocene Hemingfordian and Barstovian North American Land Mammal Ages (NALMA). Adjacent to the east, across the Squaw Peak Fault, is the Crowder Formation. Deposition of the Crowder sediments started during the Hemingfordian NALMA, as did the Cajon Valley Beds, but mammal fossils suggest that deposition of the first half of the Crowder continued through 7 Ma in the late Miocene. Projecting increased rates of deposition for the upper half of the section, the Crowder Basin may have been receiving sediment from the Victorville area until 4 Ma.

Although both Miocene basins are presently in proximity, it appears that the Crowder basin was located farther east than today. As noted above its depositional history was different from that of the Cajon basin. In addition to their Mojave source, late Barstovian elements of the northwestern Cajon Valley beds were in part derived across elements of the then-active proto-San Andreas fault.

More recent activity on the San Andreas Fault accompanied the continued rising of the San Gabriel Mountains, depositing Pleistocene sediments near the top of the In-face Bluffs. These units include the Phelan Peak Formation which records the change in drainage at 2 Ma, from south toward the Pacific Ocean to north into the internally drained Mojave Block. The Phelan Peak is overlain by the Harold Formation, Shoemaker Gravels and Noble's Old Alluvium, the latter recording the Brunhes–Matuyama reversal (781,000 years ago). The 70 Ma long biostratigraphic sequence of Cajon Pass has been exposed by northerly headward erosion along the drainages of Cajon and Crowder creeks.

Introduction

The San Andreas Fault Zone (SAFZ) in Cajon Pass marks the eastern margin of the Pacific Oceanic Plate and the western margin of the North American Continental Plate. At Blue Cut in Cajon Pass, the Pacific Plate consists of highly metamorphosed glaucophane and actinolite schist. Across the SAFZ to the east, the North American Plate consists of Mesozoic granitic rock, Cretaceous and Oligocene marine sediments, with a 20 million year history of continental basin filling, followed by the uplift of the Transverse Ranges. Students of life history can study changes in marine life and terrestrial mammals from investigate the biostratigraphic record spanning 70 million years.

Structure

Cajon Valley (Figure 1) is now bounded on the west by the San Andreas Fault, which also cuts the Cajon Valley Fault that forms the western margin of the Cajon Valley

Beds. During deposition, the proto-San Andreas Fault was forming in northern California at about 16 Ma (Nicholson et al., 1994). At this time the San Gabriel Fault was the major element of the proto-San Andreas system in the Cajon area, and it is likely that the Cajon Valley Fault was associated with the San Gabriel Fault from about 12 Ma (Woodburne, 2015). Subsequently, at about 6 Ma, the modern San Andreas Fault was developed in the Cajon Valley area, associated with the opening of the Gulf of California. The Squaw Peak thrust fault, which now separates the Crowder Formation and Cajon Valley Beds, was active from about 9 Ma (Meisling and Weldon, 1989), and led to the modern close proximity of those sedimentary units.

About 18 million years ago, the activity on the proto-San Andreas system caused clockwise rotation of regions that later became San Gabriel Mountain Range and San Bernardino Mountain Ranges (Dickinson, 1996). Rotation opened basins that were filled by the Cajon

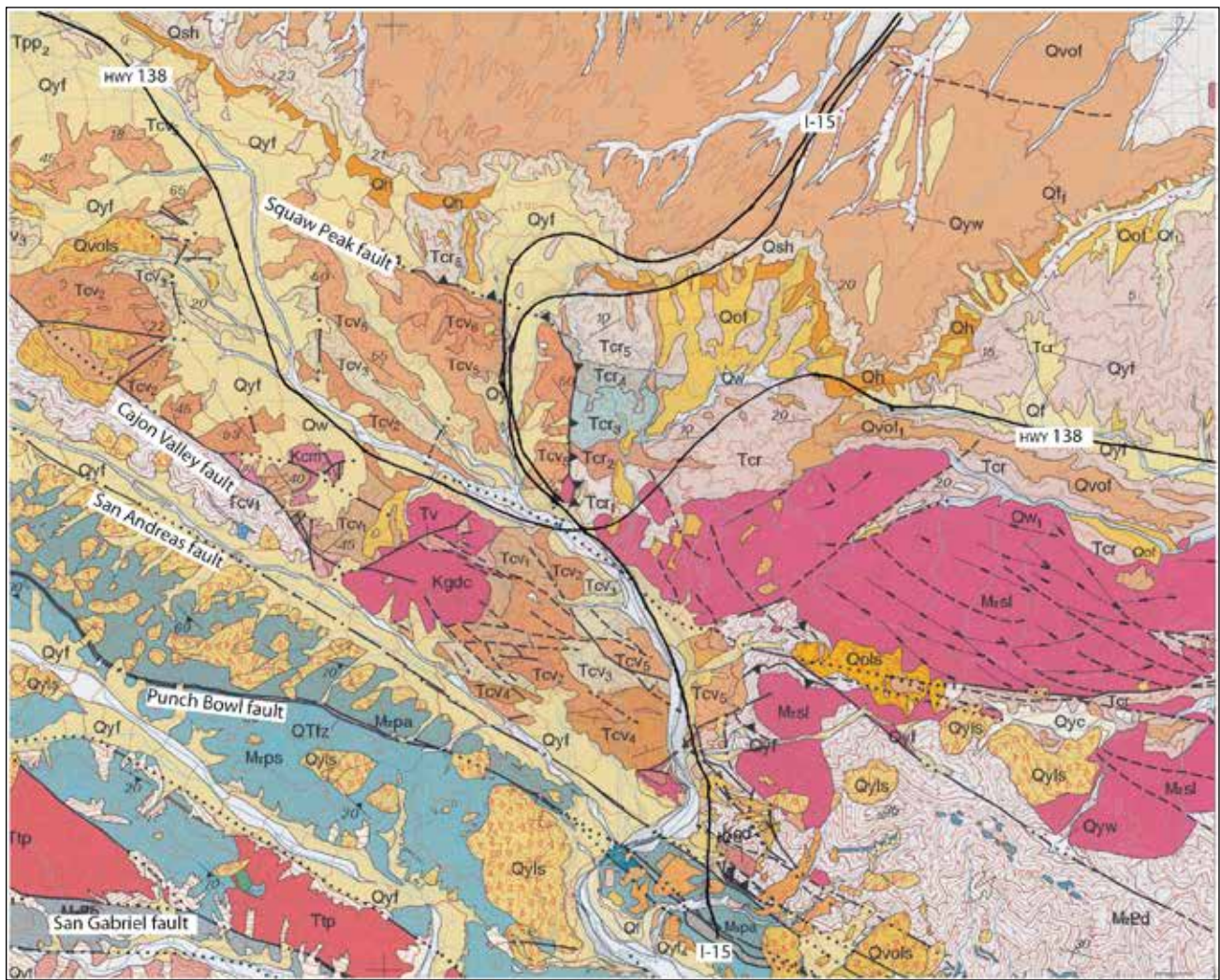


Figure 1. Geologic map of the Cajon Pass area, adapted from Morton and Miller, 2008, showing major highways and faults. Qof: Old alluvial fan deposits; Qsh: Shoemaker Gravel; Qh: Harold Formation; Tcr: Crowder Formation; Tcv: Cajon Valley Formation units; Tv: Vaqueros Formation; Kgd: Cretaceous Cosy Dell Formation.

Valley Beds (Woodburne and Golz, 1972) from 18 to 12.7 Ma (Liu, 1990) and the Crowder Formation from 18 to about 3 Ma (Weldon, 1985; Liu, 1990; Reynolds and others, 2008). The Miocene basins were covered with north-flowing Pliocene and Pleistocene debris when the eastern Transverse Ranges started rising about three million years ago. The Phelan Peak Formation is overlain by the Harold Formation, Shoemaker Gravels and Noble's Old Alluvium, the latter recording the Brunhes-Matuyama reversal (781,000 years ago), near the top of the In-face Bluffs. Those ranges reached their maximum height (11,000 ft) only a half a million years ago.

Stratigraphy and biostratigraphy

Cretaceous Cosy Dell Formation

The oldest nonmetamorphosed sediment in Cajon Pass is the Late Cretaceous marine San Francisquito Formation (Kooser, 1985; Lucas and Reynolds, 1991). The "Paleocene" San Francisquito Formation was renamed as the Cretaceous Cosy Dell Formation (Morton and

Miller, 2008) due to the presence of forty articulated elasmosaurid plesiosaur vertebrae (Lucas and Reynolds, 1991), with elasmosaur being a late Cretaceous indicator fossil. Other associated fossils include crustacean pinchers, fish scales, scaphopods, and gastropods.

Deposition of the Cretaceous Cosy Dell Formation was followed by a local 40 Ma depositional hiatus. Comparisons of other San Francisquito Formation outcrops could determine if later sediments have also been removed by an erosional event of unspecified cause.

Early Miocene Vaqueros Formation

The early Miocene Vaqueros Formation contains the long-snouted dolphin *Allodelphis woodburnei* of the superfamily Platanistoidea (Barnes and Reynolds, 2007, 2008), an early marine relative of the fresh water Ganges River dolphin. The Vaqueros Formation is rich in oyster shells and barnacle fragments. The dolphin skeleton was associated with fossils of elasmobranchs, the echinoid *Scutella fairbanksi*, and the mollusks *Crassatella granti*, *Ostrea titan subtitan*, and *Pecten sespeensis*. The presence

of the gastropod mollusk *Turritella inezana* in this marine deposit helps to establish its Early Miocene age (22Ma, Woodring, 1942).

Middle Miocene Cajon Valley Beds

The Cajon Valley Beds (Units 2 – 6) contain terrestrial land mammals that represent the late Hemingfordian through Barstovian NALMA (Woodburne and Golz, 1972; Reynolds et al., 2008). Magnetostratigraphy (Liu, 1990) shows that deposition of Units 2–6 continued for five million years from 17 Ma until 12.7 Ma. Fossil mammals include the oreodont (Woodburne and Golz, 1972), peccary, small and large camels, deerlets, small forest horses, large grassland horses, rhinoceros, chalicotheres (Coombs and Reynolds, 2015), rabbits and rodents, hedgehogs, shrews, badgers and bears (Wagner and Reynolds, 1983; Reynolds, 2015).

Miocene Crowder Formation

Magnetostratigraphy (Weldon, 1985; Liu, 1990) indicates that deposition of the Crowder Fm began 17+ Ma. Time-diagnostic rodents at the top of Unit 3 in the middle of the Crowder sequence indicate a Hemphillian age of 7.1 Ma (Reynolds and others, 2008). The greater than twelve million year depositional record has produced Hemingfordian, Barstovian and Hemphillian millipedes, lizards, small and large camel, antelope, forest horses, grassland horses, tapir, rhinoceros, weasels and badgers (Lofgren and Abersek, 2018), bone-crushing dogs, rabbits and rodents (Lindsay and Reynolds, 2008), squirrels and flying squirrels, shrews and hedgehogs (Reynolds and others, 2008).

Although presently separated from the Cajon Valley Beds by the Squaw Peak Fault, the Crowder basin was originally located farther east and its depositional history differs from that in the Cajon basin. Both formations have a source of lithic clasts from the Mojave Block. The late Barstovian elements of the northwestern Cajon Valley beds were in part derived from the northwest across elements of the then active proto-San Andreas Fault. Current directions within the lower and upper Crowder Formation developed by Foster (1980) indicate most sources for clasts in the Crowder were from the north. Projections of depositional rates (Reynolds and others, 2008) suggest that the upper Crowder Formation unit 5 may be younger than 5 Ma, and within the 4-3 Ma time range of the south flowing ancestral Mojave River (Cox and others, 1998; Cox and Tinsley, 1999; Reynolds and Cox, 1999; Cox and others, 2003).

Phelan Peak Formation

Magnetostratigraphy and clast analysis (Weldon, 1985) of the Phelan Peak Formation demonstrates that the lower unit was receiving sediment at 4 Ma from the Mojave Block to the northeast. The middle unit consists of playa silts and pond sediments deposited in a west northwesterly

trending basin parallel to the SAFZ. The upper unit started receiving clasts from the San Gabriel Mountains to the west prior to 2 Ma (Meisling and Weldon, 1989).

The Phelan Peak Formation is overlain unconformably by time- and topography-transgressive Pleistocene sediments derived from the eastern Transverse Ranges to the west and south. These units are exposed in the In-face Bluffs around the northern margin of Cajon Valley.

Harold Formation

In Cajon Pass, the Harold Formation was deposited unconformably upon the Phelan Peak Formation between 1.7 and 1.4 Ma (Weldon, 1985). The Harold Formation consists of arkosic conglomerate with occasional paleosols.

Shoemaker Gravels

The Shoemaker Gravels were deposited conformably upon the Harold Formation between 1.4 and 0.8 Ma (Weldon, 1985), and are coarse arkosic sediments with coarse clasts of varying size.

Nobles Old Alluvium

The Old Alluvium of Noble contains clasts coarser than the Shoemaker Gravels, signifying an increase in rate of uplift of the San Gabriel Mountains. The Old Alluvium was shed from the San Gabriel Mountains starting at 0.8 through 0.4 Ma and contains the Brunhes/Metayama reversal of 781,000 years (Weldon, 1985). The coarseness shows that the San Gabriel Mountains reached their maximum height only 500,000 years ago.

Victorville Fan Complex

Together, the Harold, Shoemaker and Old Alluvium make up the Victorville Fan Complex. This sequence records drainage from the Mojave Block southwest toward the Pacific Ocean and subsequent reversal of drainage northeast into the Mojave Block as the Transverse Ranges began to rise. At Victorville, deep borehole data demonstrate that south-trending streams brought clasts of Jurassic and early Miocene volcanic rocks from the Mojave Desert, not from the Transverse Ranges, and include lithologies from the Kramer Hills and outcrops near Barstow. Borehole magnetostratigraphy suggests that the top of the south-flowing lower unit is about 2.5 Ma (Cox and others, 1998). This would be within the 4 to 2 Ma range of the lower unit of the Phelan Peak Formation in western Cajon Pass, or the projected age range of the Crowder Formation (4-3 Ma, Reynolds and others, 2008) in eastern Cajon Pass.

Present Cajon Basin

Headward erosion of the Cajon Creek drainages followed the brecciated rock of the SAFZ. When encountering the softer sediments on the North American Plate, the drainage system widened to include West Cajon Wash and Crowder Creek. Broadening of the drainages systems in

the Cajon basin created an amphitheater bounded on the northwest and northeast by the In-face Bluffs.

Many questions remain in Cajon sediments to be answered by students of geology and paleontology. A few of those questions include:

- A) Does the fossil record in the Cretaceous Cosy Dell Formation suggest the presence of the Cretaceous/Tertiary Boundary? Can the basal conglomerate describe the original geographic position of this formation? What was the cause of the overlying 40 Ma erosional hiatus?
- B) What were the structural events that caused the many different sedimentary facies and inferred habitats in the Cajon Valley and Crowder formations?
- C) Do clasts and facies in the upper Crowder Formation suggest a connection with south-flowing sedimentary sources from Victorville between 4 to 3 Ma?

Acknowledgements

The authors thank David Miller for thoughtful review and comments that benefited this paper. The authors also acknowledge the many hours assistance and research contributed by students and museum volunteers that produced the current biostratigraphic picture that we have of the sequence in Cajon Pass.

References

- Barnes, L. G., and R. E. Reynolds, 2007. A primitive Early Miocene platanistoid dolphin (Cetacea: Odontoceti) from Cajon Pass, San Bernardino County, California. R. E. Reynolds (ed.), *The 2007 Desert Symposium*. Desert Studies Consortium, California State University, Fullerton, California. Abst. p. 107.
- Barnes, L. G., and R. E. Reynolds, 2008. A new species of Early Miocene allodelphinid dolphin (Cetacea, Odontoceti, Platanistoidea) from Cajon Pass, Southern California, U. S. A., in Albright, L. B., *Museum of Northern Arizona Bull.* No. 65, p. 483-508.
- Coombs, M. C. and R. E. Reynolds, 2015. Chalicotheriid material (Perissodactyla, Chalicotheriidae, Schizotheriinae) from late Hemingfordian and early Barstovian faunas of the Cajon Valley Formation in the Mojave Desert Province of southern California, p. 259-273.
- Cox, B. F., J. W. Hillhouse, A. M. Sarna-Wojcicki, and J. C. Tinsley, 1998. Pliocene-Pleistocene depositional history along the Mojave River north of Cajon Pass, California—regional tilting and drainage reversal during uplift of the central Transverse Ranges: *Geol. Soc. Amer. Abstracts with Programs*, v. 30, no. 5, p.11.
- Cox, B. F., and J. C. Tinsley, III, 1999. Origin of the late Pliocene and Pleistocene Mojave River between Cajon Pass and Barstow, California. *San Bernardino County Museum Association Quarterly* vol. 46(3):49-54.
- Cox, B. F., J. W. Hillhouse, and L. A. Owen, 2003. Pliocene and Pleistocene evolution of the Mojave River, and associated tectonic development of the Transverse Ranges and Mojave Desert, based on borehole stratigraphy studies and mapping of landforms and sediments near Victorville, California, in *Paleoenvironments and Paleohydrology of the Mojave and Southern Great Basin Deserts*, Y. Enzel, S.G. Wells, and N. Lancaster, eds. Geological Society of America Special Paper 368, p. 1-42.
- Dickinson, W. R., 1996. Kinematics of transrotational tectonism in the California Transverse Ranges and its contribution to cumulative slip along the San Andreas transform fault system. *Geological Society of America Special Paper* 305, p.1-46.
- Foster, J. H., 1980. Late Cenozoic tectonic evolution of Cajon Valley, Southern California. Ph.D. diss., University of California at Riverside, 238 pp.
- Kooser, M. A., 1985. Paleocene Plesiosaur? in *Geologic investigations along Interstate 15, Cajon Pass to Manix Lake: Redlands, San Bernardino County Museum*, p. 43-48.
- Lindsay, E. H., and R. E. Reynolds, 2008. Heteromyid rodents from Miocene faunas of the Mojave Desert, Southern California. *Natural History Museum of Los Angeles County. Science Series* 41; p. 213-236.
- Liu, Wei, 1990. Paleomagnetism of Miocene sedimentary rocks in the Transverse Ranges: The implications for tectonic history. Unpublished doctoral thesis, California Institute of Technology, Pasadena, California. p. 1-218.
- Lofgren, D. and W. Abersek, 2018. New records of *Miomustela* from the Barstow and Crowder formations of California. *California State University, Fullerton Desert Studies Consortium*, (this volume).
- Lucas, S. G., and R. E. Reynolds, 1991. Late Cretaceous (?) plesiosaurs from Cajon Pass, California. pp. 52-53 in M. O. Woodburne, R. E. Reynolds, and D. P. Whistler (eds.), *Inland Southern California: the last 70 million years*. San Bernardino County Museum Association Quarterly 38(3, 4).
- Meisling, K.E., and R.J. Weldon, 1989. Late Cenozoic tectonics of the northwestern San Bernardino Mountains, southern California. *Geological Society of America Bulletin* 101:106-128.
- Morton, D. M. and F. K. Miller, 2008. Preliminary geologic map of the San Bernardino 30'x60' quadrangle, California: United States Geological Survey Open-File Report 03-293. Available at: <http://pubs.usgs.gov/of/2003/of03-293/>. Accessed January 4, 2018.
- Nicholson, C., Sorien, C.C., Atwater, T., Crowell, J.C., and Luyendyk, B.P., 1994. Microplate capture, rotation of the western Transverse Ranges, and initiation of the San Andreas transform as a low-angle fault system. *Geology* 22, p. 491-495.
- Reynolds, R.E., R. L. Reynolds, and E. H. Lindsay, 2008. Biostratigraphy of the Miocene Crowder Formation, Cajon Pass, southwestern Mojave Desert, California. *Natural History Museum of Los Angeles County. Science Series* 41; p. 237-254.
- Reynolds, R. E., and B.F. Cox, 1999. Tracks along the Mojave: a field guide from Cajon Pass to the Manix Basin and Coyote Lake. *San Bernardino County Museum Association Quarterly* 46(3):1-26

- Reynolds, R. E., 2015. New ursid and talpid occurrences from Hemingfordian and Barstovian units of the Cajon Valley Formation, Cajon Pass, California p. 281-283.
- Wagner, H.M., and R. E. Reynolds, 1983. *Leptarctus ancipidens* (Carnivora: Mustelidae) from the Punchbowl formation, Cajon Pass, California: Bulletin of the Southern California Academy of Sciences, p. 131-137.
- Weldon, R. J. 1985. Implications of the age and distribution of the late Cenozoic stratigraphy in Cajon Pass, Southern California. *In* Geological investigations along Interstate 15, Cajon Pass to Manix Lake, California, ed. R.E. Reynolds, 59-68. Redlands, California: San Bernardino County Museum, 191pp.
- Woodburne, M. O. and D. J. Golz, 1972. Stratigraphy of the Punchbowl Formation, Cajon Valley, southern California. University of California Publications in Geological Sciences 92, p. 1-57.
- Woodring, W. P., 1942. Marine Miocene mollusks from Cajon Pass, California. *Journal of Paleontology* 16:78-83.

Fault structure and biogenic soil calcite near Ivanpah Spring, Clark Mountain, San Bernardino County, California

David K. Lynch¹, Paul M. Adams², and David S. P. Dearborn³

¹Thule Scientific, corresponding author, david@alumni.caltech.edu; ²Thule Scientific; ³Lawrence Livermore National Laboratory

ABSTRACT: Based on offset channels, soil color and vegetation lineaments along its approximately 2.5 km surface exposure, the Ivanpah Spring Fault appears to be a right lateral transform fault striking ~N45W. It shows a right-hand bend or step-over (releasing bend) near Ivanpah Spring with an offset of about 50 m. Direct surveying and topographic maps derived by stereo imagery reveals an indentation in the elevation profile through the step-over region. It appears to be a small, sag-like transtensional pull-apart that is ~35 m across and ~2 m deep. The “sag,” however, does not collect standing water because it is on a slope and has no elevation minimum. The lowest part of the sag has dark brown soil and also has the lowest slope in the transect, nearly horizontal. Surface run off would flow slower here than in steeper parts and the sag would tend to absorb more runoff water. This may explain the enhanced vegetation in the sag, which attracts herbivores, mainly cows and burros. Field inspection, photomicrography, X-ray diffraction (XRD), infrared spectroscopy (IRS), energy dispersive X-ray spectroscopy (EDS), and thermogravimetric Analysis (TGA) of soils along the transect through the sag reveal that the dark soil is due to relatively large amounts of dung (and by association urine) with elevated amounts of CaCO₃. There is a strong correlation between organic material (C-H) and pedogenic CaCO₃. We suggest that the CaCO₃ originates primarily from herbivore urine, though some of it may be the result of biomineralization by urealytic bacteria acting on decomposing dung through microbiologically induced calcite deposition (MICD).

1. Introduction

Ivanpah Spring (35.540303 -115.529610) is man-modified seep¹ in a former gold and silver mining area² on the southeast flank of Clark Mountain (Figure 1) in San Bernardino County (Ivanpah Quadrangle). The country rock is primarily a Precambrian metamorphic complex of foliated gneissic with alkali feldspar igneous intrusions and dikes³⁻⁵. Springs are often associated with faults⁶ and the Ivanpah Spring Fault passes through or near the spring. The fault was identified and mapped from aerial photographs and field inspection. In this paper we (1) report field observations of fault structures near the spring and (2) present evidence for biologically induced pedogenic CaCO₃ in a dung-rich sag-like feature.

2. Surveying the fault

We visited the site several times during 2017, and the fault trace was visually inspected on foot along its ~2.5 km long surface exposure. Particular attention was paid to a small region located ~50 m WSW of the spring

with uncharacteristically dark brown soil and showed unusual slope changes, vegetation enhancements and scattered groundwater discharge deposits. Using a handheld Garmin 60CSx receiver, we measured vertical profiles of transects that ran more or less along the line of

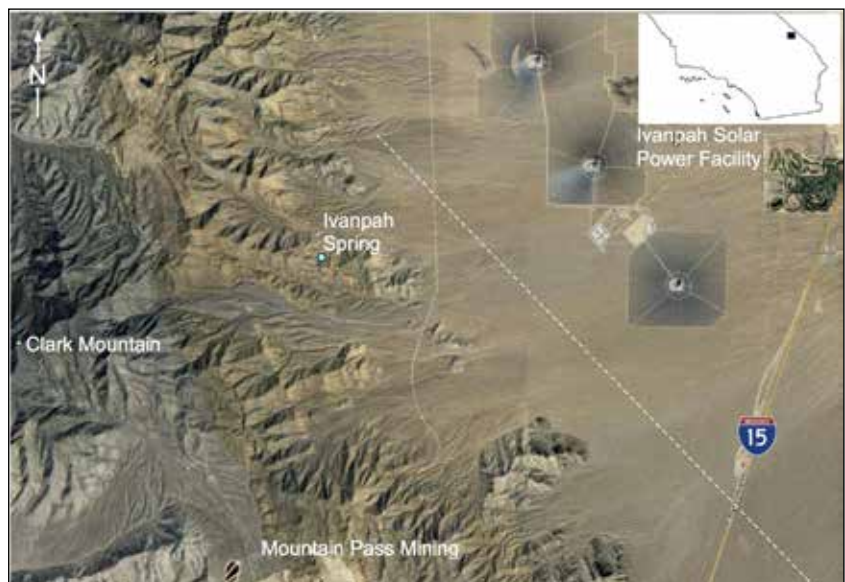


Figure 1. Annotated Google Earth map of the Ivanpah Spring area. The Clark Mountain Fault system is evident to the left as two ~N30E striking lineaments. The white dashed line is the approximate location of the putative Ivanpah Fault based on Wilkerson's map⁵.



Figure 2. (A) Google Earth image showing the location of Ivanpah Spring (yellow pushpin at the center of image). (B) Fault trace based on offset streams and soil color boundaries. (C) Fault trace when vegetation enhancements and unusual topography are included.

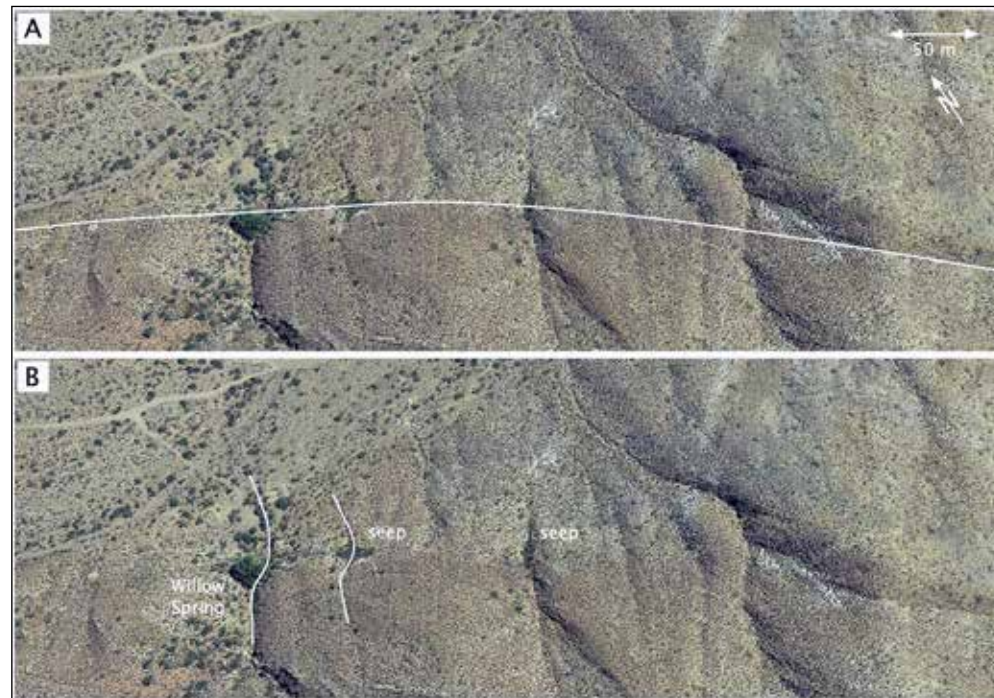


Figure 3. Two stream channels show apparent right lateral offset along the fault. (A) The white line shows the inferred fault trace. (B) Two white curved lines mark channel offset of Willow Spring and an unnamed seep.

steepest decent starting and ending in areas with typical vegetation and soil colors and passing through the brown area. The transects were nearly perpendicular to the strike of the fault. Elevation was measured approximately every

tongue of land, the curvature of the fault as seen in map view suggests that it is steeply dipping, possibly to the southwest. Mapped features highlighted on Figure 3

15 meters along the transects' 110 m lengths. Soil samples were collected at six locations, two of them in the area of brown soil.

After placing seven control point markers around the area, we took stereo pictures of the site separated by 75 m from a nearby hill that was about 23 meters above the brown area and 110 meters from it. The stereo images were later processed to produce a digital surface model of elevations and contour map of the area, from which independent measurements of the transect profile were extracted.

3. Faults p roperties

Figure 2 shows a Google Earth photograph of the fault region as far as the fault can be visually followed. Figure 2A is presented with no interpretation. Figures 2B and 2C show two possible interpretations of the trace. The northwestern portion of the fault is well marked by offset stream channels, vegetation lineaments, soil color boundaries, linear gullies, and ridge notches (topographic saddles). Our original interpretation was that the fault passed through Ivanpah Spring. Further examination of the local topography suggested that there might be a bend or step over in the vicinity of the spring.

Being on an elevated

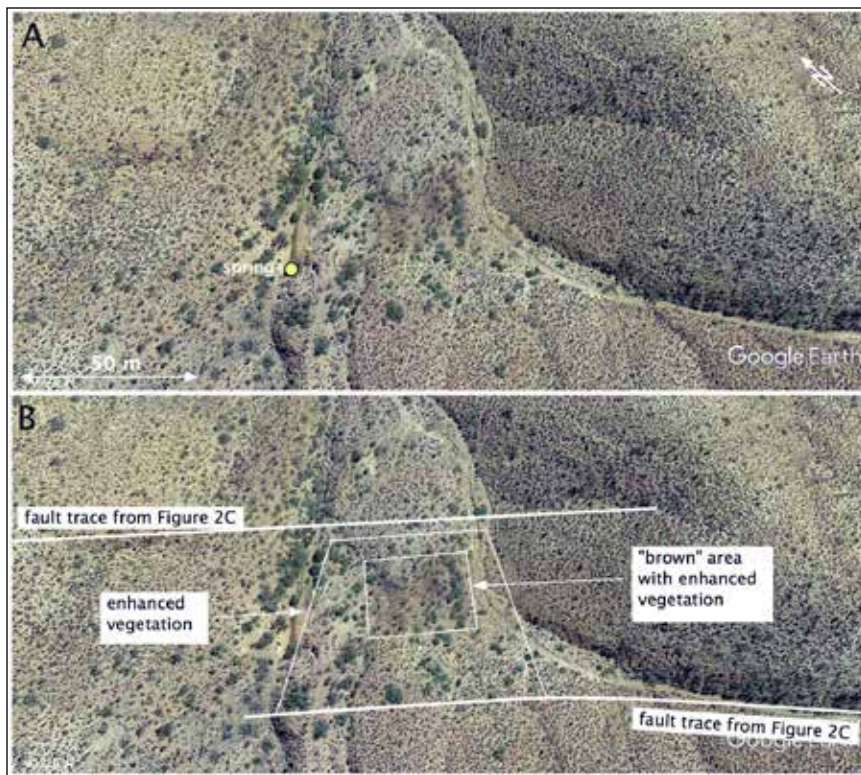
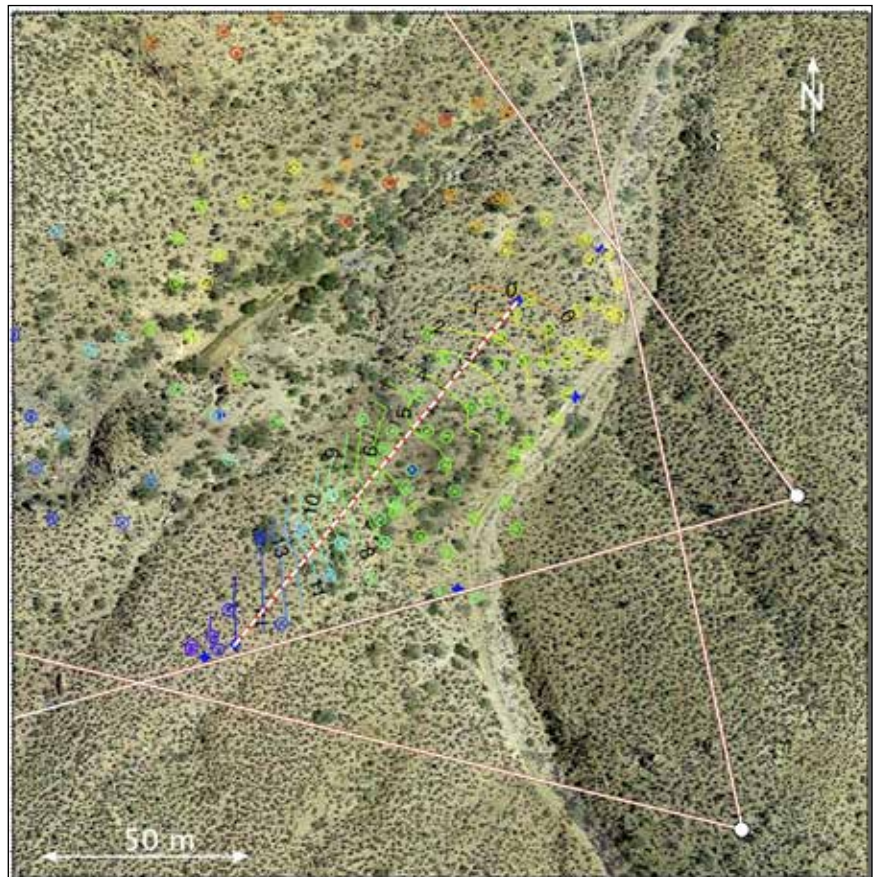


Figure 4. Step Over Region. A: Google Earth Image showing the location of Ivanpah Spring. B: Annotated Google Earth Image show the two inferred traces of the Ivanpah Spring Fault in the step over region based on field observations and Figure 2C.

suggest that the sense of slip includes a right-lateral component. Channels associated with Willow Spring and an unnamed seep both showed apparent right-hand channel offset and enhanced vegetation consistent with a subsurface barrier to groundwater flow.

Figure 5. Annotated Google Earth image of the topographic depression of interest overlaid with the derived elevation contours along the transect (dashed line). White dots are the camera locations for the stereo pair and the white lines attached to the dots show the field of view of each camera image. The contours are at 1-meter vertical elevation intervals. The stars are gps surveyed control points used to orient the cameras resulting in a defined altitude and azimuth for each pixel. Triangulated points are shown as circles with a cross. The colors vary with elevation (See PDF version of the paper in the 2018 proceedings volume at www.desertsymposium.org). The contours were generated by interpolation among these points in the area of interest within about twenty meters of the transect).



4. Survey Results

A right hand step in a right lateral transform fault should produce a pull-apart basin (sag) and we found topography consistent with geometric complexity of this type. The topographic depression is roughly rectangular (35 x 40 m) and shows a number of features that differed markedly from its surroundings (Figure 4). It contains a high concentration of visibly abundant animal dung (hence the color) that correlated with noticeably enhanced vegetation density. Soil color, composition and vegetation density outside the enhanced vegetation area is typical of the larger area. The lowest part of the brown area is nearly horizontal, in contrast to the overall $\sim 7^\circ$ slope of the region. We marked off a transect approximately 110 m long that ran downhill and through the depressed brown area. While walking along the transect, it was obvious that the

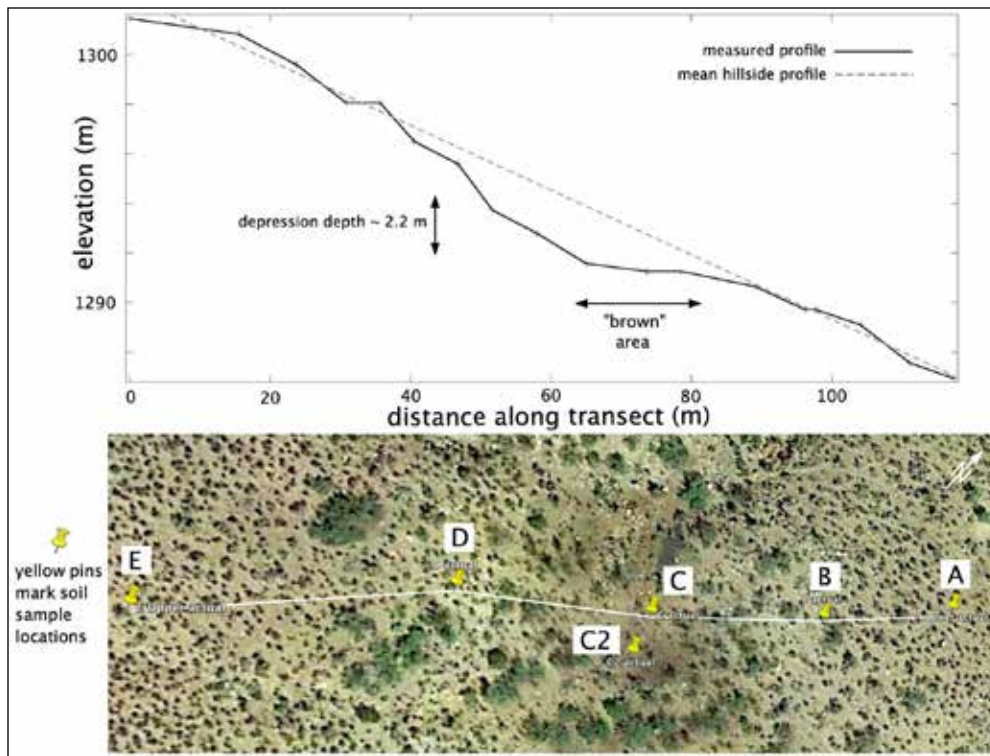


Figure 6. Upper: Transect profile. Lower: Google earth image with transect and soil sample locations. The smallest slope occurs in the brown area. C2 is about a meter lower than C.

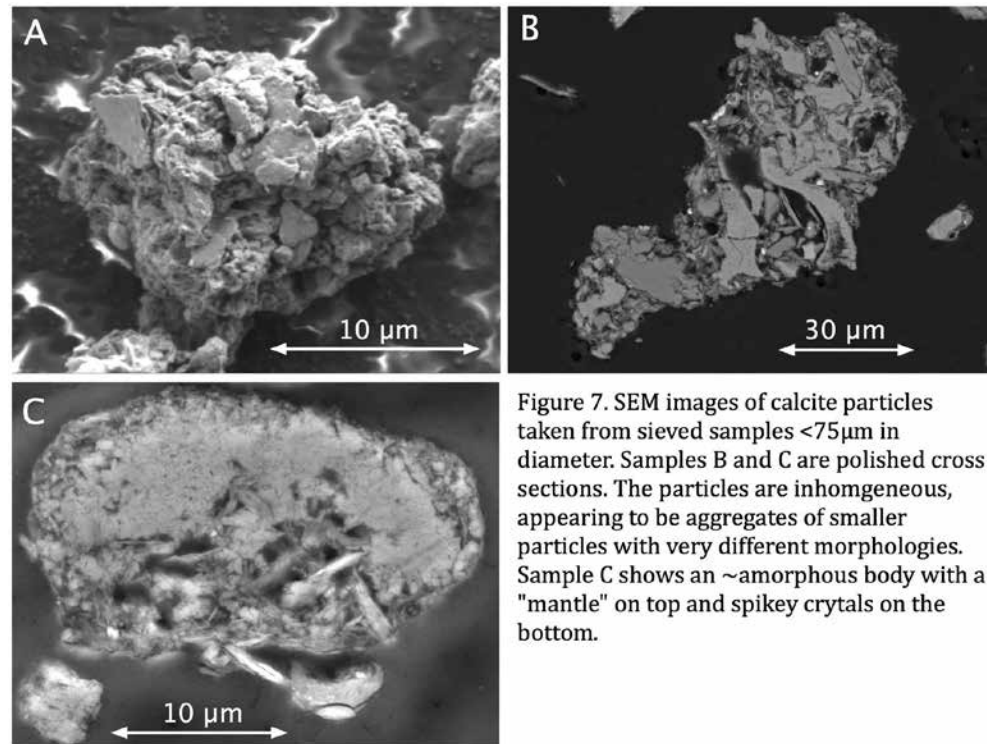


Figure 7. SEM images of calcite particles taken from sieved samples <75µm in diameter. Samples B and C are polished cross sections. The particles are inhomogeneous, appearing to be aggregates of smaller particles with very different morphologies. Sample C shows an ~amorphous body with a "mantle" on top and spikey crytals on the bottom.

slope was monotonic, i.e., at no point did it contain a local elevation minimum.

Elevation profiles of the transect were obtained three ways: (1) Google Earth topography, (2) walking the transect and marking positions with the Garmin, and (3) extracting profiles from a contour map produced from stereo imagery. All were consistent with one another.

Figure 5 shows the contour map and Figure 6 shows the profile obtained by averaging Garmin profiles.

The transect profile shows a depression about 50 m wide and 2.2 meters deep compared to the mean slope of the hillside. At its lower end the slope is small, almost horizontal but still with the same sign and the mean slope. At no place along the profile is there a minimum.

5. Soil Analysis

The purpose of analyzing the soil was to identify and map the composition, grain size and morphology of soil particles as a function of position along the transect. Surface soil samples were taken at six points along the transect (Figure 6) and sieved into three size groups: > 850 µm, 850 µm - 75 µm and <75 µm fractions, the latter of which were used for subsequent analyses. In samples C and C2 (and to lesser extent D) small seed husks and other plant debris were more common in the 850 µm - 75 µm fraction. X-ray diffraction (XRD) $\theta-2\theta$ scans were performed with copper radiation using a PANalytical X'Pert Pro diffractometer equipped with an X'celerator strip detector.

Fourier transform infrared (FTIR) measurements were

made with a Nicolet model 6700 spectrometer. Diffuse reflectance spectra were recorded with a Harrick Scientific Praying Mantis accessory using Labsphere Infragold as a background. Pseudo-transmission scans were performed with a Durascope single-bounce diamond attenuated total reflectance (ATR) accessory.

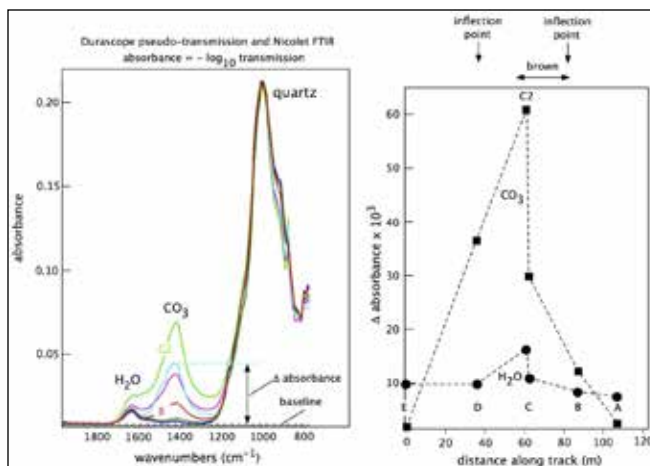


Figure 8. Left: Baseline corrected ATR reflectance FTIR spectra of the soil samples. Right: Relative signal strength of water and calcite along the transect. The upper end of the transect is at E and the lower end at A.

Soil samples in the 75 μm diameter range were potted in epoxy, sectioned and polished with 1 μm diamond paste. Automated particle analysis software in the SEM was used to measure size and composition, the latter using energy dispersive spectroscopy (EDS). Similar analyses were performed on loose particles. By number count, calcite particles were much more abundant in sample C (3.5%) than in sample E (0.13%). The calcite grains had a

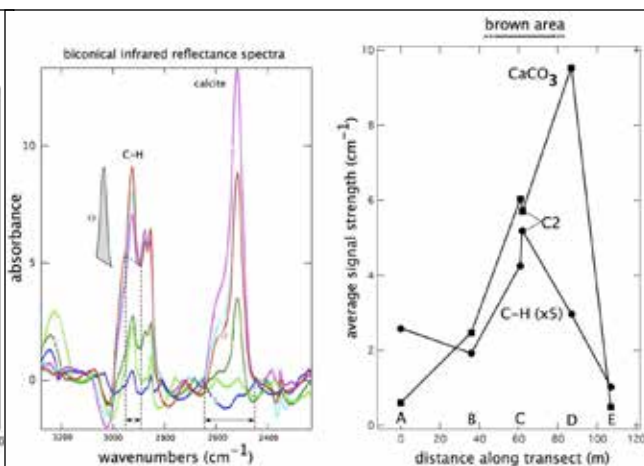


Figure 9. Left: Baseline corrected diffuse reflectance FTIR spectra of soil samples. The area of the C-H feature was measured between 2900 and 2952 cm^{-1} and is within a broader calcite feature. Another calcite feature lies between 2450 and 2650 cm^{-1} . The area of each feature was measured, an example of which is shown for location C2. Right: Peak areas of C-H and CaCO_3 along the transect. C-H and calcite clearly peak in or near the brown area (Figure 6).

coating of clay particles (Mg-Al-SiO_4) adhering to their surface and the calcite appeared to be aggregates rather than detrital (Figure 7).

Figure 8 shows ATR spectra of the soil samples normalized to the quartz peak. The CO_3 and H_2O features are well-separated, allowing relative abundance in each sample to be measured by noting height of the peak spectral features “ Δ ”. Clearly the water and calcite are well correlated. Diffuse reflectance spectra differ from ATR spectra by having very strong H_2O -OH features between 4000 and 2300 cm^{-1} . Absorption bands from C-H and CO_3 are also much stronger in this region of the reflectance spectra. Figure 9 shows baseline corrected reflectance spectra between 3200-2300 cm^{-1} . C-H features occur at 2924 cm^{-1} and 2854 cm^{-1} that are in close association with calcite peaks at 2983 cm^{-1} and 2875 cm^{-1} . C-H and CaCO_3 are evidently well correlated. Both Figure 8 and 9 show the highest concentration of C-H, H_2O and CaCO_3 in the in the brown area at locations C and C2.

Thermogravimetric analysis (TGA) and differential thermogravimetric analysis (DTG) were performed on the soil samples. The goal was to identify chemical components of the soil and estimate the relative abundance of them. Figure 10 shows the results for samples C and E. Strong peaks in DTG of sample C in the brown area show H_2O evaporation and CO_2 release as CaCO_3 dissociates. When the same analysis was performed on sample E (outside the brown area), the CO_2 peak was absent. Based on a molar analysis of sample C, the soil was 10% calcite by weight. For sample C2 it was 12%. The source of the minor peaks between 200 $^\circ\text{C}$ and 700 $^\circ\text{C}$ is not known but in view of the large amount of plant matter, they are most likely from thermal

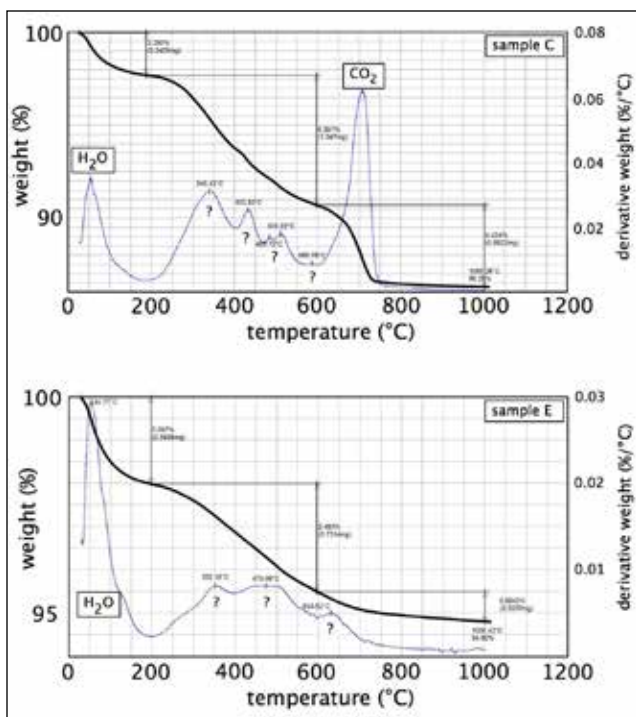


Figure 10. TGA and DTG of soil samples. Thick line is the sample weight as a function of temperature and the thin line is the negative derivative. Top: In Sample C in the brown area, the peak in the derivative at $\sim 50^\circ\text{C}$ is due to evaporation of water. Near 700 $^\circ\text{C}$ the peak is from the release of CO_2 as CaCO_3 dissociates. Bottom: Same analysis on sample E, well outside the brown area. Note the absence of the CO_2 peak

decomposition (thermolysis) of organic material, perhaps cellulose or lignin.

6. Discussion and Interpretation

The right lateral channel offsets and sag-like depression are consistent with right-lateral slip and a slight right bend or step over in the Ivanpah fault as shown in Figure 2C and Figure 4B. Fault motion may have produced a local pull-apart basin, or “sag”. Most sags collect water, and when the water evaporates, a white deposit of evaporites like halite and gypsum, are left. But this is not seen here because there is no closed basin in the vicinity of the topographic low. The depression in the profile can best be thought of as a “sag on a slope” or sidehill bench.

Enhanced vegetation is an indicator of increased soil moisture at the site. It may come from several sources: (1) tectonically crushed rock in the step-over region will open a conduit to the water table which is about few meters below the surface. Upward diffusion through the crushed rock will bring water near to the surface. (2) The speed of water (rain runoff) flowing along the surface will be lowest on the smallest slope. This occurs at the downhill part of the sag in the brown area. Thus it will spend more time in the sag and more readily percolate downward into the soil. (3) The bottom of the depression is closer to the water table than any other part of the transect, and thus one might expect enhanced vegetation. (4) Cow and burro urine will add water to the brown mantle of dung⁸⁻¹⁰.

The depression may be fairly young, formed during the Holocene or late Pleistocene. Otherwise soil creep and aeolian deposition would have likely infilled the depression. It is also not elongated along the trace as long-lived pull-apart basins are. Slippage along the fault may have recently started and present day slippage would maintain the sag. We do not know the soil movement or deposition/erosion rate in the area, but frequent visitations by herbivores might be expected to increase the infilling of the depression. There was no seismicity in the area associated with the fault¹¹ based on a full search of the USGS earthquake database. It is possible the area once did contain a minimum that collected water, which would also produce enhanced vegetation, but has since been partially filled to yield its current shape.

The brown area's color is due to animal dung, probably cows and burros that we frequently encountered near the spring. Deer and Bighorn sheep are also known in the area. Optical microscopy of soils in the brown area revealed that much of the material was organic: plant stems and seed casings. Plant fiber is composed primarily of cellulose and lignin and these materials are indigestible by herbivores. As a result, they are excreted and comprise much of the dung mass. For obvious reasons, dung and urine are spatially correlated. In view of the arid climate, the only year round source of surface water would seem to be herbivore urine.

Cow and horse (burro) urine contains CaCO_3 in solution as bicarbonate anions and in suspension as

sabulous calcite crystals^{8,9}. Additionally, the amount of calcite may be increased by the biomineralization, microbiologically induced calcite precipitation (MICP)¹⁰. Herbivore urine contains urea (CH_4NO_2), a product of protein breakdown. Dung is also rich in protein, which eventually breaks down into urea and ammonia (NH_3). In the presence of soil moisture, ureolytic bacteria produce ammonium and carbonate ions. This creates locally elevated carbonate concentrations that lead to supersaturation of soil solutions with respect to calcite. Calcite precipitates (biomineralization), thereby adding CaCO_3 to the soil where ever herbivores defecate and urinate. We have no direct evidence of this kind of biomineralization, so the C-H/ CaCO_3 correlation is most simply explained by calcite particles in herbivore urine.

The scenario that we envision is this: Right lateral slip on a fault with a right hand step produced a depression (sag). Water tables usually follow surface contours, so the depression was closer to the water table than the sounding terrain. With more available soil moisture, vegetation became enhanced. This attracted cows and burrows, which deposited dung and urine in the soil. Urine added moisture to the soil so the plants grew better. Urine also carried CaCO_3 and nutrients to the soil like urea, phosphorus and nitrogen. Plants flourished and further attracted herbivores. Thus the system is or could become self-perpetuating as herbivores watered and fertilized the soil. Eventually the depression will be filled in by soil creep unless fault slip occurs in subsequent earthquakes.

7. Summary

The Ivanpah Spring Fault is a right lateral transform fault with a right hand step that produces a sag-like structure. The sag does not collect water because it is on a slope. Herbivores are attracted to the sag where they deposit dung and urine. Soil analyses show a strong correlation between pedogenic calcite and organic material as indicated by the presence of the C-H group. In areas surrounding the sag there is very little calcite or organic material. The C-H originates from herbivore dung and the calcite is probably deposited directly as solid particles in suspension in herbivore urine.

Acknowledgements

The authors thank Jerry Treiman and Frank Jordan for useful discussions on the tectonics of the area, and Jon Chorover for drawing our attention to chemical properties of herbivore dung and urine, and to the possibility of microbiologically induced calcite precipitation. Joann Stock, George Rossman and Elizabeth Haddon contributed many helpful comments to an early draft of this paper. We are indebted to land owner Gerald Sauer for permission to visit the site and Lauria Lynch-German for assistance in the field.

References

1. Lynch, D. K. and Paul. M. Adams, Anatomy of Ivanpah Spring, In ECSZ Does it, proceedings of the 2017 Desert Symposium, R. Reynolds (ed.), Desert Studies Center, California State University Fullerton, 288-291 (2017)
2. Vredenberg, L. http://vredenburgh.org/mining_history/pages/hensher2005-ivanpah.html (retrieved 2016, current as of Feb 2018)
3. Hewett, D.E., Geology and mineral resources of the Ivanpah Quadrangle, California and Nevada: U.S. Geological Survey Professional Paper 275, (1956)
4. Miller, David M., Surficial Geologic Map of the Ivanpah 30' x 60' Quadrangle, San Bernardino County, California, and Clark County, Nevada, U.S. Geological Survey Scientific Investigations Map 3206 (2012)
5. Wilkerson , Gregg, Comparative stratigraphy of the Clark Mountains, Mescal Range, and Ivanpah Mountains, San Bernardino County, California (http://vredenburgh.org/gw/pdf/DS2016/Report_Stratigraphy.pdf)
6. Gudmundsson, A., Active fault zones and groundwater flow, *Geophys. Res. Let.*, 27 (18) 2993-2996 (2000)
7. APU (Advanced Photo Utility) © David S.P. Dearborn. APU was written for archaeologists who were interested in the location of sunrise and sunset points on the horizon and to identify stars in night time photographs. CHITO is a down-looking version of APU.
8. Diaz-Espineira M., Escolar E., Bellanato J, Medina J. A., Crystalline composition of equine urinary sabulous deposits. *Scanning Microsc.* 9(4):1071-9. (1995)
9. Finco, Delmar, Kidney Function, in *Clinical Biochemistry of Domestic Animals* (5th edition), eds Jiro J. Kaneko, John W. Harvey, Michael Bruss, Academic Press, 441 - 484 (1997)
10. Mortensen, B.M.; Haber, M.J.; DeJong, J.T.; Caslake, L.F. Nelson (2011). Effects of environmental factors on microbial induced calcium carbonate precipitation. *Journal of Applied Microbiology.* **111** (2): 338-349 (2011).
11. <https://earthquake.usgs.gov/earthquakes/search/>

20 FEB 2018

Earthwatch expedition: wildlife of the Mongolian steppe

Hal Beesley

4609 Alveo Road, La Canada, CA 91011, hcambeesley@earthlink.net

ABSTRACT—The Ikh Nart Nature Reserve in southeastern Mongolia is in a semi-desert steppe northeast of the Gobi desert and is a sister park to California’s Anza Borrego Desert State Park. Earthwatch has five expeditions every year for volunteers to assist in wildlife research and conservation at Ikh Nart. The Denver Zoo also supports Ikh Nart with biologists and funding. I participated in the Sept. 2017 expedition with 10 other volunteers and about 45 other people: wildlife biologists from the Denver Zoo and Mongolia, Mongolian graduate students, 2 veterinarians, Mongolian horsemen and motorcyclists. The Sept. team captured 9 argali sheep (*Ovis ammon*), 2 Siberian ibexes (*Capra sibirica*), and 3 goitered gazelles (*Gazella subgutturosa*) in “drive nets” to be tagged, fitted with GPS collars and so blood samples could be taken. Blood was tested for several sheep diseases and heavy metals. We also did two line transect surveys for argali sheep. The first transect was in the northern part of Ikh Nart, with 10 teams of two or three walking 4 km straight lines separated by 2 km. Each team had a GPS, a laser rangefinder and a compass to record the location of the animals seen. The first transect saw 109 argali. The second transect was in the southern part of Ikh Nart and used 6 lines of 5 km length. More than 71 argali were seen.

The argali sheep is the largest mountain sheep in the world and its conservation status is considered endangered. In Mongolia, the population has been decreasing. Poaching and competition with domestic livestock are believed to be factors affecting the populations. There is also increased mining activity near Ikh Nart. The Siberian ibex is a large goat and considered of least concern. Goitered gazelles are considered vulnerable.

There is limited trophy hunting allowed in Mongolia of argali (very few permits, thus hunting trip cost is over \$60,000) and ibex (cost over \$9,000).

We also visited the ger (yurt) home of a local herder and his family. Herders in the area raise cattle, sheep, goats, horses and camels. There were 3 children in the family. They go to a nearby boarding school and come home for the weekends. Probably very few of their generation will continue the herding life.

Ikh Nart site

Mongolia is between Russia to the north and China to the south, west and east. (Figure 1) It has an area about 90 percent of Alaska’s, and it is at latitudes of the northern US and southern Canada.

It is far from any ocean and has a continental climate with long cold winters and hot summers (Blunden 2014). The Ikh Nart Nature Reserve is in southeast Mongolia, in the Dornogobi aimag (Dornogobi means eastern Gobi. Aimags are provinces; there are 21 provinces in Mongolia) about 300 km from the Mongolia’s capital Ulaanbaatar (Figure 2). We took a 7 hour local train ride from Ulaanbaatar to a stop named Shivee-Gobi, and then a 1 hour drive to the camp on dirt roads. There is also a highway from Ulaanbaatar, which roughly parallels the railroad. This is the same railroad used by the Trans Siberian if travelling between Beijing and Moscow.



Figure 1. Location of Mongolia (CIA map).

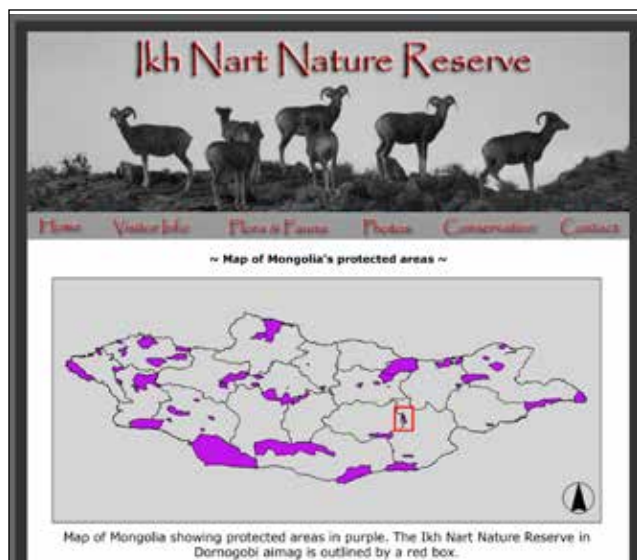


Figure 2. Location of Ikh Nart from Ikhkart.com.

Ikh Nart has an area of about 66,760 ha. By comparison, Anza-Borrego Desert State Park has an area of about 240,000 ha (600,000 acres), and Joshua Tree N.P. is nearly 800,000 acres. The elevation of the camp in Ikh Nart is 1,170 meters. Good weather data (Choir.climatemps.com) is available from the nearby town of Choir, which has an elevation of 1,286 m. Choir's annual precipitation averages 177 mm (7 inches). The hottest month is July with an average high of 25C (77F), and the coldest month is January with an average low of -25C (-13F). At Ikh Nart, the summer temperature maximum is 43C (109F) and the minimum is -40C (-40F). When we were there in September, we had some warm days and some nights below freezing. Some days were very windy, and with blowing dust.

Mongolia has national parks, special protected areas, national monuments, and nature reserves, such as Ikh Nart (Reading 2006). In and around Ikh Nart, nomadic herders live in gers and raise cattle, sheep, goats, horses and cattle. Mining is not allowed within the reserve, but there has been some illegal mining of fluorite and amethyst. In the vicinity, there is fluorite, coal, and copper mining and a non-operating uranium mine.

In 2013 dozens of calves died in Dornogobi aimag. Local herders thought it might be because of contamination from uranium mining. (Tolson 2013, wise-uranium.org 2017) Mongolian government laboratories determined that the cause was naturally occurring selenium and copper in the soil, not uranium. The groundwater in Dornogobi aimag does have high levels of naturally occurring arsenic and uranium. Because of the concern about heavy metals, they were analyzed from the blood samples taken from the animals captured on our Earthwatch expedition in Sept. 2017. Results were negative for heavy metals.

There are several cold water springs in Ikh Nart, which feed some streams (Reading 2011). One of these

springs was where our camp got drinking water (which we filtered). There are also some wells drilled for the herders, and some seasonal ponds.

Ikh Nart was established in 1996 and has received financial and technical assistance from the Denver Zoo, Anza-Borrego State Park, the Anza-Borrego Foundation, the Mongolian Academy of Sciences, the Mongolian Conservation Coalition and other organizations (Reading 2016). Anza-Borrego State Park and Foundation provided funding, ranger training, ranger salaries, and park infrastructure. People from Anza-Borrego visited Ikh Nart, and Mongolians visited Anza-Borrego. In 2008, Anza-Borrego and Ikh Nart were recognized as sister parks by the California State Park Commission.

Earthwatch

The Earthwatch Institute (Earthwatch.org) is a non-profit which has expeditions for volunteers to assist scientists in field work around the world. In 2018, there are 45 expeditions available. Most of the expeditions are for wildlife, but there are a few for archeology, plant life (one at Joshua Tree N.P.) and one for studying a volcano in Nicaragua. Volunteers make a contribution to Earthwatch and pay for their travel to the site. Earthwatch provides housing and meals for the expedition. The expedition I was on was "Wildlife of the Mongolian Steppe". It is offered five times every year in the summer months. Each of the five groups does different things. Our September group captured large animals in drive nets and did transect surveys. Other groups trap small mammals and kestrels, sample vegetation, collect radio telemetry data, and survey vultures and kestrels and their nests.

The tax-deductible contribution to Earthwatch for this expedition was about \$3100, and the roundtrip airfare from Los Angeles was about \$1200. I also got rabies pre-exposure shots before I left. This expedition was 14 days long. We had 11 volunteers in our group. Two were from Canada, one from England, one from the Netherlands (who lives in Shanghai now) and the rest from the US. Four were women and six were men.



Figure 3. The camp where we stayed. It has gers for sleeping, a kitchen ger, a dining ger, an office ger, dry toilets and showers which use solar heated bags of water.



Figure 4. The governor in her office.

One of the men was shooting a documentary about the expedition. On the first day, we met in Ulaanbaatar, Mongolia’s capital, for a group dinner and briefing. The next day, we took the train to Shivee-Gobi and then the drive to the camp. (Figure 3) We were at the camp until day 12. On that day, in the late afternoon we left camp to visit a town along the railroad, Dalanjargalan. The return train to Ulaanbaatar left about 12:30 AM, so we had several cultural activities before then. We met the governor (Figures 4, 5) and she took us to an elementary and middle school. We visited a middle school science class. The Denver Zoo has an exchange program to bring some of these students to Denver for a visit and students from Denver visit Mongolia. We visited a nursery school, a museum, had dinner and attended a musical and dance performance at the school. We went to a little store, which had everything the residents would need (like a miniature Walmart). After the musical show, we went to the Ikh Nart ranger’s office to wait for the train. Some of us went to a Karaoke place before the train. The train ride back to Ulaanbaatar took about 7 hours, so we arrived about 7:30 AM. We had time for souvenir shopping and sightseeing before our final group dinner. Some of us flew home the next day and some stayed in Mongolia for more sightseeing.

Drive Net Capture

We captured argali sheep, Siberian ibex and goitered gazelles in drive nets. The argali sheep is the largest mountain sheep in the world and its conservation status is considered endangered (Iucnredlist.org “Ovis ammon”, 2017). In Mongolia, the population has been decreasing (Lkhagvasuren 2016). Poaching and competition with domestic livestock are believed to be factors affecting the populations (Zahler 2004). The Siberian ibex is a large goat and considered of least concern (Iucnredlist.org “Capra sibirica”, 2017). Goitered gazelles are considered vulnerable (Iucnredlist.org “Gazella subgutturosa”, 2017).

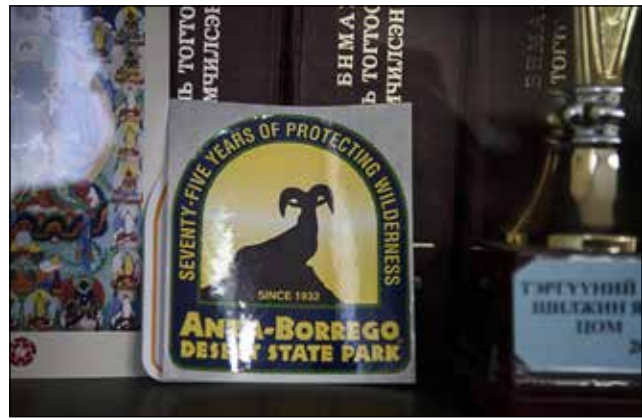


Figure 5. The Anza-Borrego Desert State Park sticker displayed in the governor’s office.

The drive nets resemble big tennis nets. (Figure 6) They are about 6 feet high and 40 feet long and are supported with 2x2 inch sticks, which have nails at one end. The nails are hooked under the top of the net. Each end of the net is supported with 2 sticks on opposite sides, and a guy rope is staked or tied around a rock. Three or four sticks at 10-12 foot spacing are installed along the length of the net. The bottoms of the nets are not staked down. Many of these nets are connected lengthwise, with a little overlap, for a total length of hundreds of feet. Two of these long nets are installed in parallel about 20 feet apart. In case an animal gets through one net, they can be caught in the next net.

After the nets are erected, everybody moves away and hunkers down, so they won’t be seen by the animals. Mongolian horsemen and motorcycle riders then go out to find animals and herd them to the nets (Figure 7). Everybody carries a radio, with one channel for English and one channel for Mongolian. We get updates on whether animals have been spotted and are coming to the net. When they hit the net, everybody runs in. The Mongolian students and riders hold the animals. A mask is put over the animals’ eyes to keep them calmer. Their rectal temperature is monitored. If it gets over 41C, the animal is released so it doesn’t get hyperthermic. If the animal is too young, it may be released too. One of the



Figure 6. Volunteers erecting the drive nets.



Figure 7. Some of the horsemen and motorcycle riders gathered before heading out to find argali.

vets takes a blood sample and monitors the animal’s condition. The others put an ear tag on and mount the GPS collar (Figure 8). Then the animal is released. Smaller animals like gazelles may be carried a distance away from the net so they don’t run back into it.

The GPS coordinates of the capture and the air temperature are recorded. The blood is analyzed for sheep diseases and heavy metals. The sheep diseases include foot and mouth and bluetongue. Mongolia has had outbreaks of foot and mouth in domestic livestock

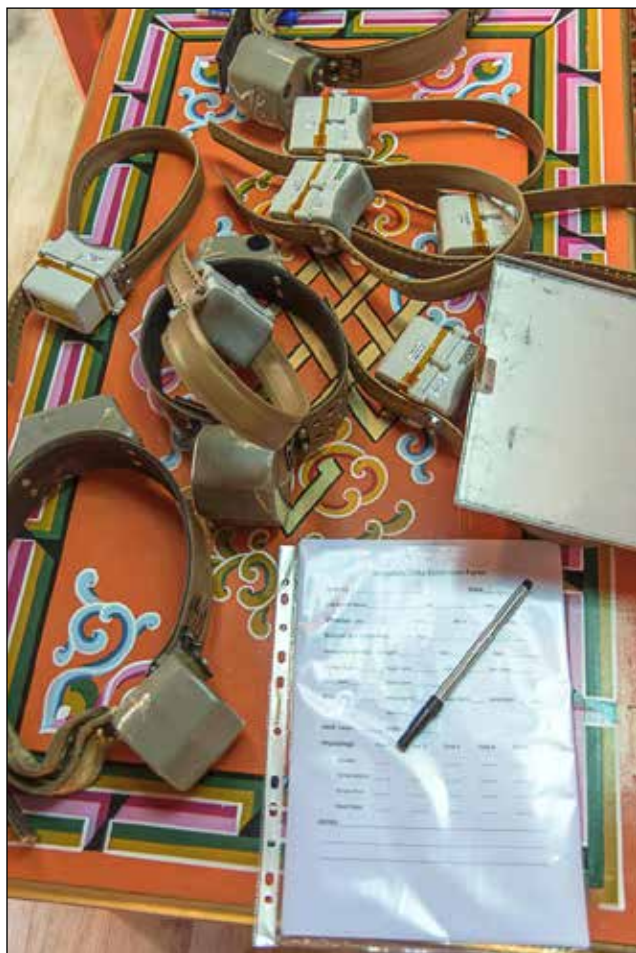


Figure 8. Some of the GPS collars.

as recently as 2010, and the disease is monitored by government veterinarians. In 2010, the disease was found in five provinces and nearly 26,000 sheep, cattle, goats and camels were infected. (McFadden 2011, www-naweb.ieaa.org)

The GPS collar location data is collected by satellite. The batteries in the collars last about 4 years.

Daily activities at camp

The first two days we set nets up in a location to capture goitered gazelles. We caught two, but one was too young and the other’s temperature was too high, so they were released (Figure 9). The third day, we moved to a different location to try to capture argali sheep. At lunchtime, we put the nets down and returned to camp. After lunch we put the nets back up and waited for argali. Finally late in the afternoon, a group was pushed to the nets and we captured 7 argali. They were all collared, tagged and sampled, then released. The nets were taken down and rolled up and we went to a different location and set the nets up to try to catch ibex the next day. After we set the nets up, they were taken down. They are always taken down at lunchtime or overnight.

The next day, we put the nets back up and captured one ibex in the morning (Figure 10). In the afternoon we



Figure 9. A goitered gazelle that was captured. This one was released without a collar because it was too young or its temperature was too high.



Figure 10. Mongolian vet taking a blood sample from an ibex.



Figure 11. The ger of the herder and his family. He lived close to our camp and was one of the motorcycle riders.

went to visit a herder and his family in their ger (Figures 11, 12). We met his wife and one daughter. There are three children in the family, who go to a boarding school during the week and come home for the weekends. The ger is a sturdy tent with wood structure inside to support the roof. It has a wood stove for heating and cooking. He had solar panels and satellite TV. They offered us some yogurt and cheese that they make. Mongolians eat a lot of meat and dairy products from the animals they keep. We were there in September and they were soon going to move to a different location for winter, which had better shelter for the animals. They animals are kept outside all year. The pastoral land in Mongolia belongs to everyone, so they can move as necessary.

After returning to camp, we had a barbecue with roast goat. Then we went to a disco at a sort of hot springs camp several miles away. Along the way, we stopped to see the ruins of a Buddhist monastery. Mongolia was communist from 1924 until 1992 (Blunden 2014), and during the 1930's, monasteries were destroyed and monks were killed.

Over the next three days we captured an ibex, 3 gazelles and 2 more argali (Figures 13-15), which used up all of the GPS collars they had for this session.



Figure 13. Right after an animal was captured in the nets.



Figure 12. The herder and his wife in their ger.

Transects

After the captures were completed, we did two transects to count argali. The first was in the northern part of Ikh Nart (Figure 16). Ten roughly parallel 4 km long lines, about 2 km apart were walked by teams of 2 or 3. Each team carried a radio, binoculars, a GPS, a compass and a laser rangefinder. Each team started to walk on their line at the same time, trying to walk at a steady pace to reach the end at about the same time. If argali were seen as we



Figure 14. A male ibex is released.



Figure 15. The vet from Denver checks the heartbeat of a captured argali with a mask over its eyes to keep it calmer.



Figure 16. The routes walked on the first transect in the northern part of Ikh Nart. The start and end of each route was programmed into the GPS's we carried.

were walking, we recorded the number of them, our GPS location at the time, the distance to them by rangefinder and the compass bearing to them. This would enable the location of the animals to be determined. My group did not see any argali along our line, but 109 argali were seen by the 10 groups.

The next day we did the second transect in the southern part of Ikh Nart. This time we walked along six lines, each 5 km long. My group saw 35 argali. They were farther from us than the rangefinder could measure, but we did record the other data. The six groups saw at least 71 total. After that transect, we drove to see a snake hibernaculum- a hill with chambers where the snakes hibernate in extreme temperatures. When we got there, a front was moving in and it was cold and windy, so we only saw one snake.

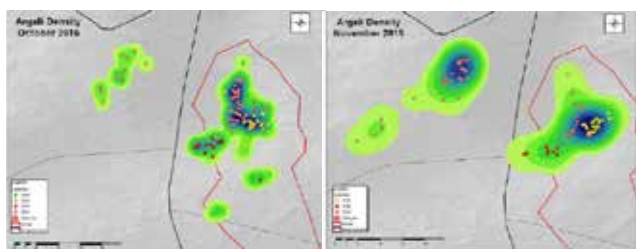


Figure 17a. Argali locations in Oct. 2015.

Figure 17b. Argali locations in Nov. 2015.

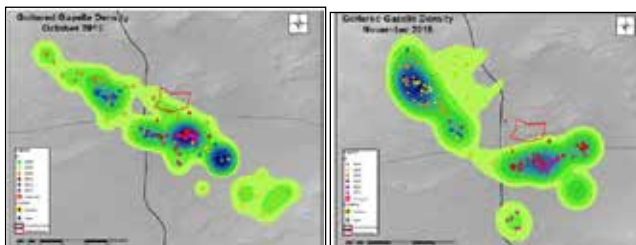


Figure 17c. Goitered gazelle locations in Oct. 2015.

Figure 17d. Goitered gazelle locations in Nov. 2015.

GPS Results

The most recent results that were available to me are from 2015 in the report on the Earthwatch website (Wingard 2015). They show locations of argali and goitered gazelles in and around Ikh Nart in October and November 2015. (Figures 17a to 17d).

References

- Blunden, J., 2014, Mongolia the Bradt Travel Guide 3rd Edn
Choir.climatemp.com
Ikhkart.com
- Iucnredlist.org, 2017, "The IUCN Red List of Threatened Species", "Capra sibirica"
- Iucnredlist.org, 2017, "The IUCN Red List of Threatened Species", "Gazella subgutturosa"
- Iucnredlist.org, 2017, "The IUCN Red List of Threatened Species", "Ovis ammon"
- Lkhagvasuren, B., Adiya, Y., Tsogtjargal, G., Amgalanbaatar, G., 2016, Current Status and Conservation of Mountain Ungulates in Mongolia, Erforsch. Boil. Ress. Mongolei, 2016 (13), p. 445-456.
- McFadden, A., 2011, Analysis of the 2010 Outbreak of Foot-and-Mouth Disease in Mongolia, Report prepared on behalf of MAF Biosecurity New Zealand and the World Bank.
- Mindat.org, "Dornogovi Aimag, Mongolia"
- Reading, R., Murdoch, J., Amgalanbaatar, S., Buyandelger, S., Davie, H., Jorgensen, M., Kenny, D., Munkhzul, T., Onloragcha, G., Rhodes, L., Schneider, J., Selenge, T., Stotz, E., Wingard, G., 2016, From "Paper Park" to Model Protected Area: The Transformation of Ikh Nart Nature Reserve, Mongolia, Parks v. 22.2 November 2016.
- Reading, R., Bedunah, D., Amgalanbaatar, S., 2006, Conserving Biodiversity on Mongolian Rangelands: Implications for Protected Area Development and Pastoral Uses, USDA Forest Service Proceedings RMRS-P-39. 2006, p. 1-17.
- Reading, R., Kenny, D., Steinhauer-Burkart, B., 2011, Ikh Nart Nature Reserve Nature Guide No. 4
- Tolson, M., July 1, 2013, earthisland.org, Earth Island Journal, "In Mongolia's Gobi Desert, Increased Mining Activities Raise Pollution Fears"
- Wingard, G., Arnold, M. 2015, Wildlife of the Mongolian Steppe 2015 Field Report, earthwatch.org.
- wise-uranium.org, 2017, "New Uranium Mining Projects – Mongolia", Last updated 9 Mar 2017. "Zoovch Ovoo deposit, Dornogobi"
- www-naweb.ieaa.org, "Mongolia successfully controls foot and mouth disease with the support of the IAEA"
- Zahler, P., Lhagvasuren, B., Reading, R., Wingard, J., Amgalanbaatar, S., Gombobaatar, S., Barton, N., Yondon, O., 2004, Illegal and Unsustainable Wildlife Hunting and Trade in Mongolia, Mongolian J. of Biological Sciences, v. 2, p. 23-31.

Eastern Joshua tree (*Yucca jaegeriana*) growth rates and survivability on Cima Dome, Mojave National Preserve

James W. Cornett

JWC Ecological Consultants, 3745 Bogert Trail, Palm Springs, CA 92264, jwcornett@aol.com

ABSTRACT: Cima Dome in Mojave National Preserve supports one of the most extensive stands of Joshua trees in existence. It is the eastern Joshua tree, *Yucca jaegeriana*, which occurs in the Preserve. This study examines rate of height increase, leaf rosette production and survivability for Joshua trees less than 3.5 m in height within a 1-hectare site. The study period covered 24 years, from 1994 through 2016. Mean annual height increase was 3.3 cm and mean annual increase in terminal leaf rosettes was 0.13 per tree. Twenty-one of 91 individuals died during the study period. Height increase was best correlated with summer precipitation whereas survivability was best correlated with annual precipitation. No significant correlation existed between leaf rosette production and measures of precipitation.

Introduction

Cima Dome in Mojave National Preserve supports one of the most extensive stands of Joshua trees in existence with densities often exceeding 130 trees per hectare (Figure 1). On the dome, trees are particularly abundant above 1,500 m in elevation where climatic conditions appear particularly favorable for establishment of recruits and growth. With elevation considered to be a major factor in vigor and survival of Joshua tree populations in a changing climate (Barrows, 2012; Cole et al., 2011), growth rates of the high-elevation Cima Dome population of eastern Joshua trees (*Yucca jaegeriana*) have special significance.

In 1987, I established a one-hectare study site on the dome to measure growth rates of a cohort of Joshua trees. The site was at a higher elevation than sites described in three previous studies of Joshua tree growth rates (Comanor and Clark, 2000; Esque et al., 2015; Gilliland et al., 2006; Table 1). Compared with previous studies, this study involved a larger number of trees and covered a longer time span (Table 1). Tree height and leaf rosette production were measured annually for trees less than 3.5 m in height from 1993

to 2016 (24 years). Within this time frame there was a six-year drought from 2011 through 2016, one of the most intense and persistent droughts ever experienced in the California desert region.



Figure 1. Joshua tree study site on Cima Dome, Mojave National Preserve.

Site Description

The site was located on a northwest-facing bajada with a 3% grade. It was selected because of high tree density including dozens of juveniles less than 1 m in height and more than 30 adult trees exceeding 3.5 m. Lower slopes of the Ivanpah Mountains were located 0.9 km to the southeast. Soil consisted of coarse sand interrupted by occasional exposed quartz monzonite bedrock. Perennial plant species within site boundaries in 1993 and listed in decreasing order of cover were spiny menodora (*Menodora spinescens*), blue sage (*Salvia dorrii*), Nevada ephedra (*Ephedra nevadensis*), Joshua tree (*Yucca brevifolia*), antelope brush (*Purshia tridentata*), blackbrush (*Coleogyne ramosissima*), golden cholla (*Cylindropuntia echinocarpa*), banana yucca (*Yucca baccata*), pancake prickly pear (*Opuntia chlorotica*), Cooper’s box thorn (*Lycium cooperi*), California juniper (*Juniperus californica*), plains prickly-pear (*Opuntia polyacantha*), Mojave mound cactus (*Echinocereus triglochidiatus*), beehive cactus (*Escobaria vivipara*) and fishhook cactus (*Mammillaria tetrancistra*). There were no paved roads within 1 km of the site and signs of human presence were minimal. No evidence of past wildfires was detected. Though evidence of cattle was recorded on most site visits, cattle browsing on Joshua trees was never observed nor detected. Mean annual temperature for the 24-year study period was 13.9°C and mean annual precipitation was 219 mm (data accessed at <https://raws.dri.edu/> on 10 Feb 2018). The area experiences a bimodal precipitation regimen with annual precipitation divided almost equally between winter and summer.

Methods

The square, 1-hectare study plot was permanently marked with steel stakes driven into the corners (corner coordinates: northwest 35°19’7.5”N, 115°32’52.4”W; northeast 35°19’8.7”N, 115°32’48.7”W; southwest 35°19’4.4”N, 115°32’51.4”W; southeast 35°19’5.6”N, 115°32’47.7”W). Trees were numbered with aluminum tags wired loosely around trunks to allow expansion. Data was collected annually in April. A tree with one or more green terminal leaf rosettes was considered living while those with no green leaf rosettes were considered dead. Height increases of trees that could be accurately measured, those < 3.5 m, were recorded to nearest centimeter. New leaf rosettes were recorded as soon as they could be visually discerned.

Precipitation and temperature data were obtained from the Western Regional Climate Center (data accessed at

Table 1. Current and published Joshua tree growth rate studies. Mean height increases and mean leaf rosette increases (or decreases) are per tree per year of study. Height increases are in centimeters. Study durations are inclusive.

Study authors	# trees in study	height increase	rosette increase	Study Duration	Site elevation	Site location
current study	93	3.3	0.13	1993-2016	1,529	Cima Dome Mojave National Preserve
Comanor/Clark	21	5.3	0.28	1975-1995	875	Victorville San Bernardino County
Comanor/Clark	19	4.1	-0.03	1975-1995	1,125	Cima Dome Mojave National Preserve
Comanor/Clark	31	3.1	0.15	1975-1995	1,265	Yucca Flat Nevada Test Site
Esque et al.	53	3.1	not measured	1989-2011	1,245	Yucca Flat Nevada Test Site
Gilliland et al.	77	3.8	not measured	1987-2001	850	Lytle Preserve Utah

<https://raws.dri.edu/> on 10 Feb 2018). Climate data from the Mid Hills recording station was used in this study. Because the Mid Hills station was 24 km SSE of the study site and 121 m higher in elevation, the data from Mid Hills was compared with the Southeast Desert Basins of California and Extreme Southern Nevada region-wide data sets obtained from NOAA (Climate at a Glance accessed <https://www.ncdc.noaa.gov/cag/time-series/usat> on 10 February 2018). These two regional data sets were highly correlated with the Mid Hills data ($r > 0.9$; $P < 0.01$). For this reason, it was concluded Mid Hills data was a reliable indicator of climatic trends and weather events for the Cima Dome study site.

Results

Mean growth rate of 93 plants was 3.3 cm over the 24-year study period. This is similar to annual growth rates demonstrated in previous studies (Table 1). Some trees showed no measurable annual growth in height. This differed from Esque et al. (2015) who found growth rates were highly variable “but positive, even during years with average precipitation.” (Esque et al. made no mention of growth in years of below average precipitation.) In the current study, a maximum growth rate of 14 cm was recorded between May of 2014 and April of 2015 for juvenile tree #143. Though such a growth rate was exceptional, rates ≥ 10 cm were recorded in 15 of the 23 years. Comanor and Clark (2000) recorded annual growth rates ≥ 10 cm per year as well. The Pearson correlation coefficient was calculated to reveal any relationship between height increase and precipitation in the 12 months prior to annual site assessments. This yielded no significant relationship ($r = 0.23$, $P = 0.29$). However, a moderate correlation ($r = 0.53$, $P = 0.009$) was found between height increase and summer rainfall as recorded

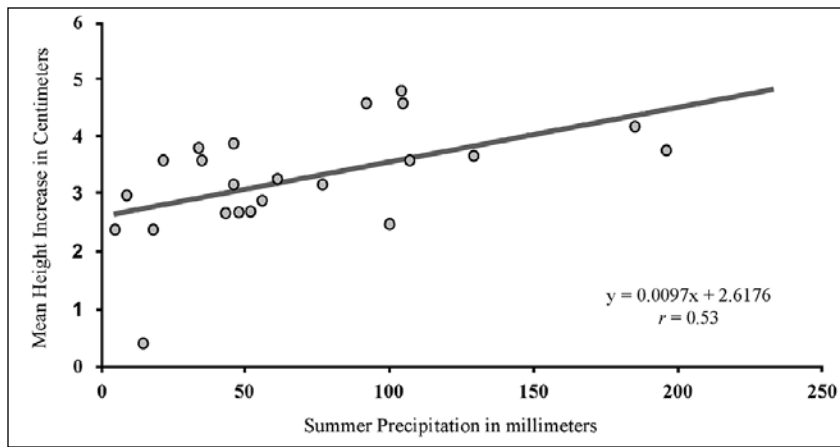


Figure 2. Correlation between mean annual growth rate of Joshua trees <3.5 m in height and summer precipitation from 1994 through 2016 at Cima Dome, Mojave National Preserve, California.

in July, August and September. A regression line and data points for this relationship are shown in Figure 2.

The appearance of new leaf rosettes (potentially growing into future branches) for trees < 3.5 m was an uncommon event. The entire cohort generated a mean of only 0.13 new rosettes per year over 24 years (Table 2). Data collected in 2016 revealed the greatest number of rosettes: 0.38 per tree or just over one leaf rosette for every 3 trees (Table 2). Though most trees did not produce new leaf rosettes in most years, production was occasionally far above the annual mean. Examples include trees #116 and #213 that both grew four new rosettes in 1998-99, tree #297 that grew five new rosettes in 2004-5 and tree #137 that grew six new rosettes in 2015-6. Tree #274 produced 21 rosettes during the study period, nearly one each year. Nine trees failed to produce any new rosettes in 24 years. I found no statistically significant correlations between leaf rosette production and either annual ($r = 0.20, P = 0.35$) or summer ($r = 0.33, P = 0.13$) precipitation.

Maximum number of living trees < 3.5m in height within the study site reached 77 by April of 2008. At the end of the study in 2016 the number had dropped to 72 or a decrease of 6.5%. A total of 21 trees in the cohort died during the study period. Gnawing indicated that 2 were killed by rodents or lagomorphs and 6 were gone and had presumably been eaten as well. The remaining 13 trees appeared to have expired due to drought as no green remained in the leaves and no physical damage was apparent. I found a moderate correlation between tree survivability (percentage of trees that survived since the previous data collection) and annual precipitation ($r = 0.51, P = 0.01$). No statistically significant correlation existed between survivability and summer rainfall ($r = 0.30, P = 0.159$). Percentages of surviving trees from each preceding year are shown in Table 2.

Discussion

I hypothesized increases in height and new leaf rosettes would be positively correlated with annual precipitation as shown in the paper by Esque et al. (2015). Although I could not repeat that finding, I did find a moderate correlation between summer rainfall and height increase. The explanation for this would most likely be that warm temperatures in summer increase growth rates so long as moisture is available. Growth at other times of year would cease or be reduced due to lower temperatures. It would be interesting to know the relationship between seasonal precipitation and growth in the western Joshua tree, *Yucca brevifolia*. The latter species occurs in areas where summer rainfall is much less likely.

Table 2. Mean height increases, mean leaf rosette increases and percentage of trees surviving from previous year. Height increases are in centimeters. Also shown are precipitation totals for 12 months and summer months prior to annual data collection. Mean annual precipitation from 1993 through 2016 was 219 mm. Precipitation totals in table are in millimeters.

Year	height increase	rosette increase	% trees surviving	Prior 12-month precipitation	Prior Summer precipitation
1994	3.0	0.15	100	106	9
1995	2.9	0.08	100	332	56
1996	2.7	0.05	100	136	43
1997	0.4	0.05	98.7	87	15
1998	2.5	0.13	98.7	275	100
1999	3.8	0.22	100	256	196
2000	4.6	0.08	100	242	105
2001	3.2	0.03	100	234	77
2002	2.7	0.13	96.0	93	48
2003	2.4	0.09	100	185	18
2004	3.9	0.14	98.6	221	46
2005	3.6	0.28	100	551	22
2006	3.3	0.05	98.6	154	61
2007	3.6	0.14	96.1	117	35
2008	3.6	0.08	100	227	107
2009	3.2	0.10	96.1	147	46
2010	2.7	0.15	97.2	203	50
2011	2.4	0.08	100	232	5
2012	3.8	0.28	91.8	58	34
2013	4.2	0.29	100	212	185
2014	3.7	0.11	100	228	129
2015	4.6	0.28	100	189	92
2016	4.8	0.38	100	225	104

My inability to discover an association between precipitation and new leaf rosettes probably reflects the incredibly slow process of branch development. As stated previously, most trees did not produce any new leaf rosettes in most years. Twenty-four years may be insufficient time to generate enough data to demonstrate associations with either annual or seasonal precipitation. Leaf rosette production may also be associated with Joshua tree flowering cycles, a phenomenon not addressed in this paper. The western Joshua tree, *Yucca brevifolia*, branches only after production of an inflorescence on a terminal leaf rosette (Rowland, 1978). *Y. brevifolia* may be a masting species with flowering and seed production (and ultimately new leaf rosette production) occurring irregularly (Borchert and DeFalco, 2016). *Y. jaegeriana* produces new leaf rosettes without flowering but the energetic requirement of producing large inflorescences at irregular intervals (author's unpublished data) likely influences rate of branching.

Twenty-one individuals monitored in this study died during the time span 1994 through 2016. There was a net loss to the cohort, however, of only 5 individuals as total mortality was largely offset by sixteen new population recruits. Drought appeared to be the cause of death for most of the expired individuals. Even the 8 that were presumed killed by rodents, lagomorphs or deer may have been attacked, in part, for the moisture they contained during times of drought. Esque et al. (2015) noted jackrabbits were more likely to attack Joshua trees during drought and I have noted this as well particularly in areas where *Y. brevifolia* is the only succulent plant available (author's unpublished notes). During the current study period below-average-precipitation prevailed for five consecutive years, from 2011 through 2015. No recruits were detected during this period and 6 members of the cohort expired. Unlike increase in height that was correlated with summer precipitation, survivability was correlated with annual precipitation. This suggests growth and survivability are separate phenomena and the distinction seems worthy of additional investigation.

The current study indicates young Joshua trees established near the species' historical elevational limit have the capacity to survive and continue to grow despite the long-term drought experienced during the current study. There was, however, a net cohort loss of 6.5%. If this decline were to persist decades into the future, *Y. jaegeriana* would eventually disappear from the site. The current study also suggests summer rainfall is most important for Joshua tree growth. Future studies should examine all aspects of Joshua tree population dynamics and climate from the perspective of seasonal patterns, not just annual climate summaries.

Acknowledgments

I thank the Garden Club of the Desert and Joshua Tree National Park Association for their financial support. T. Johnson and V. Rohrback assisted with collection of

field data. Mark Borchert and David Miller reviewed the manuscript and made many helpful suggestions which were incorporated into the text. My gratitude is extended to each of these individuals and organizations.

Literature cited

- Barrows, C. W. and M. L. Murphy-Mariscal. 2012. Modeling impacts of climate change on Joshua trees at their southern boundary: how scale impacts predictions. *Biological Conservation* 152:29–36.
- Borchert, M. I. and L. A. DeFalco. 2016. *Yucca brevifolia* fruit production, predispersal seed predation, and fruit removal by rodents during two years of contrasting reproduction. *American Journal of Botany* 103 (5): 830 – 836.
- Cole, K.L., K. Ironside, J. Eischeid, G. Garfin, P. B. Duffy and C. Toney. 2011. Past and ongoing shifts in Joshua tree distribution support future modeled range contraction. *Ecological Adaptations* 21(1):137-149.
- Comanor, Peter L. and William H. Clark. 2000. Preliminary growth rates and a proposed age-form classification for the Joshua tree, *Yucca brevifolia* (Agavaceae). *Haseltonia* 7:37-46.
- Esque, T. C., P. A. Medica, D. F. Shryock, L. A. DeFalco, R. H. Webb and R. B. Hunter. 2015. Direct and indirect effects of environmental variability on growth and survivorship of pre-reproductive Joshua trees, *Yucca brevifolia* Engelm. (Agavaceae). *American Journal of Botany* 102(1): 85–91.
- Rowland, Peter G. 1978. The vegetation dynamics of the Joshua tree (*Yucca brevifolia* Engelm.) in the Southwestern United States of America. Doctoral dissertation, University of California, Riverside.

Rare ant populations in the headwaters of Mojave drainages: new records for *Temnothorax paiute* in the Clark and San Gabriel Mountains

James Des Lauriers¹ and Mark Ikeda²

¹Dept Biology, Chaffey College, Alta Loma, CA 91763, JIMDESL39@gmail.com

²Dept. Biology, San Bernardino Valley College, San Bernardino, CA 92410, mikeda56@gmail.com

The ant species *Temnothorax paiute* (formerly known as *Temnothorax* sp. CA-08) was recently described by Snelling, et al. (2014). The description was based on the only three known specimens of the species which were collected more than fifty years ago. The label data of those specimens and their accession codes appear in the paper (Snelling, et al. 2014, p 63).

This note presents new records of the species that have resulted from studies of the ants of the Mojave National Preserve (Ikeda & Des Lauriers, 2011) and the ants of the San Gabriel Mountains (Des Lauriers & Ikeda, 2017). The specimens reside in three collections, Univ. Calif., Davis [UCDC] and the personal collections of James Des Lauriers [JDL] and Mark Ikeda [MKI]. The San Bernardino Co. records listed below do not appear in Ikeda and Des Lauriers (2011) because they were misidentified as the common *T. nevadensis* in that study. The correction of their identification was prompted when Snelling et al. (2014) appeared and JDL reviewed his personal collection. Identification was confirmed by both Philip S. Ward and Matthew M. Prebus.

CALIFORNIA: Los Angeles Co; Hwy N4, 1.1 km e Valyermo Post Office, 1168 m, 34.43994° -117.84362°, 1 worker, 19.vii.2014, (J. Des Lauriers), (15118JDL), [JDL]. 1 worker, 16.v.2015 (J. Des Lauriers), (15693JDL), [MKI]. 1 worker, 20.ix.15, (J. Des Lauriers), (15988JDL), [JDL]. 1 worker, 12.xii.2015, (J. Des Lauriers), (16204JDL), [JDL]. Hwy N4, 1.5 km e Valyermo Post Office, 1171 m, 34.43876° -117.84164°, 1 worker, 16.viii.2014, (J. Des Lauriers), (CASENT0758796), [UCDC]. Largo Vista Rd, 2.6 km n Hwy N4, 1411 m, 34.43235° -117.76752°, 3 workers, 16.vi.2016, (J. Des Lauriers), (16493JDL), [JDL]. 1 worker, 15.ix.2016, (J. Des Lauriers), (16824JDL), [JDL]. 2 workers, 16.x.2016, (J. Des Lauriers), (16918JDL), [JDL]. 1 worker, 19.vi.2017, (J. Des Lauriers), (17325JDL), [JDL].
San Bernardino Co; Curtis Cyn Rd, NN699, Clark Mtns, 1657 m, 35.55077° -115.57217°, 1 worker, 5.v.2006, (J. Des Lauriers), (CASENT0732595), [UCDC]. 1 worker, 4.viii.2006, (J. Des Lauriers), (4850JDL), [JDL]. 1 worker, 7.x.2006, (J. Des Lauriers), (14651JDL), [MKI]. Rd NN699 x Perimeter Rd, Clark Mtns, 1463 m, 35.56242° -115.59698°, 3 workers, 4.viii.2006, (J. Des Lauriers), 4878JDL), [JDL].

These 13 records include 16 individual workers from 5 locations with collection dates ranging from May to

December and at elevations between 1168 – 1657 m. All of them were collected from pitfall traps that accumulated 9440 trap nights of sampling effort. Each trap array consisted of four 9 cm. dia. disposable plastic beverage cups containing ethylene glycol. A stiff plastic roof supported by 4 long nails embedded in the ground was placed about two cm above the cup to keep rain and litter from falling into the cup while not restraining the ground movement of arthropods. Traps were haphazardly placed on the north sides of bushes or overhanging boulders under the dripline, thus protecting the trap from intense summer heat. Traps were left in place for a year or more and refreshed five or more times per year, generally monthly to allow sampling across seasons.

Searching for nests at two of the sites included visually scanning stems, turning stones, digging under bushes, breaking stems and opening galls and beetle galleries in stems. The searches were not successful.

The collecting sites are dominated by *Pinus monophylla*, *Juniperus* sp., and *Yucca brevifolia*. *Tetradymia* sp. and *Ephedra* sp. are moderately abundant at the three Los Angeles Co. sites. All of the sites are in north-facing drainages on well-drained sandy or gravelly soils.

Gordon C. Snelling provided helpful comments about the manuscript.

References

- Des Lauriers, James & Dana Ikeda, 2017. The Ants (Hymenoptera: Formicidae) of the San Gabriel Mountains of Southern California, USA with an Annotated List. 264-277 p. IN: Reynolds, R.E. (ed), 2017. Desert Studies Symposium. California State University Desert Studies Consortium. 342 pp.
- Ikeda, M. & J. Des Lauriers, 2011. The Ant Fauna of the Mojave National Preserve. p 104-113. IN: Reynolds, R.E., ed. 2011. The Incredible Shrinking Pliocene and Abstracts of Proceedings: the 2011 Desert Symposium. California State University Desert Studies Consortium. 136 pp.
- Snelling, R.R., M.L. Borowiec, M.M. Prebus. 2014. Studies on California Ants: a Review of the Genus *Temnothorax* (Hymenoptera, Formicidae). ZooKeys 372: 27-89. doi: 10.3897/zookeys.372.6039www.zookeys.org

Recognition of a *Glaucomys* subspecies population isolated at the headwaters of the Mojave River

Tom Howe and Peggy Howe

P. O. Box 1231, Lake Arrowhead, CA 92352; peby2thowe@cs.com

DNA studies of North American flying squirrel species have revealed a third, genetically distinct new species, *Glaucomys oregonensis*, or Humboldt's flying squirrel. Humboldt's flying squirrel represents one of "two distinctive clades" (Arbogast et al, 2017) that were previously embedded in the *Glaucomys sabrinus* or northern flying squirrel designation. Within the Humboldt flying squirrel species are 5 subspecies previously known as subspecies of *G. sabrinus*, including *Glaucomys oregonensis californicus*. *G. o. californicus* was designated as the subspecies *G. sabrinus* in the San Bernardino Mountains, isolated at the end of the Ice Age by the development of the Mojave Desert. The southernmost *G. californicus* flying squirrels were initially described as three isolated populations in the San Jacintos, San Bernardinos, and the San Gabriels within California's Transverse Ranges. While the *G. o. californicus* subspecies populations in the San Jacintos and San Gabriels have yet to be observed in recent inventories, *G. o. californicus* populations are well documented, observed, and studied in the San Bernardino Mountains with specimens from this population being used in the recent DNA study.

The San Bernardino Mountains, as the headwaters of the Mojave River, offer critical environmental components to ensure successful populations of *G. o. californicus* flying squirrels from the middle Pleistocene to present. These squirrels represent the southernmost population of flying squirrels, who have benefited from the niche provided by the Transition life zone with open deciduous and pine forests and 18 to 26 inches of precipitation annually. More recent investigation of preferred habitat for *G. o. californicus* stress "moist environment close to a water source," dense forest canopy, and accumulated thick forest duff, which encourages the growth of preferred food, fungi (Yuan, 2017; Winchell, 2017). Meyer and others (2005) specified that "nest trees were usually close to riparian habitat; 86% of nest trees were <150 m from a perennial creek". The San Bernardino Mountains have abundant water sources, which are manifested in above-ground creeks, as well as Little Bear Valley (Lake Arrowhead), and Big Bear Valley (Big Bear Lake), where natural marshy meadows and seasonal lakes eventually were reconfigured as man-made lakes. This represents the headwaters of the Mojave River. Around 0.25 Ma, the flora preferred by *Glaucomys* was widespread, the rising San

Bernardino Mountains and the Mojave River drainage provided abundant water and food sources. At the end of the Ice Age when the arid Mojave Desert formed in the rain shadow of several mountain ranges, the then isolated *G. o. californicus* survived as an isolated population.

With the relationship of *G. o. californicus* to the Sierra Nevada squirrels, the obvious path to the San Bernardinos would be by way of the southern Sierra Nevada and the Tehachapi Mountains. During the continued rising of the Transverse ranges, including the San Gabriels and the San Bernardinos, the late middle Pleistocene flora that *Glaucomys oregonensis* thrived within, would have allowed easy and regular migration from the southern Sierras, Tehachapi Mountains and subsequently to the Transverse ranges. Recent studies in the San Bernardino Mountains of *G. o. californicus* have demonstrated flexibility in preferred canopy environment showing an inclination for oak and fir for nesting. Both forest types display hollows that occur naturally or are developed by woodpeckers, which the squirrels take advantage of for nests. These would have allowed even more unrestricted southward migration during climatic change. Today, the Tehachapi Mountains continue to be a corridor for both wildlife and plant populations between the Sierra Nevada Mountains and the Transverse Ranges.

The question is: when and how did *G. o. californicus* arrive in the San Bernardino Mountains? The time of divergence of *Glaucomys oregonensis* from *G. sabrinus* occurred approximately 1.32 million years ago. Other California flying squirrels from the northern Sierra Nevada in Plumas County, *G. o. lascivus*, and San Bernardino Mountains, *G. o. californicus*, show a significant "genetic divergence" from other populations of *G. oregonensis*. Based on the genetic data estimate, these two subspecies became isolated from the main population of *G. oregonensis* 70,000 b. p. This same mitochondrial DNA analysis determined *G. o. californicus* had a strong DNA relationship with the northern Sierra Nevada *G. oregonensis* subspecies of squirrels in the study. Unfortunately, these two populations were the only California squirrels used in the study. The extant Sierra Nevada subspecies and *G. o. californicus* are in turn "surprisingly divergent" from each other indicating a "complex biogeographic" process that ultimately brought *G. o. californicus* to the San Bernardinos (Arbogast and



Figure 1. On the bird feeders – how we first saw *Glaucomys*.



Figure 2. Taking advantage of available water.



Figure 3. Feeding during original study. Close up taken with a cell phone, ignoring our intrusion.

others, 2017). Ultimately, this does not define *when* they first appeared in the San Bernardinos.

Established in the headwaters of the Mojave River in the San Bernardinos, *G. o. californicus* has shown itself to be very adaptable in regard to varied preferred foods vs. available foods. Today they enjoy natural lichen on trees, dogwood berries, and fungi on the forest floor. The strength of their population in the human habitations (Figures 1–3) indicates they can live with

humans, automobiles, and learn to love bird seed from the residents’ feeders in the summer when other sources of food are scarce.

References

- Arbogast, B. S., Schumacher, K. I., Kerhoulas, N. J., Bidlack, A. L., Cook, J. A., Kenagy, G. J., (2017, Sept). Genetic data reveal a cryptic species of New World flying squirrel: *Glaucomys oregonensis*. *Journal of Mammalogy*, 98(4): 1027-1041, 2017. Retrieved September 10, 2017 from <http://www.academic.oup.com/jmammal/article-abstract/98/4/1027/3807034/Genetic-data-reveal-a-cryptic-species-of-New-World>
- Brylski, P. V. (1998). San Bernardino flying squirrel, *Glaucomys sabrinus californicus*, in Bolster, B.C., editor. 1998. *Terrestrial Mammal Species of Special Concern in California*. Draft Final Report prepared by P.V. Brylski, P.W. Collins, E.D. Pierson, W.E. Rainey and T.E. Kucera. Report submitted to California Department of Fish and Game Wildlife Management Division, Nongame Bird and Mammal Conservation Program for Contract No.FG3146WM.
- Ingles, L. G. (1965). *Mammals of the Pacific States, California, Oregon and Washington*. Stanford University Press, Stanford, California.
- Meyer, M. D., Kelt, D. A., North, M. P., (2005, April) Nest Trees of Northern Flying Squirrels in the Sierra Nevada. *Journal of Mammalogy*, 86(2):275-28, 2005 Retrieved February 13, 2018 from <https://academic.oup.com/jmammal/article/86/2/275/891029>
- Yuan, S, Winchell, C. (2017) Squirrels who don’t follow the rules: Defining the habitat of the San Bernardino Flying Squirrel. ESYS Senior Internship Program, Environmental Systems University of California San Diego and U. S. Fish and Wildlife Service, Poster 2017.

Review of Amphicyonidae (Mammalia, Carnivora) from the Barstow Formation of California

Donald Lofgren¹, Maya Fassler², and Stephanie Aldaz²

¹Raymond M. Alf Museum of Paleontology, Claremont, California, 91711

²The Webb Schools, Claremont, California, 91711

Introduction

The first major report describing Miocene vertebrate fossils from the Barstow Formation was by Merriam (1919). Shortly thereafter in 1923, C. Frick and his field crews began a long-term project to recover fossils, mainly mammals, from the abundant outcrops of the Barstow Formation in the Mud Hills north of the city of Barstow (Figure 1), efforts that continued into the early 1950's (Woodburne et al., 1990). Later, Frick's massive collection was donated to the American Museum of Natural History (AMNH) in New York.

The amphicyonids, *Amphicyon*, *Pliocyon*, and *Ischyrocyon* have been reported from the Barstow Formation based on the Frick collections at the AMNH (Woodburne et al., 1990; Hunt, 1998; Pagnac, 2005, 2009). *Pliocyon* was originally described by Matthew (1918) and the genotypic species was designated as *P. medius*. There are two additional species of *Pliocyon*, *P. robustus* (Berta and Galiano, 1984) and *P. ossifragus* (Douglass, 1903; Tabrum et al., 2001). The AMNH sample of *Pliocyon* from the Barstow Formation is small and was briefly described by Pagnac (2005), but the species represented was not determined. However, Berta and Galiano (1984) had already noted that undescribed lower jaws housed at the AMNH from the Barstow Formation represented *P. medius*.

The remaining sample of amphicyonid specimens from the Barstow Formation at the AMNH represent two taxa

that differ in size. The larger taxon is *A. ingens* (Hunt, 1998, 2003; Pagnac, 2005). The smaller taxon was referred to both *Amphicyon* sp. indeterminate (Pagnac, 2005) and *Ischyrocyon gidleyi* (Hunt 1998, 2003), but these specimens now appear to represent *I. gidleyi* (Pagnac, 2009).

Here we describe the large AMNH collection of Barstow Formation amphicyonids, as well as the small collection of Barstow amphicyonids housed at the Raymond M. Alf Museum of Paleontology (RAM). A revised biostratigraphy of amphicyonids from the Barstow Formation is presented based on Pagnac (2009) and our study of AMNH and RAM specimens.

Materials and methods

Specimens housed at the AMNH were photographed and studied by D. Lofgren in 2015-2016. For each FAM or AMNH specimen a brief description of the material, as well as the locality and collection date are provided, if available. Frick collection specimens that are not cataloged are listed by their box number (BAR for Barstow) followed by a field number (example, BAR 95-51). Measurements of amphicyonid teeth were taken in mm using a Mitutoyo digital caliper. A cm tape measure was used to measure limb elements. *Hemicyon* Quarry is also commonly referred to as the *Hemicyon* Stratum, so AMNH specimens listed as either are considered the same locality. The unnamed middle member and unnamed upper member of the Barstow Formation are not formal stratigraphic units, but are referred to as middle member and upper member in the text to avoid the repetitive use of unnamed.

Institutional Abbreviations: AMNH, American Museum of Natural History, New York, New York; CM, Carnegie Museum of Natural History, Pittsburgh, Pennsylvania; FM, Field Museum of Natural History, Chicago, Illinois; FAM, Frick Collection, American Museum of Natural History, New York, New York; MCZ, Museum of Comparative Zoology, Cambridge, Massachusetts; RAM, Raymond M. Alf Museum of Paleontology, Claremont, California; FSGS, Florida State Geological Survey, Florida; UCMP, University of California Museum of Paleontology, Berkeley, California; UF, University of Florida, Gainesville, Florida.

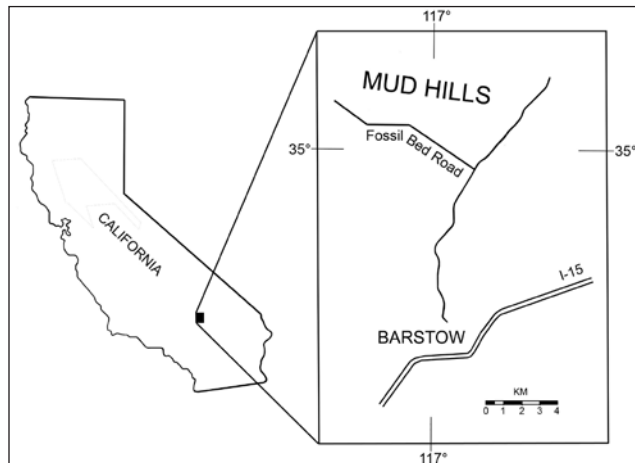


Figure 1: Location of the Barstow Formation within the Mud Hills, Mojave Desert, California (adapted from Steinen, 1966).

Other Abbreviations: **Ba1** and **Ba2**, biochrons of the Barstovian NALMA; **NALMA**, North American Land Mammal Age.

Systematic paleontology

FAMILY AMPHICYONIDAE

Pliocyon Matthew, 1918

Pliocyon medius Matthew, 1918

Pliocyon medius was described by Matthew (1918) who designated AMNH 17207, a nearly complete skull from the Olcott (“Snake Creek”) Formation in Nebraska, as the genotype. Based on AMNH 17207, *Pliocyon* was differentiated from *Amphicyon* based on its smaller molars, canines, and incisors (Matthew, 1918).

Currently, there are three known species of *Pliocyon*: *P. robustus*, *P. ossifragus*, and *P. medius*. The holotype and only known specimen of *P. robustus* is a partial left mandible (UF 24013) from the Upper Bone Valley Formation in Florida (Berta and Galiano, 1984).

Table 1: Measurements in mm of the p2-m3 of *Pliocyon robustus* from the Bone Valley Formation (UF 24013), *P. medius* from the Barstow Formation (FAM 27316, FAM 27504, FAM 27503), and *P. medius* from the Olcott Formation (AMNH 54323, AMNH 54348, AMNH 54344, AMNH 54319, AMNH 54342, AMNH 54330, AMNH 54339, AMNH 13849).

Tooth	UF 24013	FAM 27316	FAM 27504	FAM 27503	AMNH (various)
p2					
Length	11.0	10.2	10.7	10.4	9.6-12.0
Width	7.7	6.5	7.0	6.9	5.1-7.4
p3					
Length	10.7	--	--	12.2	11.4-13.7
Width	7.4	--	--	6.8	5.5-7.2
p4					
Length	19.5	18.1	16.9	18.2	12.1-24.2
Width	8.1	9.7	8.3	10.2	6.9-16.3
m1					
Length	33.2	29.3	28.3	30.4	19.3-31.2
Width	14.8	15.8	14.6	15.0	12.5-25.5
m2					
Length	21.5	20.0	17.4	--	15.9-21.4
Width	10.2	14.9	13.8	--	9.6-15.6
m3					
Length	11.3	11.4	--	--	11.0-11.5
Width	7.0	10.1	--	--	6.5-10.8

Compared to specimens of *P. medius* from the Olcott and Barstow formations, the mandible of *P. robustus* is more robust, the p2-3 are more reduced, the p2 is larger than the p3, and the m1 is relatively longer in *P. robustus* (Berta and Galiano, 1984). Based on a larger sample from the Olcott Formation and the three mandibles of *Pliocyon* from the Barstow Formation, the Barstow and Olcott dentaries have a smaller p2 compared to p3 and a relatively shorter m1 than the holotype of *P. robustus* (Table 1). Also, the three mandibles of *Pliocyon* from the Barstow Formation are very similar in size (Table 1) and morphology to those of *P. medius* from the Olcott Formation. There is little doubt the Barstow Formation sample of *Pliocyon* represents *P. medius*.

The holotype of *Pliocyon ossifragus* (CM 790) is a partial skull with an incomplete dentition from Miocene strata in the Lower Madison Valley of Montana that was originally identified as an ursid similar to *Dinocyon* (Douglass, 1903). In his description of CM 790, Douglass (1903) noted that the P4 and M1-2 were very large, comparable in size to those of *Amphicyon major* from Europe. Subsequently, *Dinocyon ossifragus* was referred to *Pliocyon ossifragus* by Tabrum et al. (2001) without comment. *Pliocyon ossifragus* is much larger than *P. medius* and is similar in size to *Amphicyon ingens*. For example, the M1 of *A. ingens* from the Barstow Formation has a length of 29.5 mm and a width of 38-39 mm and the M1 of *Pliocyon ossifragus* is 30 mm in length and 41 mm in width (Douglass, 1903). Thus, if CM 790 is correctly referred to *Pliocyon*, *P. ossifragus* would represent the largest species of the genus.

Specimens of *Pliocyon medius* are rarely recovered from the Barstow Formation. There are only seven AMNH specimens and no examples of the species are present in the RAM collections. Although the cheek teeth of *P. medius* and *Ischyrocyon gidleyi* are similar size (Figure 2), the canine of *Pliocyon medius* (approximately 20 mm in



Figure 2: Labial view of FAM 27130, right dentary of *Ischyrocyon gidleyi* with p2-4, m1-2 (above) and labial view of FAM 27503, right dentary of *Pliocyon medius* with p2-4 and m1 (below).

maximum diameter and 13 mm in minimum diameter at gum line) is smaller than the canine of *Ischyrocyon gidleyi* (approximately 22-23 mm in maximum diameter and 15.5 mm in minimum diameter at gum line). As would be expected, the canine of *Amphicyon ingens* from the Barstow Formation is much larger than either of the other two amphicyonids (approximately 28 mm in maximum diameter and 19 mm in minimum diameter at gum line). All AMNH specimens of *Pliocyon medius* that have locality data are from the middle member of the Barstow Formation. They include:

- FAM 68201, right radius, Spade Quarry, 1937.
- FAM 68203, right metatarsal IV, 2nd Division, 1933.
- FAM 27316, left mandible with p2, p4, m1-3, and damaged p3, Yermo Quarry, 1932.
- FAM 27504, right mandible with c, p2, p4, m1-2, Green Hills, no date.
- FAM 27503, right mandible with p2-4 and m1, Green Hills, no date.
- FAM 27102, juvenile palette, no locality or date.
- FAM 27103, juvenile mandibles and upper teeth, no locality or date.

AMPHICYON Lartet, 1836

AMPHICYON INGENS Matthew, 1924

The holotype of *Amphicyon ingens* (FAM 18272) is from the Snake Creek beds (Matthew, 1924) and the species

is the largest of the North American amphicyonids (Hunt 1998, 2003). In addition to *Pliocyon medius*, two other amphicyonid species are present in the Barstow Formation, *Amphicyon ingens* (Hunt, 1998, 2003; Pagnac, 2005) and *Ischyrocyon gidleyi* (Hunt, 1998; Pagnac, 2009). Postcranial specimens of *Amphicyon ingens* are usually about 20 to 40% larger than those of *Ischyrocyon gidleyi* (Table 2) (Figure 3). However, an ulna from Turbin Quarry (FAM 68193A, middle member) is 33 cm in length, similar in length to the only complete ulna known of *Ischyrocyon gidleyi* from Deep Quarry in the Barstow Formation (FAM 27153, upper member). The most complete specimen of *Amphicyon ingens* from the Barstow Formation is FAM 23788, a partial skeleton from Valley View Quarry. The mandible of FAM 23788 is much larger than the mandible of *Ischyrocyon gidleyi* (Figure 4) and the skull of FAM 23788 is massive, although crushed (Figure 5).

A skeletal cast of *Amphicyon* was created as part of a major renovation of the AMNH paleontology displays in the 1990s. Many elements of *A. ingens* from Nebraska and Colorado (FAM 68117, FAM 54262, UCMF 36279) were molded to make the cast which is now on display in the Lila Acheson Wallace Wing of Mammals and their Extinct Relatives at the AMNH. An additional cast of *Amphicyon* made by AMNH staff is on display at the RAM in the Hall

Table 2: Measurements in cm of postcranial elements of *Amphicyon ingens* and *Ischyrocyon gidleyi* from various localities in the Barstow Formation (Q= quarry).

<i>Amphicyon ingens</i>			<i>Ischyrocyon gidleyi</i>		
Locality	Specimen	Length	Length	Specimen	Locality
Radius					
Valley View Q	FAM 23788	35	27	FAM 27153	Deep Q
Skyline Q	FAM 23794	33	--		
Steepside Q	FAM 68193	40	--		
Ulna					
Valley View Q	FAM 23788	42	33	FAM 27153	Deep Q
East of Yermo Q	FAM 27300A	40	--		
Valley View Q	FAM 23794	40	--		
Skyline Q	FAM 23792	40	--		
Turbin Q	FAM 68193A	33	--		
Humerus					
Valley View Q	FAM 23788	42	26	FAM 27088	1 st Division
Oreodont Q	FAM 68191	35	25	FAM 68198	<i>Hemicyon</i> Q
Tibia					
Valley View Q	FAM 23788	36	24	FAM 27099G	1 st Division
			29	FAM 68200	New Year Q
			30	FAM 27153A	Deep Q
			29	FAM 68197	2 nd Division



Figure 3: Comparison of FAM 23788, ulna of *Amphicyon ingens* (above) and FAM 27153, ulna of *Ischyrocyon gidleyi* (below).



Figure 4: Labial view of the left dentary (FAM 23788) of *Amphicyon ingens* (above) and the left dentary of *Ischyrocyon gidleyi* (FAM 27095) (below).

of Footprints (Figure 6), mounted over the only known trackway of *Amphicyon* from North America (RAM 100, holotype of ichnotaxon *Hirpexipes alfi*, Sarjeant et al., 2002). The trackway was collected from the middle member in 1964 by Raymond Alf and Webb Schools students (Lofgren et al., 2006; Lofgren and Anand, 2010). The RAM cast was a gift from the AMNH in exchange for the rights to mold the holotype of *Hirpexipes alfi*. Thus, the record of *Amphicyon ingens* from the Barstow Formation includes a spectacular trackway on exhibit at the Raymond M. Alf Museum of Paleontology.

RAM specimens of *Amphicyon ingens* from the Barstow Formation are all postcranial elements from the middle member. RAM 7332 is a large astragulus from RAM locality V94026, a site that also yielded a smaller amphicyonid astragulus (RAM 7308) (Figure 7). The

larger astragulus (RAM 7332) compares favorably in size to a damaged astragulus of *A. ingens* from Valley View Quarry (Figure 7) and almost certainly represents this species. The smaller astragulus (RAM 7308) probably represents *Ischyrocyon gidleyi* or a smaller species of *Amphicyon*.

Twenty four cataloged and eight uncataloged specimens of *Amphicyon ingens* from the Barstow Formation are housed at the AMNH. One is an uncatalogued partial metapodial (BAR 328) from Hidden Hollow Quarry, the only specimen identified as *A. ingens* from the upper member of the Barstow Formation. The fragmentary condition of BAR 328, and the fact that all other AMNH specimens of *A. ingens* are from the middle member, suggests that BAR 328 may represent some other amphicyonid. Thus, AMNH and RAM specimens confidently identified as *A. ingens* that have precise locality data are all from the middle member of the Barstow Formation. These specimens include:

FAM 23788, partial skeleton, including left mandible with c, p2-4, and m1-2, right mandible with c, p1-4, m1, crushed skull with right P1-4 and M2 and left C, P2-4, and M1-2, left and right radius, left and right ulna, patella, assorted metapodials and phalanges, broken astragulus, humerus, tibia, distal end of femur, crushed innominate, left and right scapula, rib fragments, proximal femur lacking head, twelve fragmented vertebrae, and axis, Valley View Quarry, 1933.

FAM 27097, left m3, Green Hills, no date.

FAM 27096A, right M1, Green Hills, no date.

FAM 27099A-H, associated (?) isolated teeth (M1, M2, m2, P4), Green Hills, no date.

FAM 27098, left mandible with p3-m1, right mandible with p3-p4, Green Hills, no date.



Figure 5: Palatal view of FAM 23788, a crushed but nearly complete skull of *Amphicyon ingens* from Valley View Quarry.



Figure 6: Skeletal cast of *Amphicyon ingens* mounted over trackway of *Amphicyon* (RAM 100, *Hirpexipes alfi*) on display in the Hall of Footprints at the Raymond M. Alf Museum of Paleontology.



Figure 7: Comparison of the astragulus of *Amphicyon ingens*, FAM 23788 (left) and RAM 7332 (middle), with the astragulus of *Ischyrocyon gidleyi*, RAM 7308 (right).

FAM 50070, broken ulna, right mandible with i2-3, c, p1-4, m1-3 (m3 in crypt), left mandible with i2-3, c, p1-4, m1-2, Bar 374c-3259-st-5Q-lo. Lev., no date.

FAM 23794A, left radius, Skyline Quarry, 1933.

FAM 23792, left ulna, Skyline Quarry, 1933.

FAM 68191, left humerus, Oreodont Quarry, 1934-35.

FAM 27300, left mandible with damaged p2-3, p4-m2, and m3 alveolus, and right mandible with i3, c, p2-4, m1, 5 miles east of Yermo, 1932.

FAM 27300A, left ulna, 5 miles east of Yermo, 1932.

FAM 27300B, right metatarsal IV, 5 miles east of Yermo, 1932.

FAM 68193, left radius, Steepside Quarry, 1937.

FAM 68193A, right ulna, Turbin Quarry, 1937.

FAM 68192, proximal end of humerus, Valley View Quarry, 1933.

FAM 68196, proximal right femur without head, Valley View Quarry, 1933.

FAM 68196A, distal end of left femur, Valley View Quarry, 1933.

FAM 68210, metatarsal II, Skyline Quarry, 1936-37.

FAM 68210A, metatarsal III, Skyline Quarry, 1936-37.

FAM 23794, ulna, Valley View Quarry, 1933.

FAM 23794A, metacarpal V, Valley View Quarry, 1933.

FAM 23793, right metacarpal IV, Skyline Quarry, 1933.

FAM 68207, right metatarsal III, Mayday Quarry, 1937.

FAM 27096, maxilla fragments with right M2 and left P4-M2,

2nd and 3rd Division Green Hills, 1929.

BAR 328, distal half of metapodial, Hidden Hollow Quarry, 1934-35.

BAR 277, calcaneum, Mayday Quarry, 1933.

BAR 242, 258, 261, 262, 265, 267A, metapodials and phalanges, Valley View Quarry, 1933.

RAM 6811, left scapholunar, RAM locality V95082 (middle member), 2000.

RAM 7556, right metacarpal V fragment, RAM locality V94180 (middle member), 1994.

RAM 9439, left scapholunar, RAM locality V94026 (middle member), no date.

RAM 7332, left astragulus, RAM locality V94026 (middle member), no date.

ISCHYROCYON Matthew and Gidley, 1904

ISCHYROCYON GIDLEYI Matthew, 1902

Numerous specimens in the Frick Collections at the AMNH are labelled *Amphicyon* sp. and they are about 30% smaller than AMNH specimens referred to *Amphicyon ingens* (Pagnac, 2005). These smaller AMNH amphicyonid specimens were identified as *Ischyrocyon gidleyi*, an exclusively North American genus, based mainly on numerous skulls and mandibles recovered from the *Hemicyon* Stratum of the Barstow Formation (Hunt, 1998). In contrast, Pagnac (2005) noted that criteria proposed by Hunt (1998) to differentiate *Amphicyon* from *Ischyrocyon* were not useful in assigning specimens from the Barstow Formation labelled *Amphicyon* sp. in the ANNH collections to either genus.

Table 3: Measurements in mm of the m1-2 and P4-M2 of *Amphicyon ingens* and *Ischyrocyon gidleyi* from the Barstow Formation, *Amphicyon frendens* from the Sheep Creek Formation, and *A. galushai* from the Runningwater Formation (measurements of *A. galushai* and *A. frendens* from Hunt (2003, tables 4.2 and 4.5).

Tooth	<i>Amphicyon ingens</i>	<i>Ischyrocyon gidleyi</i>	<i>Amphicyon frendens</i>	<i>Amphicyon galushai</i>
m1				
Length	35.9-42.1	27.2-32.6	33.5-39.8	30.2-32.2
Width	17.1-19.6	11.8-14.3	--	15.7-16.5
m2				
Length	29.0-36.0	--	21.9-32.1	18.5-20.6
Width	19.0-20.4	--	--	13.3-15.9
P4				
Length	32.5-33.7	22.6-29.7	24.9-32.4	24.8-31.4
Width	19.6-20.0	12.1-16.2	--	14.9-17.9
M1				
Length	29.4-29.5	18.5-24.9	23.2-29.3	20.4-24.8
Width	38.3-39.5	25.6-31.3	29.4-37.0	27.3-32.9
M2				
Length	22.1	--	19.5-26.5	15.7-19.6
Width	30.6	--	31.4-39.9	24.9-28.9

Pagnac (2005) argued that the parastylar cusp of P4 and the relative size of M2 and M1 of these AMNH specimens were characteristic of *Amphicyon*, but that they could not be assigned to any existing species of the genus, although they compare most favorably to *A. frendens* based on size. Apparently this conflict was resolved as this smaller amphicyonid is listed as *Ischyrocyon gidleyi* in a subsequent biostratigraphic review of the Barstow Formation by Pagnac (2009, figure 3).

According to Hunt (2003), the *Amphicyon* lineage in North America is restricted to these species, *A. galushai*, *A. frendens*, and *A. ingens*. As noted earlier, *A. ingens* is much larger than any other species of *Amphicyon* and the size of the dentition of *A. frendens* is significantly larger than that of *A. galushai* (Hunt, 2003, table 4.2 and table 4.5). When comparing the size of the M1 and m1 of AMNH specimens of *Ischyrocyon gidleyi* from

the Barstow Formation to those of *Amphicyon galushai* and *A. frendens*, the Barstow specimens are similar in size to *A. galushai* and smaller than those of *A. frendens* (Table 3). It is important to note that postcranial elements labelled as *Amphicyon* sp. (now *Ischyrocyon gidleyi*) from the Barstow Formation in the AMNH collections are from sites throughout the middle and upper member of the formation and it is unsure if all of these isolated elements actually represent *Ischyrocyon gidleyi*.

The remains of a smaller species of *Amphicyon* are commonly found in Barstovian rocks in North America. In addition to *A. frendens* and *A. galushai*, four other species of *Amphicyon* smaller than *A. ingens* have been described: *A. longiramus*, *A. intermedius*, *A. pontoni*, and *A. riggsi*. (Simpson, 1930; McGrew, 1939; White, 1940, 1942). However, Hunt (2003) restricted *Amphicyon* in North America to *A. galushai*, *A. frendens*, and *A. ingens* without comment on the status of *A. longiramus*, *A. intermedius*, *A. pontoni*, and *A. riggsi*. We provide a brief review of these taxa.

Two species were described from the Thomas Farm area of Florida, *Amphicyon intermedius* and *A. longiramus* (White, 1940, 1942). The holotype of *A. intermedius* is a mandible with p3-m2 (MCZ 3631), whose respective length and width of the m1-2 are 29 mm x 14 mm (m1) and 20.5 mm x 14.5 mm (m2) (White, 1940), dimensions more similar in size to *A. galushai* (Table 3). The holotype of *A. longiramus* (MCZ 3919) is a mandible with p2-m2 (White, 1942) whose m1 length is 32 mm and m2 length is 23 mm, dimensions more similar to *A. frendens* than *A. galushai*. Thus, if these specimens still represent *Amphicyon*, they indicate that two species are present in Miocene strata from Florida.

Interestingly, another species of *Amphicyon*, *A. pontoni*, was described by Simpson (1930) from Florida based on an isolated m2 (FSGS V4112) with a length of 18.6 mm and a width of 14.3 mm. If valid, *A. pontoni* would be most similar in size to *A. galushai* (Table 3).

The other species is *Amphicyon riggsi* from the Deep River Beds (Renova Formation) of Montana (McGrew,



Figure 8: Palatal view of FAM 27107, a relatively complete skull of *Ischyrocyon gidleyi*.



Figure 9: Occlusal view of FAM 27117, partial right maxilla of *Ischyrocyon gidleyi* with P4-M3, compared to the M1-3 of FAM 23788, partial skull of *Amphicyon ingens*.

1939), whose holotype (FM P12029) includes a partial skull with mandible. The m1 and m2 of *A. riggsi* are 31.0 mm x 14.3 mm (m1) and 21.6 mm x 16.0 mm (m2) in length and width respectively (McGrew, 1939). These dimensions are most similar to *A. galushai* (Table 3).

The validity of *A. longiramus*, *A. intermedius*, *A. pontoni*, and *A. riggsi* are in doubt as they were dismissed without comment by Hunt (2003). However, the disagreement between Hunt (1998) and Pagnac (2005) over the identification of the smaller sized amphicyonid in the AMNH collections was resolved (Pagnac, 2009). Thus, *Ischyrocyon gidleyi* appears to represent this smaller sized amphicyonid from the Barstow Formation, but if any of these specimens were later identified as *Amphicyon*, they would be more similar to *A. galushai* than *A. frendens* based on size (Table 3).

Ischyrocyon gidleyi is known from 103 cataloged and four uncataloged specimens labelled *Amphicyon* sp. (*Ischyrocyon gidleyi*) in the AMNH collections. Thirty-three of these are from the *Hemicyon* Stratum, including numerous skulls and mandibles (Figure 8) as noted by Hunt (1998). The dentition of *Ischyrocyon gidleyi* is much smaller than that of *Amphicyon ingens* (Figure 9). It is important to note there is repetitive numbering of specimens of *Ischyrocyon gidleyi* (“*Amphicyon* sp.”) in the AMNH sample. One example is FAM 27106, the catalog number for a maxilla and two mandibles from the Rak Division (no collection date) and also the catalog number for a maxilla with no locality or collection date. Another is FAM 27107, which refers to an M2 with no data, as well as a skull from the *Hemicyon* Stratum (Figure 8) with no collection date. Specimens labelled *Amphicyon* sp. in the AMNH collections also include 40, mostly isolated, postcranial elements. We assume that most of these specimens represent *Ischyrocyon gidleyi*, but it is possible that the sample could include specimens of a species of *Amphicyon* smaller than *A. ingens*.

The RAM sample of smaller amphicyonid specimens from the Barstow Formation includes an astragalus (RAM 7308) and a calcaneum fragment (RAM 7322) from the



Figure 10: Comparison of canines of *Ischyrocyon gidleyi*, RAM 7347 (above) and FAM 27139 (below).

middle member, and a canine (RAM 7347) from the upper member. RAM 7347 compares closely to canines labelled *Amphicyon* sp. (*Ischyrocyon gidleyi*) in the AMNH collections (Figure 10) and RAM 7308 is much smaller than the astragalus of *Amphicyon ingens* from the Barstow Formation (Figure 7).

AMNH and RAM specimens identified as *Ischyrocyon gidleyi* that have locality data are all from the middle and upper members of the Barstow Formation. These specimens include:

- FAM 68206, left metatarsal III, Valley View Quarry, 1933.
- FAM 68205, proximal half of metapodial, Valley View Quarry, 1933.
- FAM 68205A, proximal end of metapodial, Valley View Quarry, 1933.
- FAM 68205B, proximal end of metapodial, Valley View Quarry, 1933.
- FAM 68200, right tibia, New Year Quarry, 1934.
- FAM 68198, right humerus, *Hemicyon* Quarry, 1938.
- FAM 68198A, distal half of humerus, Hidden Hollow Quarry, 1933-36.
- FAM 68199, proximal half of femur, *Hemicyon* stratum, 1930.
- FAM 27153B, astragalus, *Hemicyon* Stratum, 1930.
- FAM 27303A, metatarsal III, *Hemicyon* Stratum, 1931.
- FAM 68208, proximal end of metacarpal III, *Hemicyon* Quarry, 1931.
- FAM 68209, metacarpal II, Hidden Hollow Quarry, 1935-36.
- FAM 68209A, metatarsal III, Hidden Hollow Quarry, 1935-36.
- FAM 68209B, metatarsal I, Hidden Hollow Quarry, 1935-36.

- FAM 27095, left mandible with c, p2-4, m1-2, m3 alveolus and right mandible with i3, c, p1-4, m1-3, Barstow Bluff, 1927.
- FAM 27095A, left and right calcaneum and four metapodials, Barstow Bluff, 1927.
- FAM 27153, radius, two metapodials, and ulna, Deep Quarry, Green Hills, west of camp, 1931.
- FAM 27153A, crushed tibia, Deep Quarry, 1931.
- FAM 27153A, partial femur without head, Camp Quarry, 1931.
- FAM 68195, proximal half of femur, Steepside Quarry, upper level, 1935-36.
- FAM 68197, right tibia, 2nd Division, 1927.
- FAM 68202, right metacarpal V, Steepside Quarry, upper level, 1935-36.
- FAM 68202A, right metacarpal III without proximal end, Steepside Quarry, upper level, 1935-36.
- FAM 68206, left metatarsal III, Valley View Quarry, 1933.
- FAM 68205, proximal half of metapodial, Valley View Quarry, 1933.
- FAM 68205A, proximal end of metapodial, Valley View Quarry, 1933.
- FAM 68205B, proximal end of metapodial, Valley View Quarry, 1933.
- FAM 27301, left and right maxilla fragments with M2s and an isolated M3, 5 miles east of Yermo Quarry, 1932.
- FAM 27304, right maxilla with broken C and P4-M1, *Hemicyon Stratum*, 1931.
- FAM 50086, right mandible with p3-4, and erupting m1, May Day Quarry, 1933.
- FAM 50087, left mandible with m1, May Day Quarry, 1933.
- FAM 50088, left maxilla with P4-M2 and right maxilla with P4-M1, May Day Quarry, 1934.
- FAM 50082, left maxilla fragment with P4 and erupting M2, Hidden Hollow Quarry, 1935.
- FAM 50083, left mandible with p4-m2, Hidden Hollow Quarry, 1935.
- FAM 50089, crushed skull with left P4-M2, damaged right P4-M1 and M2, Hailstone Quarry, 1937.
- FAM 27302, right mandible with i2-3, c, p1-2, p4, m1, and left mandible with c, p1-4, *Hemicyon Stratum*, 1931.
- FAM 23791, tibia, Skyline Quarry, 1933.
- FAM 23789, four metacarpals, Skyline Quarry, 1933.
- FAM 23793, two metapodials, Valley View Quarry, 1933.
- FAM 50075, skull with left P1-3, P4, and M1-2, and right P1-3, P4-M1-3, and atlas, Leader Quarry, 1935.
- FAM 20085, partial femur without head, no locality, 1925.
- FAM 27106, left mandible with p4-m2, right mandible with i2-3, c, p1, p3-4, m1-2, and left maxilla with I1-3, damaged P1, and P2-M3, Rak Division, no date.
- FAM 27116, left maxilla with P3-M2, 1st Division, no date.
- FAM 68194, right femur, 2nd division, no date.
- FAM 50105, M3, Green Hills Quarry, no date.
- FAM 27126, left maxilla with P4-M2, *Hemicyon Stratum*, no date.
- FAM 27141, left mandible with m1 and erupting m3, *Hemicyon Stratum*, no date.
- FAM 27097A, metatarsal and three phalanges, 1st Division, no date.
- FAM 27097E, metatarsal, 1st Division, no date.
- FAM 27097F, proximal half of metatarsal, 1st Division, no date.
- FAM 27099G, tibia, 1st Division, no date.
- FAM 27099H, proximal half of metatarsal, 1st Division, no date.
- FAM 27088, left humerus, 1st Division, no date.
- FAM 27127A, right P4, *Hemicyon Stratum*, no date.
- FAM 27096B, right metacarpal V, *Hemicyon Stratum*, no date.
- FAM 27124, right maxilla with P4-M2, *Hemicyon Stratum*, no date.
- FAM 27117, right maxilla with P4-M3, 1st Division, no date.
- FAM 27107, partial skull with left I3, C, P2, P4, M1-2, and right I3, C, P2-4, M1-2, *Hemicyon Stratum*, no date.
- FAM 27123, skull fragment with left and right P1, *Hemicyon Stratum*, no date.
- FAM 27137, left mandible with c, p2-3, m1, right mandible with p2-4, m1, and metapodial, *Hemicyon Stratum*, no date.
- FAM 50081, brain case, partial innominate, distal femur, astragulus, two metapodials, Hidden Hollow Quarry, no date.
- FAM27107A, skull with left C1, P203, M1-2, and right I2-3, C1, P3-4, M1, *Hemicyon Stratum*, no date.
- FAM 27109, skull with left I1-3, C1, P1-2, P4, M1-3, and right I1-3, C1, P1-4, M1-3, *Hemicyon Stratum*, no date.
- FAM 27210, juvenile skull with erupting left P4, *Hemicyon Stratum*, no date.
- FAM 27127, right P4, *Hemicyon Stratum*, no date.
- FAM 27108, skull with damaged teeth, *Hemicyon Stratum*, no date.
- FAM 27110, skull with left I3, C, P2-3, M1-2, and right C, P1-4, and M1, *Hemicyon Stratum*, no date.
- FAM 27133, left mandible with c, p1-4, and m1-2, 1st Division, no date.

- FAM 27119, left maxilla with M1-2, 1st Division, no date.
- FAM 27115, skull fragments with right P4-M1 and broken left P4-M1, *Hemicyon* Stratum, no date.
- FAM 27142, right mandible with i3, p1, p3-4, m1, *Hemicyon* Stratum, no date.
- FAM 27143, right mandible with p2, p4, m1-2, *Hemicyon* Stratum, no date.
- FAM 27120, right maxilla with M1-2, 1st Division, no date.
- FAM 27132, left mandible with broken m1, and right mandible with c, p2-4, m1, *Hemicyon* Stratum, no date.
- FAM 27148, left mandible with m1-2, *Hemicyon* Stratum, no date.
- FAM 50078, right mandible with damaged p3-4 and m1-2, and left mandible with p4, and damaged m1, New Hope Quarry, no date.
- FAM 27113, juvenile skull with erupting left P4-M2, right M1, and left and right DP3-4, *Hemicyon* Stratum, no date.
- FAM 27125, right maxilla fragment with P3-4, *Hemicyon* Stratum, no date
- FAM 27111, mandible with c, p1-2, m1 and erupting c and m2, skull with right M1-2 and left P4-M2, *Hemicyon* Stratum, no date.
- FAM 27118, right maxilla with M1-2, 1st Division, no date
- FAM 27144, left mandible with p4-m2, and upper molars, *Hemicyon* Stratum, no date.
- FAM 27146, left mandible with p2-4 and m1, *Hemicyon* Stratum, no date.
- FAM 27139, right mandible with c, p1, and p3 and left isolated c, 1st division, no date.
- FAM 27147, right mandible with m1, *Hemicyon* Stratum, no date.
- FAM 27135, right mandible with p4-m2, *Hemicyon* Stratum, no date.
- FAM 27100, right mandible with p4 and m3, Green Hills, no date.
- FAM 27140, mandible fragments, no locality or date.
- FAM 20823, braincase, no locality or date.
- FAM 27104, left M2, no locality or date.
- FAM 27105, right M3, no locality or date.
- FAM 27107, right M2, no locality or date.
- FAM 27138, right mandible with m1-2, no locality or date.
- FAM 27106A, right maxilla with P4-M1, no locality or date.
- FAM 27106, right maxilla with I3 and C, no locality or date.
- FAM 27095B, left metacarpal II and IV, no locality or date.
- FAM 27136, right mandible with m2-3, no locality or date.
- FAM 27131, left mandible with m1-2, no locality or date.
- FAM 27145, left mandible with damaged teeth, no locality or date.
- FAM 27130, right mandible with p2-4, m1-2, no locality or date.
- FAM 27134, left mandible with p1, p4, m1-3, no locality or date.
- FAM 27128, broken left P4, no locality or date.
- FAM 27121, left M2, no locality or date.
- FAM 20822, braincase, no locality or date.
- BAR 192, two molars, Green Hills Quarry, 1930.
- BAR 420, calcaneum, Yermo Quarry, 1938.
- BAR 80, braincase, *Hemicyon* Stratum, 1927.
- BAR 156, phalanges, Skyline Quarry, no date.
- RAM 7347, lower canine, RAM locality V94039 (upper member), 1999.
- RAM 7308, left astragulus, RAM locality V94026 (middle member), no date.
- RAM 7322, left calcaneum fragment, RAM locality V94026 (middle member), no date.

Biostratigraphy

Mandibles of *Pliocyon medius* were recovered from Yermo Quarry (FAM 27316) and two sites noted as “Green Hills” (FAM 27504 and FAM 27503). The Green Hills Fauna of the Barstow Formation occurs in strata that extend from Stepside Quarry up to just below Valley View Quarry (Figure 11), an interval that is part of the Ba1 biochron of the Barstovian NALMA (Tedford et al., 2004; Pagnac, 2009) and includes the Orodont Tuff dated at 15.8 Ma (Woodburne et. al., 1990). *Pliocyon medius* is also well known from late Hemingfordian to early Barstovian strata in Nebraska (Hunt, 1998).

Amphicyon ingens is best known from the Barstow Formation based on FAM 23788, a partial skeleton from Valley View Quarry. The record of *A. ingens* from the Barstow Formation appears to be restricted to the Ba1 biochron of the Barstovian NALMA as it occurs from Stepside Quarry up to Mayday Quarry and Skyline Quarry, an interval that represents most of the middle member (Woodburne et. al., 1990; Pagnac, 2009). As noted earlier, BAR 328 is a partial metapodial from Hidden Hollow Quarry identified as *A. ingens*. If the locality data for BAR 328 is correct, the range of *A. ingens* would extend into the upper member of the Barstow Formation, up into the Ba2 biochron (Figure 11). *Amphicyon ingens* is also known from early to medial Barstovian strata in Nebraska, Oregon, New Mexico, and Colorado (Hunt, 1998), so its occurrence in the

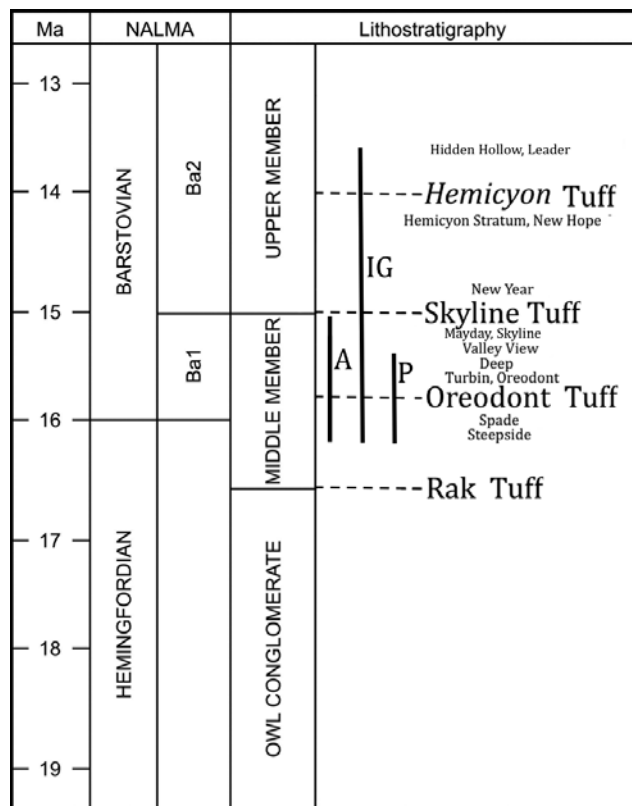


Figure 11: Geochronology and biostratigraphic subdivision of the Barstow Formation (adapted from Pagnac, 2009 and Woodburne et al., 1990), showing stratigraphic ranges of *Amphicyon ingens* (A), *Ischyrocyon gidleyi* (IG), and *Pliocyon medius* (P). The stratigraphic positions of some of the Frick quarries mentioned in the text are noted.

upper member of the Barstow Formation would not be a biochronologic range extension for the taxon.

Skulls and mandibles labelled as *Amphicyon* sp. in the AMNH collections from the *Hemicyon* Quarry were referred to *Ischyrocyon gidleyi* (Hunt, 1998). Postcranial elements labelled as *Amphicyon* sp. are from sites throughout the middle and upper members, from Steepside Quarry up to Hidden Hollow Quarry. It is unsure if all of these isolated elements actually do represent *Ischyrocyon gidleyi*, and analysis of postcranial remains was beyond the scope of this study. *Hemicyon* Quarry specimens represent a small form of *Ischyrocyon*, and Claredonian strata in Texas yield much larger individuals (Hunt, 1998). Thus, whether a second species of *Ischyrocyon* should be erected is an open question (Hunt, 1998).

Summary

The Frick collections at the American Museum of Natural History include 156 amphicyonid specimens from the upper and middle members of the Barstow Formation that are referred to *Amphicyon ingens*, *Pliocyon medius*, and *Ischyrocyon gidleyi*. A much smaller amphicyonid collection is housed at the Raymond M. Alf Museum of Paleontology and is composed of seven isolated

postcranial elements and the only known trackway (*Hirpexipes alfi*) of *Amphicyon* from North America.

The presence of *Pliocyon medius* in the Barstow Formation (seven isolated AMNH elements) is confirmed as three mandibles from the middle member are very similar to mandibles of the species from the Olcott Formation in Nebraska. *Amphicyon ingens* is much larger (about 30%) than either *Pliocyon medius* or *Ischyrocyon gidleyi* and is known from thirty-two AMNH and four RAM specimens. This large amphicyonid is best known from the Barstow Formation based on a partial skeleton (FAM 23788) from Valley View Quarry (middle member). *Ischyrocyon gidleyi* is the most abundant amphicyonid known from the Barstow Formation as 117 AMNH and three RAM specimens were recovered. This species is best known from the *Hemicyon* Stratum in the upper member as multiple skulls and mandibles were collected by Frick crews from the site over 60 years ago.

The biostratigraphic records of *Pliocyon medius* and *Amphicyon ingens* (including *Hirpexipes alfi*) are restricted to the middle member except for an uncataloged metapodial (BAR 328) from Hidden Hollow Quarry in the upper member. If BAR 328 is correctly identified and if locality data is accurate, the range of *Amphicyon ingens* would be extended up into the upper member of the Barstow Formation. This occurrence would not be a biochronologic range extension for *A. ingens* as it is known from medial Barstovian strata elsewhere in North America. Besides the excellent sample from the *Hemicyon* Stratum, *Ischyrocyon gidleyi* has been recovered from multiple sites in both the middle and upper members of the Barstow Formation. The sample includes over 40 postcranial elements which would be very difficult to distinguish from various smaller species of *Amphicyon* known from Barstovian strata. If any of these elements were indeed referable to *Amphicyon*, based on size, *A. galuslai* would be the most likely species represented by the specimens.

Acknowledgments

We thank J. Shearer of the California Bureau of Land Management for permits, M. Woodburne for reviewing the manuscript, J. Galkin, R. O'Leary, and J. Meng of the AMNH for access to specimens, and the Mary Stuart Rogers Foundation, Augustyn Family Fund of the Raymond M. Alf Museum of Paleontology, and the David B. Jones Foundation for financial support.

References cited

- Berta, A., and H. Galliano. 1984. A Miocene amphicyonid (Mammalia, Carnivora) from the Bone Valley Formation of Florida. *Journal of Vertebrate Paleontology* 4:122-125.
- Douglass, E., 1903. New vertebrates from the Montana Tertiary. *Annals of the Carnegie Museum* 2:145-199.
- Hunt, Jr., R. M. 1998. Amphicyonidae. pp. 196-221, in *Evolution of Tertiary Mammals of North America, Volume 1: Terrestrial Carnivores, Ungulates, and ungulate-like*

- Mammals (C. M. Janis, K. M. Scott, and L. L. Jacobs, eds.), Cambridge University Press, Cambridge, United Kingdom.
- Hunt, Jr., R. M. 2003. Intercontinental migration of large mammalian carnivores: earliest occurrence of the Old World bearded *Amphicyon* (Carnivora, Amphicyonidae) in North America. *Bulletin of the American Museum of Natural History* 279:77-115.
- Lartet, E., 1836. Nomenclature des mammifères et des coquilles qu'il a troves dans un terrain d'eau douce pres de Simorre at de Sansan (Gers). *Bulletin de al Societe geologique de France* 7:217-220.
- Lofgren, D. L., Greening, J. A., Johnson, C. F., Lewis, S. J, and M. A. Torres. 2006. Fossil Tracks at the Raymond Alf Museum of Paleontology and management of tracks on public lands. *New Mexico Museum of Natural History & Science Bulletin* 34:109-118.
- Lofgren, D. L., and R. Anand. 2010. 75 years of fieldwork in the Barstow Formation by the Raymond M. Alf Museum of Paleontology. pp. 169-176, in: R. E. Reynolds and D. M. Miller (eds.). *Overboard in the Mojave: 20 Million Years of Lakes and Wetlands*. Desert Studies Consortium: Fullerton, California.
- Matthew, W. D., 1902. A skull of *Dinocyon* from the Miocene of Texas. *Bulletin of the American Museum of Natural History* 16:129-136.
- Matthew, W. D., 1918. Contributions to the Snake Creek fauna with notes upon the Pleistocene of Western Nebraska American Museum Expedition of 1916. *Bulletin of the American Museum of Natural History* 38:183-229.
- Matthew, W. D., 1924. Third contribution to the Snake Creek fauna. *Bulletin of the American Museum of Natural History* 50:59-210.
- Matthew, W. D., and J. Gidley, 1904. New or little known mammals from the Miocene of South Dakota. Parts I-III. *Bulletin of the American Museum of Natural History* 20:241-268.
- McGrew, P. O., 1939. A new *Amphicyon* from the Deep River Miocene. *Field Museum of Natural History Geological Series* 6:341-350.
- Merriam, J. C., 1919. Tertiary mammalian faunas of the Mohave Desert. University of California Publications in Geological Sciences 11:437a-437e, 438-585.
- Pagnac, D. C., 2005. A systematic review of the mammalian megafauna of the middle Miocene Barstow Formation, Mojave Desert, California (PhD dissertation). University of California-Riverside. 384 pp.
- Pagnac, D. C., 2009. Revised large mammal biostratigraphy and biochronology of the Barstow Formation (Middle Miocene), California. *Paleobios* 29:48-59.
- Sarjeant, W. A. S., Reynolds, R. E., and M. M. Kissell-Jones, 2002. Fossil creodont and carnivore footprints from California, Nevada, and Wyoming, pp. 37-50, in (Reynolds, R. E. ed.), *Between the Basins: Exploring the Western Mojave and Southern Basin and Range Province*. California State University-Fullerton, Desert Studies Consortium.
- Simpson, G. G., 1930. Tertiary Land Mammals of Florida. *Bulletin of the American Museum of Natural History* 59:1-64.
- Steinen, R. P., 1966. Stratigraphy of the middle and upper Miocene, Barstow Formation, California. (m.s. thesis): University of California-Riverside, 150 pp.
- Tabrum, A. R., Nichols, R., and A. D. Barnosky. 2001. Tertiary paleontology of southwest Montana and adjacent Idaho. *Museum of the Rockies Occasional Paper* 3:93-112.
- Tedford, R. H., Albright III, L. B., Barnosky, A. D., Ferrusquia-Villafranca, I., Hunt, Jr., R. M., Storer, J. E., Swisher III, C. C., Voorhies, M. R., Webb, S. D., and D. P. Whistler. 2004. Mammalian biochronology of the Arikareean through Hemphillian interval (Late Oligocene through Early Pliocene epochs). pp 169-231, *in Late Cretaceous and Cenozoic Mammals of North America; Biostratigraphy and Geochronology* (M. O. Woodburne ed.), Columbia University Press, New York.
- White, T. E. 1940. New Miocene vertebrates from Florida. *Proceedings of the New England Zoological Club* 18:31-38.
- White, T. E. 1942. The lower Miocene mammal fauna of Florida. *Bulletin of the Museum of Comparative Zoology* 92:1-49.
- Woodburne, M. O., Tedford, R. H., and C. C Swisher III. 1990. Lithostratigraphy, biostratigraphy, and geochronology of the Barstow Formation, Mojave Desert, southern California. *Geological Society of America Bulletin* 102:459-477.

New records of *Miomustela* from the Barstow and Crowder formations of California

Donald Lofgren¹ and Will Abersek²

¹Raymond M. Alf Museum of Paleontology, Claremont, California

²The Webb Schools, Claremont, California.

Introduction

Miomustela was originally described by as *Martes? minor* based on CM 848, a left dentary from Miocene strata in the Madison River Valley of Montana (Douglass, 1903) which later was designated as the genotype of *Miomustela madisonae* (Douglass, 1929; Hall, 1930). *Miomustela* has been reported from late Arikareean to late Barstovian strata in Canada and the United States (Baskin, 1998), including the Barstow Formation of California (Figure 1) (Pagnac 2005, 2009). Of the twelve specimens of small mustelids from the Barstow Formation housed at the AMNH, UCMP, and RAM, eleven were referred to *Plionictis ogygia* and one to *Miomustela* (Lofgren et al., 2016). Two additional specimens of *Miomustela* are present in the collections of the San Bernardino County Museum (SBCM), a dentary from Skyline Quarry in the Barstow Formation, as well as a crushed skull with a dentary and associated phalanges from the Crowder Formation. These specimens are described and their biostratigraphic importance discussed.

Abbreviations

AMNH, American Museum of Natural History, New York, New York; **Ba1**, Barstovian Biochron 1; **Ba2**, Barstovian Biochron 2; **CM**, Carnegie Museum of Natural History, Pittsburgh, Pennsylvania; **FAM**, Frick Laboratory Collections, American Museum of Natural History, New York, New York; **NALMA**, North American

Land Mammal Age; **RAM**, Raymond M. Alf Museum of Paleontology, Claremont, California; **SBCM**, San Bernardino County Museum, Redlands, California; **UCMP**, University of California Museum of Paleontology, Berkeley, California.

Miomustela

Miomustela was reported from the Barstow Formation (Pagnac, 2005; 2009) apparently based on two dentaries (UCMP 311688 and UCMP 315119) and one maxillary fragment (UCMP 320005). These specimens were referred to *Plionictis* as the two genera can easily be distinguished by size, *Plionictis* being significantly larger (Lofgren et al. 2016). For example, the m1 of the holotype of *Miomustela madisonae* (CM 848) is about half the size of the m1 of holotype of *Plionictis ogygia* (AMNH 9042) (Table 1). Thus, only a single specimen of *Miomustela* (RAM 16254) has been described from the Barstow Formations (Lofgren et al. 2016).

The Crowder Formation has yielded a skull and dentary of a small mustelid (SBCM L1585-1613, from SBCM locality PS-1, Quarry A). The Crowder Formation dentary was compared to the holotype of *Miomustela madisonae*, a partial dentary with p3-m1 (FAM 100010, a cast of CM 848), and both the SBCM dentary (Figure 2) and the holotype have a p2 that is narrow antero-posteriorly

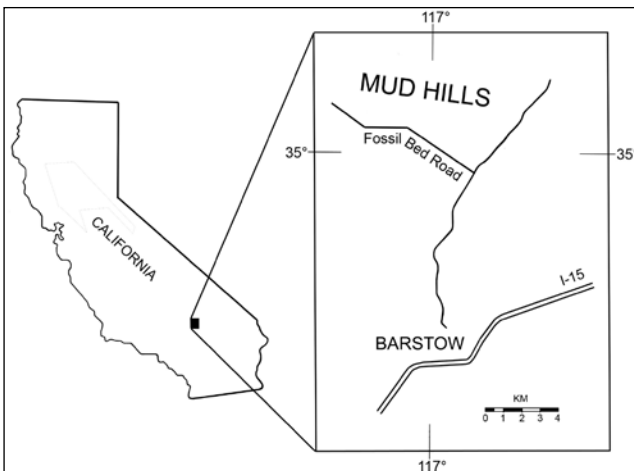


Figure 1. Location of the Barstow Formation within the Mud Hills, Mojave Desert, California (adapted from Steinen 1966).

Table 1. Comparison of the measurements in mm of the lower dentition of the holotypes of *Miomustela madisonae* (FAM< 100010, cast of CM 848) and *Plionictis ogygia* (AMNH 9042) and a dentary of *Miomustela* (AMNH 104680) from Observation Quarry (Nebraska) with *Miomustela* from the Crowder and Barstow formations.

Specimen		p2	p3	p4	m1
FAM 100010	L	—	2.4	3.3	5.0
	W	—	1.1	1.5	2.1
AMNH 104680	L	—	1.9	2.7	4.2
	W	—	1.0	1.3	2.0
SBCM L1585-1613	L	1.4	2.2	2.6	4.2
	W	.8	1.2	1.4	1.9
SBCM 1-130-32N	L	—	2.4	—	5.5
	W	—	1.2	—	2.1
AMNH 9042	L	3.3-3.4	4.3-4.4	4.9-5.2	7.5
	W	1.7-1.9	2.1-2.2	2.4-2.5	3.3-3.6

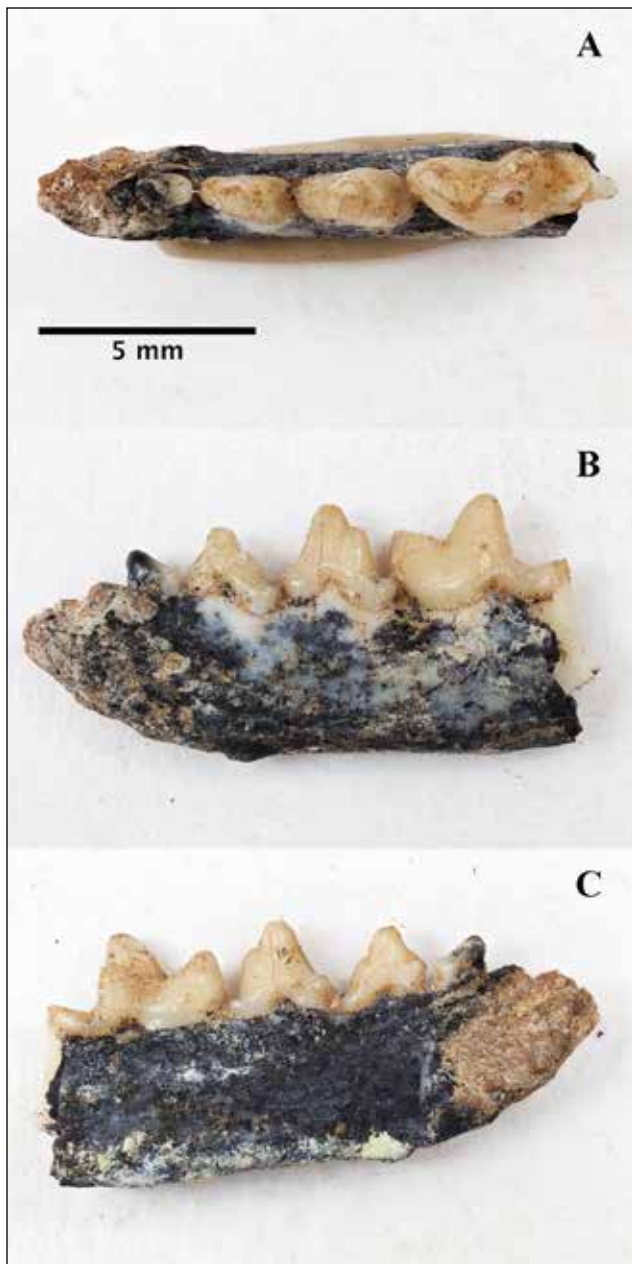


Figure 2. Occlusal (A), labial (B), and lingual (C) view of SBCM L1585-1613 a left dentary with p2-m1 of *Miomustela* from the Crowder Formation.

and broad transversely, a p3 that is transversely narrow with a small heel, and a p4 with a larger heel and a taller main cusp than p3. In both specimens the m1 has a large anteriorly projecting and low paraconid, a large protoconid which is much taller than the paraconid, and a small metaconid that is positioned slightly posterior to the large protoconid, a deep notch separating the paraconid and protoconid, a trigonid that opens lingually, and a talonid basin with a rounded posterior margin. The size of the dentition of CM 848 and the SBCM L1585-1613 is similar except that the m1 of the holotype is larger (Table 1). The Crowder Formation dentary is more similar in size to AMNH 104680, a dentary fragment of *Miomustela*

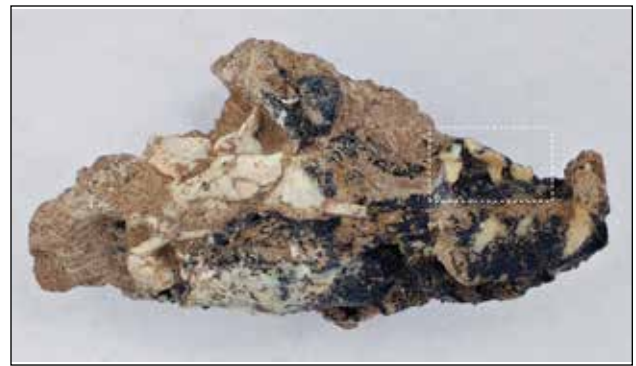


Figure 3. Palatal view of SBCM L1585-1613, a skull of *Miomustela* from the Crowder Formation. White dashed box is 12 mm in length and denotes location of Figure 4.

with p3-4, m1 from Observation Quarry (Lofgren et al. 2016, fig. 2) (Table 1), an early Barstovian site in Nebraska (Tedford et al. 2004; Korth and Evander, 2016). In any case, SBCM L18585-1613 represents *Miomustela*, but a smaller individual than that represented by the holotype (Table 1).

The skull of L1585-1613 has been significantly damaged by compaction (Figure 3) and a number of isolated phalanges are positioned adjacent to its dorsal surface, apparently from the same individual. The only known Barstow Formation specimen of *Miomustela madisonae* is RAM 16254, a maxilla fragment with P3-4 (Lofgren et al. 2016). Both the P3 and P4 of SBCM L1585-1613 and RAM 16254 are about the same size (Table 2) and both P4s have a well-developed metastylar blade that lacks a metastyle or carnassial notch (Figures 4-5), features that characterize *Miomustela* (Baskin, 1998). The P4s also have a small protocone and parastyle that are subequal in size and positioned transversely parallel. Because of these similarities and the fact that the premolars are similar in size (Table 2), SBCM L1585-1613 may also represent *Miomustela madisonae*. In addition, the dentition of SBCM L1585-1613 is also similar to that of AMNH 104677, a skull of *Miomustela* from Observation Quarry (see Lofgren et al. 2016, fig. 4) (Table 2).

Table 2. Measurements in mm of the upper dentition of *Miomustela* from the Barstow and Crowder formations of California, compared to the holotype of *Plionictis ogygia* (AMNH 9042) and a skull of *Miomustela* (AMNH 104677) from Observation Quarry, Nebraska.

Specimen		P3	P4	M1
AMNH 104677	L	2.8	4.3	2.0
	W	1.2	1.8	3.9
RAM 16254	L	2.3	4.4	—
	W	1.3	2.2	—
SBCM L1585-1613	L	2.9	4.6-4.8	—
	W	1.3	2.3-2.4	—
AMNH 9042	L	4.7	7.3-7.4	3.5
	W	2.8	4.2-4.3	6.7

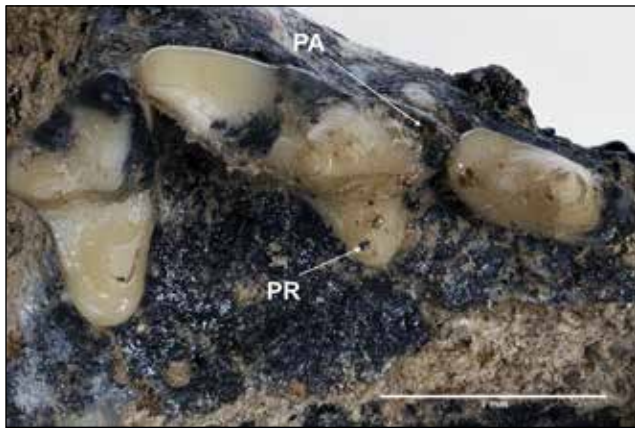


Figure 4. Occlusal view of the right P3-M1 of SBCM L1585-1613, a skull of *Miomustela* from the Crowder Formation (PR, protocone; PA, paracone). Scale bar equals 3 mm.

Also, the SBCM collections include a partially prepared dentary with p3 and m1 (SBCM 1-130-32N) of what appears to be *Miomustela* from Skyline Quarry East, a site from the uppermost part of the middle member. SBCM 1-130-32N has the typical m1 morphology of *Miomustela*; large and anteriorly projecting paraconid and large protoconid positioned slightly anterior to small metaconid (Figure 6). But the m1 of this specimen has a relatively wider talonid basin and is 30% longer than the m1 of the Crowder Formation dentary (L1585-1613). The m1 of SBCM 1-130-32N is also about 10% larger than the m1 of the holotype of *Miomustela madisonae* (Table 1). Thus, there may be two species of *Miomustela* in Barstovian or late Hemingfordian strata from southern California. A larger species represented by SBCM 1-130-32N and a smaller species represented by RAM 16254 and SBCM L1585-1613. More specimens are needed from both the Barstow and Crowder formations to fully address this uncertainty.

Biostratigraphy

The Barstow Formation in the Mud Hills consists of about 1,000 meters of nonmarine strata that is subdivided into three members which, in ascending stratigraphic order, are the Owl Conglomerate Member, the middle member, and the upper member (Woodburne, et al., 1990). Small mustelids from the Barstow Formation were reviewed by Pagnac (2005) and only a single specimen of *Miomustela madisonae* (RAM 16254) was identified from the Barstow Formation (Lofgren et al., 2016). RAM 16254 is from RAM locality V98004, a site in the upper member, about 30 meters below the *Hemicyon* Tuff (Lofgren et al., 2014). Thus, RAM 16254 is slightly older than 14.0 Ma and is from strata that correlate to the Ba2 biochron of the Barstovian NALMA (Figure 6). The additional specimen of *Miomustela* from the Barstow Formation described here (SBCM 1-130-32N) is from the uppermost part of the

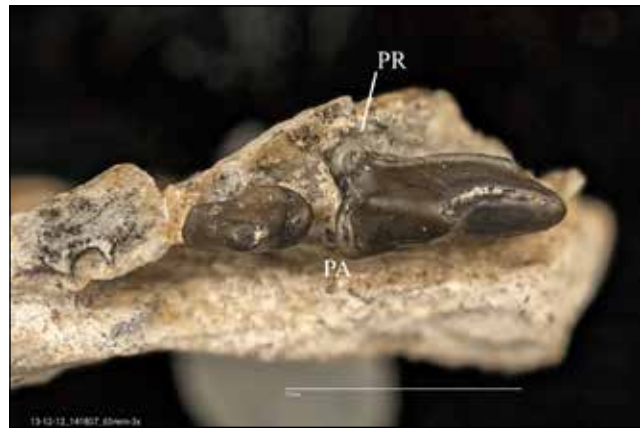


Figure 5. Occlusal view of RAM 16254, a right maxilla fragment of *Miomustela madisonae* with P3-4 from RAM locality V98004 (PR, protocone; PA, paracone). Scale bar equals 5 mm.

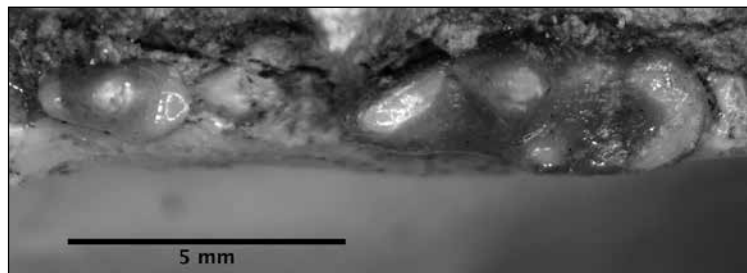


Figure 6. Occlusal view of the p3 and m1 of SBCM 1-130-32N, a right dentary from Skyline Quarry East from the middle member of the Barstow Formation. Scale bar equals 5 mm.

middle member, strata that correlate to the Ba1 biochron (Figure 7).

The Crowder Formation record of *Miomustela* (SBCM L1585-1613) is part of the Wye Local Fauna which was recovered from Bed 1 of Unit 1 of the formation (Reynolds et al. 2008). The Wye Local Fauna resembles that of the Red and Rak divisions of the Barstow Formation, and several of its taxa indicate an affinity to the He2 biochron of the Hemingfordian NALMA (Reynolds et al. 2008) (Figure 7). The dentition of SBCM L1585-1613 is very similar in morphology and size to specimens of *Miomustela* from Observation Quarry, an early Barstovian AMNH excavation in the Sand Canyon Beds of Nebraska (Tedford et al., 2004). A recent study of the small mammals from Observation Quarry indicates that it yields a transitional Hemingfordian-Barstovian fauna, with the greater number of species of Barstovian affinity also suggesting an early Barstovian age (Korth and Evander, 2016).

Summary

Two specimens of *Miomustela* are known from the upper and the middle member of the Barstow Formation. These specimens differ significantly in size and it is unsure which represents *Miomustela madisonae* and if there are two species present. The biostratigraphic range of *Miomustela* includes parts of both the Ba1 and Ba2 biochrons. Because the recovery of a small mustelids

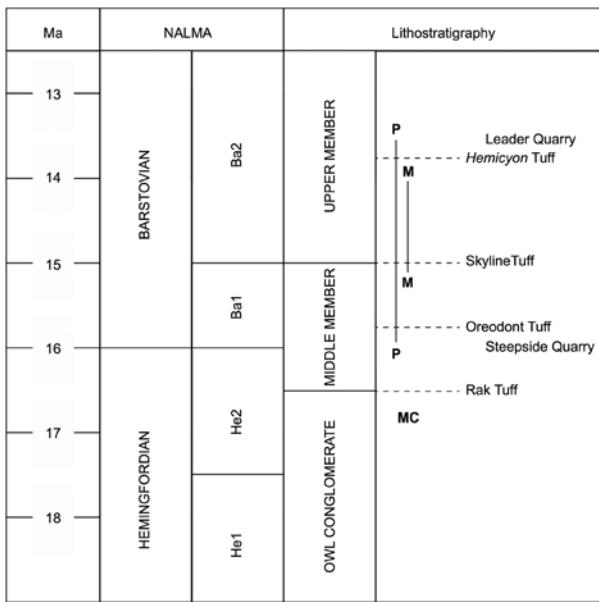


Figure 7. Geochronology and biostratigraphic subdivision of the Barstow Formation (adapted from Pagnac, 2009 and Woodburne et al., 1990), showing stratigraphic ranges of *Plionictis* (P) and *Miomustela* (M), as well as an approximation of the correlated stratigraphic position of L1518-1613 (MC), a skull and dentary of *Miomustela* from the Crowder Formation, in relation to Barstow Formation strata.

from the Barstow Formation is a rare event, any new discovery might significantly change the currently known biostratigraphic range of *Miomustela*.

The Late Hemingfordian strata (He2) of Crowder Formation also contain *Miomustela* based on a skull and dentary. This specimen is more similar in size to RAM 16254 than SBCM 1-130-32N and it is unknown if it represents *Miomustela madisonae* or a smaller species of the genus.

Acknowledgements

We thank J. Shearer of the California Bureau of Land Management for permits, R. Reynolds for encouragement and information, M. Woodburne for reviewing the manuscript, P. Holroyd of the UCMP, I. Gilbert and J. Reynolds of the SBCM, and J. Galkin, R. O'Leary, A. Gishlick, and J. Meng of the AMNH for access to, loan of, and/or photos of specimens, and the Mary Stuart Rogers Foundation, Augustyn Family Fund, and the David B. Jones Foundation for financial support.

References cited

- Baskin, J.A., 1998. Mustelidae. pp.152-173, in C.M. Janis, K.M. Scott, and L.L. Jacobs (eds.), *Evolution of Tertiary Mammals of North America 1: Terrestrial Carnivores, Ungulates, and Ungulate-like mammals*. Cambridge University Press, United Kingdom.
- Douglass, E., 1903. New Vertebrates from the Montana Tertiary. *Annals of the Carnegie Museum* 2:145-199.

- Douglass, E., 1929. General notes. *Journal of Mammology* 11:146-155.
- Hall, E.R., 1930. Three New Genera of Mustelidae from the Later Tertiary of North America. *Journal of Mammology* 11:146-154.
- Korth, W. W., and R. L. Evander. 2016. Lipotyphla, Chiroptera, Lagomorpha, and Rodentia (Mammalia) from Observation Quarry, Earliest Barstovian (Miocene), Dawes County, Nebraska. *Annals of the Carnegie Museum* 83:219-254.
- Lofgren, D. L., C. Kwon, J. Todd, S. Marquez, A. Holliday, R. Stoddard, and P. Kloess. 2014. Preliminary analysis of an important vertebrate bearing horizon with abundant avian material from the upper member of the Barstow Formation of California. Pp. 155-164, in Reynolds, R.E. (ed.), *Not a drop left to drink. California State University-Fullerton Desert Studies Consortium, 2014 Desert Symposium Field Guide and Proceedings*.
- Lofgren, D. L., A. Holliday, and R. Stoddard. 2016. Review of small mustelids from the Barstow Formation of California. Pp. 295-302, in Reynolds, R. E. (ed.), *Going Loco, Investigations along the Lower Colorado River. California State University-Fullerton Desert Studies Consortium, 2016 Desert Symposium Field Guide and Proceedings*.
- Pagnac, D. C., 2005. *A Systematic Review of the Mammalian Megafauna of the Middle Miocene Barstow Formation, Mojave Desert, California* (PhD Dissertation). University of California-Riverside, 384 pp.
- Pagnac, D. C., 2009. *Revised Large Mammal Biostratigraphy and Biochronology of the Barstow Formation (Middle Miocene), California*. *Paleobios* 29:48-59.
- Reynolds, R. E., Reynolds, R. L., and E. H. Lindsay. 2008. *Biostratigraphy of the Miocene Crowder Formation, Cajon Pass, southwestern Mojave Desert, California*. *Natural History Museum of Los Angeles County, Science Series* 41:237-253.
- Steinen, R. P., 1966. *Stratigraphy of the middle and upper Miocene, Barstow Formation, California*. (m.s. thesis): University of California-Riverside, 150 pp.
- Tedford, R. H., L. B. Albright III, A. D. Barnosky, I. Ferrusquia-Villafranca, R. M. Hunt Jr., J. S. Storer, C. C. Swisher II, M. R. Voorhies, S. D. Webb, and D. P. Whistler. 2004. *Mammalian biochronology of the Arikarean through Hemphillian interval (late Oligocene through early Pliocene epochs)*. Pp. 169-231, in M. O Woodburne (ed.), *Late Cretaceous and Cenozoic mammals of North America*. Columbia University Press, New York.
- Woodburne, M. O., Tedford, R. H. and C. C. Swisher III. 1990. *Lithostratigraphy, Biostratigraphy, and Geochronology of the Barstow Formation, Mojave Desert, Southern California*. *Geological Society of America Bulletin* 102:459-477.

A notable canid baculum from the Miocene Barstow formation, Mud Hills, California

Robert E. Reynolds

CSU Desert Studies Research Associate, Redlands, CA 92373, bob.reynolds220@gmail.com

ABSTRACT: A fossil baculum was recognized during preparation of fossils at the San Bernardino County Museum. The specimen is from the Miocene Barstow Formation of the central Mojave Desert, specifically from Robbins Quarry in Hell Gate Basin, approximately 13 meters above the Hemicyon Tuff (14.0+/-0.1 Ma). Robbins Quarry strata have produced a record of 21 vertebrate taxa, including two felids and five canids, from the upper Barstovian Land Mammal Age (Ba2) of the early Miocene.

Baculae are composed of dense bone, and lack surfaces for articulation. Rarely preserved as fossils, it is a challenge to determine the source taxon. This specimen differs morphologically from the straight and grooved baculae of modern canids. The process of elimination suggests that the Robbins Quarry baculum belongs to the borophagine *Aelurodon asthenostylus*, a bone-crushing dog slightly larger than a modern coyote.

The baculum is the penile bone, or os penis, that occurs in carnivora (canids, felids, procyonids, bear, and pinnipeds), rodents, insectivores, bats, and some primates. Baculae are rare fossil occurrences, and the recovery of this element from Robbins Quarry in Hell Gate Basin (HGB) prompted a search for the identity of the source taxon.

Stratigraphy and age

The upper part of the Barstow Formation in the Mud Hills contains the Barstow Fauna (Woodburne and Reynolds, 2010). Hell Gate Basin (HGB) is located in the western Mud Hills, north of Fossil Canyon, along the Carnivore Canyon drainage. The sedimentary section in HGB (Woodburne and Reynolds, 2010) includes the Skyline Tuff (ST) and Dated tuff (DT; 14.8 Ma), the Hemicyon Tuff (HT; 14.0 Ma) and the Lapilli Tuff (LT; 13.4 Ma). Robbins Quarry is located 13 m above the HT and is therefore slightly younger than 14 Ma.

Description

The 10 cm long baculum is a 9 mm diameter dense bone with a small, medial hole at the broken proximal end. The lateral views (Fig. 1, 2) show a slight sinusoidal curve, with the distal tip arching dorsally. In dorsal view (Fig. 3), the shaft is straight. The tip is slightly flattened dorsally, with small lateral ribs along both sides of the distal margin.

Elimination of suspects

Strata containing the Robbins Quarry fauna include two felids, the mountain lion size *Pseudaelurus intrepidus* (Browne, 2002) and the bob cat size *Nimravides marshi* (Browne and Reynolds, 2015). Extant felids (*Felis concolor*,

Lynx rufus) have bullet-shaped baculae that are less than 3 cm long. The small size and morphology suggests that the baculum is not from a felid.

Canid-like carnivores (Browne, 2002; Pagnac, 2009) from the Barstow Fauna include, from small to large, the caninae (Wang and others, 1994) *Leptocyon* sp. and the borophagines (Wang and others, 1999) *Cynarctus*



Figure 1 Robbins Quarry baculum L1816-5832. A: left lateral view, B: right lateral view; C: dorsal view.



Figure 2. *Amphicyon* baculum replica RAM 18272/ V—2017001. A: dorsal view; B: lateral view.

galushai, *Paracynarctus kelloggi*, *Paratomarctus temerarius* and *Aelurodon asthenostylus*. Large amphicyonids *Amphicyon*, *Pliocyon*, and *Ischyrocyon* are also present. The specimen differs morphologically from the straight and grooved baculae of modern canids and from that of *Canis dirus*.

The moderately curved structure (Fig. 1) of the Robbins Quarry baculum excludes the straight baculum of the bear-dogs (Amphicyonidae, Fig. 2a) which have an anterior groove that extends for more than one-third the length of the shaft. Additionally, the *Amphicyon* baculum (Fig. 2) is 30 cm in length, much longer than the baculum under study.

The baculum of extant coyotes and fox is straight, with a posterior groove that extends two-thirds of the length of the shaft. The structure and small size of coyotes (7 cm) and smaller fox (including *Leptocyon* sp.) baculum excludes that group. In contrast, the baculum of the Miocene fox (*Hesperocyon gregarius*, Wang, 1994, Fig 12) is highly curved.

Based on skull measurements, the borophagines *Paratomarctus temerarius* (15 cm skull) and *Cynarctus galushai* (17 cm skull) are structurally too small to have a 10 cm long baculum. The process of elimination suggests that the Robbins Quarry baculum belongs to the Borophagine *Aelurodon asthenostylus*, a bone-crushing

dog with a 20 cm skull that was slightly larger than a modern coyote.

Discussion

Body size and morphology of extant and fossil carnivores, including two felids and seven canid-like carnivores from the Robbins Quarry stratigraphic horizon, were compared to the fossil baculum from Robbins Quarry. The process of elimination suggests that the taxonomic source of the baculum from Robbins Quarry is *Aelurodon asthenostylus*.

Acknowledgements

The author thanks Dr. Xiaoming Wang for discussions and direction with this research. Dr. M. O. Woodburne provided constructive comments during review. Access to specimens in the Raymond Alf Museum for photography was provided by Gabriel Santos and Dr. Andrew Farke. Specimen RAM 18272/ V-2017001 was photographed by Dr. Andrew Farke. SBCM specimens were photographed by Ian Gilbert, curator of earth science. Thanks to James Shearer, BLM archaeologist, and BLM Barstow Field Office staff for providing paleontologic use permits for access to localities. The author acknowledges the generous assistance from many SBCM volunteers who collected specimens from Robbins Quarry specimens over the last 30 years.

References

- Browne, Ian D., and Reynolds, R.E., 2015, *Nimravides marshi* (Felidae): an early scimitar-cat from the upper Barstovian section of the Mud Hills, Mojave Desert, California, 2015 Desert Symposium Volume, California State University, Desert Studies Consortium, p. 136-144.
- Browne, I. D., 2002, Late Barstovian Mammalian Fauna of Robbins Quarry (Barstow Formation, San Bernardino County, California) [Master's Thesis]: University of California, Riverside, p. 111.
- Pagnac, D. 2009. Revised large mammal biostratigraphy and biochronology of the Barstow Formation (middle Miocene), California. *PaleoBios* 29(2): 48-59.
- Reynolds, Robert E., and Ian Browne, 2015, Robbins Quarry: Taphonomy and stratigraphic position in the Barstow Formation, Mojave Block, California. 2015 Desert Symposium Volume, California State University, Desert Studies Consortium, p. 145-148.
- Wang, Xiaoming, 1994, Phylogenetic systematics of the Hesperocyoninae (Carnivora: Canidae). *Bulletin of the American Museum of Natural History* 221:1-207).
- Wang, Xiaoming, Tedford, R. H., and Taylor, B. E., 1999, Phylogenetic systematics of the Borophaginae (Carnivora: Canidae): *Bulletin of the American Museum of Natural History*, no. 243, p. 391.
- Woodburne, Michael O. and Robert E. Reynolds, 2010, The mammalian litho- and biochronology of the Mojave Desert Province; 2010 Desert Symposium Volume, California State University, Desert Studies Consortium. p. 124-147.

Size variation in *Cynarctus galushai* (Canidae) dentition from the Barstow Fauna, Mud Hills, California

Robert E. Reynolds

CSU Desert Studies Research Associate, Redlands, CA 92373; bob.reynolds220@gmail.com

ABSTRACT—Newly recovered specimens of teeth from a borophagine dog, *Cynarctus galushai*, from the upper Barstow Fauna in the upper half of Barstow Formation in the western Mud Hills exhibit a wide range of size. Specimens discussed here were collected from 12 m below to 120 m above the Hemicyon Tuff (HT). The 0.7 Ma span of time in which the specimens were deposited is within the early Miocene, constrained by the HT (14.0 Ma) and the Lapilli Tuff (LT) (13.4 Ma).

Molar specimens under study include a small M2/ recovered from below the HT in Hell Gate Basin (HGB) and a large maxilla with molars from 120 m above the HT in Truck Top Wash (TTW). The molars' size and morphology were compared to the large *Cynarctus galushai* from Robbins Quarry located 13 m above the HT in HGB. Size was also compared with specimen measurements from the Frick American Museum (AMNH) collections. The *Cynarctus* from immediately below the HT in HGB is shorter and narrower than AMNH specimens. Three molars of *Cynarctus galushai* from above the HT are larger than those from the AMNH collections.

The size variation of *Cynarctus* reported in this study is not statistically significant due to the limited sample size. Examination of additional dentition from within the 0.7 Ma span of these stratigraphic limits may allow conclusions about species diversification in the early Miocene upper Barstovian North American Land Mammal Age.

Introduction

The upper part of the Barstow Formation in the Mud Hills contains the Barstow Fauna (Woodburne and Reynolds, 2010). Canid-like carnivores from the Barstow Fauna include the canine *Leptocyon* sp. and the borophagines *Cynarctus galushai*, *Paracynarctus kelloggi*, *Paratomarctus temerarius* and *Aelurodon asthenostylus*. Large amphicyonids *Amphicyon*, *Pliocyon*, and *Ischyrocyon* are also present. Recently recovered specimens of a borophagine dog identified as *Cynarctus galushai* from the upper Barstow Fauna in Hell Gate Basin (HGB) and Truck Top Wash (TTW) exhibit a wide range of size.

Location and age range

Hell Gate Basin is located in the western Mud Hills along the Carnivore Canyon drainage and north of Fossil Canyon. The sedimentary section includes the Skyline Tuff and Dated Tuff (14.8 Ma), the Hemicyon Tuff (HT, 14.8 Ma) and the Lapilli Tuff (LT, 13.4 Ma).

Truck Top Wash is located in the far northwestern Mud Hills. The pair of white tuffs in TTW is tentatively referred to the Hemicyon Tuff and the Hemicyon Tuff of Lindsay. A *Cynarctus* palate with dentition (RAM 18788) was collected from paleosol sediments approximately 120 meters above the pair of tuffs. The HGB specimens are clustered around the HT, while the TTW specimen was recovered from slowly accumulated paleosols much higher

in the section. Differing rates of sediment accumulation in HGB wetland/lacustrine sediments and TTW paleosol sections prevent precise stratigraphic comparison of specimens.

The stratigraphic range of specimens collected is from 12 m below the HT in HGB, to 120 m above the HT in TTW. The 0.7 Ma span of time in which the specimens were deposited is roughly constrained by the HT (14.0 Ma) and the LT (13.4 Ma).

Occurrence

Pagnac (2009) reports six canids of the Barstow Fauna stratigraphically near the HT (14.0 Ma) and below the LT (13.4 Ma): *Aelurodon asthenostylus*, *Cynarctus galushai*, *Paracynarctus kelloggi*, *Tomarctus brevirostis*, *Paratomarctus temerarius*, and *Microtomatctus conferta*. Three of these, *C. galushai*, *P. temerarius* and *A. asthenostylus*, were recovered from Robbins Quarry in HGB by SBCM paleo crews between 1970 and 1998 (Browne, 2002).

Comparisons

Of the six canid taxa, the genus *Aelurodon* is significantly larger than all the other five. Upper molars of *Aelurodon* can be distinguished by the reduction of the M2/ relative to the M1/. The width of M2/ is only 55% that of M1/ and a labial cingulum on M2/ is not illustrated. Adaptations



Figure 1. *Cynarctus galushai*. Occlusal view of left M1/, M2/ (L1816-3477; SBCM 1-130-1, Robbins Quarry).



Figure 2. *Cynarctus galushai*. Occlusal view of left M2/ (L1816-5833; SBCM 1-130-8, SBCM Quarry P).



Figure 3. *Cynarctus galushai*. Occlusal view of left P4/, M1/, M2/ (RAM 18788; SBCM 1-130-424, Truck Top Quarry).

toward hypocarnivory are accompanied by significant reduction of the metacone relative to the size of the paracone in both M1/ and M2/. The size and morphology of *Aelurodon* eliminates that genus from comparison to molars under study.

Tomarctus has a “C” (bean-shaped) M2/, with metacone reduced in relation to paracone. The lingual cingulum is strong on M1/ and on the paracone of M2/, but much reduced on the metacone of M2/.

Paratomarctus has a “C” (bean-shaped) M2/, with hypocone extended posteriorly, making the tooth wider lingually than labially.

Browne (2002) indicates that “*P. temerarius* shows a number of adaptations toward hypercarnivory and is differentiated from the similarly sized, more hypocarnivorous *C. galushai* by teeth gracile [slender] in appearance with structural emphasis on increased shearing.”

The M2/ of *Paracynarctus* is slightly elongate relative to the M1/ (Wang and others, 1999).

Cynarctus galushai has a rhombohedral-shaped M2/, with metacone half the size of the paracone. Comparison with other *Cynarctus* species suggests that the new rhombohedral M2/ specimens can be referred to *C. galushai*. The inflated, non-rhomboidal M2/ of *Carpocyon compressus* excludes that taxon from consideration.

Measurements and distinguishing morphologic characteristics support the identification of SBCM L1816-3477 from Robbins Quarry (SBCM 1-130-1), SBCM L1816-5833 from HGB SBCM Quarry P (1-130-8), and the maxilla from TTQ, SBCM 1-130-424 (RAM18788) as *Cynarctus galushai*.

Size variation

The M1/s of *Cynarctus galushai* (L1816-3477, RAM 18788) from above the HT are up to 15% longer and 24% wider than the AMNH mean. The M2/s of *Cynarctus galushai* (L1816-3477, RAM 18788) from above the HT are up to 19% shorter and almost equal in width to the AMNH mean. The M2/ of *Cynarctus* (L1816-5833) from 12 meters below the Hemicyon Tuff in Hell Gate Basin is 26 % shorter and 17% narrower than the norm from the AMNH collections.

Summary

There is notable size variation in *Cynarctus galushai* from the Barstow Fauna of the Mud Hills. The M1/s of

Table A: Average measurements (mm) of upper molars of *Cynarctus galushai*.

LOC	Taxon	LM1	WM1	LM2	WM2
SBCM 1-130-1* Robbins Quarry	<i>Aelurodon asthenostylus</i> L1816-3609	14.68	17.75		
SBCM 1-130-1* Robbins Quarry	<i>Paratomarctus temerarius</i> L1816-4098; L1816-5598	11.37	14.44	6.38	9.25
SBCM 1-130-1* Robbins Quarry	<i>Cynarctus galushai</i> L1816-3477 (lt & rt)	11.00	13.80	6.27	9.63
SBCM 1-130-8 Quarry P	<i>Cynarctus galushai</i> L1816-5833			5.8	9.0
SBCM 1-130-424 Truck Top Quarry	<i>Cynarctus galushai</i> RAM 18788	12.4	14.5	7.4	9.8
AMNH Mean **		10.80	11.70	7.70	9.90

* Browne, 2002; ** Wang and others, 1999, Appendix III.

Cynarctus galushai (L1816-3477, RAM 18788) from above the HT appear to be longer and wider than the AMNH mean. The M2/s (L1816-3477, RAM 18788) from above the HT appear to be reduced in length compared to the AMNH mean. The M2/ (L1816-5833) from below the HT is much shorter and narrower than all other *Cynarctus* M2/s. The sample size is too limited to allow erection of separate species. Examination of additional dentition from within the 0.7 Ma span of these stratigraphic limits may allow conclusions about species diversification in the early Miocene upper Barstovian North American Land Mammal Age.

Acknowledgements

I thank Dr. Xiaoming Wang for discussions and direction with this short paper and Ian Gilbert for photographing SBCM specimens. Dr. M. O. Woodburne provided constructive comments during review. Specimen RAM 18788 was photographed by Lucy Herrero of the Alf Museum in Claremont. Thanks to James Shearer, BLM archaeologist at Barstow Field Office for providing paleontologic use permits for access to localities. Several specimens were collected under permit CA-16-08P; exp. date Sept. 2019. Quintin Lake, Mark Roeder, and Tom Howe assisted with collecting these specimens over the past 30 years.

References

- Browne, I. D., 2002, Late Barstovian Mammalian Fauna of Robbins Quarry (Barstow Formation, San Bernardino County, California) [Master's Thesis]: University of California, Riverside, p. 111.
- Pagnac, D. 2009, Revised large mammal biostratigraphy and biochronology of the Barstow Formation (middle Miocene), California. *PaleoBios* 29(2): 48-59.
- Wang, Xiaoming, Tedford, R. H., and Taylor, B. E., 1999, Phylogenetic systematics of the Borophaginae (Carnivora: Canidae): *Bulletin of the American Museum of Natural History*, no. 243, p. 391.
- Woodburne, M. O. and R. E. Reynolds, 2010, Litho- and biochronology of the Mojave Desert Province, California. *California State University, Fullerton Desert Studies Consortium*, p. 124-147.

A small invertebrate fauna from the middle Miocene Monterey Formation, including a possible new species of bivalve, in southern Orange County, California

N. Scott Rugh

Paleo Environmental Associates, Inc. srugh@sbcglobal.net

During excavation work for a new residential development (Reata Glen), in Orange County, California in 2016 and 2017, large numbers of fairly well preserved invertebrate fossils from the middle Miocene Monterey Formation were recovered. Five bivalve species, three gastropod species and one species of echinoid were obtained. Reata Glen is located a few miles east of the I-5 Freeway northeast of San Juan Capistrano, and less than half a mile west of San Antonio Parkway, just north of the Ortega Highway (State Route 74). The property was formerly Planning Area 1 of Rancho Mission Viejo (RMV). A substantial quantity of matrix blocks containing fossil shells was recovered from 25 fossil collecting localities. Almost all of the material was collected by Archaeological Resources Management Corporation (ARMC) field monitor Carrie Lambert. Fossils occurred in a light to dark gray, mostly very fine- to fine-grained sandy siltstone layer one to two feet thick with an approximately one-inch thick layer of dark gray to predominately black, very fine-grained clayey silt, most commonly observed at the base of the gray sandstone layer, but sometimes occurring

as another nearly one-inch thick layer at the top of the sandstone bed.

Methods

Within the gray sandstone layer, where the majority of the fossils were collected, two lithologies could be noted: 1. Laminated light to dark gray, silty, very fine-grained sandstone that breaks easily along fine bedding (depositional) planes and is fairly easy to prepare, and 2. A mix of silty sand with a high clay content, usually a dark gray color, but often greenish, which does not fracture easily and is more difficult to prepare. At many localities, the sediments were oxidized to cream and tan colors and fossils were only preserved as internal and external molds. The unoxidized, darker gray colored sediments contained specimens with the original shell material preserved, although much of this shell material was chalky and frequently prone to crumbling. Many specimens were deformed and fractured, and some shells were literally flattened. Fortunately, several specimens were undeformed, and these were selected with the best of the less well-preserved examples for the final collection.

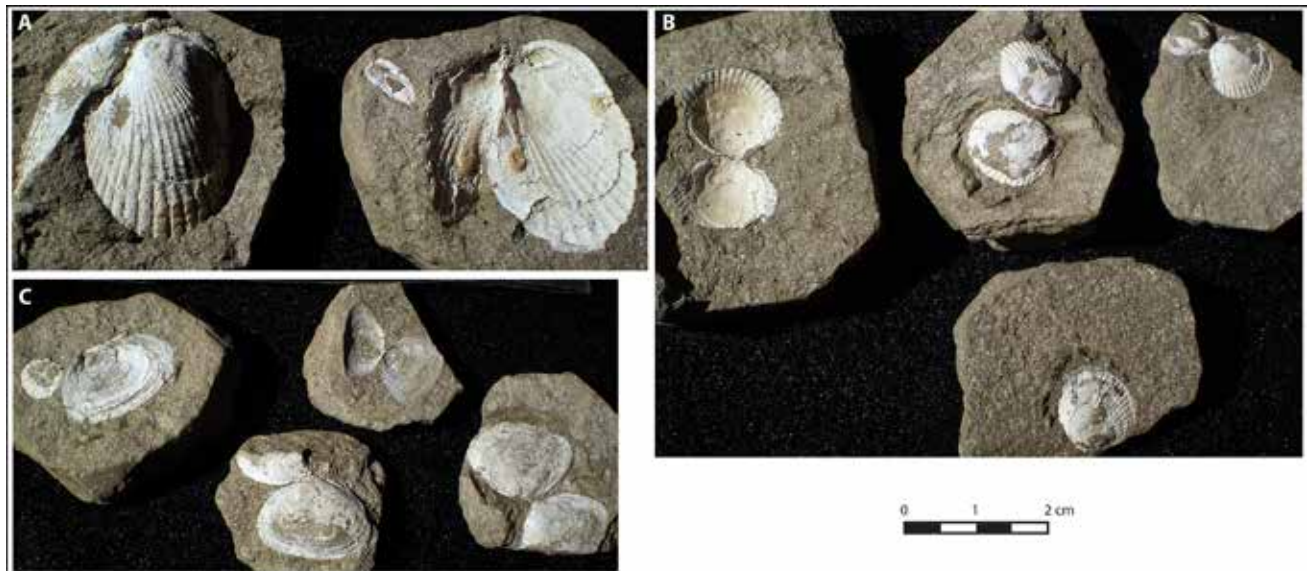


Figure 1. Common bivalve species from Reata Glen: A. Ark clam *Anadara* sp. cf. *A. montereyana*, paired valves, part-counterpart; B. Carditid cf. *Cyclocardia ventricosa*, including three paired valves; C. Tellinid *Macoma albaria*, paired valves.



Figure 2. Locally abundant transparent scallop *Delectopecten peckhami*, only present in a few of the collecting sites. Many of the specimens are paired valve molds. The patches of cracked, whitish material is original thin, fragile shell material that has been sealed to internal and external molds with a dilute glue and water solution.

Specimens (on reduced matrix) were removed from the sediment blocks by breaking away pieces of the block with the beveled edge of a rock hammer, chopping pieces off with a crimper tool, or sawing out specimens with a carbide blade on a hacksaw handle (Figures 1 to 5). To consolidate the chalky shell material and attach as much of the thin shell as possible to the internal and external molds, a 1:10 mixture of glue and water was dripped on

the surface of the specimen, often applying two coats of the milky solution. In addition to hardening and bonding the shell to fossil mold surfaces, the dilute glue solution effectively filled in the pores and cracks in the siltstone and solidified it. When dry, the glue and water solution is compatible with acetone based waterproof polymers, such as Paraloid B-72 or PVA (Vianc).

Results

The collections contain a fairly low diversity of invertebrate fossils, including five bivalves, the ark clam *Anadara* sp. cf. *A. montereyana*¹, the carditid cf. *Cyclocardia ventricosa*, the tellinid *Macoma albaria*, the transparent scallop *Delectopecten peckhami*, and the nut clam *Nuculana* (*Saccella*?) sp., three gastropods, the mud nassa *Nassarius* sp. cf. *N. arnoldi*, the moon snail cf. *Polinices* sp. and a possible whelk species, and the echinoderm, cf. *Astrodapsis* sp. Scattered bony fish remains, including scales and tiny bones (opercula, spines and vertebrae) were also present. A couple of the best-preserved fish specimens include a fairly well-preserved part-counterpart tail end of a small fish from locality DAA-0403-2017-1 collected by David Alexander, and a

¹ *Anadara* cf. *montereyana* is used after Stanton's (1966) paper on the Castaic Formation. This species is easily confused with the middle Miocene species *Anadara obispoana* (Moore, 1983). Perhaps they are synonymous.

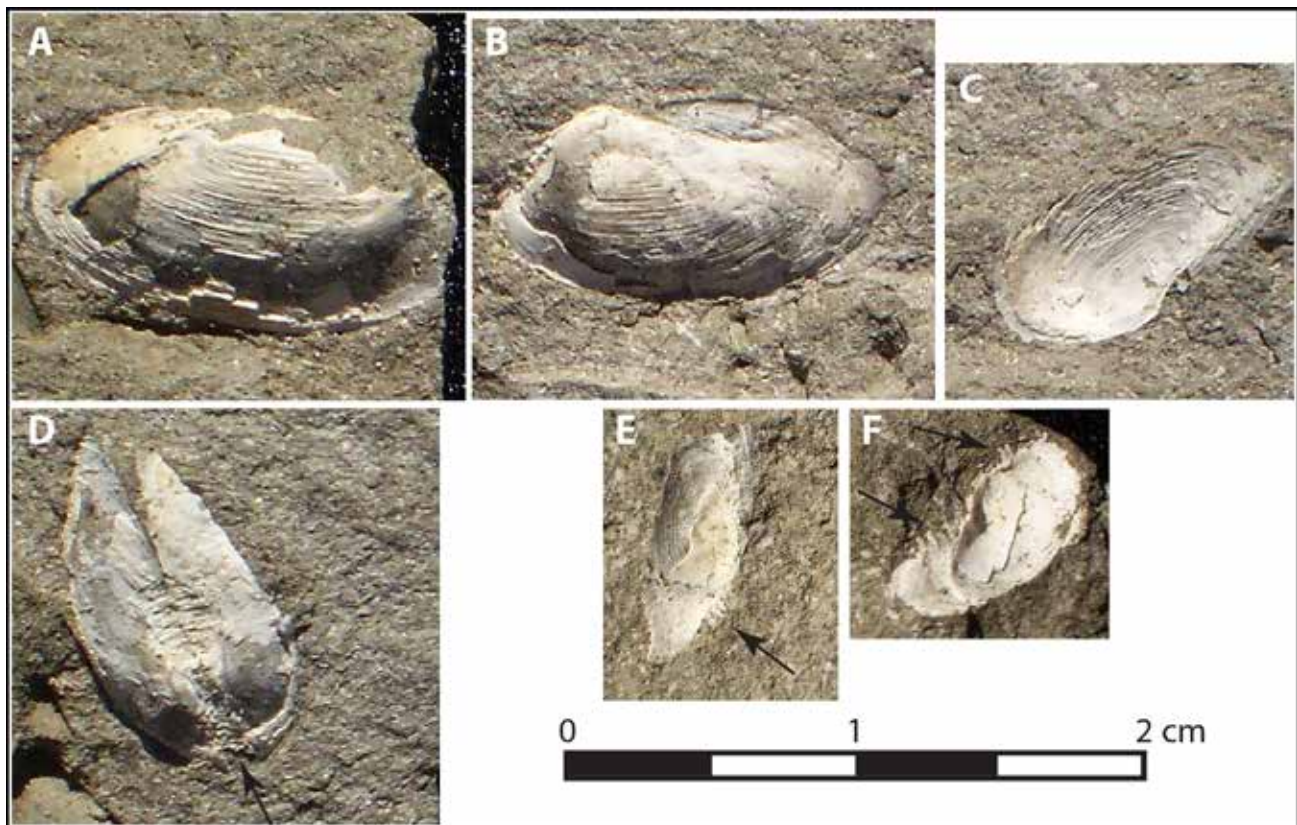


Figure 3. *Nuculana* (*Saccella*?) A-C. Valves showing external sculpture. Specimen C is an internal view of valve, worn along ventral edge to external sculpture. D-F. Valves showing teeth along the hinge line of a pair, external view (D), and on the dorsal edges of valves showing internal views (E and F).



Figure 4. *Nassarius* sp. cf. *N. arnoldi*. Left, Internal mold with crushed spire. Right, Partial external mold.

nicely preserved blackish vertebra from site CEL-0412-2017-2 collected by Carrie Lambert.

Paleoenvironment

The preservation state and species composition of the Reata Glen fossils give good clues about the paleoenvironment. Many bivalves were preserved in the open “butterfly” position (i.e. paired valves). This indicates a fairly undisturbed ocean bottom environment with a relative lack of currents, which is typical of deeper waters. This is consistent with the very fine-grained sediment types in which the specimens are preserved. Several of the bivalve genera in the collection such as *Cyclocardia*, *Delectopecten*, and *Nuculana* are known to live in great ocean depths hundreds and even thousands of feet deep. It is harder to interpret depth from species of *Anadara*, but *A. sp. cf. A. montereyana* is believed to have lived in considerable ocean depths (Savdra and Bottjer, 1987).



Figure 5. cf. *Astrodapsis* sp., part-counterpart. Some detail of the ornate radial arrangement of test elements is clearly visible in this highly oxidized specimen.

Discussion

The fauna is typical of those collected from similar deposits in southern Orange County, many of which have yielded the same set of species, often with one species being dominant. *Anadara* sp. cf. *A. montereyana* and *Delectopecten peckhami* typically occur in monotypic concentrations. The invertebrate material from Reata Glen provides a better understanding of these projects. Because of the very large numbers of fossils recovered, a few were well enough preserved to adequately compare with material from other projects in the area. For example, a species identified as “*Clinocardium* sp.” from a former RMV project collected in 2012 is now more likely to be considered as *Cyclocardia* sp. cf. *C. ventricosa*.

Eastern Pacific *Cyclocardia* species tend to have fewer ribs than species of *Clinocardium*, and the beak of the former genera tends to occur more anteriorly on the valve than that of the later.

More importantly, examples of a species of bivalve not previously identified in material from other projects is now identified as a *Nuculana*, due to the abundance of this species in the Reata Glen project (only found on the first day from field sites CEL-1118-2016-1 and -2) which provided a few good examples for comparison. Based on poor examples from another project, the species was previously thought to be a species of “*Petricola*”. A few of the Reata Glen examples were found with the taxodont teeth exposed, allowing placement of this species in *Nuculana*, probably in the subgenus *Saccella*. This may represent a new species of nut clam. The specimens from Reata Glen differ from other *Nuculana* species, which are typically tapered to a narrow or pointed posterior end, whereas the Reata Glen specimens are gracefully rounded both anteriorly and posteriorly. No similar examples could be found in a search of literature on the middle Miocene (e.g. Moore, 1963 and 1983), nor could any *Nuculana* with a similar shape and surface sculpture be found in the modern literature, except a line drawing of one living deep water species from the western Atlantic, *Nuculana (Saccella(?)) jeffreysi* (figured in Abbott, 1974).

At the time of writing of this paper PEAI Paleo consultants are working on the Paleo monitoring reports for Reata Glen. The fossils will soon be received by The Doctor John D. Cooper Paleontological and Archaeological Center to be curated and stored in the collections.

Acknowledgements

I would like to thank the personnel of Reata Glen CCRC for the opportunity to collect and research the fossils. Carol Demcak, president of Archaeological Resource Management Corporation (ARMC) provided support for the paleontology work on the project. Thanks to Mark Roeder for oversight of the collection and curation of the invertebrate fossil material. An extra thanks to Carrie Lambert for providing a working paleontology lab in her backyard complete with shade canopy, a sturdy table, and preparation tools. Paleontological monitors Carrie Lambert, David Alexander, and Benjamin Scherzer collected the fossils. Much thanks to George Kennedy for kindly reviewing the paper, and to David Miller for working with the photographs for desired placement of photos and adjustments to the clarity of the *Nuculana* images.

References

- Abbott, R. T. 1974. American Seashells. Second Edition. Van Nostrand Reinhold, New York. pp. 1 - 663
- Moore, E. J. 1963. Miocene Marine Mollusks from the Astoria Formation in Oregon. Geological Survey Professional Paper 419: 1 - 109
- Moore, E. J. 1983. Tertiary marine pelecypods of California and Baja California: Nuculidae through Malleidae. United States Geological Survey Professional Paper 1228-A: A1- A108
- Stanton, R. J. 1966. Megafauna of the upper Miocene Castaic Formation, Los Angeles County, California. Journal of Paleontology 40 (1): 21 - 40
- Savrda, C. E. and Bottjer, D. J. 1987. The exaerobic zone, a new oxygen-deficient marine biofacies. Nature. 327: 54-56

A diverse freshwater molluscan fauna from the latest Pleistocene deposits from Salt Creek, Menifee, California

N. Scott Rugh and Mark A. Roeder

Paleo Environmental Associates, Inc., srugh@sbcglobal.net

Introduction

In February 2011, earth-moving activities associated with the realigning and widening of Goetz Road and construction of a bridge over Salt Creek in Riverside County, southern California resulted in the recovery of a diverse fauna of late Pleistocene invertebrate and vertebrate fossil remains. The Goetz Road Project is located between the I-15 freeway to the west and the I-215 freeway to the east. Goetz Road/Salt Creek Bridge runs south to north at the boundary of the communities of Canyon Lake to the west and Menifee to the east. Salt Creek is a tributary of the Santa Ana River drainage system. The fossils were obtained from a light gray mudstone of a late Pleistocene alluvium, approximately 11,340 years old on basis of accelerator mass spectrometry carbon-14 radiometric dating analysis (Lander, 2015). This sediment was washed in the field to fine to medium-grained sand containing fossil shells. A total of 12,634 mollusk fossils were identified to species level. Many other specimens occurred in the sample but were not counted due to being rejected for the final collection or were too small to isolate. A possible new species of *Gyraulus* is recognized and informally described.

Methods

Specimen totals were obtained from three separate samples of shell material. The first two batches were comprised of miscellaneous collections of specimens that were initially processed by monitors from Paleo Environmental Associates, Inc. (PEAI). One of the samples consisted of shells enclosed by a comparatively hard, grayish matrix. The second sample, in a softer (more friable) matrix was sieved with a 20-mesh screen. The larger specimens were then picked by hand from the resulting residue and the many smaller specimens caught on the screen were collected with forceps. The quantity of specimens obtained was sufficient for the determination of the percentage of different species, so finer mesh sizes were not needed. Shells from the friable matrix were combined



Figure 1. The Goetz Road, Salt Creek Bridge excavation, view toward the south. The position of the fossil beds is low in the gray layer in the cut, angled slope to the east (left) a few feet above the light colored sediment. The fossil layer has been replaced with construction boulders in dark fill in the adjacent bank seen in the center of the photo. The south foundation of the bridge is visible in the background, and a worker stands at the bottom of the excavation for the north end of the bridge. Photo by Jeffrey Cassidy

with those from the more compact matrix. The first two combined samples contained 2,609 identifiable specimens. The third sample included a large bag of dry grass and leaf litter that had been reduced by floating the sample in water to separate any shells from the denser bone occurring in the initial sample. Much of the leaf litter was removed by hand, and then screened over a larger screen to remove much of the remaining leaf detritus. The remaining mix of silt, leaf fragments and shells was screened with a 20-mesh screen to collect the shell specimens. The third batch was by far the most productive sample, with 10,019 specimens. Most of the shells from that batch were in excellent condition and relatively few fragmented or worn specimens were rejected. Species percentages were calculated by combining the specimen totals for each species from all three batches (Table 3). Only six specimens of the fingernail clam *Pisidium* sp. in all were retained. Although this total of 6 was used in the calculation of the frequency of species in Table 2, they are

Table 1.—Molluscan taxonomic list, PEAI locality JDC 2011-02-15-02.

Class Gastropoda (snails)

Order Mesogastropoda

Family Valvatidae

Valvata humeralis (glossy valvata)

Order Branchiopulmonata

Family Lymnaeidae

Fossaria cubensis (Carib fossaria)

Stagnicola elodes (marsh pondsnail)

Family Pysidae

Physella cf. *heterostropha* (tadpole snail)

Family Planorbidae

Gyraulus circumstriatus (modern contaminant)

Gyraulus parvus (ash gyro)

Gyraulus new sp.?

Planorbella tenuis (Mexican rams-horn)

Ferrissia cf. *fragilis* (fresh-water limpet)

Order Sigmurethra

Family Succineidae

Succinea rehderi (chrome ambersnail)

Family Pristilomatidae

Hawaiiia miniscula (minute gem snail) (modern contaminant?)

Family Limacidae

?*Deroceras laeve* (slug)

Order Unknown

Unidentified gastropod species

Class Bivalvia (clams)

Order Veneroida

Family Pisiidiidae

Pisidium spp. (fingernail clams)

Table 2. Frequencies and habitats of molluscan taxa from PEAI locality JDC 2011-02-15-02.

Species	Common Name	Frequency	Habitat
<i>Gyraulus new sp.?</i>	gyro	44.0%	presumably slow-flowing water
<i>Gyraulus parvus</i>	ash gyro	16.4%	slow-flowing water with mud substrate
<i>Physella</i> cf. <i>heterostropha</i>	tadpole snail	13.0%	shallow, slow-flowing creek, spring, or river
<i>Stagnicola elodes</i>	marsh pondsnail	10.2%	shallow, slow flowing or standing water
<i>Valvata humeralis</i>	glossy valvata	7.4%	lakes, ponds, marshes, or slow-flowing streams with mud substrate
<i>Planorbella tenuis</i>	Mexican rams-horn	5.3%	slow-flowing or standing water with mud substrate
<i>Fossaria cubensis</i>	Carib fossaria	1.8%	amphibious, edges of streams or ponds with mud substrates
<i>Pisidium</i> sp.	fingernail clam	0.1%	bottoms of lakes, streams, and rivers
<i>Succinea rehderi</i>	chrome ambersnail	<0.01%	damp or moist plants and under rocks and logs
<i>Hawaiiia miniscula</i>	minute gem snail	<0.01%	moist protected areas in wooded habitats
? <i>Deroceras laeve</i>	slug	<0.001%	terrestrial, moist plant debris, near water bodies
<i>Ferrissia</i> cf. <i>fragilis</i> ^a	fresh-water limpet	<0.001%	quiet, subpermanent to permanent water less than 6 feet deep and with muddy to sandy substrate

^aSpecific identification and habitat after Groves (2015).

Table 3. Specimen counts for molluscan taxa from PEAI locality JDC 2011-02-15-02 by sample.

Species	Sample			Total
	1	2	3	
<i>Planorbella tenuis</i>	145	264	354	663
<i>Physella</i> sp.	274	42	1130	1,646
<i>Valvata humeralis</i>	240	41	901	1,182
<i>Stagnicola elodes</i>	116	223	944	1,283
<i>Gyraulus parvus</i>	249	144	1673	2,066
<i>Gyraulus new sp.?</i>	650	300	4612	5,562
<i>Fossaria cubensis</i>	20	1	205	226
Total	1694	915	10,019	12,628

Note: Six specimens of *Pisidium* from samples 1 and 2 not included because substantial number of additional specimens not counted.

not included in the total counts for Table 3, resulting in a reduced total of 12,628 for that table. Several additional tiny specimens were observed but not collected due to the very fragile nature of these specimens which break easily, even with fine forceps. A technique using a fine paint brush to collect the specimens would have permitted the collection of many of these specimens, but time was limited. As a result, in this study, the calculation of a 0.1 % frequency of *Pisidium* sp. is underestimated.

A large *Physella* shell from the Salt Creek fossil bed not selected for the collection was submitted to Beta Analytic, Inc., Florida for radiocarbon dating analysis (Appendix B, Lander, 2015). The result was a conventional radiocarbon age of 11,340 +/- 50 years BP. The 2 Sigma calibration ages are 13290 to 13130 calibrated years BP.

Results

The fossil molluscan assemblage from PEAI locality JDC 2011-02-15-02 represents a high diversity of extant mollusk species, mostly freshwater snails and a freshwater clam (Table 1). There are only three completely terrestrial species in the assemblage, including a slug, which is represented by only one specimen, and two land snail species, each represented by three specimens. For one of those species, *Hawaiiia miniscula*, two of the specimens appear to be modern. Thus, the entire suite of species constitutes a dominantly freshwater assemblage.

The species found at the Salt Creek bridge excavation are presented in Table 2 in order of decreasing abundance (modern species omitted). The percentage represented by each species in the molluscan assemblage was based on a total sample of 12,634 specimens. The most common snails were two species of the freshwater gastropod genus *Gyraulus*. The more abundant taxon might represent a new species. That species was also the larger bodied, with the largest specimen measuring 8.5 mm in diameter. The second species was identified as *G. parvus*, with the largest individual measuring 6.5 mm in diameter. A third species, *G. circumstriatus*, was also recognized in the sample, but

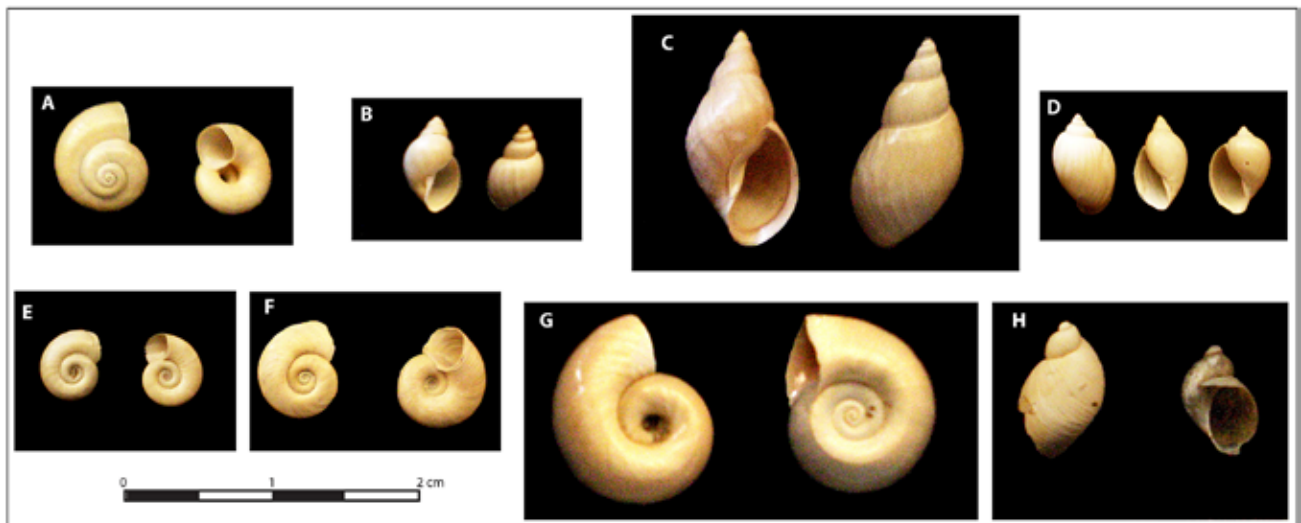


Figure 2. Large gastropods (over 5 mm in size). Top row: A. *Valvata humeralis*, B. *Fossaria cubensis*, C. *Stagnicola elodes*, D. *Pysella* sp. cf. *P. humerosa*. Bottom row: E. *Gyraulus parvus*, F. *Gyraulus* new sp.?, G. *Planorbella tenuis*, H. *Succinea rehderi*.

appeared to be modern occurrences or contaminants because its shells were shiny and amber in color. A total of 31 specimens of this last species was identified. It was the smallest-bodied species of the three, the largest individual measuring just 4.0 mm in diameter. The species was not included in the calculations of species percentages because its remains were not considered fossilized. However, it did prove useful when comparing with the other two species because species of *Gyraulus* are very difficult to identify.

After carefully examining specimens of *G. circumstriatus* and *G. parvus*, it was observed that the aperture of *G. circumstriatus* tended to be rounded and aligned horizontally with the flattened shell, whereas the aperture in *G. parvus* tended to be stretched outward and somewhat downward and, consequently, appears to be diamond-shaped. In both *G. circumstriatus* and *G. parvus*, the aperture is about a third the length of the shell when viewed with the aperture facing towards the viewer and to the right. The most abundant and possibly

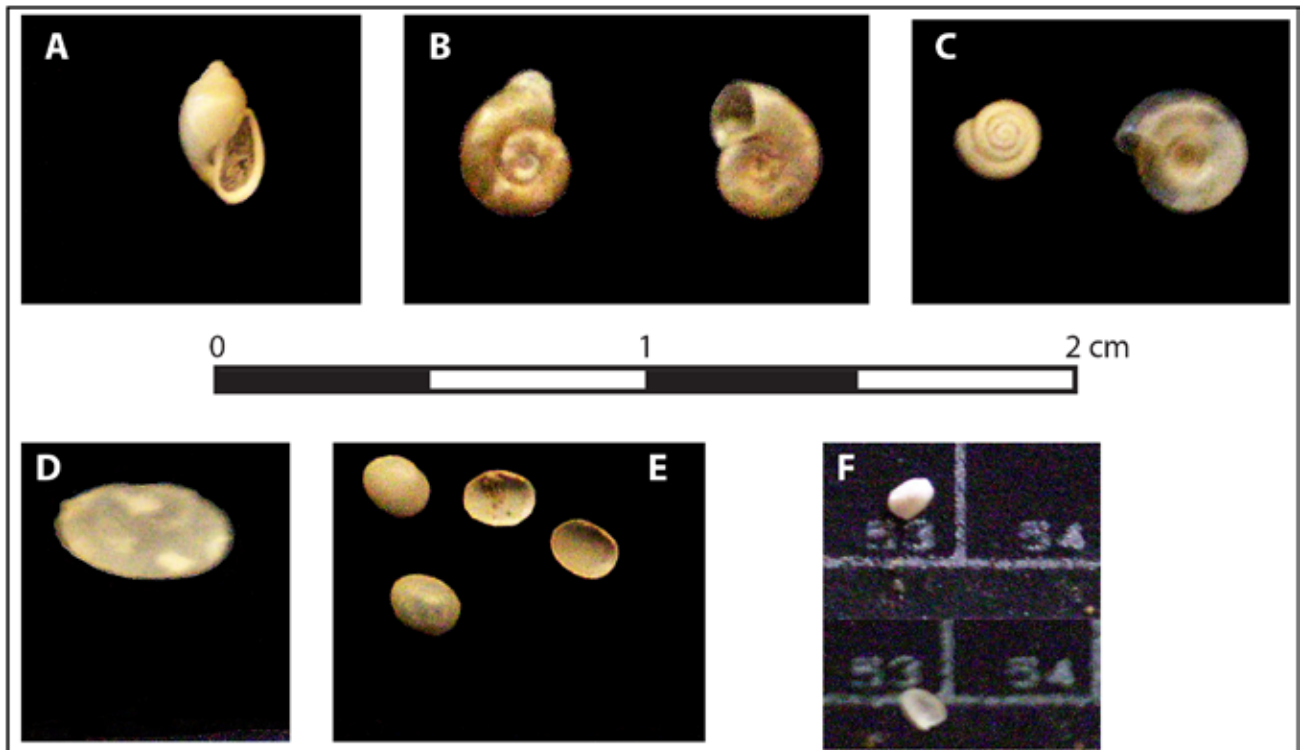


Figure 3. Small gastropods (under 5 mm in size). Top row: A. Order unknown, unidentified gastropod, B. *Gyraulus circumstriatus**, C. *Hawaiiia miniscula**. Bottom row: D. ? *Deroceas* sp., E. *Pisidium* sp., F. *Ferrissia* sp. cf. *F. fragilis*. *species that appear to have mixed into the fossil material from overlying modern sediment.

new species of *Gyraulus* is described below. In contrast to the morphology of the new species, it is more difficult to distinguish shells of the two other *Gyraulus* species.

The largest shells of the other species in the assemblages include those of *Stagnicola elodes* (15 mm in height, but the largest specimen, also measuring 15 mm, missing spire, would probably have been about 20 mm if complete), *Planorbella tenuis* (10.5 mm in diameter), *Physella* sp. cf. *P. heterostropha* (largest 10.5 mm in height, although all other specimens were 8.0 mm or less), *Fossaria cubensis* (9.0 mm in height), and *Valvata humeralis* (6 mm in diameter).

The respective specimens are preserved extremely well, with most being unbroken and many having lips with little or no chipping. The shell surface of most shells is not even slightly chalky. Many of the *Valvata humeralis* specimens have a yellowish hue and are glossy, and many of the *Stagnicola elodes* shells have an orangish or purplish band along the inside of the outer lip. This color band is not as intense as that of modern shells, and because the overall color of these shells is an opaque cream color, not a transparent amber color typical of the family, they are not thought to be modern.

Description: *Gyraulus* new sp? (Figure 2.F.). The possible new species of *Gyraulus* is the largest of the three *Gyraulus* species from this project, the largest specimen measuring 8.5 mm in diameter. The second largest species is *G. parvus*, the largest individual measuring 6.5 mm in diameter, and no example of the smallest species, *G. circumstriatus* (a modern contaminant) is over 4.0 mm in diameter. The potentially new species of *Gyraulus* has an aperture wider than the others associated, which extends almost halfway into the shell, making the shell more globose, and the umbilicus is noticeably more constricted than in the other two species. In addition, while the other two species always have thin lips, the presumed new species only sometimes has a thin lip. Instead, there is a shelf-like widening around the edge of the lip in most specimens of the apparently new species, including juveniles, making it possible to identify specimens down to 1 or 2 millimeters in diameter. In contrast, it is more difficult to distinguish shells of the two other *Gyraulus* species. The potential new species is similar to *G. hornensis* of the Great Lakes region illustrated by Burch and Tottenham (1980) in having a wide aperture that extends more than a third of the way into the shell.

Vertebrate fauna

Like the invertebrate fossils (Table 2), ninety percent of the vertebrate remains recovered from this site were species that today inhabit fluvial and/or lacustrine environments (three-spine stickleback, arroyo chub, chorus frog, true frog, western pond turtle) (Table 4). The remaining ten percent are vertebrates that today inhabit the riparian corridors and/or upslope drier scrub or chaparral habitats on either side of the present-day Salt Creek drainage (lizards, snakes, birds, and rodents). Notably absent from

this latest Pleistocene aged site were the remains of large extinct land mammals. Large modern species like ground squirrel, rabbits, and deer were not recovered. Since the paleoenvironment of the project site appears to have been mostly aquatic, the conditions must not have favored the preservation of these medium to large mammals.

Discussion

Very nearly all of the molluscan species in the assemblage are aquatic species that live in slow-flowing or standing water over a soft substrate. Some species, such as *Valvata humeralis* and *Stagnicola elodes*, prefer areas with dense bottom vegetation. The tadpole snail, *Physella* sp. cf. *P. heterostropha*, might prefer scattered hard surfaces, suggesting that rocks might have been present on the bottom. However, terrestrial taxa, such as *Succinea rehderi* and *Deroceras* sp., are extremely rare or, as in the case of the land snail *Hawaiiia miniscula*, probably modern. Those habitat preferences suggest that the depositional environment represented by the molluscan assemblage was completely aquatic.

Other modern and fossil freshwater molluscan faunas may be compared with that from the Goetz Road PEAI locality JDC 2011-02-15-02. The most common species, or similar species, from the Salt Creek locality are species common in southern California water systems today. For example, in both Tecolote Creek, San Diego, and Mission Creek, Santa Barbara, *Physella* sp. cf. *P. heterostropha* and *Fossaria parva* (similar to *F. cubensis* from Salt Creek) are common species. In Mission Creek, *Gyraulus parvus* is also common. These species also occur in Pleistocene-aged fossil collections of freshwater invertebrates in southern California museums. In San Diego, these collections from near the Pacific Coast tend to have a relatively low diversity of freshwater mollusk species. One of the most diverse collections is from the Robertson Ranch, Mastodon site, SDSNH Locality 6044 with 4 freshwater gastropod species and 2 species of land snails. All three of the above living freshwater species present in Mission Creek were present in the mastodon site, as well as *Planorbella tenuis*. The two fossil land species from that site are the slug *Deroceras* sp. and *Succinea rehderi*. The San Diego Natural History Museum has Holocene aged collections from the Imperial Valley near the Salton Sea. These collections often contain *Physella* and *Gyraulus* species, but lack the *Fossaria* species. The addition of a few species unique to the region such as the subfossil gastropod *Tryonia protea*, the brackish water clam *Rangia* sp. in some places, and small species of Hydrobiid snails tends to increase the diversity of freshwater fossil faunas in that region. For example, the Brawley Bypass, SDSNH locality 6224 contains 8 freshwater species, including 2 bivalve species.

A collection with a species diversity of 12 freshwater species including 9 mollusk species and 3 land snail species was obtained in 2000 during monitoring of the Ameridge development project in Fullerton, Orange

Table 4. Counts and frequency of vertebrate taxa recovered from PEAI JDC2011-02-15 -02

Common Name	Scientific Name	Number of Remains	Percentage
Three-spined stickleback	<i>Gastrosteus aculatus</i>	ca 725	69%
Arroyo chub	<i>Gila cf. orcuttii</i>	172	16
Chorus frog	<i>Pseudacris</i> sp.	40	4
True frog	<i>Rana</i> sp.	5	1
Western pond turtle	<i>Actinemys marmorata</i>	2	.2
Whiptail	<i>Aspidoscelus</i> sp.	2	.2
Spiny lizards	Phrynosomatidae	2	.2
Lizards	Lacertilia	12	1
Rubber boa	<i>Charina bottae</i>	1	.1
Ring-necked snake	<i>Diadophis punctatus</i>	2	.2
Gopher snake	<i>Pituophis cf. catenifer</i>	2	.2
Racer	<i>Coluber</i> sp.	3	.3
Two-striped garter snake	<i>Thamnophis cf. hammondi</i>	1	.1
Garter	<i>Thamnophis</i> sp.	2	.2
Garter	<i>cf. Thamnophis</i> sp.	1	.1
Snakes	Serpentes	29	3
Shorebirds	Charadiiformes	1	.1
Thrush	Turdidae	1	.1
Medium-sized songbird	Passeriformes	1	.1
Shrew	<i>Sorex</i> sp.	1	.1
Weasel?	Mustelidae (small)	1	.1
Pocket gopher	<i>Thomomys bottae</i>	9	1
Pocket mouse	<i>Perognathus/Chaetodipus</i> sp.	18	2
Pocket mouse	<i>cf. Chaetodipus</i> sp.	3	.3
Vole	<i>Microtus</i> sp.	2	.2
Wood rat	<i>Neotoma</i> sp.	2	.2
Pinyon mouse	<i>Peromyscus cf. truei</i>	1	.1
Deer mouse	<i>Peromyscus</i> sp.	3	.3
Deer mouse	<i>cf. Peromyscus</i> sp.	2	.2
Harvest mouse	<i>Reithrodontomys</i> sp.	3	.3
Rodent	Rodentia	8	1
Total		ca. 1056	

County by PEAI. Many of the species described above (including all 6 species from the Robertson Ranch project) were present in the material from the Ameridge project. A few species found in the Salt Creek project not present in any of the above-mentioned locations include *Stagnicola elodes*, *Valvata humeralis*, and the potential new species of *Gyraulus*.

Valvata humeralis and *Stagnicola elodes* are known from the fossil record in southern California. Both occur at Rancho La Brea, the former also in the Palos Verdes Formation of Los Angeles County and the Manix Formation of the Mojave Desert (Lamb, 1989), and the

latter in the Rancho Labrean of Michigan (Lander, 2015). *Valvata humeralis* also occurred in the high elevation late Pleistocene Basin deposits of Lake Owens around 11,000 years before the present (Koehler, 1995).

Conclusions

The species composition of mollusks of the Goetz Road/Salt Creek project provides strong evidence that the depositional environment was predominately an aquatic habitat as indicated by the high percentage of strictly freshwater mollusk species versus the low percent of land snail species. Here the same relative frequency pattern was observed for the vertebrate fossils: The number of specimens of the few freshwater vertebrates, especially fish and frog species, were far more abundant than the relatively fewer specimens of the many terrestrial vertebrate species (Table 4). The same kind of direct relationship between the relative percentages of mollusks versus vertebrates is observed in the recent PEAI Pacific City development project located approximately 1 kilometer south of Huntington Beach, Orange County and about 1 kilometer inland from the current shoreline (Wake and Roeder, 2009). In the Pacific City project, fossil elements from aquatic vertebrate species such as fish, toads, frogs and pond turtles along with species that live near the edge of streams and ponds, including salamanders and garter snakes were predominant. Confirming the presence of a slow-moving body of water and associated riparian zone, the three most common species of snails in that study, comprising 88% of the fauna, were *Gyraulus parvus*, *Physella* cf. *P. heterostropha*, and *Fossaria parva*.

The assemblage from Goetz Road/Salt Creek PEAI locality JDC 2011-02-15-02 is notable by its taxonomic diversity. Not counting two modern taxa (*Gyraulus circumstriatus* and *Hawaiiia minisucula*), there are 12 fossil mollusk species present in the collection including 8 freshwater and 2 terrestrial gastropod species, and a single freshwater bivalve species. One additional unidentified fossil pulmonate snail is present (Figure 3. A.). It is not known if this species is an aquatic, or a terrestrial snail. The only living gastropod species that could be found resembling this unknown snail is the Neotropical land snail *Streptostyla labida* (Roth, 2018).

Valvata humeralis and *Stagnicola elodes* are two species most common in northern latitudes (see Burch, and Tottenham, 1980). These species do not appear to be extant in southern California, but do occur rarely in the fossil record in southern California. The apparent new species of *Gyraulus* may be related to the species *G. hornensis* of the Great Lakes region. These last three

species have more northern ranges today, and this suggests that the temperature in the region of Menifee, Riverside County may have been cooler 11,000 years ago than that of today. The single specimen of the freshwater limpet *Ferrissia* sp. cf. *F. fragilis* is also important because it represents only the fourth fossil occurrence of the species known from the western United States (Groves, 2015).

Acknowledgements

We are grateful for the review of this paper provided by Bob Reynolds. We thank Mr. Andrew L. Huneck, a Senior Transportation Planner with the Riverside County Transportation and Land Management (TLMA) Department. TLMA retained Paleo Environmental Associates for oversight of all phases of the project from monitoring to curation of identified fossil material. Dr Sinéad Ní Ghabhláin of ASM Affiliates, Inc., (prime cultural resource contract for Project) provided mitigation program oversight and helped ensure Project compliance with any TLMA guideline regarding paleontologic resources. The fossil specimens were accessioned into the Riverside Metropolitan Museum (RMM) by M. Roeder under the supervision of Mr. James Bryant, the RMM Curator of Natural History. Teresa Woodard provided access to N.S. Rugh to photograph the specimens at RMM.

Lindsey T. Groves, Collections Manager at the Natural History Museum of Los Angeles County Malacology Department identified the freshwater limpet. Barry Roth provided his time to attempt an identification of the unknown gastropod. Dr Thomas Wake of the UCLA Zooarchaeology Department identified the vertebrate remains. Jeffrey D. Cassidy and Patrick W. Riseley, PEAI monitors, collected the fossils, and recorded specimen and geologic data. The senior author would like to thank Bruce Lander, PEAI principal paleontologist for the Project mitigation program for corrections on fossil species range on the early technical report. The editor, David Miller produced the excellent plates of the fossil mollusks.

References

- Burch, J.B., and J.L. Tottenham. 1980. North American freshwater snails: species list, ranges, and illustrations. *Walkerana* 3: 1–125.
- Koehler, P.A. 1995. Late Pleistocene mollusks from the Dolomite site, Owens Lake playa, California. *Veliger* 38(4): 312 – 318.
- Groves, L.T. Collections Manager, Natural History Museum of Los Angeles County Malacology Department. Written communication dated 4-3-2015 to E.B. Lander (PEAI).
- Lamb, R.V. 1989. The nonmarine mollusks of Pit 91, Ranch La Brea, southern California, and their paleoecologic and biogeographic implications. California State University, Northridge. MS thesis. pp. 1 - 365
- Lander, E.B. 2015. Goetz Road Project Canyon Lake and Menifee, Riverside County, California – Paleontological Resource Impact Mitigation Program final technical report of results and findings. Unpublished final project report

submitted to ASM Affiliates, Inc., Carlsbad, CA on behalf of Riverside County Transportation and Land Management Agency Transportation Department. 29 p.

Lander, E.B. Ph.D. (PEAI), Written communication dated 6-15-2015 to N.S. Rugh.

Roth, B. Ph.D. (Paleontology, Berkeley) Written communication dated 2-21-2018 to N.S. Rugh.

Wake, T. A. and M.A. Roeder. 2009. A diverse RanchoLabrean vertebrate microfauna from southern California includes the first fossil record of ensatina (*Ensatina eschscholtzii*: Plethodontidae). *Quaternary Research* 72: 364-370.

A glance to the east: Lake Ivanpah— an isolated southern Great Basin paleolake

W. Geoffrey Spaulding¹ and Douglas B. Sims²

¹*Terra Antiqua, 2320 Cordelia Street, Henderson, NV 89044; wgeoffrey@terrantqua.com;*

²*Department of Physical Sciences, College of Southern Nevada, North Las Vegas, NV 89030*

Setting

Lower Colorado River Corridor Ivanpah Dry Lake lies east of the Ivanpah, Mescal, and Clark mountains, just west of the Nevada border in San Bernardino County, California. Interstate 15 (I-15) crosses its barren flat, leaving California at the northeastern end of the playa, ca. 50 km south of Las Vegas (Fig. 1). Ivanpah playa is nearly contiguous with Roach Dry Lake, Nevada; the elevation of both playas is 794 m amsl. The northern portion of Ivanpah basin hosts solar-energy generation facilities, commercial developments, and regional transmission and transportation corridors. Large alluvial fans encroach on the playa from both the east and the west (Fig. 2); as a result, while it is nearly 20 km long, it is never more than 3 km wide. On the southern margin of the dry lake, the delta-fan of Cima Wash¹ (Fig. 1) spreads onto the playa (Fig. 3). Saltscrub (*Atriplex polycarpa*) rings most of the playa, and extends upslope typically to between 810 and 820 m amsl, where it gives way relatively abruptly to creosote bush (*Larrea tridentata*) scrub.

Hydrography

The Ivanpah drainage is in the southern hydrographic Great Basin, which extends south through the Mojave and Colorado deserts, to about the U.S.–Mexico border (Smith and Street-Perrott, 1983). Tributaries to the lower Mojave River lie only 20 km to the west in Shadow Valley. On the other side of the mountains to the east and south, drainage is to the Colorado River (Fig. 1). Ivanpah's playa covers ca. 53 km², Roach Dry Lake in Nevada, only ca. 15 km². The California portion of Ivanpah Dry Lake's catchment covers ca. 1,128 km² and, in Nevada, its catchment (including that of Roach Dry Lake) is approximately 831 km², for a total drainage basin area of ca. 1,959 km². This drainage network extends from Cima



Figure 1. The Ivanpah Drainage Basin and Vicinity. The irregular line defining the drainage basin is dark-colored in Nevada, and light-colored in California. IDL, Ivanpah Dry Lake; RDL, Roach Dry Lake. Other places are (1) Clark Mountain Range; (2) southern Spring Mountains; (3) Lucy Gray Mountains; (4) Mid Hills; (5) Mescal Range (to west) and Ivanpah Mountains (to east and south); (6) Cima Wash; (7) Valley Wells paleospring deposits, Shadow Valley. Base for this and all remote imagery following are courtesy of *Google Earth*[®] and copyright by *Google*.

Dome to the southwest in California, to Potosi Mountain to the northeast in Nevada (Fig. 1).

Studies of pluvial lakes (e.g. Mifflin and Wheat, 1979; Wells et al., 2003) stress not only the size of a drainage basin and runoff, but also the relationship between the height of topography in a basin and the amount of runoff sufficient to support a lake. The higher the topography, the greater the amount of orographically induced precipitation triggered within that basin. In this light, it is notable that the Ivanpah drainage basin is not only almost 2,000 km² in area, but it is contiguous with the highest mountains in this part of the Mojave Desert including:

- New York Mountain, California (2296 m amsl)
- Clark Mountain, California (2417 m)
- Potosi Mountain, Nevada (2,595 m)
- McCullough Mountain, Nevada (2,142 m)

Previous research

Snyder et al. (1964) mapped a pluvial lake in the Ivanpah basin, but offered no evidence for a paleolake

¹ We are unaware of a formal name for this large wash. For the purpose of this study, we name it after the historic town of Cima near its headwaters.

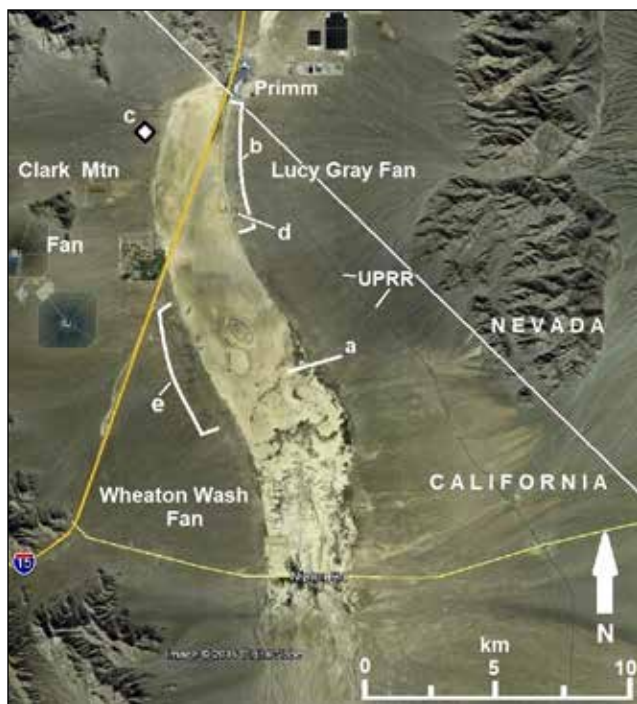


Figure 2. Ivanpah Dry Lake and vicinity. Other localities are (a) transect of Sims and Spaulding (2017) in the Lucy Gray Swale; (b) distribution of wave-cut strath surfaces on the toe of the Lucy Gray alluvial fan; (c) beach ridge buried beneath alluvium of Clark Mountain Fan (CMF-76); (d) the Alpha Longshore Basin; (e) arcuate lineaments of the northern limb of the Wheaton Wash fan toe; UPRR, Union Pacific Railroad.

in the valley. Nor has any evidence been produced for a paleolake here prior to Sims and Spaulding (2017). To the contrary, Mifflin and Wheat (1979) proposed that this, and other similar basin floors, were at most paludal habitat and supported no substantial lakes during the Late



Figure 3. Low-angle remote view south to the Cima Wash Delta-Fan. Dotted line marks the edge of the debouchment. Circles = localities discussed in text. p, stranded playa sediments. Small arrows to the right show the position of the shoreline lineament discussed in text.

Pleistocene. The presumed absence of a paleolake here is reflected in the maps of Smith and Street-Perrott (1983), Spaulding et al. (1983), and Morrison (1991). However, investigations in the southern Ivanpah basin (Spaulding, 1999) revealed the presence of lacustrine sediments ca. 6 m above the elevation of the modern playa (794 m amsl). More recently, no shoreline features distant from the current playa were mapped by House et al. (2006) or Ramelli et al. (2006a, b) near Roach Dry Lake, nor by Schmidt and McMackin (2006) on the fans of the Clark Mountain Range (Figs. 1, 2).

The Valley Wells paleospring deposits, to the west in Shadow Valley (Pigati et al., 2011; Quade et al., 1995), as well as the paleosprings in the Las Vegas Valley to the northeast (Fig. 1; Quade et al., 1995, 1998; Springer et al., 2015), provide evidence for enhanced glacial-age precipitation, ending rather abruptly between 18,000 and 19,000 cal B.P. (calibrated ¹⁴C years before present²). A reemergence of springs from ca. 13,500 to 8,100 cal B.P. occurs in many areas (e.g. Pigati et al., 2011). Pluvial lakes along the Mojave River (Enzel et al., 2003; Reheis et al., 2012; Kirby et al., 2015), particularly Lake Mojave only 70 km to the southwest (Ore and Warren, 1971; Wells et al., 2003), provide another important paleohydrologic data base extending from the last glacial age into the early Holocene. But while paleospring deposits are records of recharge in the form of precipitation on the surrounding mountains (Springer et al., 2015), runoff to pluvial Lake Mojave originates in the San Bernardino Mountains (Enzel et al., 1992; 2003), outside of the Mojave Desert. Thus, a lacustrine record from the Ivanpah basin, recording run-off in an entirely desert basin, would be the first of its kind in the region.

During their study of a 4.5 km long soil-boring transect on the eastern margin of Ivanpah playa ("a" in Fig. 2), Sims and Spaulding (2017) identified two localities where subsurface geochemical changes suggested former beach-zones, distant from the modern dry lake. An excavation to examine one of these geochemical anomalies exposed stratigraphic evidence of at least four high-lake stands, discussed below. These initial findings showed that, even though it lacks prominent wave-cut shorelines, the Ivanpah

² In this study, we use calibrated radiocarbon ages before the present, basing calibrations on conventional ¹⁴C ages corrected for δ¹³C using CalPalOnline (University of Cologne, 2007).

basin possesses a complex lacustrine history warranting further study.

Objectives

Ivanpah Dry Lake, like several other playas in the southern Great Basin lacking obvious shorelines (Smith, 1991), has received comparatively little research, in part because it was thought to have hosted no pluvial lakes. Mifflin and Wheat's (1979) model explaining this apparent absence in terms of the lower topography of the southern desert basins, meager precipitation, and extreme evaporation rates (see also Morrison, 1991; Enzel et al., 2003), essentially codified the assumption that no Late Quaternary lakes existed in these basins. Sims and Spaulding (2017) provided initial basis to challenge that assumption in the Ivanpah basin, and the objective here is to summarize the principal geomorphic and stratigraphic evidence for Lake Ivanpah. We also discuss aspects of the basin's geology and geomorphology that contributed to this paleolake remaining essentially unknown into the 21st century.

Methods

We prioritize evidence that allows discrimination between water bodies of considerable depth and expanse, paleolakes, and other wetland deposits common in the valleys of the northern Mojave Desert (e.g. Quade et al., 1995; Springer et al., 2015). In the past, paleospring deposits in the southern Great Basin were often misidentified as pluvial lake sediments (see discussions in Mifflin and Wheat, 1979; Quade et al., 1995; Enzel et al., 2015, 2016). These criteria include the presence of

- Internal drainage leading to a dry lake bed
- Shoreline (littoral) features
- Bedded, fine-grained (lacustrine) sediments generally horizontally bedded and laterally continuous
- Fossils of aquatic biota

Studying a paleolake in a basin with subdued topography requires relatively precise elevation estimates. Elevations established by total-station survey can differ by several meters from those interpolated from U.S. Geological Survey 7.5 provisional topographic sheets. We therefore discriminate between elevations established by benchmarks and total station surveys, reported as meters above mean sea level (m amsl), and those derived by interpolation, commercial GPS units, and digital elevational models (DEMs), reported as estimated meters amsl (est. m amsl). A geo-positioned survey base station and field unit were used to fix the elevations of key stations to within ± 0.2 m. These elevations were then to the elevation of the playa floor to determine paleolake depth, expressed as change in water level (Δ_w) relative to 794 m amsl ($\Delta_w = 0$ m).

GoogleEarth Pro™ remote imagery was used to initially identify shoreline features. These include lineaments caused by spatially abrupt changes in color and albedo

subparallel to, but well-removed from, the current playa margin. In the field, these contrasts correspond to marked changes in soil conditions (Sims and Spaulding, 2017), as well as vegetation composition and shrub density. Less commonly, a steeper in-board slope is evident, and interpreted as a wave-cut foreslope in front of a littoral beach crest. Broad beach planation (strath) surfaces, and patterns created by the truncation of drainages at relict shorelines, were also identified and related to lake-shore (littoral) geomorphic processes. These features were ground-truthed and documented in the field. In addition, stratigraphic sections were found in natural exposures, and in excavations, that displayed not only lacustrine sediments, but also relict playa surfaces, transgressive sequences, and buried beach features, all >0.5 km from the modern playa.

Shoreline features

This discussion focusses on some of the most obvious shoreline features in the Ivanpah basin. A separate, more comprehensive survey of all evidence identified to date is in review (Spaulding and Sims, 2018).

Lucy Gray Alluvial Fan

Alluvium comprising the Lucy Gray fan (LGF) splays onto the northeastern Ivanpah and the western Roach basins to cover more than 54 km² (Fig. 2; Ramelli et al., 2006a, b; House et al., 2006). The western toe of the LGF describes an arc 16 km long with west-northwest to west-southwest exposures. Several geomorphic features on the toe of this fan are best explained as results of near-shore and shoreline erosion.

Beach surfaces

Remote imagery of the LGF toe ("b" in Fig. 2) reveals elongated, bright patches up to 190 m long, with their long axes oriented perpendicular to the contour lines (Fig. 4a). Their surfaces are barren and covered by a gravel lag that lacks desert pavement development (i.e., settling, interlocking of clasts, presence of desert varnish, iron staining of clast bottoms; Waters, 1992; Fig. 4b, c). These barren surfaces are uniformly inclined toward the playa, and planed flat to the extent that they lack the bar-and-swale topography typical of alluvial fans. Most are floored by a carbonate duricrust (Stage 2 caliche) below a thin (≤ 5 cm) mantle of buff (7.5 YR7/3), bedded silt or, closer to the playa, grey-green (gley1 8/1) playa mud (Fig. 4b). In their topographic position and relationship to the playa they correspond to linear surfaces on the east margin of Roach Dry Lake mapped "Qpf" (playa fringe deposits) and "Qea" (sand sheet deposits; Ramelli et al., 2006b).

At their edges, eolian ablation can be seen stripping away the overlying saltscrub hummocks and exhuming these paleosurfaces. The gravel lag is a product of this deflation; its parent material is a gravelly sand at the base of the saltscrub hummocks. After exposure by ablation



Figure 4. Strath surfaces on the Lucy Gray Fan toe. **a (Top):** Contrast-enhanced oblique aerial view east showing strath surfaces (SS; only a few are labeled for example). **b (Middle):** View northwest across surface; note person in distance. **c (Bottom):** Winnowing of exhumed gravelly beach sand (left, A-B) to produce gravel lag (right, C).

of the overlying hummock, the sand is winnowed out by the prevailing wind, producing a lag of small gravel clasts (Fig. 4c). This mantling lag may correspond to the “Thin (~single-grain) veneer of subangular fluvial gravel commonly at surface” of map unit Qea (Ramelli et al., 2006a, b). However, a fluvial (alluvial) origin for this gravel is not the only possibility. The unconsolidated, gravelly sand that is its parent material (“b” in Fig. 4c) appears no different from the gravelly beach sand of today’s littoral zone (Fig. 5; Spaulding and Sims, 2018), and is considered a beach deposit here too.

These barren areas appear to be wave-planed strath, or beach, surfaces, and represent paleosurfaces being exhumed by eolian ablation of their salt-scrub mantle. Their orientation, proximity to the playa, and microstratigraphy suggest they were created by erosion, as wave action levelled the original bar-and-swale topography of the alluvial fan, during more than one prehistoric high-lake stand. In this model, the gravelly sand at the base of the eroding hummocks (Fig. 4c) relates to the regressive phase of the last lake high-stand, and is a beach deposit analogous to that on the edge of the dry lake today. Its lateral extent and uniform character do not support a fluvial origin (Ramelli et al., 2006a, b);



Figure 5. Gravelly sand of the beach zone of Ivanpah Dry Lake. Depending on locality, this zone is from 5 m to more than 50 m wide. **a (Top):** Beach sand along the shoreline. Debris to lower left and lower right mark the grounding line of flotsam during an undated but recent inundation. Station is 8 km south of Primm (Fig. 2). **b (Bottom):** Close-up of the gravelly sand. Position of trowel is same as top photo.

instead, it is likely littoral. For kilometers along the LGF toe (Fig. 2), these exhumed surfaces extend from the playa upward to ca. 802 m amsl. The mapped upper limit of the mantling beach sand provides a minimum depth for Lake Ivanpah of 7.7 m ($\Delta w \geq 7.7$ m; Fig. 6).

Truncated drainages

In a dry-lake basin with uniformly sloping sides, ephemeral washes would end in a splay of debris, losing their walls and dropping their bedload on the playa margin. However, these terminal debris fans, or debouchments (we reserve the term “alluvial fan” for the kilometer-scale constructs comprising the bajadas of the region), usually don’t occur at the playa edge because the washes seldom reach the dry lake uninterrupted. Remote imagery shows that larger washes usually end >0.5 km from the playa. To investigate these further, stations were established remotely at the apices of debouchments at principal washes. Excluding washes that appear affected by flood-control modifications or recent roadways, these debouchments occur 0.7 to 1.2 km from the edge of the current playa, at 804 est. m amsl ($804.4 \text{ m} \pm 2.1 \text{ m}$, $n = 18$). Their distance from the current playa and generally

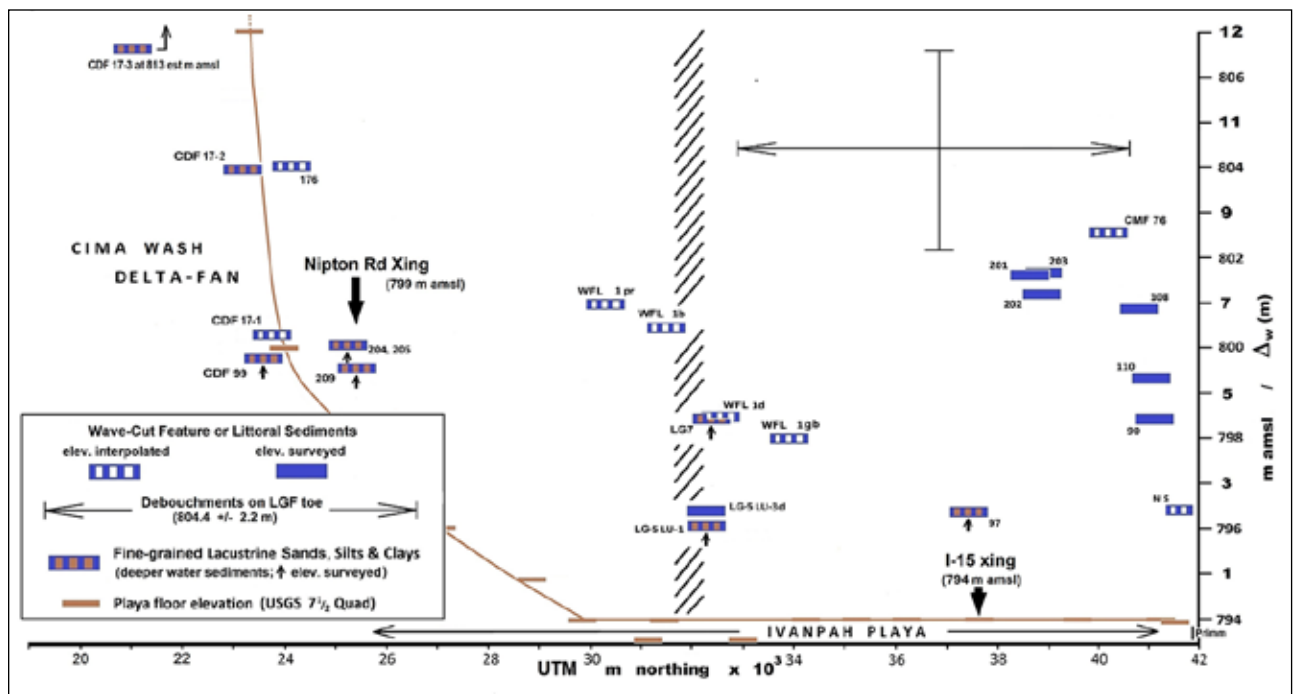


Figure 6. Diagram showing indicators of high water in m above the floor of Ivanpah playa (bottom line); the north end of the playa is to the right, at Primm (Fig. 2; following Spaulding and Sims, 2018). Hachured line shows approximate northern limit of evidence for neotectonic displacement.

consistent elevation indicate that these debouchments are responding to a geomorphic control other than the dry-lake floor. They typically occur just inboard of the lower limit of creosote bush scrub, likely in response to a subtle change in basin morphometry at ca. 804 m elevation. This is likely to be a beach ridge. The elevation of the shoreline indicated by these debouchments, 804 est. m amsl ($\Delta_w = 10.4 \pm 2.1$ m; Fig. 6), is consistent with Sims and Spaulding's (2017) detection of a high-lake stand at $\Delta_w = 9.8$ m.

Wheaton Wash and Mineral Hill Fans

Remote imagery of the western margin of Ivanpah Dry Lake reveals a nearly continuous shoreline lineament extending ca. 13 km, from I-15 corridor to south of Nipton Road (Fig. 2). This feature differs from the east margin of the playa, which displays a range of geomorphologic features attributable to littoral erosion, but no uninterrupted shoreline lineaments.

Wheaton Wash Fan

In the treatment below, we distinguish between the lineament's appearance and attributes on the north limb of the Wheaton Wash Fan (WWF) toe, and its behavior farther south nearer the southern end of the basin. The shoreline lineament on the northeast-facing limb of the WWF toe describes a series of curvilinear features suggesting wave-cut embayments, at some distance from the playa margin (0.5 – 0.8 km; Figs. 2, 7). Knick points were found in the field along some of these lineaments, with steeper slopes on the inboard side, typical of beach morphology, at about where creosote-bush scrub gives

way to saltscrub downslope. The arcuate profiles of these embayments may reflect the cross-sections of alluvial fan lobes, cut by wave action at the edge of a water body. Their development may also reflect cusp-and-embayment topography, typical of beaches subject to strong on-shore flow (Davidson-Arnott, 2010). In the remote images available (e.g. Fig. 7), the albedo contrast representing the shoreline is most evident in the embayments, and least discernable on the cusps, consistent with erosion dominating in the embayments but not on the cusps.

Remote imagery of the WWF shoreline also shows linear, low-albedo, dendritic features primarily down gradient of the shoreline lineament and perpendicular to the contours ("rd" in Fig. 7). Their orientation and shape suggest that these features are relict drainages. In the field they are filled-in, and possess neither bank, nor bed, nor channel. Their presumed deeper soils support dense stands of vegetation, contributing to their low albedo. Their outlines suggest a different surface hydrology than exists today with broad, possibly sluggish drainages and a lower gradient. The shorelines of the WWF embayments range from ca. 798 to 802 est. m amsl, an implied water-depth (Δ_w) of 4 to 8 m.

Southern shoreline lineament

Although it appears flat, the floor of southern Ivanpah playa is not level (Spaulding, 1999). It drops gradually at about 1 m/km to the north, where it attains an essentially level surface about 4 km north of Nipton Road (Fig. 8c). Given this, it seemed appropriate to determine whether the shoreline lineament along the basin's western margin



Figure 7. Shoreline lineaments of the northern WWF (arrows). “rd” = relict drainages. Line on east side of playa is the transect of Sims and Spaulding (2017).

maintains the horizontal, as it should absent neotectonic displacement. We found that this is not the case. Instead, a topographic profile of that lineament reveals a steep initial decline, from ca. 815 est. m amsl at its southern end, opposite the CDF, to 805 est. m amsl where it crosses Nipton Road (Fig. 8b). A more gradual decline in the elevation of the shoreline lineament continues north from Nipton Road for another 3.5 to 4.0 km. The northern limit of this zone of flexure appears to coincide with the northern limit of saltscrub and associated polygonal desiccation cracks on the playa (Fig. 2), and its approximate position is shown by the hachured line in Figure 6.

The decline to the north of the shoreline lineament therefore mirrors the tilt of the axial basin floor (Fig. 8). Since displacement of the basin floor must have occurred *after* the high-lake stand responsible for the shoreline lineament, estimating Δ_w based on field evidence within this zone of flexure (south of the hachured line in Figure 6) may yield spurious results. We anticipate this in our estimates of lake depth moving forward. Finally, neotectonics aside, we note that the elevation of the shoreline lineament near its southern terminus is about the same as that of the surface of the CDF (810 to 815 est m amsl; Fig. 8a). This fulfills another criterion of Enzel et al. (2016) for validating the presence of a paleolake. They point out that, in an actual paleolake, delta-fans must enter the basin at about the same elevation as the shoreline.

Lacustrine and littoral sediments

The results of this study indicate that, in favorable topography, fan-toe progradation and resultant burial obscures, but often preserves, the stratigraphic record of past high-lake stands. The example from the Clark Mountain fan (CMF; below) is particularly instructive,

because shorelines substantially above the modern playa appear absent here.

Clark Mountain Fan

Around the northern part of Ivanpah playa, there is a singular absence of high-lake ($\Delta_w > 2.5$ m) features on the alluvial fans extending from the mountains. But this is likely due to burial of littoral features by fan-toe progradation, rather than to the actual absence of high-lake stands. At CMF-76, on the toe of the Clark Mountain Fan (“c” in Fig. 2), excavations for a solar-energy center exposed littoral features and sediments ca. 85 cm below the surface (Spaulding and Sims, 2018). At this depth, basal gravelly sands comprise a low berm with the in-board slope dipping toward the playa, now ca. 0.75 km distant. This unit is over-topped by charcoal-rich beach sand, interpreted as organic material incorporated in flotsam of an over-bank deposit. Two separate samples from this stratum yielded ^{14}C dates of 5465 ± 100 and 5390 ± 55 cal B.P. (Spaulding and Sims, 2018). This middle-Holocene beach feature lies at ca. 803 est. m amsl ($\Delta_w \approx 9$ m; Fig. 6). The alluvial fan sediment unconformably overlying these features entirely masks any shoreline signature in remote imagery, at least in the visible spectrum. Thus, later Holocene fan-toe progradation (e.g., Harvey et al., 1999; Harvey and Wells, 2003) is a mechanism by which surface evidence of past high-lake stands is entirely masked.

The Alpha Longshore Basin

Relatively large (70 to 250 m), elongate basins can be found along the eastern edge of Ivanpah playa, separated from the playa itself and lying inland (Fig. 9). Their floors are cut off from the playa by ridges 2 to 3 m high. The east wall of one of these, the alpha longshore basin (ALB), reveals a sequence of massive, oxidized, silty, gravelly sands interbedded with thinner silt units containing expansive clays (Fig. 9b). This section shows that the basin walls appear to be composed predominantly of oxidized, alluvially reworked playa and playa-fringe sediments, including eolian and beach sands. The thin, discrete clay-silt units lie approximately horizontally, and can be followed for >50 m, indicating they are not interdunal swale deposits, nor paludal or “palustrine” deposits. The lowest mud in the section, ALB LU-1 lies on a hummocky paleosurface and displays limited, meter-scale evaporite inflorescences. These clay-rich units display no peds, no soil horizonation, and no pedogenic carbonate, all consistent with a lacustrine origin. Three separate lake inundations appear represented by this section (Fig. 9b),

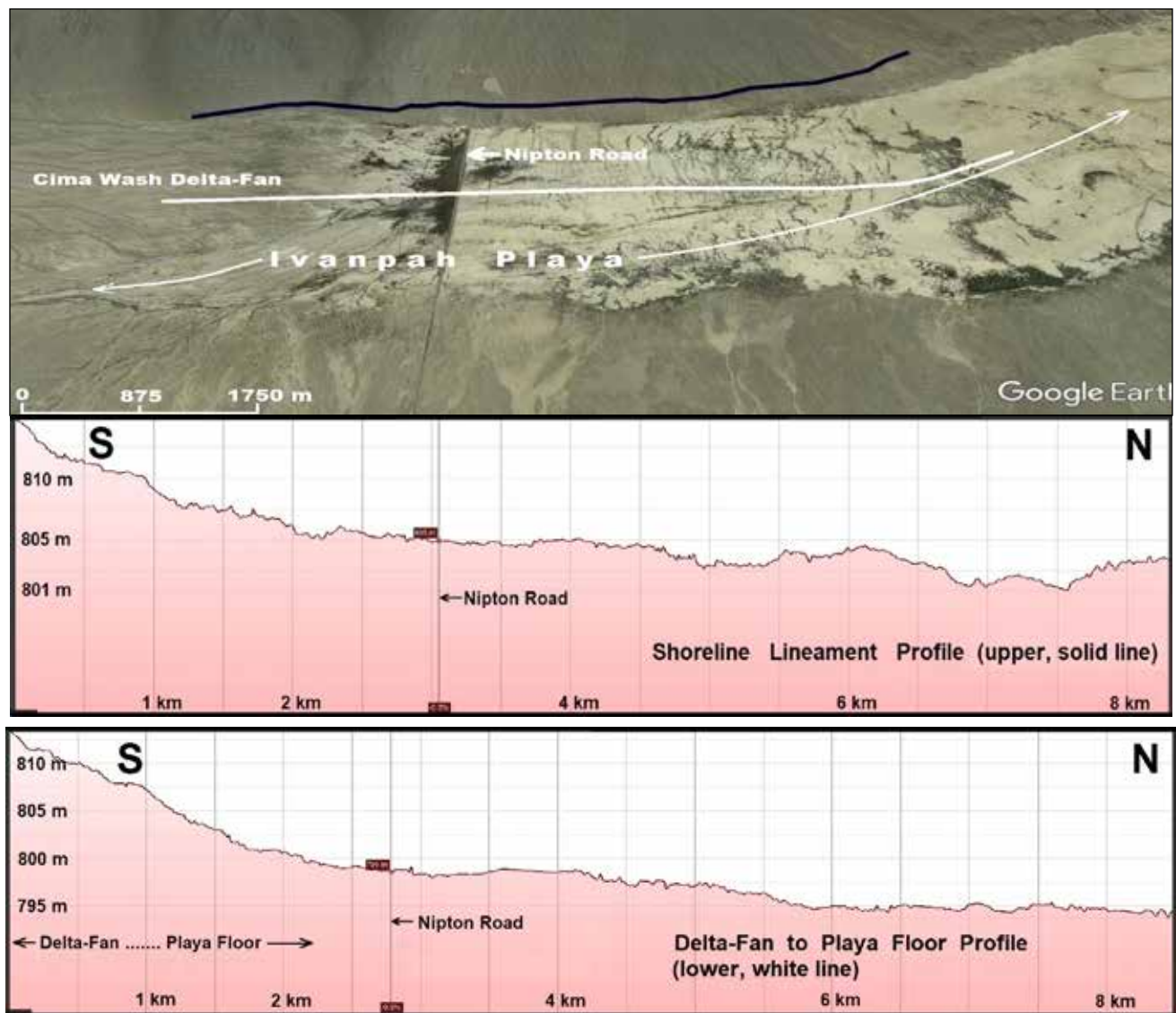


Figure 8. Comparison of two topographic profiles in the southern Ivanpah basin. **a (Top):** Oblique aerial view west showing the relative position of profiles of the southern shoreline lineament (solid line) and the basin floor (white line). **b (Middle):** DEM-based elevational profile of the shoreline lineament (upper, solid line). **c (Bottom):** Profile of the basin floor (lower, white line).

with intervening periods of alluvial deposition. Relatively deep water³ and/or some distance to shoreline is implied by the fine-grained sediment. Evaporites are limited to the lowest unit, and are limited in extent.

The Lucy Gray Swale

Sims and Spaulding (2017) established a transect of bore-holes across the Lucy Gray swale (Fig. 2) to study subsurface sediment-chemical alterations in response to basin-wide inundation. Two excavations along that transect, ca. 0.7 km and 1.1 km east of the playa, provided stratigraphic evidence for several highlake stands below a veneer of alluvium and eolian sand sheet. The most recent lake stage, recorded at LG5, is a transgressional

³ In their study of Pluvial Lake Manix, Reheis et al. (2012) used the following scale: “shallow” lake conditions, <5 m deep; “moderate” lake depths, $\Delta w = 5$ to 8 m; “deep” conditions, $\Delta w > 8$ m. We employ this relative scale here as well.

sequence yielding a ¹⁴C date of 980 ± 35 cal B.P. An unconformity below separates it from horizontally bedded, clean fine lacustrine sand, dated at 7405 ± 40 cal B.P. This lacustrine sand in turn lay above two relict playa surfaces of early Holocene (8820 ± 115 to 9450 ± 25 cal B.P.) and latest Pleistocene age (ca. $13,070 \pm 115$ cal B.P.; Sims and Spaulding, 2017). With the top of the youngest, transgressive sequence of LG5 at 796.4 m amsl, waters in this embayment must have exceeded 2.4 m depth ($\Delta_w > 2.4$ m). At LG7, ca. 1.1 km east of the playa margin, another mud-cracked, relict playa surface was encountered at ca. 125 cm depth. Radiocarbon dating of this lacustrine sequence proved it to be younger than the lacustrine units encountered at LG5. Four stratigraphically separated ¹⁴C dates falling in a narrow range of 5830 ± 60 to 6245 ± 30 cal B.P., close to the age of the buried beach features at CMF-76, discussed above.

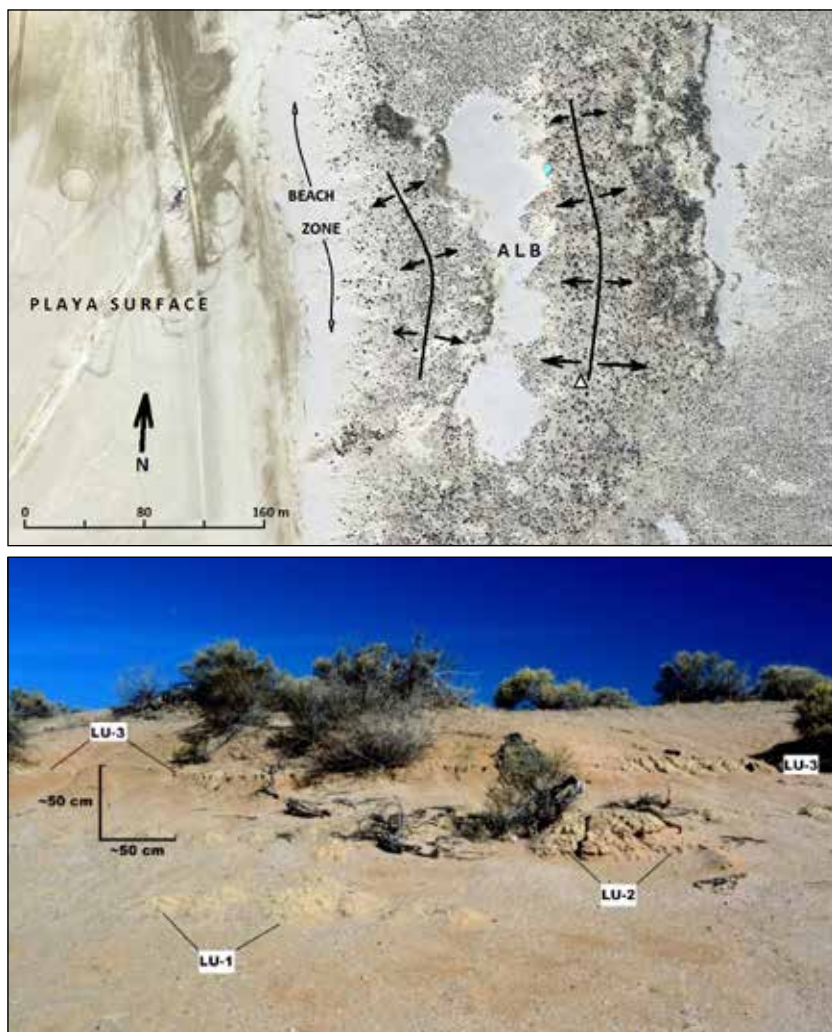


Figure 9. The Alpha Longshore Basin (ALB), east of Ivanpah Dry Lake (Fig. 2). **a (Top):** Remote image of the ALB. Curved lines show crests of low (2-3 m) ridges, arrows point downslope. White triangle is location of benchmark "Skit" (796.8 m amsl). Blue push-pin shows location of profile, below. **b (Bottom):** The east wall of the ALB. Lacustrine units are labeled ALB LU-1 through ALB LU-3.

Southern Ivanpah basin

The playa floor south of Nipton Road (Fig. 2) is complicated, low-relief terrain. Bordering it to the south and east, the Cima Delta-Fan (Fig. 3) rises several meters above it (Figs. 3, 8a). East and north of the foot of the CDF (dotted line in Fig. 3) channeling and sheet wash have exposed a mosaic of lacustrine sediments ranging from light brown (7.5YR 6/3), oxidized playa muds higher in section, to buff to white (2.5YR 7/3) lacustrine silts lower in section. Gravel lag deposits are common. Some consist of allochthonous granitics from the bedload of Cima Wash, or basalts from the alluvial fans to the east. Autochthonous, tufa-nodule gravel lags also cover wide areas.

Elevated playa sediments

In the southern Ivanpah basin, yardangs and larger erosional remnants preserving lacustrine sediment

become common. For example, on the east margin of the playa, from Nipton Road south past Murphys Well, an expanse of playa sediment (areas marked "p" in Fig. 3) separates the alluvial fan to the east from the basin floor to the west. This oxidized light-brown, gritty mud appears little different from that comprising the current playa. It is horizontally bedded and rises to 805 est. m amsl. Shells of a dextrally whorled, conspiral gastropod (cf. Succineidae; the amber snail family) are weathering from this sediment (Spaulding and Sims, 2018). Amber snails are terrestrial pulmonate gastropods that require perennially moist to wet ground, and thrive in habitats ranging from marshes to the edges of freshwater lakes (e.g. Lannoo and Bovbjerg, 1985).

Cima Delta-Fan

Elsewhere in the southern part of the basin, the discovery of lake muds below alluvium of Cima Wash (CDF99-1; Spaulding, 1999) led us to return to the CDF. These dark brown, bedded, charcoal-rich, sandy silts are separated from the overlying Cima Wash alluvium by a sharp discontinuity at 799.9 m amsl (CDF 991; Figs. 3, 6). Carbon from 5 to 25 cm below the discontinuity yielded an age of $10,920 \pm 145$ cal B.P. Additional localities on the delta-fan margin, CDF-17-1, -17-2, and -17-3 (Fig. 3), provide exposures of lacustrine sediment extending laterally for distances approaching a kilometer.

All these sites display the same sequence of lacustrine to littoral sediments, capped by alluvium of the CDF. At the base of the exposed sections lies a >2 m thick bedded, light gray (2.5Y 7/2) to buff (2.5Y 7/3) lacustrine silt. It grades upward to a gray-brown (10YR 7/2) sandy silt, interpreted as littoral muds (Spaulding and Sims, 2018). The elevation of the lacustrine sediments at CDF-17-1 is ≤ 803 est. m amsl ($\Delta_w \leq 9$ m).

Gastropod shells (only the taxon cf. Succineidae, again) are relatively common in this apparently regressive sequence, along with the endocarps (fruit pits) of net-leaf hackberry (*Celtis reticulata*). Net-leaf hackberry is a long-lived, riparian tree, nearly extinct in the Mojave Desert (Jahren et al., 2001; Thorne et al., 1981). The grey-brown littoral muds appear to thicken to the south, and surface exposures of lake muds can be traced to a point almost 4 km south of Nipton Road (Fig. 3), where they lie at 820 est. m amsl. As noted previously, neotectonic displacement may be partly attributable to the high elevation of the lake

sediments exposed along the toe of the CDF, 10>20 m above the playa floor base level (794 m amsl). Also, at this point it is unclear whether these lake sediments are intercalated with and underlain by alluvium of the CDF, or simply lap onto sediments comprising the delta-fan toe.

Discussion and conclusions

Strath surfaces, recently exhumed by ablation but eroded by wave action, extend for kilometers along the LGF toe. Their preferential occurrence on some exposures is likely related to the orientation of wave-generating (in this case, west to northwest) paleowinds. Equal-elevation debouchments marking a subtle beach ridge also extend for kilometers along the LGF toe. Shoreline lineaments on the fan west of the Ivanpah playa display cusp-and-bay morphometry, and suggest another orientation for wave-generating paleowinds, this time from the northeast. Paleodrainages also occur here, with shapes suggesting lower gradients and sluggish drainage on the edge of a paleolake.

Excavations and natural exposures on both sides of this dry lake reveal relict playa surfaces, beach ridges, and littoral as well as lacustrine sediments, largely concealed beneath overriding alluvium. Some of these exposures can be followed for >1 km, and they display the uniform bedding and homogeneity characteristic of lacustrine sediments, not paleospring deposits (Enzel et al., 2015, 2016). Complicating estimates of paleolake depth relative to the current playa floor elevation of 794 m amsl, the basin rises to the south while the dry lake retains its

Table 1. Key stations showing paleolake depth in the northern portion of the basin.

Sta. No.†	Locality and Evidence	Δ_w (m)
90, 90b	Upper limit, strath surfaces, WNW limb of LGF toe	4.4
108	Upper limit, beach sand associated with LGF toe strath surfaces, WNW limb	6.9
202	Upper limit, strath surfaces, WSW limb of LGF toe	7.2
201, 203	Upper limit, beach sand associated with LGF toe strath surfaces, WSW limb	7.7
97	Deep-water sediment exposed in the ALB, uppermost unit	>2.4
LG7	Lake muds below playa surface, 125 cm bgs	>4.5
-	Highest subsurface anomaly marking shoreline (Sims and Spaulding, 2017)	9.8
-	Mean est. elev., drainage debouchments (n=18) marking subdued shoreline, 0.6 – 1.4 km from playa	8.3–12.5***
WFL-1	WWF shoreline lineaments north of the zone of flexure	7.0**
CMF-76	Beach ridge buried beneath alluvium of the CMF toe	9.0**

* Range at 1 σ .

** Elevation estimate based on commercial GPS or DEM; all others surveyed in.

† See Figure 5 and Spaulding and Sims, 2018.

appearance as a playa (Figs. 2, 6, 8). A relatively prominent shoreline lineament on the west side of the basin also is deflected upward to the south. Therefore, we avoid using any shoreline features or lacustrine sediments from south of this zone of flexure (the hachured line in Fig. 6) to estimate paleolake water depth. Fortunately, there are a number of datum points north of this zone, summarized in Table 1.

Based on this evidence, it appears that paleolakes in the Ivanpah basin attained, and likely exceeded, a depth of 10 m (ca. 33 ft). If “deep” water exceeds 8 m,



Figure 10. Outline map of Paleolake Ivanpah at $\Delta_w = 10$ m (804 m amsl), based on current topography, and uncorrected for crustal displacement.

then Lake Ivanpah is an episodically deep paleolake. This evidence falsifies the assumption that there were no Late Quaternary lakes of substantial depth in this basin. Mapped on current topography, a lake of 10 m depth would have covered ca. 121 km² in two states (Fig. 10).

Our objective has been to describe some of the evidence for recurrent high-lake stands in the Ivanpah basin, not to focus on the lake's chronology. The latter is secondary to the main objective of determining whether or not lakes periodically occupied this basin during geologically recent times. And such appears to have been the case. Most high-lake events recorded to date appear to be early and middle Holocene. The dates from some units suggest that high-lake stands may have persisted for centuries. The fossils of net-leaf hackberry, a long-lived, riparian tree, also indicate perennially available water. In the Mojave Desert, almost all *Celtis* fossils have been found in early-Holocene sediments or in similar-age packrat middens (Spaulding, 1994; Jahren et al., 2001), and such is likely to be the case here as well.

So while some postglacial lakes in this basin may have been ephemeral, initial dating suggests that others may have lasted for centuries. But regardless, duration *per se* is not part of the definition of a lake. Runoff from the Ivanpah drainage basin, with its size of ca. 1,959 km² and relatively high, mountainous terrain, occasionally has been sufficient to fill this basin to depths of at least 10 m. A similar event today would have catastrophic effects on regionally important infrastructure (Figs. 6, 10). The initial distribution of ¹⁴C dates from these lacustrine sediments and littoral features also reveal more frequent post-glacial high-lake episodes than expected, with a number occurring during the "modern", middle to late Holocene climatic regime (see also Enzel et al., 1992; Kirby et al., 2015).

Fan-toe progradation appears to have been particularly effective in burying evidence of past high-lake stands in the northern portion of the Ivanpah basin. A model of alluvial fan dynamics in which early postglacial fan aggradation is followed by fan-toe progradation (e.g. Harvey et al., 1999; Harvey and Wells, 2003), fits these findings well. Perhaps not coincidentally, this process appears to have been pronounced in the northern Ivanpah basin, where the surface appears to have dropped >10 m, relative to the southern basin (Fig. 8). This sort of displacement could theoretically accelerate fan-toe progradation in the northern basin, further accounting for the apparent absence of paleoshorelines there.

The paleohydrogeography of dry lakes in the southern Great Basin should be revisited in light of these findings. The usefulness of hydrologic models such as that of Mifflin and Wheat (1979) is not in dispute. However, their value as predictive, rather than reconstructive, tools can be questioned based on the data from the Ivanpah basin. Despite the quantitative support that can be generated by the models, the "assumption of absence" (that is, that outside of basins fed by runoff from the

Sierra and Transverse Ranges, no Late Quaternary lakes of substantial size or depth existed) appears falsified by this record. These results invite replication, but they also suggest further investigations of other interior paleolakes would be fruitful, if they were focused on the fringes of the basins, where later Quaternary stratigraphic evidence may be found.

References cited

- Enzel, Yehouda, W. J. Brown, R. Y. Anderson, L. D. McFadden, and S. G. Wells. 1992. Short-duration Holocene lakes in the Mojave River drainage basin, southern California. *Quaternary Research* 38: 60-73.
- Enzel, Y., S. G. Wells, and N. Lancaster. 2003. Late Pleistocene lakes along the Mojave River, southeast California. In *Paleoenvironments and Paleohydrology of the Mojave and Great Basin Deserts* (Y. Enzel, S.G. Wells, and N. Lancaster, eds.). Geol. Soc. Amer. Special Paper 368: 61-77.
- Enzel, Y., Y. Kushnir and J. Quade. 2015. The middle Holocene climatic records from Arabia: Reassessing lacustrine environments, shift of ITCZ in Arabian Sea, and impacts of the southwest Indian and African monsoons. *Global and Planetary Change* 129: 69-91.
- Enzel, Y., Y. Kushnir and J. Quade. 2016. Response to Engel et al. (in press): Lakes or wetlands? A comment on "The middle Holocene climatic records from Arabia: Reassessing lacustrine environments, shift of ITCZ in Arabian Sea, and impacts of the southwest Indian and African monsoons" by Enzel et al. (2015). *Global and Planetary Change* in press. pdf. on researchgate.net.
- Harvey, A. M., P. E. Wigand, and S. G. Wells. 1999. Response of alluvial fan systems to the late Pleistocene to Holocene climatic transition: contrasts between the margins of pluvial Lakes Lahontan and Mojave, Nevada and California, USA. *Catena* 36: 255-281.
- Harvey, A. M. and S. G. Wells. 2003. Late Quaternary variations in alluvial fan sedimentologic and geomorphic processes, Soda Lake basin, eastern Mojave Desert, California. *Paleoenvironments and Paleohydrology of the Mojave and Great Basin Deserts* (Y. Enzel, S.G. Wells, and N. Lancaster, eds.). Geol. Soc. Amer. Special Paper 368: 207-230.
- House, P. K., B. J. Buck and A. R. Ramelli. 2006. Preliminary Surficial Geologic Map of the Ivanpah Valley Part of the Hidden Valley, Sloan NE and Sloan SE 7.5' Quadrangles, Clark County, Nevada. Nevada Bureau of Mines and Geology. Open-file Report 06-11D. Carson City, NV.
- Jahren, A. H., R. Amundson, C. Kendall and P. Wigand. 2001. Paleoclimatic reconstruction using the correlation in $\delta^{18}\text{O}$ of hackberry carbonate and environmental water, North America. *Quaternary Research* 56: 252-263.
- Kirby, M.E., E.J. Knell, W. T. Anderson, M.S. Lachniet, J. Palermo, H. Eeg, R. Lucero, R. Murrieta, A. Arevalo, E. Silveira, and C.A. Hiner. 2015. Evidence for insolation and Pacific forcing of late glacial through Holocene climate in the Central Mojave Desert (Silver Lake, CA). *Quaternary Research* 84: 174-186.

- Mifflin, M. D., and M. M. Wheat. 1979. *Pluvial Lakes and Estimated Pluvial Climates of Nevada*. Nevada Bureau of Mines and Geology Bulletin 94. Carson City.
- Morrison, R. B. 1991. Quaternary stratigraphic, hydrologic, and climatic history of the Great Basin, with emphasis on Lakes Lahontan, Bonneville, and Tecopa. In *Quaternary Nonglacial Geology: Conterminous U.S.* (R. B. Morrison, ed.). The Geology of North America Volume K-2, pp. 283-320.
- Ore, T. H., and C. N. Warren. 1971. Late Pleistocene-early Holocene geomorphic history of Lake Mojave, California. *Geological Society of America Bull.* 82, 2553-2562.
- Pigati, J. S., D. M. Miller, J. E. Bright, S. A. Mahan, J. C. Nekola, and J. B. Paces. 2011. Chronology, sedimentology, and microfauna of groundwater discharge deposits in the central Mojave Desert, Valley Wells, California. *Geol. Soc. America Bull.* 123: 2224-2239.
- Quade, Jay, M. D. Mifflin, W. L. Pratt, W. McCoy, and L. Burckle. 1995. Fossil spring deposits in the southern Great Basin and their implications for changes in water-table levels near Yucca Mountain, Nevada, during Quaternary time. *Geological Society of America Bull.* 107:213-230.
- Quade, Jay, R.M. Forester, W.L. Pratt, and C. Carter. 1998. Black mats, spring-fed streams, and late-glacial-age recharge in the southern Great Basin. *Quaternary Research* 49: 129-148.
- Ramelli, A. R., P. K. House, and B. J. Buck. 2006. Preliminary Surficial Geologic Map of the Ivanpah Valley Part of the State Line Pass and Ivanpah Lake 7.5' Quadrangles, Clark County, Nevada. Nevada Bureau of Mines and Geology. Open-file Report 06-11E. Carson City, NV.
- Reheis, M. C., J. Bright, S. P. Lund, D. M. Miller, G. Skipp and R. J. Fleck. 2012. A half-million-year record of paleoclimate from the Lake Manix Core, Mojave Desert, California. *Palaogeography, Palaeoclimatology, Palaeoecology* 365–366 (2012) 11–37
- Robinson, M. C., S. Flint, and W. G. Spaulding. 1999. Molycorp, Inc. Mountain Pass Mine cultural resources investigations testing and evaluation report for CA-Sbr9387, CA-SBr-9388, and CA-SBr9389/H, Ivanpah Dry Lake, San Bernardino County, California. Applied EarthWorks, Hemet, CA.
- Schmidt, K. M., and M. McMackin. 2006. Preliminary surficial geologic map of the Mesquite Lake 30' x 60' Quadrangle, California and Nevada. U.S. Geological Survey Open File Report 2006-1035. Denver, CO.
- Sims, D. B. and W. G. Spaulding. 2017. Shallow Subsurface Evidence for Postglacial Holocene Lakes at Ivanpah Dry Lake; an Alternative Energy Development Site in the Central Mojave Desert, California, USA. *J Geography and Geology*. <http://www.ccsenet.org/journal/index.php/jgg/article/view/65389>.
- Smith, G. I. 1991. Stratigraphy and Chronology of Quaternary-age Lacustrine Deposits. In *The Geology of North America, Volume K-2, Quaternary Non-Glacial Geology: Conterminous U. S.*, edited by R.B. Morrison, pp. 339-346. Geol. Soc. Amer., Boulder, CO.
- Smith, G. I. and F. A. Street-Perrott. 1983. Pluvial Lakes of the western United States. In *The Late Pleistocene* (S.C. Porter, ed.), pp. 190-214. University of Minnesota Press, Minneapolis.
- Snyder, C. T., G. Hardman, and F. F. Zdenek. 1964. *Pleistocene lakes in the Great Basin*. Miscellaneous Geologic Investigations Map I-416. U. S. Geological Survey, Washington, D. C.
- Spaulding, W. G. 1999. Results of larger scale geomorphologic reconnaissance. In Molycorp, Inc. Mountain Pass Mine cultural resources investigations testing and evaluation report for CA-Sbr9387, CA-SBr-9388, and CA-SBr9389/H, Ivanpah Dry Lake, San Bernardino County, California (M. C. Robinson, S. Flint, and W. G. Spaulding eds.). Applied EarthWorks, Hemet, CA. pp. 79-89. Retrieved from <https://www.scribd.com/doc/314014653/Robinson-et-al-1999-Ivanpah-CA-Report>.
- Spaulding, W. G., E. B. Leopold, and T. R. Van Devender. 1983. Late Wisconsin paleoecology of the American Southwest. in S.C. Porter, ed. *The Late Pleistocene*. Univ. Minnesota Press, Minneapolis. pp. 259-293.
- Spaulding, W. G., and D. B. Sims. 2018. Lake Ivanpah: An Overlooked Paleolake in the Southern Great Basin, California and Nevada, U. S. A. In review.
- Springer, K.B., C.R. Manker, and J. S. Pigati. 2015. Dynamic response of desert wetlands to abrupt climate change. *PNAS* 112: 14522-14526.
- Thorne, R. F., B. A. Prigge, and J. Henrickson. 1981. A flora of the higher ranges and the Kelso Dunes of the eastern Mojave Desert in California. *Aliso* 10: 71-186.
- University of Cologne, 2007. *CalPalOnline*. quickcal2007 ver.1.5. Cologne Radiocarbon Calibration and Paleoclimate Package. <http://www.calpal-online.de>.
- Wells, S. G., W. J. Brown, Y. Enzel, R. Y. Anderson, and L. D. McFadden. 2003. Late Quaternary geology and paleohydrology of pluvial Lake Mojave, southern California. In *Paleoenvironments and Paleohydrology of the Mojave and southern Great Basin Deserts* (Y. Enzel, S. G. Wells, and N. Lancaster, eds.). Geol. Soc. Amer. Special Paper 368: 79-114.

An overview of stamp mills of the California Desert

Larry M. Vredenburg¹ and Charlie Cornell²

¹Tehachapi, California, vrede@bak.rr.com

²Litchfield Park, Arizona, minercon@aol.com

The Mojave Desert Heritage and Cultural Association's two historic stamp mills, situated at Goffs, California, are the only operational stamp mills within the California Desert. The American Boy first saw service in 1887 in Montana, the Stotts, which was located about 20 miles northwest of Goffs, probably dates from the early 1900s.

The stamp mill is now an obsolete technology, akin to the steam locomotive. However, at one time nearly every significant historic mine throughout the west had a stamp mill associated with it. The stamp mill was used to pulverize crushed ore to a powder prior to extracting valuable metals.

A stamp mill essentially is an oversized mechanical mortar and pestle. Powered by water, steam, electricity, or an internal combustion engine, the pestle (or stamp) is lifted by a cam fixed to a rotating shaft, then dropped repeatedly onto a steel shoe in a mortar box. Water is added to the mix of crushed rock in the mortar box and a screen on the front only allows ore pulverized to a small enough size to pass through.

This technology is ancient, dating to as early as the third century B. C. Stamp mills were used throughout the Roman Empire. They were used in the medieval Islamic world as well as throughout Europe during this time. Water-powered stamp mills are illustrated in Georg Agricola's *De Re Metallica* published in 1556. The first stamp mill in the United States was built in 1829 at the Capps mine near Charlotte, North Carolina.

Until the 1970s, when heap-leaching began to be used on low-grade gold ore, milling of ore principally involved four steps: 1) crush ore to a size small enough to be fed into the pulverizer, 2) pulverize the ore, 3) concentrate the ore, and 4) refine the metal.

Historically throughout California, the first step of concentrating gold ore was a simple amalgamation process. Pulverized rock in a slurry passed from the mortar box over a gently slanting copper plate, which was typically electro-plated with silver. These plates were then coated with mercury. Gold would adhere to

(amalgamate with) the mercury. Periodically the stamp mill would be shut down and the amalgam would be scraped from the copper plate. The amalgam would then be processed in a retort where the mercury would vaporize and was recovered, leaving the gold behind for final refining. Both of the restored MDHCA stamp mills are fitted with sluice tables where the copper plate would have been. The sluice table has riffles like its cousin the sluice box that is used extensively in placer gold recovery.

After passing over the copper plate, the slurry was usually sent to a shaker table, which concentrates heavy minerals in a gravity process not unlike a gold pan. Depending on the amount of "free gold" in the ore, this process would recover about 70 percent of the assayed value of the ore. Gold ore combined with sulfide minerals such as pyrite typically will not amalgamate, requiring much more expensive alternatives.

During the 1890s the cyanide process was developed, bypassing the need for amalgamation. In this process, the slurry is combined in a weak cyanide solution. Gold dissolves in the cyanide solution, then the precious metal is recovered from the solution.

Large stamp mills of the California Desert

We won't go into all the variations in mills here, but one variation is worth mentioning.



1975 photo of the Stotts mill, Round Valley. BLM photo

The Mining and Scientific Press on April 7, 1894, published an article about two 10-stamp mills erected at the gold camp of Vanderbilt, 30 miles north of Goffs and about 15 miles from Interstate 15. This article contrasted the two mills operating there. One was referred to as a Colorado stamp mill; the other, a California stamp mill. The stamps in the Colorado mill dropped twice as far and half as fast as the California mill.

The stamps at the Vanderbilt Mining and Milling Company's "Colorado mill" weighed 650 pounds each and dropped 16 inches 30 times per minute. At the "California mill," erected by Alan Green Campbell, the 750-pound stamps dropped seven inches 90 times per minute. The article summarized that, when used on the same ore, the mills are essentially equivalent and that "both are good."

Both small and large stamp mills were used throughout the deserts of California. The largest mills include the following:

- the Tumco (Hedges) Mine located in Imperial County, supported two mills which totaled 140 stamps
- the 50-stamp Randsburg-Santa Fe Reduction Company Mill, later renamed the Bagdad Chase Mill, was located in Barstow
- at Daggett the 60-stamp Waterloo Mining Company mill, and other smaller mills processed silver ore from the mines at Calico
- the Yellow Aster Mine in Randsburg supported an 100-stamp mill
- the Lucky Baldwin Mine, also known as the Gold Mountain Mine, located northeast of Big Bear had a 40 stamp mill.

Mojave Desert Heritage and Cultural Association stamp mills

A handful of mills remain in place within the California desert and its fringes. A 10-stamp mill remains at Skidoo in Death Valley. The Wall Street 2-stamp mill erected by William Keyes can be found within Joshua Tree National Park. Also within Joshua Tree National Park is 10-stamp mill at the Lost Horse Mine. Just outside of the California Desert in Keyesville, Kern County, there is a 10-stamp mill, and a 5-stamp mill can be found high in the Inyo Mountains at Beveridge.

Currently there are two refurbished operational stamp mills at the Mojave Desert Historic and Cultural Association museum at Goffs, California: the 10-stamp American Boy Mill and the 2-stamp Stotts Mill. The Mojave Desert Heritage and Cultural Association was founded by Dennis Casebier in 1993.

In the mid-1970s while conducting field work, Bureau of Land Management staff stumbled on an intact 2-stamp mill located at the south end of Round Valley, about 20 miles northwest of Goffs. BLM manager Wess Chambers mentioned the



Restored Stotts mill. Photo by Larry Vredenburg

mill to Dennis Casebier, and years later, in February 1999, Dennis and Chris Ervin went searching and found it.

Little is known about the mill. Between 1908 and 1910 there was mining activity just to the south in Gold Valley. During this time a mill was erected in the vicinity but the location is not known; perhaps this is the mill. On August 14, 1931, the property that embraced the mill was patented



Location of the Jay Gould mine and millsite 28 miles northwest of Helena, Montan. 1924 General Land Office Survey of T13N, R7W



Restored American Boy stamp mill. Photo by Larry Vredenburg by Ambrose Stotts under the Stock-Raising Homestead Act.

The mill was purchased from the land owner Bud Smith III. By September 1999, MDHCA volunteers began disassembling and hauling the mill to Goffs. Reconstruction began a year later and continued until 2003. After a hiatus, work resumed in earnest in 2008. The project was much more than reassembling a jigsaw puzzle. The mill needed a new power source. A new bull wheel had to be fabricated as did bearings and a cam shaft. A cam had to be repaired. It was finally operational March 28, 2010. Approximately 2,460 hours of volunteer labor was expended on this project. The mill is powered by a 10-horsepower electric motor; it has an automatic feeder that delivers crushed rock to the mortar box.

The history of the 10-stamp America Boy Mill is nothing short of amazing. The mill is a portion of the 60-stamp mill erected in 1887 at the Empire Mine, Montana. The mine was located on the west slope of Mount Belmont, about 2 miles west of Marysville and about 20 miles north of Helena, Montana. In 1928, 10 of the 60 stamps were moved to the Jay Gould mine. The mill was located about 1,100 feet south of the mine at 46°52'45.93"N 112°27'28.07"W.

Sometime in the 1950s Glenn Allman acquired the mill to serve his American Boy mine, and moved it about a mile to the northwest, to the south side of Stemple Pass. Allman refurbished the mill; however, the mine failed to yield a profit. The mill structure still stands in Stemple Pass at 46°53'42.99"N 112°28'10.03"W.

The mill was then purchased by Joe Pauley of Rosamond, California. He had hoped to sell the mill to Walt Disney when Euro Disney was under construction in Paris, France, but deal didn't go through. In 1996, Dennis Casebier purchased the mill from Pauley. Restoration began in October 2010 and was completed three years later after an estimated 4,100 hours of volunteer labor. The mill is powered by a 30-horsepower diesel engine; it has

automatic feeders that deliver crushed rock to the mortar box.

Both mills were refurbished under the direction of Charlie Cornell. Restoration of these mills was a herculean effort that involved many individuals and generous financial donations.

References

- Agricola, Georg, 1986, *De Re Metallica*. Translated by Herbert Clark Hoover and Lou Henry Hoover. (New York: Dover Publications) Reprint of the 1950 reprint of the 1912 edition.
- Bureau of Land Management, "Tumco Historic Mine," <https://www.blm.gov/visit/tumco-historic-mine>
- Connell, Charlie, 2013, "American Boy 10-Stamp Mill Progress," <http://stampmillman.blogspot.com/2013/04/american-boy-10-stamp-mill-progress.html>
- Connell, Charlie, 2015, "California Stamp Mills, America Boy Mine 10-Stamp Mill; Stotts Millsite 2-stamp mill," <http://stampmillman.blogspot.com/2015/10/operational-stamp-mills-in-usa.html>
- Connell, Charlie, 2013, "115 Year Old Stamp Mills Run Again," http://stampmillman.blogspot.com/2013/10/115-year-old-stamp-mills-run-again_9910.html
- Connell, Charlie, 2014, "Stamp Mill Mortise & Tenon," <http://stampmillman.blogspot.com/2014/08/stamp-mill-mortise-tenon.html>
- Connell, Charlie, ND, "American Boy 10-Stamp Mill History," PowerPoint Presentation, 32 pp.
- Connell, Charlie, ND, "Stotts 2-Stamp Mill Restoration," PowerPoint Presentation, 31 pp.
- Del Mar, Algernon, 1912, "Stamp Milling, a Treatise on Practical Stamp milling and Stamp Mill Construction" (McGraw – Hill Book Company: New York).
- Knopf, Adolph, 1913, "Ore Deposits of the Helena mining Region Montana," U. S. Geological Survey Bulletin 527, p. 75
- Pardee, J. T., and F. C. Schrader, 1933, "Metalliferous Deposits of the Greater Helena Mining Region Montana," U. S. Geological Survey Bulletin 842
- Serpico, Phil, 2004, "A Road to Riches, The Randsburg Railway Company and Mining District," (Omni Publications: Palmdale, California).
- Swope, Karen K and Carrie J. Gregory, 2017, "Mining in the Southern California Deserts: A Historic Context Statement and Research Design," U. S. Bureau of Land Management Technical Report 17-42. p2.24
- Vredenburg, L. M., Shumway, G.L., Hartill, R. D., 1981, "Desert Fever, an overview of mining in the California Desert" (Living West Press: Canoga Park, CA), p. 95.
- Wikipedia, "Wall Street Mill," https://en.wikipedia.org/wiki/Wall_Street_Mill
- Wikipedia, "Stamp Mill," https://en.wikipedia.org/wiki/Stamp_mill
- Wikipedia, "Gold Extraction," https://en.wikipedia.org/wiki/Gold_extraction

Geology of the Old Mojave Road and surrounding areas, San Bernardino County, California and Clark County, Nevada: a field guide

Gregg Wilkerson
 gwilkerson@bak.rr.com

This field guide to the geology and history of the Old Mojave Road is organized in four sections that are posted on line at Academia.com and in my Google Drop Box

Section	Academia.edu	Dropbox: yosoygeologo@gmail.com
Part 1: Text (16M)	https://www.academia.edu/35530815/Geology_of_the_Old_Mojave_Road_and_Surrounding_Areas_San_Bernardino_County_California_and_Clark_County_Nevada_PART_1_Text	https://www.dropbox.com/s/naudb750e2bybgl/PART%201%20GEOLOGY%20AND%20HISTORY%20OF%20THE%20OLD%20MOJAVE%20ROAD%20AND%20SURROUNDING%20AREAS.pdf?dl=0
Part 2: Appendices (3 MB)	https://www.academia.edu/35530837/Geology_of_the_Old_Mojave_Road_and_Surrounding_Areas_San_Bernardino_County_California_and_Clark_County_Nevada_PART_2_Appendices	https://www.dropbox.com/s/4fx0tw3z7irg7hh/PART%202%20APPENDICES%20p%20200.pdf?dl=0
Part 3: Area Maps (43 MB)	https://www.academia.edu/35530880/Geology_of_the_Old_Mojave_Road_and_Surrounding_Areas_San_Bernardino_County_California_and_Clark_County_Nevada_PART_3_Area_Maps	https://www.dropbox.com/s/01r4178swq35uf8/PART%203%20AREA%20MAPS.pdf?dl=0
Part 4: Geologic Index and Mosaic (26 mb)	https://www.academia.edu/35530900/Geology_of_the_Old_Mojave_Road_and_Surrounding_Areas_San_Bernardino_County_California_and_Clark_County_Nevada_PART_4_Geologic_Mosaic	https://www.dropbox.com/s/auyymx3gye9w2yj/PART%204%20GEOLOGIC%20MOSAIC.pdf?dl=0

Acknowledgement and disclaimer

This work is a compilation of geologic information and mine history data gathered from a variety of published and unpublished sources. I have not attempted to harmonize these disparate and sometimes contradictory sources but have presented the data mostly as I found it. I have changed verb tenses and used some paraphrase for readability. When print is in Italics, these are quotations, the sources of which are noted at the end of each paragraph. OMR means “Old Mojave Road”. I also have done original research for many places of interest along that OMR that supplement information contained in these published and unpublished sources. My research adds or changes some inaccurate or incomplete previous descriptions of places and histories along the OMR.

I used and adapted GIS data for the mileage points from the OMR website (<http://www.mojave-road.com/>) but corrected several of those points and added several of my own. Those adjustments are based on comparison with USGS digital on-line maps and the geologic maps referenced in my References and Bibliography section.

I use many of the same mileage points that were described in Mojave Road Guide: An Adventure Through Time (Dennis Casebeer, 2016). The locations and mileage points given in that book are similar, but not identical with mile points at <http://www.mojave-road.com>. I have used mileage points from the website, and the mileage distances describe in Casebeer’s book.

I ask that you support the Mojave Desert Heritage and Cultural Association by going on line and purchasing Casebeer’s book at <https://www.mdhca.org/store>. Have it with you when using my guidebook to get additional interesting historical information about the Old Mojave Road and adjacent areas.

Avenza and georectified .pdf maps

All the on-line maps in this report are in georectified .pdf format. You can get the Avenza .pdf maps application at <https://www.avenza.com/avenza-maps/>. Download the maps to your cell phone and use it to locate yourself as you drive along the field trip route. Don’t worry about keeping track of mileage from the beginning. Just use the mile markers as destination waypoints.

Geographic overview

The Old Mojave Road starts at the Colorado River in Nevada 14 miles north of Needles, California, 0.6 miles east of the Casino on the Fort Mojave Indian Reservation. This starting point is in the floodplain of the Colorado River which has cut down through older units and exposed them, from youngest to oldest as we drive west to the northeastern flank of the Dead Mountains. From there we drive up on to the east-sloping pediment of the Dead Mountains, turning northwest and driving more-or-less parallel to the California–Nevada state line until we come to the southern slopes of the Newberry Mountains of Nevada. From there we turn west and cross the Piute Valley to the Piute Mountains. We make a detour around the Piute Mountain Wilderness area at Fort Piute, crossing the Piute Mountains at Telephone Cable Pass to the south. From there we cross eastern Lanfair Valley to the northern end of the Vontrigger Hills. From the Vontrigger Hills we cross western Lanfair Valley and pass to the south of Lanfair Buttes (Eagle Mountain) and Grotto Hills, which are on our right (to the north). We pass out of western Lanfair Valley at the northeastern end of Table Mountain. Then we traverse southwest of Pinto Mountain and go up and across the Mid Hills. We cross the Mid Hills at Cedar Canyon. Exiting the Mid Hills, we cross Kelso Wash to an unnamed hill at mile 66.9 and then skirt the northern flank of the Marl Mountains. We drive west and northwest along the southern edge of the Club Mountain volcanic field to Willow Wash. Traveling northwest we greet the north end of Seventeen Mile Point in the Old Dad Mountains. From Seventeen Mile point we go southwest across Devil’s Playground to the Little Cowhole and Cowhole Mountains. The Old Mojave Road goes between those two mountains to the eastern edge of Soda Lake. Crossing Soda Lake we come to the southeastern end of the Soda Mountains. From there we skirt the southeast end of the Soda Mountains and the southeast flank of the Cave Mountains. Near the southwest end of the Cave Mountains we enter Afton Canyon on the Mojave River. For the Afton Canyon portion of our journey, the Cady Mountains are on the south and southwest of the Old Mojave Road. Afton Canyon ends at the Afton Canyon Campground. From there we are in sediments of the Lower Mojave River and Glacial Lake Manix to the end of our field trip near Camp Cady.

0.0 to 5.4—Floodplain for the Colorado River and Bouse Formation

(Figure 1)

In this first geologic segment of the OMR, we start at the Colorado River. It has been down-cut into older floodplain and alluvial deposits. The sequence of rocks, from generally younger to older as we move west are:

Qcr1a—Post-Davis Dam channel and floodplain deposits (approximately 1937 to 1954), includes deposits that

predate channelization in the southern part of the map area

Qcr2b—Inset sequence of alluvial terraces (late Holocene), includes mud, sand, and gravel B

Qcr2c—Inset sequence of alluvial terraces (late Holocene), includes mud, sand, and gravel C **Qcr2d** Inset sequence of alluvial terraces (late Holocene), includes mud, sand, and gravel D **Qcr2c** Inset sequence of alluvial terraces (late Holocene), includes mud, sand, and gravel C **Qaa** Deposits of most frequently inundated alluvial channels and fans, (late Holocene)

Qa1b—Deposits of intermittently active alluvial channels, sheetflow areas, and alluvial fans (late Holocene)

Qaa—Deposits of most frequently inundated alluvial channels and fans, (late Holocene) **Qa1** with **QTa** on the flanks

Qa1—Alluvium (late Holocene to modern), recently active channel and alluvial fan deposits, unconsolidated sand

QTa—Alluvium, undivided (Pleistocene and Pliocene) and gravel

Qa1b—Deposits of intermittently active alluvial channels, sheetflow areas, and alluvial fans (late Holocene)

Qa1—Alluvium (late Holocene to modern), recently active channel and alluvial fan deposits, unconsolidated sand

Qaa—Deposits of most frequently inundated alluvial channels and fans, (late Holocene)

5.4 to 9.8—Northeast flank of the Dead Mountains

(Figure 2)

The Dead Mountains are made of Pre-Cambrian rocks. Jennings (1961) shows the north part of the Dead Mountains as “Earlier Precambrian Metamorphic Rocks” (ep€) and the middle part as “Undivided Precambrian gneiss” (e€g). Bishop (1963) shows the southern Dead Mountains to be “Undivided Precambrian gneiss” (p€g) to the west with “Pleistocene non-marine” (Qc) and “Quaternary nonmarine terrace deposits” (Ql) to the east. The northeastern flank of the Dead Mountains is made of the “Earlier Precambrian Metamorphic Rocks” (ep€) unit of Jennings (1961). These rocks are in the Proterozoic (Xf and Xfl) unit of House and others (2004).

9.8 to 12.5—Southern flank of the Newberry Mountains, Nevada

(Figure 3)

The southern flank of the Newberry Mountains of Nevada was mapped by House and others (2010). Their mapping shows that the Newberry Mountains are dominated by Felsic Plutonic Rocks (lpf). The USGS 750K digital map of Nevada shows these as Tertiary Felsic Intrusives (Tfi). The Kingman 250K Map by Jennings (1961) mapped these plutonic rocks in California as Early Pre-Cambrian Undivided granitic rocks (ep€). The hills hosting the

Gibraltar claims (T13N, R.20E, Section 32, SBM) at the California-Nevada state line were mapped as Undivided pre-Cambrian by Jennings, 1961 (ep€) and as High-grade Metamorphic rocks (Mh) by House and others, 2010.

These are the rocks we traverse on the OMR between mile 9.8 and 11.4.

The southwest flank of the Newbery Mountains, from east to west are composed of

Afo—Middle Pleistocene Old alluvial fan deposits

Afx—Pliocene to Late Miocene

Afy—Holocene Young alluvial fan deposits

Afi—Late Pleistocene Intermediate alluvial fan deposits

Afxk—Pliocene to Late Miocene Extremely Old Alluvial fan, k denotes massive calcrete

12.5 to 28.2—Piute Valley

(Figure 4)

The Piute Valley section of the OMR is dominantly alluvial materials of Holocene and Pleistocene age. In this segment we pass through several old homesteads, and see evidence of WWII desert training maneuvers.

28.2 to 30.9—Piute Mountains

(Figure 5)

The OMR crosses through the center of the Piute Mountains. The Northern Piute Mountains are mostly Tertiary dacite (Td) with a few outcrops of Early Proterozoic Gneiss and granitoids (undivided, Xg) and Cretaceous Younger Granitoid Rocks (Kg1) on the eastern edge. The southern Piute Mountains are mostly Cretaceous Porphyritic Granodiorite (Kpg) with bodies of Early Proterozoic Younger Granitoids (Xg1) to the east and Miocene Basalt Flows (Tb, 10 m.y.) to the west (Miller and others, 2007).

30.9 to 35.1—Eastern Lanfair Valley

(Figure 6)

The Lanfair Valley was mapped by Miller and others (2007) as Holocene and Pleistocene Alluvial Fan Deposits and Alluvium (Qaf). In 2012 Miller produced a Quaternary surface geology map for the Ivanpah 30o x 60o quadrangle. That map shows two major depositional groupings, one west and one east of the “Large Unnamed Wash” at mile 32.2.

From the western edge of the Piute Mountains to the Large Unnamed Wash at mile 32.2, the mapped units, from east to west along the OMR are (Miller, 2012):

Qmc—Holocene and Pleistocene Mass-Movement colluvial deposits

Qya—Holocene and Latest Pleistocene Young alluvial fan deposits

Qia—Late and Middle Pleistocene Intermediate alluvial deposits

Qya+Qaa—Holocene and Latest Pleistocene Young alluvial fan deposits and Latest Holocene active alluvial fan deposits

From the Large Unnamed Wash to the northeastern edge of the Vontrigger Hills, the mapped units, from east to west along the OMR are (Miller, 2012):

Qiaq—Late to Middle Pleistocene Intermediate alluvial fan deposits composed of grus

Qyw+Qaw—Holocene and Latest Pleistocene Young wash deposit and Active wash deposit

Qoag—Middle to Early Pleistocene Old alluvial fan deposit composed of grus

Qiaq/Qoag—Late to Middle Pleistocene Intermediate alluvial fan deposit composed of grus / Middle to Early Pleistocene Old alluvial fan deposit composed of grus

Qiaq/fpg—Late to Middle Pleistocene Intermediate alluvial fan deposit composed of grus / Felsic plutonic rocks that weather to grus

Qoag—Middle to Early Pleistocene Old alluvial fan deposit composed of grus

35.1 to 37.0—North flank of Vontrigger Hills

(Figure 7)

The Vontrigger Hills are mostly Early Proterozoic Younger Granitoids (Xg1) with a small amount of Miocene Younger Volcanic Rocks (Tv1) northwest of the California Mine and another mass of Tv1 northeast of the American Flag Gold mines.

37.0 to 43.7—Western Lanfair Valley: Vontrigger Hills to Grotto Hills

(Figure 8)

Between the northwestern edge of the Vontrigger Hills and Grotto Hills (mile 43.3) the quaternary rocks of Lanfair valley are Late to Middle Pleistocene Intermediate alluvial fan deposits composed of (Qiaq) of Miller (2012).

43.7 to 48.6—Grotto Hills to Mid Hills

(Figure 9)

From the Grotto Hills to the Mid Hills, the OMR is atop Quaternary Alluvium (Qal of Jennings, 1961) and Quaternary Fanglomerate (Qaf of Miller and others, 2007). Miller (2012) mapped these rocks as Qiaq.

48.6 to 58.4—Mid Hills

(Figure 10)

The Mid Hills are mostly Cretaceous Mid Hills Adamelite (Kmh). There are two major faults in the Mid Hills. The northern one is the Cedar Canyon Fault. It strikes north-northeast in the middle-eastern part of the Mid Hills. On Jenkin’s map (1961) this fault extends 27 miles southwest from Caruther’s Canyon in the south-central New York Mountains to the town of Kelso (See Appendix 48.6B). Miller and others (2007) do not extend the Cedar Canyon Fault that far west. Instead, they show the East

Providence Fault zone cropping out along the centerline of the southern Mid Hills. This fault crosses, but does not off-set, the Cedar Canyon Fault at Mile 58.4. There is a band of Early Proterozoic Intermediate-age Granitoids (Xg2, 1,7000 -1,715 m.a.) that follows the strike of the East Providence Fault in the southern part of the Mid Hills. South of the Cedar Canyon Fault, in the northern Mid Hills (Pinto Mountains) is Miocene Rhyolite Tuff of White Horse Mesa (Tw, 15.8 m.a.), Between the Mid Hills Campground and Table Top Mountain is a mass of Cretaceous Black Canyon Hornblende Gabbro (Kbc). The flanks of Table Top Mountain are Cretaceous Rock Springs Monzodiorite (Krs). The summit of Table Top Mountain is capped with Miocene Rhyolite Tuff of White Horse Mesa (Tw). See map in Appendix 48.6A.

58.4 to 66.9—Cedar Wash between Mid Hills and Unnamed Hill At Mile 66.9

(Figure 11)

Between the Mid Hills and an unnamed hill south of Mile 66.9, the OMR traverses Quaternary fanglomerate (Qaf of Miller and others, 2007) of the Cedar Wash drainage.

The Quaternary rocks between the Mid Hills and the Marl Mountains are mostly

Qyag—Holocene and Latest Pleistocene Young alluvial fan deposit composed of grus.

Qiaq—Late to Middle Pleistocene Intermediate alluvial fan deposit composed of grus.

Qyw—Holocene and Latest Pleistocene Young wash deposit.

At Mile 66.9 to the north are views of the granitic Cima Dome.

66.9 TO 70.7—Unnamed Hill At Mile 66.9 to Marl Springs

(Figures 12 and 13)

Traversing the Unnamed Hill at Mile 66.9 westward to the Marl Springs in the Marl Mountains, the OMR crosses more Quaternary Alluvial Fanglomerate (Qaf of Miller, 2007). The Quaternary Geologic map for the Ivanpah Quadrangle (Miller and others, 2012) shows these rocks as Qyag+Qiaq (Holocene and Latest Pleistocene Young Alluvial fan deposit composed of gruss and Late to Middle Pleistocene Intermediate alluvial fan deposit composed of gruss).

70.7 to 74.0—Marl Mountains

(Figure 14)

The Marl Mountains are mostly Cretaceous Teutonia Adamellite (Kt), and Pliocene and Miocene gravels (Tg) with large masses of Early Proterozoic Gneiss and Granitoids (Xg of Miller and others, 2007).

74.0 to 85.7—Cinder cones And lava flows of southern Club Peak Volcanic Field

(Figure 15)

After exiting the Marl Mountains, the OMR crosses a wash and then skirts the southern flank of the Club Peak Volcanic Field, a collection of Pleistocene to Miocene basalt cinder cones (QTbc) and lava flows (QTbl). There are several abandoned cinder mines in the volcanic field as well as some lava tubes. The volcanic rocks lie above Cretaceous Teutonia Adamellite (Kt) and Undifferentiated Proterozoic Gneiss and Granitoids (Xg of Miller and others, 2007). The geology of the Club Peak Volcanic Field mapped at a scale of 1:24,000 is included in the Wilshire, 2002 ("Digital ...Geologic Map of the Indian Spring Quadrangle.)

85.7 to 89.4—Seventeen Mile Point

(Figure 16)

Seventeen Mile Point is the northern tip of the Old Dad Mountain. Vredenburg (2017 p. 120) described the geology of the Old Dad Mountains:

No single rock type dominates Old Dad Mountain and its surrounding area. Rock types include Early Proterozoic gneiss and granitoid rocks (Xg), Jurassic Aztec Sandstone (Ja), Mesozoic volcanic and sedimentary rocks (Mzv), Late Proterozoic and Cambrian siliciclastic rocks (PZs), and Tertiary volcanic rocks (Tv1). Old Dad Mountain is underlain by a resistant knob of limestone which is part of the Devonian to Permian limestone (PDI). Hewett (1956) reported the presence of granite, schist, and quartzite intruded by syenite dikes in the Proterozoic rocks in this general area (Theodore, 2007, p. 111). The oldest structure is a Lower (?) Jurassic unconformity overlain by Aztec Sandstone. The northwesttrending Powerline Canyon shear zone is exposed just south of Jackass Canyon. The Playground thrust fault truncates these older structures. Extensional tectonics during Miocene time resulted in the Old Dad normal fault. The steep slopes that formed on both sides of the Old Dad Mountain fault block by erosion or downfaulting became the source of numerous landslides of brecciated rock, as well as glide blocks, during Neogene time (Dunne, 1977). Hewett (1956, p. 113) surmised gold mineralization at mines in the north of Old Dad Mountain may be related to the intrusion of the Sands granite. At the Paymaster Mine, a massive quartz vein occurs in pre-Cambrian gneiss. Gold bearing quartz veins at the Brannigan and Oro Fino Mines occur in quartzite, shale, and dolomite of the Upper Precambrian to Lower Cambrian Wood Canyon formation, Stirling quartzite and Johnnie formation (Hewitt, 1956, p. 38; from Vredenburg, 2017).

89.4 to 94.8—Devil's Playground

(Figure 17)

Between Seventeen Mile Pine and the Little Cowhole Mountains, the OME traverses Quaternary Alluvium and Lake deposits. These were mapped by Miller (2012). From east to west these are:

Qia—Late to Middle Pleistocene Intermediate alluvial fan deposit

Qya/Qia—Holocene and latest Pleistocene Young alluvial fan deposit/Late to Middle Pleistocene Intermediate alluvial fan deposit

Qia—Late to Middle Pleistocene Intermediate alluvial fan deposit

Basinal Contact—Between alluvial and debris flow deposits to the east and eolian deposits to the west

Qyae/Qiae—Holocene to Latest Pleistocene Young mixed alluvial and eolian sand deposit / Late to Middle Pleistocene Intermediate mixed alluvial and eolian sand deposit

Qiae—Late to Middle Pleistocene Intermediate mixed alluvial and eolian sand deposit

Qiea—Late to Middle Pleistocene Intermediate mixed eolian sand and alluvial deposit

Qyea+Qaed—Holocene and Latest Pleistocene Young Mixed alluvial and aeolian sand Deposit + Holocene and Latest Pleistocene Young Eolian Sand Dune Deposit.

94.8 to 96.6—Cowhole and Little Cowhole Mountains

(Figure 18)

The Cowhole Mountains are south of the OMR and the Little Cowhole Mountains are north of it.

The east side of the Little Cowhole Mountains are (KJcm) and the eastern side is €d and (€Zs, Milller and others, 2007).

The Cowhole Mountains have a northern, central and southern portions delineated by faults. The northern block has:

TKf—Felsite dikes (Tertiary or Cretaceous)

KJc—Granitoid Rocks of Cowhole Mountain (Cretaceous or Jurassic) PD = Permian and Devonian

€d—Dolomite (Cambrian)

€Zs—Siliciclastic rocks (Cambrian and Late Proterozoic)

Xg—Granitoids (Proterozoic)

The central block has:

TKf—Felsite dikes (Tertiary or Cretaceous)

KJcm—Granitoid Rocks of Cowhole Mountains (Cretaceous or Jurassic)

Ja—Aztec Sandstone (Jurassic)

Jd—Diorite (Jurassic)

Mzv—Volcanic and Sedimentary Rocks (Mesozoic) PDI—Permian and Devonian limestone

€d—Dolomite (Cambrian)

The southern block has

TKf—Felsite dikes (Tertiary or Cretaceous)

KJcm—Granitoid Rocks of Cowhole Mountains (Cretaceous or Jurassic)

Ja—Aztec Sandstone (Jurassic)

Jd—Diorite (Jurassic)

Mzv—Volcanic and Sedimentary Rocks (Mesozoic) PDI—Permian and Devonian limestone

€d—Dolomite (Cambrian)

96.6 to 102.5—Soda Lake

(Figures 19 and 20)

Soda Lake has sand dunes along it’s eastern edge. There is a clay central section surrounded by a halo of alkali materials. There is a 2-mile long section of brown-black clays at the western edge of Soda Lake along the OMR. The lake was mapped as Qaf by Miller and others (2007).

102.5 to 110.6—Southern Soda Mountains

(Figure 21)

Mapped units in the southern Soda Mountains are given in Table 1.

Table 1. Mapped units in the southern Soda Mountains			
Formation Name	Age	Symbol	Author
Alluvium	Holocene or Pleistocene	Qa	Dibblee, 2008a
Clay or Mud Playa Deposits	Holocene or Pleistocene	Qc	Dibblee, 2008a
River Terrace Gravel	Holocene or Pleistocene	Qg	Dibblee, 2008a
Non Marine	Pleistocene	Qc	Jennings and others, 1962
Older Fanglomerate	Pleistocene	Qof	Dibblee, 2008a
Older Gravel	Pleistocene	Qog	Dibblee, 2008a
Non-Marine	Pliocene to Pleistocene	QP	Jennings and others, 1962
Undifferentiated Mafic Volcanic Rocks	Pliocene?	Tv	Dibblee, 2008a
Gravel	Pliocene and Miocene	Tg	Miller and others, 2007
Andesite	Tertiary	Tva	Jennings and others, 1962
Rhyolite	Tertiary	Tvr	Jennings and others, 1962
Granitoid Rocks	Cretaceous and Jurassic	KJg	Miller and others, 2007
Quartz Monzonite	Late Jurassic or Early Cretaceous	qm	Dibblee, 2008a
Granite to Quartz Monzonite	Late Jurassic or Early Cretaceous	gqm	Dibblee, 2008a
Metavolcanic Rocks	Jurassic-Triassic	JTrv	Jennings and others, 1962
Granite	Mesozoic	Gr	Jennings and others, 1962
Volcanic and Sedimentary Rocks	Mesozoic	Mzv	Miller and others, 2007
Metavolcanic Rocks	Mesozoic or older	mv	Dibblee, 2008a
Carbonate Rocks	Paleozoic	Pzc	Miller and others, 2007

Formation	Age	Symbol
River Sand	Holocene	Qrs
River Gravel	Holocene	Qrg
Windblown Sand	Holocene	Qs
Clay	Holocene	Qc
Alluvium	Holocene	Qa
Alluvial fan gravel	Holocene	Qf
Manix Lake Gravel	Pleistocene	Qmg
Manix Lake Sand	Pleistocene	Qms
Manix Lake Clay	Pleistocene	Qmc
Older Alluvium	Pleistocene	Qoa
Older Gravel	Pleistocene	Qog
Older Lake Sediments	Late Pleistocene	Qol
Older Fanglomerate	Late Pleistocene	Qof
Coarse Breccia	Pliocene	QTbr
Gravel	Pliocene to Miocene	QTg
Clay	Pliocene to Miocene	QTc
Cobble Gravel	Miocene	Tg

The oldest rocks are Paleozoic carbonates roof pendants followed by Mesozoic sediments and volcanics, Jurassic and Triassic metavolcanics. These are preserved in pendants in slightly younger Late Jurassic and Early Cretaceous granitoid rocks. These were eroded and upon them were deposited Miocene and Pliocene volcanic rocks of andesitic or rhyolitic composition. Erosion and uplift of all these rocks produced Miocene to Holocene gravels and other continental clastic deposits. The most recent Holocene and Pleistocene sediments are related to Lake Manix and evolution of the Mojave River.

110.6 to 114.8: Upper Mojave River Wash

(Figures 22 and 23)

This segment of the OMR traverses Quaternary alluvium shed from the southeastern Cave and southwestern Soda Mountains. The main channel of the Mojave River Wash is to the south.

114.8 to 120.5: Cave and Northern Cady Mountains

(Figure 24)

Cave Mountain geology

The northern boundary of Cave Mountains is the Cronese Valley through which Interstate 15 passes. A splayed fault system marks Cronese Valley. This fault is traced 23 miles westward all the way to Coyote Lake.

The Cave Mountains were mapped by Dibblee (2008a). They are mostly granite-quartz monzonite (g- qm) in

Formation	Age	Symbol
Volcanic fanglomerate	Miocene	Tvf
Andesitic fanglomerate	Miocene	Tva
		Tfb
Basalt	Miocene	Tb
Basalt breccia	Miocene	Tbb
Fanglomerate of basaltic detritus	Miocene	Tfa
Andesite	Oligocene	Ta
Tuff breccia	Oligocene	Tt
Sandstone	Oligocene	Tss
Andesite porphyritic	Oligocene	Tap
Dioritic dike	Post-Early Cretaceous	d
Granite	Late Jurassic and Early Cretaceous	gr
Metavolcanics	Paleozoic or older	mv

the northeast with Older Quaternary gravel (Qog) in the southwest. There is a roof pendant of Mesozoic sedimentary rock (ms) between two west-southwest-east-northeast trending faults at the Cave Mine in the southeastern part of the mountains. The southern boundary of the Cave Mountains is the Manix fault. This fault controls the location of eastern Afton Canyon and can be traced westward to the town of Manix (T.10N, R.04E, Section 5) (Wilkerson, 2013).

A map of the Cave Mountains is provided in Appendix 114.8

Northern Cady Mountain geology

South of the Manix fault, between the northwest branch of Baxter Wash and the upper reaches of Afton Canyon, the northern Cady Mountains expose, from west to east, expose Tertiary gravel (Tg), Older gravel (Qog), granite-quartz monzonite, and a metasedimentary roof pendant (ms). At the southeast end of the northern Cady Mountains, the older gravels surround Tertiary andesite (Ta). The western northern Cady Mountains are a fault blocks of granite (gr) to the east, Tertiary tuff (Ta) and Tertiary andesite (Ta) in the middle, and Tertiary andesite (Ta) to the east. These fault blocks are up to the west. The middle block has some Tertiary basalt (Tb) on top of the Tertiary andesite (Ta). In the eastern part of the western northern Cady Mountains, there are exposures of Tss. These sandstones (Tss) are in depositional and in fault contact with Tertiary andesite (Ta) and Tertiary basalt (Tb). The southern boundary of the northern Cady mountains, for this report are Wilhelm Wash and Baxter Wash (Wilkerson, 2013).

120.5 to 139.3: Lower Mojave River and Lake Manix sediments

(Figure 25)

Beginning at mile 120.5 and continuing to the end of this field guide at Camp Cady (mile 139.3), we will be following the Mojave River and its associated clastic sedimentary rocks. On our left, to the south are the northeastern Cady Mountains. A list of the Tertiary sediments we will see on this journey is given in Table 2 (from Dibblee, 2008a and 2008b).

Volcanic, sedimentary and metamorphic rocks of the northwestern Cady Mountains to the south of our field trip route, given in Table 3, are from Dibblee (2008b) The northwestern Cady Mountains are bounded to the north by the Manix Fault. We cross it at mile 118.7, 119.6, 129.1, 135.0 and 138.5.

References and bibliography

- Antil, R.J., A. Cunningham and M. Schaffer, 1957, Geology and Mineral Resources of Township 12, Range 5 and 6 East, San Bernardino County, California, San Francisco, Southern Pacific Land Company (Silver Sericite Mine).
- Aubury, Lewis .E., 1902, The Copper Resources of California: California Mining Bureau Bulletin 23, p. 254;
- Aubury, L.E. 1906, The structural and industrial materials of California: California Mining Bureau. Bulletin. 38, 412 pp (Cave Mine p. 299).
- Aubury, Lewis E., 1908. The Copper Resources of California. California, State Mining Bureau, Bulletin 50. 336p.
- Bailey, G.E. 1902, Register of mines and minerals, San Bernardino County : California Mining Bureau Registers of Mines, no. 11, 20 pp. (Cave Mine p.:13).
- Balley, H. D., February 2, 1956, Rare earths and the Mountain Pass mine: Address at the National Western Mining Conference of the Colorado Mining Association, Denver, Colorado.
- Bancroft, Peter, "Royal Gem Azurite a new gemstone," *Lapidary Journal*, April, 1978, p. 66 (Copper World Mine).
- Bateman, P.C., 1965, Geology and tungsten mineralization of the Bishop district, California, with a section on Gravity study of Owens Valley, by L.C. Pakiser and M.F. Kane, and a section on Seismic profile, by L.C. Pakiser: U.S. Geological Survey Professional Paper 470, 208 p.
- Barca, Richard A., 1960, Geologic map of portions of the northern portion of the Old Dad Mountains, San Bernardino County, California, California Division of Mines and Geology Map Sheep MS-7 (1:62:500).
- Beckerman, G.M., Robinson, J.P., and Anderson, J.L., 1982, The Teutonia batholith—A large intrusive complex of Jurassic and Cretaceous age in the eastern Mojave Desert, California, in Frost, E.G., and Martin, D.M., eds., *Mesozoic-Cenozoic tectonic evolution of the Colorado River region, California, Arizona, and Nevada*: San Diego, California, Cordilleran Publishers, p. 205–220.
- Bezore, Stephen P. and Stephen E. Joseph. 1985, *Mineral Land Classification of the Northern Portion of the Kingman 1 x 2 Degree Quadrangle*, California Department of Conservation, Division of Mines and Geology, Open-File Report 85-15 LA.
- Billinger, Charles, "Legendary River of Gold Not Forgotten," *Los Angeles Times*, Section II, Dec. 5, 1976;
- Halliday, William R., 1959, *The Cave of Gold in Adventure is Underground* (New York: Harper and Row) p 27-35. Patchick, 1961, p. 8; Casebier, 1988, p. 239-244, cited in Vredenburg, 1989, p. 76
- Bishop, Charles C., 1963, *Geologic Map of California*, Olap R. Jenkins Edition, Needles sheet: California Division of Mines and Geology, scale 1:250,000.
- Boalich E.S., 1923, Notes on iron ore occurrences in California: California Min. Bur. Rept. 18, pp. 110-113 (Cave Mine, p. 112).
- Blackwelder, Elliot, and Elbworth, E. W., 1936, Pleistocene lakes of the Afton Basin, California: *Am. Jour. Sci.*, vol. 31, pp. 453-463.
- Bradley, W.W., and others, 1918, Manganese and chromium in California: California Div. Mines Bull. 76, 248 pp.
- British Geological Survey, 2007, Rare Earth Elements, PDF file, p.25, 29.
- Bradsher, Keith, 2010a, (2010-09-24). "China halts exports of minerals crucial to Japanese industry HONG: Customs officers at ports stop rare earth elements amid fishe". *International Herald Tribune, Hong Kong (thejakartapost)*. Retrieved 2010-11-01.
- Bradsher, Keith, 2010b, "Challenging China in rare earth mining," *New York Times*, 21 April 2010.
- Brown, H. J., and Larry Monroe, 2000. Geology and mineral deposits in the Baxter–Basin area south of Cave Mountain, San Bernardino County, California. *San Bernardino County Museum Association 38 Quarterly*, 47(2):42-46.
- Bryers, F.M., Jr., 1960, Geology of the Alvord Mountain Quadrangle, San Bernardino County, California, US Geological Survey; Bulletin 1089-1, 71 p., map scale 1:62:500
- Business Wire, 2012, "Molycorp Announces Start-Up of Heavy Rare Earth Concentrate Operations at Mountain Pass, Calif.," *Business Wire* (August 27, 2012
- Burchard, E.F., 1934, Fluorspar deposits in western United States: *Am. Inst. Min. Met. Engr. Trans.*, vol. 109, pp. 373-374, 1934. (Afton Canyon Fluorite p. 373, 374).
- Burchard, E.F., 1948: Summary of the iron-ore situation in California: California Div. Mines Bull. 129, pp. 207-229 (Cave Mine, p. 220).
- Burchfiel, B.C., and Davis, G.A., 1971, Clark Mountain thrust complex in the Cordillera of southeastern California—Geologic summary and field trip guide, in Elders, W.A., ed., *Geological excursions in southern California: Riverside, University of California, Campus Museum Contributions Number 1*, p. 1–28.
- Burchfiel, B.C., and Davis, G.A ,1981, Mojave Desert and environs, in Ernst, W.G., ed., *The geotectonic development of California (Rubey Vol. I): Englewood Cliffs, N.J., Prentice-Hall*, p. 217–252.

- Burchfiel, B.C., and Davis, G.A., 1988, Mesozoic thrust faults and Cenozoic low-angle normal faults, Eastern Spring Mountains, Nevada, and Clark Mountains Thrust Complex, California: in D.L. Weide and M.L. Faber eds., *This Extended Land Fieldtrip Guidebook: Las Vegas, Nevada*, Cordilleran Publishers, p. 87-106.
- Burchfiel, B.C., and Davis, G.A., 1971, Clark Mountain thrust complex in the Cordillera of southeastern California: Geologic summary and field trip guide: California University, Riverside Campus Museum
- Contribution, no. 1, p. 1-28.
- California State Mining Bureau; 1908, Bull. 50. (Copper World Mine).
- California Journal of Mines and Geology, 1953, V. 49, Tabulated list no. 341, p. 108 (Teutonia Mine).
- Capps, R.C., and J.A. Moore, 1997, Geologic Map of the Castle Mountains, San Bernardino County, California and Clark County, Nevada, Nevada Bureau of Mines and Geology, Map 108
- Carlisle, D.L., Luyendyk, B.P., and McPherron, R.L., 1980, Geophysical survey in the Ivanpah Valley and vicinity eastern Mojave Desert, California, in Fife, D.E., and Brown, A.R., eds., *Geology and mineral wealth of the California desert: Santa Ana, California*, South Coast Geological Society, p. 485-494.
- Casebier, D.G., 1988, *Guide to the East Mojave Heritage Trail, Ivanpah to Rocky Ridge (Tales of the Mojave Road Publishing Co.: Norco, CA.)* 304 pp.
- Castor, Stephen B., 2008, "Rare Earth Deposits of North America". *Resource Geology* 58 (4): 337
- Clary, M.R., 1967, *Geology of the eastern part of the Clark Mountain Range, San Bernardino County, California: California Division of Mines and Geology Map Sheet 6* (adapted from Dobbs, 1961).
- Clary, Michael R., 1967, *Geology and Sections of the Eastern Part of the Clark Mountain Range, San Bernardino County, California, California Division of Mines and Geology, Map Sheet 6.*
- Cloudman, H. E., Huguenin, E., and Merrill, F. J. H., 1919, *San Bernardino County: California Min. Bur. Rept. 15*, pp. 771-899 (Cave Mine, p. 818).
- Cox, D.P., and Singer, D.A., eds., 1986, *Mineral deposit models: U.S. Geological Survey Bulletin 1693*, 379 p.
- Crosby, J. W., III, and Hoffman, S. R., 1951 *Fluorspar in California: California Jour. Mines and Geology*, vol. 47, pp. 619-638.
- Crosby, J. W., III, and S.R. Hoffman, 1951, *Fluorspar in California: California Jour. Mines and Geology*, vol. 47, pp. 619-638 (Afton Canyon Fluorite p. 633-636).
- Crossman, J. H., 1890-1891, *San Bernardino County, its mineral and other resources: Min. and Sci. Press*, vols. 61 and 62. A series of weekly articles from July- 12, 1890 to January 31, 1891. 39
- Danelski, David, 2009, *Expansion in works for S.B. County mine with troubled environmental past*, The Biz Press, February 9, 2009
- Davis, W. M., 1933, *Geomorphology of mountainous deserts: Report XVI, IGC, Washington.*
- Davis, W. M., 1933, *Granitic domes of Mohave Desert: Trans. San Diego Soc. of Nat. History*, pp. 213-257.
- Davis, W. M., 193B, *Sheetfloods and streamfloods: Geol. Soc. Am., Bull.*, vol. 49, no. 9, pp. 1337-1416.
- DeGroot, Henry, 1890, *San Bernardino County, its mountains, plains, and valleys: California Min. Bur. Rep!*. 10, pp. 518-539.
- Denver Business Journal, 2010. "Molycorp announces details of IPO," *Denver Business Journal*, 13 July 2010.
- DeWitt, E., 1987, *Proterozoic ore deposits of the southwestern U.S.: Society of Economic Geologists Guidebook Series*, v. 1, 189 p.
- Destination 4x4, 2016, *Government Holes*, <https://www.destination4x4.com/government-holes/>, Posted April 10, 2016. Accessed Dec. 20, 2017.
- DeWitt, E., Armstrong, E.L., Sutter, J.F., and Zartman, R.E., 1984, U-Th-Pb, Rb-Sr, and Ar-Ar mineral and whole-rock isotope systematics in a metamorphosed granitic terrane, southeastern California: *Geological Society of America Bulletin*, v. 95, no. 6, p. 723-739.
- Dibblee, Thomas W., 1967, *Geologic Map of the Broadwell Lake Quadrangle, San Bernardino County, California, U.S. Geological Survey Miscellaneous Investigations, Map I-475*, 1:62,500 scale.
- Dibblee, Thomas W., 2008a, *Geology of the Alvord Mountain and Cave Mountain 15 Minute Quadrangles, California*, Dibblee Foundation, Map DF-398, 1:62,500 scale..
- Dibblee, Thomas W., 2008b, *Geology of the Newberry and Cady Mountain 15 Minute Quadrangles, California*, Dibblee Foundation, Map DF-394, 1:62,500 scale.
- Dibblee, Thomas W., 2008c, *Geology of the Barstow and Dagget 15 Minute Quadrangles, California*, Dibblee Foundation, Map DF-393, 1:62,500 scale.
- Dibblee, Thomas W., 2008d, *Geology of the Broadwell Lake 15 Minute Quadrangles, California*, Dibblee Foundation, Map DF-395, 1:62,500 scale.
- Dibblee, Thomas W., 2008e, *Geology of the Ludlow and Bagdad 15 Minute Quadrangles, California*, Dibblee Foundation, Map DF-396, 1:62,500 scale.
- Dibblee, Thomas W., 2008g, *Geology of the Opal Mountain and Lane Mountain 15 Minute Quadrangles, California*, Dibblee Foundation, Map DF-403, 1:62,500 scale.
- Dibblee, Thomas W., 2008h, *Geology of the Apple Valley and Ord Mountain 15 Minute Quadrangles, California*, Dibblee Foundation, Map DF-377, 1:62,500 scale.
- Dibblee, Thomas W., 2008i, *Geology of the Lake Arrowhead and Lucern Valley 15 Minute Quadrangles, California*, Dibblee Foundation, Map DF-379, 1:62,500 scale.
- Dibblee, Thomas W., 2008j, *Geology of the Old Woman Springs and Emerson Lake 15 Minute Quadrangles, California*, Dibblee Foundation, Map DF-380, 1:62,500 scale.
- Dibblee, Thomas W., 2008k, *Geology of the Deadman Lake and Lead Mountain Lake 15 Minute Quadrangles, California*, Dibblee Foundation, Map DF-388, 1:62,500 scale.

- Dibblee, Thomas W. and A.M. Bassett, 1966, Geology of the Cady Mountain Quadrangle, San Bernardino County, California, U.S. Geological Survey, Miscellaneous Investigations, Map I-476, 1:62,500 scale..
- Dobbs, Phillip Hale, 1961, Geology of the central part of the Clark Mountain Range, San Bernardino Co., Unpublished Master of Science Thesis, Univ. of South. Calif., Los Angeles, 115 pp.
- Dohrenwend, J.C., 1987, Basin and Range, in Graf, W.L., ed., Geomorphic systems of North America: Boulder, Colo., Geological Society of America, Centennial Special Volume 2, p. 303-342.
- Dohrenwend, J.C., 1988, Age of formation and evolution of pediment domes in the area of the Cima volcanic field, Mojave Desert, California, in Weide, D.L., and Faber, M.L., eds., This extended land—Geological journeys in the southern Basin and Range: Las Vegas, Nevada, Geological Society of America, Cordilleran Section, Field Trip Guidebook, p. 214-217.
- Dorton, N. H., 1910, A reconnaissance of parts of northwestern New Mexico and northern Arizona: U.S. Geol. Survey Bull. 435, 88 pp.
- Dunne, G.C., 1977, Geology and structural evolution of Old Dad Mountain, Mojave Desert, California: Geological Society of America Bulletin, v. 88, no. 6, p. 737-748.
- Eric, John H., 1948, Tabulated list of copper deposits in California : California Div. Mines Bull. 144, pp. 199-357.
- Evans, J. R., 1961, Volcanic cinders near Baker: Mineral Information Service, vol. 1.4, no. 9, pp. 10-11.
- Evans, J. R., 1966, California's Mountain Pass mine now producing europium oxide, Mineral Information Service, vol. 18, no. 2, pp. 23-32.
- Evans, James R., 1971, Geology and mineral deposits of the Mescal Range quadrangle, San Bernardino County, California. California Division of Mines and Geology map sheet 17, scale 1:62,500, 40
- Evans, J. R., 1974, "Relationship of Mineralization to major structural features in the Mountain Pass area, San Bernardino County, California," California Geology, Vol. 27, No. 7 p. 147-157.
- Faulds, J.E., House, P.K., and Ramelli, A.R., 2000, Geologic map of the Laughlin area, Clark County, Nevada, Nevada Bureau of Mines and Geology, Open File Report 00-06 (1:24,000).
- Faulds, J.E., House, P.K., Ramelli, A.R., Bell, J.W., and Pearthree, P.A. 2001, Preliminary geologic map of the Davis Dam Quadrangle, Clark County, Nevada, and Mohave County, Arizona, Nevada Bureau of Mines and Geology, Open File Report 03-5.
- Faulds, James E., P. Kyle House, Philip A. Peartree, John W. Bell and Alan R. Ramelli, 2004, Preliminary geologic map of the Davis Dam Quadrangle and the Eastern Part of the Bridge Canyon Quadrangle, Clark County Nevada, and Mohave County, Arizona, Nevada Bureau of Mines and Geology, Open File Report 2003-05.
- Fleck, Robert, Mattinson, J.M., Busby, Cathy J., Carr, M.D., Davis, G.A., and Burchfiel, B.C., 1994, Isotopic complexities and the age of the Delfonte volcanic rocks, eastern Mescal Range, southeastern California: Stratigraphic and tectonic implications: Geological Society of America Bulletin, v. 106, p. 1242-1253.
- Frickstad, W.N., 1955, A century of California Post Offices, 1848 to 1954 (A Philatelic Research Society Publication: Oakland) Geological Sciences Department, CSU Pomona (2008). "Mountain Pass Rare Earth Mine". California State Polytechnic University, Pomona. Retrieved 2009-03-04
- Goldfarb, R.J., Miller, D.M., Simpson, R.W., Hoover, D.B., Moyle, P.R., Olson, J.E., and Gaps, R.S., 1988, Mineral resources of the Providence Mountains Wilderness Study Area, San Bernardino County, California: U.S. Geological Survey Bulletin 1712 , chap. D, 70 p.
- Goodwin, Joseph Grant (1957) Lead and zinc in California. California Journal of Mines and Geology, Division of Mines: 53(3&4): 622-623. (Carbonate King Mine).
- Gregory, H. E., 1916, The Navajo county--a geographic and hydrographic reconnaissance of parts of Arizona, New Mexico, and Utah: U.S. Geol. Survey Water Supply Paper no. 380, 219 pp.
- Hafen, L. R. and A.W. Hafen, 1998. Journals of forty-niners—Addison Pratt's diary: 94-107.
- Hague, Arnold, 1BB3, Geology of the Eureka district, Nevada: U.S. Geol. Survey Ann. Rept. 3, pp. 237-290.
- Hart, Herbert M., 2017, Camp Marl Springs Military History, posted at <http://mojavedesert.net/military/camp-marl-springs.html> accessed Dec. 20, 2017:
- Haxel, Gordon B., 2005, Haxel, James B. Hedrick, and Greta J. Orris, "Rare earth elements – Critical resources for high technology," US Geological Survey, Fact Sheet 087-02, 17 May 2005.
- Hazard, J. C., 1937a, Cambrian Girvanellas from the southern Great Basin region [abs.]: Geol. Soc. America Proc. 1936, p. 354-355.
- Hazard, J. C., 1937b, Lower Triassic rocks in San Bernardino County, California [abs.]: Geol. Soc. America Proc. 1936, p. 329.
- Hazard, J. C., 1937 c, Paleozoic section in the Nopah and Resting Springs Mountains, Inyo County, California: Calif. Jour. Mines and Geology, v. 33, p. 289-339.
- Hazard, J. C., 1939, Possibility of pre-Cambrian glaciation in southeastern California [abs.]: Pan Am. Geologist, v. 71, p. 47-48.
- Hensher, A., 1979, Ghost towns of the central Mojave, (Alan Hensher: Los Angeles).
- Hirschberg, D.M., and Pitts, G.S., 2000, Digital geologic map of Arizona: a digital database derived from the 1983 printing of the Wilson, Moore, and Cooper, 1:500,000-scale map: U.S. Geological Survey, Open-File Report OF-2000-409, scale 1:500,000
- Hess, F. L., 1917, Tungsten minerals and deposits: U. S. Geological Survey Bulletin 652, p.41
- Hewett, D. F., 1931, Geology and ore deposits of the Goodsprings quadrangle, Nevada: U.S. Geol. Survey Prof. Paper 162, 172 pp.

- Hewett, D.E., 1956, Geology and mineral resources of the Ivanpah Quadrangle, California and Nevada: U.S. Geological Survey Professional Paper 275, 172 p.
- Hewett, D.F. and others, 1936a, Mineral resources of the region around Boulder Dam: U. S. Geol. Surv. Bull. 871, 197 pp. (Cave Mine, p.78).
- Hewett, D.F. and others, 1936b, Mineral resources of the region around Boulder Dam: U. S. Geol. Survey Bull. 871, 197 pp. (Afton Canyon Fluorite p. 171,172).
- Hewett, D.F. and others, 1936c, Mineral resources of the region around Boulder Dam: U. S. Geol. Survey Bull. 871, 197 pp. (Cave Mountain. P.76).
- Hewett, D.F., Stone, Jerome, and Stieff, L.R., 1969, The ages of three uranium minerals, Mojave Desert, California, IN Geological Survey Research 1969: U.S. Geological Survey Professional Paper, 650-B, p. B84-B88. (Teutonia Quartz Monzonite, Late Cretaceous or early Tertiary).
- Hodge, E.T., 1935, Available raw material for a Pacific Coast iron industry: War Dept., vol. 8, North Pacific Division, appendix E-5, California iron ore deposits, pp. 10-13, vol. 1, d : 44; and vol 3, ap. E- 5:4.
- Hogue, Arnold, 1892, Geology of the Eureka district, Nevada: U.S. Geol. Survey Monograph 20, 419 pp.
- House, P. Kyle, Keith A. Howard, Philip a Pearthree and John W. Bell, 2004, Preliminary Geologic Map of the Nevada and Arizona Parts of the Mount Manchester (1:24:000) Quadrangle, Open File Report 04-04, Nevada Bureau of Mines and Geology in Cooperation with U.S. Geological Survey.
- House, P. Kyle, Heather Green, Abbey Grimmer and the Nevada Digital Mapping Team, 2010, Preliminary Geologic Map of Clark County, Nevada, Open File Report 10-7, Nevada Bureau of Mines and Geology
- Howard, Keith A., 2002, Geologic Map of the Sheep Hole Mountains 30° x 60° Quadrangle, San Bernardino and Riverside Counties, California, U.S. Geological Survey, Miscellaneous Field Studies, MF-2344, Sheet 1 of 2.
- Howard, K.A., Kilburn, J.E., Simpson, R.W., Fitzgibbon, T.T., Detra, D.E., Raines, G.L., and Sabine, C., 1987, Mineral resources of the Bristol/Granite Mountains Wilderness Study Area, San Bernardino County, California: U.S. Geological Survey Bulletin 1712-C, 18 p.
- Hsu, Jeremy, 2010a, "Shortage of rare earth minerals may cripple U.S. high-tech, scientists warn Congress," Popular Science, 17 March 2010
- Hsu, Jeremy, 2010b "U.S. military supply of rare earth elements not secure," TechNewsDaily, 14 April 2010.
- Ireland, William, 1888, San Bernardino County: California Mining Bureau Report 8, 948p (Bullion Mine).
- Jaffe, Howard W., 1955, Precambrian monozite and zircon from the Mountain Pass rare-earth district, San Bernardino County, California: Geol. Soc. Am. Bull., vol. 66, pp. 1247-1256.
- Jamasmie, Cecilia, 2015, (August 26, 2015). "Molycorp shuts down Mountain Pass rare earth plant". mining.com. Retrieved November 8, 2015
- Jennings, C. W., 1961, Geologic map of California, Olaf P. Jenkins edition, Kingman sheet, California Division of Mines and Geology scale 1:250,000.
- Jennings, Charles Q., John L. Burnett and Bennie W. Troxel, 1962, Geologic map of California, Olaf P. Jenkins Edition, Trona Sheet, California Division of Mines and Geology, scale 1:250,000
- Jessey, David R., Don W. Tarman, Miho Waki and Suzanne M. Baltzer, 2001, A field investigation of the Clark Mountain fault complex, San Bernardino County, in The Changing Face of the East Mojave Desert. Zzyzzx Desert Symposium, California p. 46-49.
- Jones, C.C. 1916, The Pacific Coast iron situation- the iron ores of California and possibilities of smelting: Am. Inst. Min. Met. Eng. Trans., vol. 53, pp. 306-323, 1916.pp 08; 16 (Cave Mine).
- Joseph, Steven E., 1984. Mineral land classification of the Mescal Range 15' quadrangle, San Bernardino County, California. California Division of Mines and Geology open file report 84-2
- Joseph, Steven E., 1985. Mineral land classification of the Ivenpah-Crescent Peak – Searchlight 15' Quadrangles, San Bernardino County, California. California Division of Mines and Geology open file report 84-7.
- Kupfer, Donale H. and Allen M. Basset, 1962, Geologic Reconnaissance Map of Part of the Southeastern Mojave Desert, California, U.G. Geological Survey Mineral Investigations Field Studies Map MF-205 and California Division of Mines and Geology Special Report 83 "A Geological Reconnaissance in the Southeastern Mojave Desert, California
- Lamey, C.A., 1948, Cave Canyon iron-ore deposits, San Bernardino, California: California Division of Mines Bulletin, 129: pp.69-83 (Cave Mine). Leith, C.K., 1906, Iron ores of the western United States and British Columbia: U. S. Geol. Survey Bulletin 285: pp 194-200 (Cave Mine, page 198).
- Larsen, S. E. Jr., Gottfried, D., Jaffe, H. W., and Waring, C. L., 1958, Lead-alpha ages of the Mesozoic batholiths of western North America: U.S. Geol. Survey Bull. 1070-B, 62 pp.
- Lingenfelter, R.E., 1986, Death Valley and the Amargosa, a land of illusion (University of California Press: Los Angeles) p. 135-136.
- Logan, C. A., 1947, Limestone in California: California Jour. Mines and Geology, vol. 43, pp. 175-357. 42
- Longwell, C. R., 1925, The pre-Triassic unconformity in southern Nevada: Am. Jour. Sci., 5th ser., v. 10, p. 93-106.
- Longwell, C. R., 1928, Geology of the Muddy Mountains, Nevada: U. S. Geol. Survey Bull. 798.
- Lucas, J.M., 1992, Gold: U. S. Bureau of Mines, Annual Report 1991, 43 p.
- Lyon, D.A., 1914, D. A., The electric furnace in pig-iron manufacture : U. S. Bur. Mines Bull. 67, pp. 7-57 (Cave Mine, page 40).
- Malach, R., 1977, Adventurer John Moss, gold discovery in Mohave County (Mohave County Board of Supervisors: Kingman, AZ) 32 p.

- Margonelli, Lisa (2009). "Clean Energy's Dirty Little Secret". The Atlantic. Retrieved 2009-08-05
- Meek, Norman, 1989, eomorphic and hydrologic implications of the rapid incision of Afton Canyon, Mojave Desert, California, *Geology* (1989) 17 (1): 7-10; [https://doi.org/10.1130/0091-7613\(1989\)017%3C0007:GAHIOT%3E2.3.CO;2](https://doi.org/10.1130/0091-7613(1989)017%3C0007:GAHIOT%3E2.3.CO;2)
- Mendenhall, W. C., 1909, Some Desert Watering Places in Southeastern California and southwestern Nevada: U.S. Geological Survey Water Supply Paper 224. p. 56.
- Merriam, Charles W., 1964, Cambrian rocks of the Pioche mining district, Nevada, U.S. Geol. Survey Prof. Paper 469, pp. 1-SB.
- Miller, David M., 2012, Surficial Geologic Map of the Ivanpah 30' by 60' Quadrangle, San Bernardino County, California and Clark County, Nevada, U.S. Geological Survey, Scientific Investigations Map 3206.
- Miller, D.M., Glick, L.L., Goldfarb, R., Simpson, R.W., Hoover, D.B., Detra, D.E., Dohrenwend, J.C., and Munts, S.T., 1985, Mineral resources and resource potential map of the South Providence Mountains Wilderness Study Area, San Bernardino County, California: U.S. Geological Survey Miscellaneous Field Studies Map MF-1780-A, scale 1:62,500
- Miller, D.M., Frisken, J.G., Jachens, R.C., and Gese, D.D., 1986, Mineral resources of the Castle Peaks Wilderness Study Area, San Bernardino County, California: U.S. Geological Survey Bulletin 1713-A, 17 p.
- Miller, D.M., and Wooden J.L, 1993, Geologic map of the New York Mountains area, California and Nevada: U.S. Geological Survey Open-File Report 93-198, 10 p., scale 1:50,000.
- Miller, D.M., and Wooden, J.L., 1994, Field guide to Proterozoic geology of the New York, Ivanpah, and Providence Mountains, California: U.S. Geological Survey Open-File Report 94-674, 40 p
- Mining and Scientific Press, 1897, v. 74, p. 94; 1899, v. 78, p. 35 (Copper World Mine).
- Miller, David M, Robert J. Miller, Jane E. Nielsen, Howard G. Wilshire, Keith A. Howard and Paul Stone, 2007, Geologic Map of the East Mojave National Scenic Area, California, U.S. Geological Survey Bulletin 2160, Plate 1.
- Mills, Christina, 2016, Rock Springs Loop Trail, <https://www.nps.gov/moja/planyourvisit/rock-spring-loop-trail.htm> accessed Dec. 20, 2017
- Molycorp Inc., 2008, Prospectus for Initial Public Offering
- Molycorp Inc, 2010. Press Release,, "Business Wire", 06 Sep 2010.
- Molycorp Inc., 2015. "Molycorp reports first quarter 2015 financial results". Molycorp. May 7, 2015
- Morton, D.M., K. D. Watson, and A. K. Baird, 1991. Alkalic silicate rocks of the Mountain Pass district, San Bernardino County, CA. San Bernardino County Museum Association Special Publication, SP 91-1:90 - 96.
- Mueller, P.A., Ragland, P.C., Ranson, W.A., and Burchfiel, B.C., 1979, High-K calc-alkaline plutonic rocks from southeastern California: *The Mountain Geologist*, v. 16, p. 105-115
- Murdoch, Joseph and Robert W. Webb, 1948, Minerals of California,: California Div. Mines Bull. 136, p. 285, 1948.
- Murdoch, Joseph and Robert W. Webb, 1966, Minerals of California, Centennial Volume (1866-1966): California Division Mines & Geology Bulletin 189: 126, 218, 223, 341. (Carbonate King Mine). 43
- Myrick, D.F., 1963. Railroads of Nevada and Eastern California, vol 2, the southern roads. Berkeley: Howell-North Books.
- Myers, W.A. 1983. Iron Men and Copper Wires. Glendale: Trans_Anglo Books.
- New York Times, 2010, Amid Tension, China Blocks Crucial Exports to Japan, *New York Times*, 22/SEP/10
- Nielson, J.E., Frisken, J.G., Jachens, R.C., and McDonnell, J.R., Jr., 1987, Mineral resources of the Fort Piute Wilderness Study Area, San Bernardino County, California: U.S. Geological Survey Bulletin 1713-C, 12 p.
- Nielson, Jane E and Ryan D. Turner, 1999, Geologic Map of the Hart Peak 7.5 Minute Quadrangle, California and Nevada: A Digital Database, U.S. Geological Survey, Open File Report 99-34.
- Noble, L. F., 1914, The Shinumo quadrangle, Grand Canyon district, Arizona: U. S. Geol. Survey Bull. 549. (Tapeats Sandstone).
- Nolan, T. B., 1929, Notes on the stratigraphy and structure of the northwest portion of Spring Mountain, Nevada: *Am. Jour. Sci.*, 5th ser., vol. 17, pp. 461-472.
- Nolan, T. B., 1943, The basin and range province in Utah, Nevada, and California: U.S. Geol. Survey Prof. Paper 197-D, pp. 141-196.
- Nolan, T. B., Merriam, C. W., and Williams, J. S., 1956, The stratigraphic section in the vicinity of Eureka, Nevada: U.S. Geol. Survey Prof. Paper 276, 77 pp.
- Novitsky-Evans, J.M., 1978, Geology of the Cowhole Mountains, southeastern California: Houston, Tex., RiceUniversity, Ph.D. dissertation, 100 p.
- Olson, J.E., and Pray, L.C., 1954, The Mountain Pass rare-earth deposits, in Mineral deposits and mineral industry, chap. 8 of Jahns, R.H., ed., *Geology of southern California*: California Division of Mines Bulletin 170, p. 23-39.
- Olson, J. C., Shawe, D. R., Pray, L. C., and Sharp, W. N., 1954, Rare earth mineral deposits of the Mountain Pass district, San Bernardino County, California: U.S. Geol. Survey Prof. Paper 261, 75 pp.
- Page, L.R. and J.H. Wiese, 1945. The Evening Star tin deposit and adjacent tungsten deposits, San Bernardino County, California. USGS technical reports section.
- Page, L. R., and Wiese, J. H., 1946, The Evening Star tin deposit and adjacent tungsten deposits, San Bernardino County, California: U.S. Geol. Survey Strategic Minerals Investigations, unpublished.
- Patchick, P. F., 1959, Economic geology of the Bullion Mining District, San Bernardino County, California: University of Southern California, unpublished M.S. thesis, p. 172;
- Patchick, P., 1961, "A geologist's notes on the Ivanpah Mountains," *Desert Vol.* 24, No. 5, p. 8-11.

- Pemberton, H. Earl (1983), Minerals of California; Van Nostrand Reinhold Press: 85, 229-230, 233, 514. (Carbonate King Mine).
- Powell, K.B., 1948, Raw materials, Kaiser Company, Inc., Fontana plant : Unpublished paper presented before Los Angeles Fall Meeting, Amer. Inst. Min. Engrs., 18 pp (Cave Mine).
- Pratt, J. H., 1896, On northupite; pirssonite, a new mineral; gaylussite and hanksite from Borax Lake, San Bernardino Co., California : Am. Jour. Sci., 4th ser., vol. 2, pp. 123-135 (Cave Mine).
- Pray, L. C., 1957, Rare earth elements: California Div. Mines Bull. 176, pp. 467-474.
- Proctor, Cathy, 2010, "Molycorp gets OK for rare-earths processing plant," Denver Business Journal, 13 December 2010.
- Prommel, H. W. C, 1937, Sampling and testing of a goldscheelite placer deposit in the Mojave Desert, Kern and San Bernardino Counties, California : U. S. Bur. Mines Inf. Circ. 6960, 18 pp. (Cave Mine).
- Reynolds, R.E., and Nance, M.A., 1988. Shadow Valley Basin: late Tertiary deposition and Gravity Slides from the Mescal Range. Cordilleran Section, Geological Society of America, Field Trip Guidebook.
- Reynolds, R. E., Allen F. Glazner, and Norman Meek, 1989, Field Trip Log, The west-central Mojave Desert: Quaternary studies between Kramer and Afton Canyon, a special publication of the San Bernardino County Museum Association 2024 Orange Tree Lane, Redlands, California 92374, prepared in conjunction with the 1989 Mojave Desert Quaternary Research Center Symposium May 19 - 21, 1989
- Reynolds, R.E., and Reynolds, J., 1991. Crossing the borders: the 1991 MDQRC field trip, in Crossing the borders: Quaternary studies in eastern California and southwestern Nevada, R.E. Reynolds, ed. Redlands, San Bernardino County Museum Association Special Publication MDQRC 91:5-35.
- Reynolds, R.E., R.L. Reynolds, C.J. Bell, N.J. Czaplowski, H.T. Goodwin, J.I. Mead, and B. Roth, 1991. The Kokoweef Cave faunal assemblage. San Bernardino County Museum Association Special Publication, SP91-1:97-103.
- Reynolds, R.E., 1993. Erosion, deposition, and detachment: the Halloran Hills area, California, p. 21-24, in Extended terranes, California, Arizona, Nevada, D.R. Sherrod and J.E. Nielson, eds. U.S. Geological Survey Bulletin, 2053: 250 p.
- Reynolds, R.E. (compiler), and Reynolds, J. (ed), 1995. Ancient surfaces of the Eastern Mojave Desert. San Bernardino County Museum Association Quarterly, 42(3): 160 p.
- Reynolds, R.E., and Reynolds, J. (eds), 1996. Punctuated chaos in the northeastern Mojave Desert. San Bernardino County Museum Association Quarterly, 43(1,2): 156 p.
- Reynolds, R. E., G. T. Ririe, D. Miller, and L. Vredenburg, 1996. Punctuated Chaos: a field trip guide in the northeastern Mojave Desert. San Bernardino County Museum Association Quarterly, 43(1 & 2):5-26.
- Reynolds, R.E., and Calzia, James, 2001. Neogene erosional surfaces in the northeastern Mojave Desert, California, in Reynolds, R.E. (ed.), 2001. The changing face of the east Mojave Desert. California State University, Desert Studies Center: 41-43.
- Reynolds, Robert E. and Ted Weasma, 2005, Old ores: mines and mineral marketing in the east Mojave Desert—a field trip guide, in Old Ores: mines and mineral marketing in the east Mojave Desert—a field trip guide, Robert E. Reynolds and Ted Weasma editors, California State University, Desert Studies Consortium and LSA Associates, Inc.. April 2005, p. 2-19.
- Rich, Mark, 1961, Stratigraphic section and fusulinids of the Bird Spring formation near Lee Canyon, Clark County, Nevada; Jour. Paleontology, vol. 35, pp. 1159-1180.
- Richards, Arthur, and Brokow, A. L., 1944, Geology and ore deposits of the Carbonate King zinc mine, Kokoweef Mountain area, Son Bernardino County, California: U.S. Geol. Survey open file report, 3 pp.
- Ririe, G. T. and Geoff Nason, 1991. Molycorp's Mountain Pass Mine. San Bernardino County Museum Association Special Publication, SP 91-1:87-89.
- Rocks & Minerals (1947): 22: 439. (Carbonate King Mine).
- Rodman, E.J., 1989, A detailed structural analysis of the Clark Mountain fault in SE California: [M.S. Thesis] University of California-Davis, 76 p.
- Rogers, Thomas H., 1967, Geologic Map of California: San Bernardino Sheet, California Division of Mines and Geology, Geologic Atlas of California, San Bernardino 1:250,000 scale sheet.
- Reynolds, Robert E. and Ted Weasma, 2005, Old ores: Mines and Mineral Marketing in the East Mojave Desert – A field trip guide, 2005 Desert Symposium, Zzyzzx, California State University, Desert Studies
- Schlocker, J., 1942 Magnesium-bearing minerals in the Boulder Dam area for the production of magnesium metal: U. S. Bur. Mines Inf. Circ. 7216, 16 pp.
- Schwartz, Scott, 2017, Fort Piute - Rocky Redoubt On The Mojave Road, Desert USA, <https://www.desertusa.com/desert-trails/fort-piute.html> accessed Dec. 21, 2017
- Stone, Paul, David M. Miller, Calvin H. Stevens, Jose Rosario, Jorge A. Vazquez, Elmira Wan, Susan S. Priest, and Zenon C. Valin, 2017, Geologic Map of the Providence Mountains in Parts of the Fountain Peak and Adjacent 7.5 Quadrangles, San Bernardino County, California, U.S. Geological Survey: Scientific Investigations Map 3376.
- Theodore, Ted. G., 2007, Geology and Mineral Resources of the East Mojave National Scenic Area, San Bernardino County, California, U.S. Geological Survey Bulletin 2160.
- Tucker, W. B., 1921, Los Angeles Field Division, San Bernardino County: California Division of Mines Report 17, p. 3-20
- Tucker, W. B., and Sampson, R. J., 1931, San Bernardino County: Calif. State Min. Bur., Mining in California, v. 27. p. 262-401.
- Tucker, W. Burling, and Sampson, R. J., 1930, Commercial grinding plants in California, Southern California Plants, Los Angeles field division [San Bernardino County] : California Div. Mines Rept. 26, pp. 202-345.
- Tucker, W. Burling, and Sampson, R. J., 1931, Los Angeles field division [San Bernardino County] : California Div. Mines Rept. 27, pp. 262-401.

- Tucker, W. Burling, and Sampson, R. J., 1943, Mineral resources of San Bernardino County, California Div. Mines Rept. 39, p. 484, 1943.
- Turner, R.D., and Glazner, A.F., 1990, Miocene volcanism, folding, and faulting in the Castle Mountains, southern Nevada and eastern California, Wernicke, B.P., ed., Cenozoic tectonics of the Basin and Range Province at the latitude of Las Vegas: Geological Society of America Memoir 176, p. 23–35.
- Segerstrom, Richard J., 1941, Tin in California, California Journal of Mines and Geology, v. 37, p. 551-554.
- Sharp, R. P., 1957, Geomorphology of Cima Dome, Mohave Desert, California: Geol. Soc. Am. Bull. vol. 68, no. 3, pp. 273-290.
- Sharp, J.E., 1984, A gold mineralized breccia pipe complex in the Clark Mountains, San Bernardino County, California; in J. Wilkins Jr. ed., Gold and silver deposits of the Basin and Range Province, western USA: Volume XV, Arizona Geol. Soc. Digest, Tucson AZ, p. 119-139.
- Shaw, Van E., 1959, Extraction of rare-earth elements from bastnoesite concentrate; U.S. Bureau of Mines Report of Investigations 5474, 12 pp.
- Shawe, D.R., 1988, The case for gold—An introduction to geology and resources of gold in the United States, in Shawe, D.R., Ashley, R.P., and Carter, L.M.H., eds., Introduction to geology and resources of gold and geochemistry of gold: U.S. Geological Survey Bulletin 1857-A, p. A1–A8.
- Shumway, G.L., L. Vredenburgh and R. Hartill, 1980. Desert fever: an overview of mining in the California Desert Conservation Area. BLM Contract No. CA_060_CT7_2776.
- Sillitoe, R.H., 1991, Intrusion-related gold deposits, in Foster, R.P., ed., Gold metallogeny and exploration: Glasgow and London, Blackie and Son Ltd., p. 165–209.
- Spencer, J.E., and Turner, R.D., 1985, Geologic map of Homer Mountain and the southern Piute Range, southeastern California: U.S. Geological Survey Miscellaneous Field Studies Map MF-1709, scale 1:24,000
- Sperisen, F. J, 1897. Mineral Resources U. S. United States Geological Survey:504.
- Sperisen, F. J, 1938. Gem minerals of California. California Journal of Mines and Geology, 34(1):34-74.
- Spieker, E. M., 1946, Late Mesozoic and early Cenozoic history of central Utah: U.S. Geol. Survey Prof. Paper 205-D, pp. 117-161.
- Stone, Paul, and Howard, K.A. 1979, Compilation of geologic mapping in the Needles 1 degree x 2 degree sheet, California and Arizona, U.S. Geological Survey, Open File Report 79-388.
- Storms, W. H., 1893 San Bernardino County: California Mining Bur., Rept. 11, pp. 337-369 (Morning Star Mine)
- Theodore, Ted. G., 2007, Geology and Mineral Resources of the East Mojave National Scenic Area, San Bernardino County, California, U.S. Geological Survey Bulletin 2160
- Thomas, W.M., Clarke, H.S., Young, E.D., Orrell, S.E., and Anderson, J.L., 1988, Proterozoic high-grade metamorphism in the Colorado River region, Nevada, Arizona, and California, in Ernst, W.G., ed., Metamorphism and crustal evolution of the western United States (Rubey Vol. VII): Englewood Cliffs, N.J., Prentice-Hall, p. 526–537.
- Thompson, D.F., 1978. The geology of the Evening Star tin mine and surrounding region, San Bernardino County, California. MS Thesis, University of Missouri, Rolla.
- Tucker, W. Burling, 1921, Los Angeles field division: California Mining Bureau. Report 17: 363. (Carbonate King Mine).
- Tucker, W. Burling, 1921, San Bernardino County: California Mining Bureau. Rept. 17, pp. 333-374.
- Tucker, W. Burling, 1924, Los Angeles field division: California :Min. Bur. Rept. 20. (San Bernardino County and other counties).
- Tucker, W. Burling, and Sampson, R. J., 1930, San Bernardino County: Calif. Div. Mines Rept. 26, pp. 202-325.
- Tucker, W. Burling, and Sampson, R. J., 1931, Los Angeles field division [San Bernardino County] : California Div. Mines Rept. 27, pp. 262-101.
- Tucker, W. B., and Sampson, R. J., 1940, Current mining activity in southern California: California Div. Mines Rept. 36, pp. 9-B2.
- Tucker, W. B., and Sampson, R. J., 1941, Recent developments in the tungsten resources of California: California Div. Mines Rept. 37, pp. 565-588.
- Tucker, W. B., and Sampson, R. J., 1943, Current mining activity in southern California: California Div. Mines Rept. 39, pp. 118-138.
- Tucker, W. Burling and Reid J. Sampson. 1943, Current mining activity in southern California: California Journal of Mines and Geology, California Division Mines Report 39(4): 478-479. (Carbonate King Mine).
- Tucker, W. B., and Sampson, R. J., 1943, Mineral resources of San Bernardino County: California Div. Mines Rept. 39, pp. 427-549.
- Turner, R.D., and Glazner, A.F., 1990, Miocene volcanism, folding, and faulting in the Castle Mountains, southern Nevada and eastern California, Wernicke, B.P., ed., Cenozoic tectonics of the Basin and Range Province at the latitude of Las Vegas: Geological Society of America Memoir 176, p. 23–35.
- U.S. Bureau of Land Management, 1980, The California desert conservation area plan: U.S. Bureau of Land Management, 173 p.
- U.S. Bureau of Land Management, 1982, Final environmental impact statement and proposed plan California Desert Conservation Area, Appendix 14, volume G (revised), Geology-Energy-Minerals: U.S. Bureau of Land Management, p. 1–202.
- U.S. Bureau of Mines, 1990b, Copper, gold: U.S. Bureau of Mines Mineral Commodity Summaries, 1990, p. 52–53, 70–71.
- U.S. Bureau of Mines and U.S. Geological Survey, 1980, Principles of a resource/reserve classification for minerals: U.S. Geological Survey Circular 831, 5 p.
- U.S. Bureau of Land Management, 1988, East Mojave National Scenic Area Final Management Plan: Needles, Calif., Department of Interior, Bureau of Land Management, Needles Resource Area, May 1988.

- U.S. Bureau of Mines, 1990a, Minerals in the East Mojave National Scenic Area, California—A minerals investigation, v. 1: U.S. Bureau of Mines Open-File Report MLA 6-90, 356 p.
- U.S. Bureau of Mines, 1990b, Minerals in the East Mojave National Scenic Area, California—A minerals investigation, v. 1: U.S. Bureau of Mines Open-File Report MLA 6-90, Table 2, p. 108 (Teutonia Mine).
- U.S. Department of Energy, 1979b, Airborne gamma-ray spectrometer and magnetometer survey, Las Vegas quadrangle (Arizona, California, Nevada), William quadrangle (Arizona), Prescott quadrangle (Arizona), and Kingman quadrangle (Arizona, California, Nevada): U.S. Department of Energy Open-File Report GJBX-59(79), 993 p.17, no. 6, p. 414.
- U.S. Department of Energy, 1979a, Aerial radiometric and magnetic survey, Trona National Topographic Map, California: U.S. Department of Energy Open-File Report GJBX-65 (79), 204 p.
- U.S. Geological Survey, 2009, The Mojave River and Associated Lakes, <https://pubs.usgs.gov/of/2004/1007/river.html> accessed Sept. 24, 2017.
- U.S. Geological Survey, 2017, Geologic Maps of Nevada, California and Arizona (on line maps).
- Ver Planck, W.E., 1961. History of mining in northeastern San Bernardino County. California Division of Mines, Mineral Information Service, 14(9).
- Vitnliano, C. J., 1950 Needles magnesite deposit San Bernardino County, California: California Jour. Mines and Geol., pp. 307-372, pls. 62-65.
- Vredenburg, Larry M., 1994. Fort Irwin and vicinity: mining history and development. San Bernardino County Museum Association Special Publication, SP 94-1:
- Vredenburg, Larry M., 1995. A brief summary of the history of mining in the East Mojave Desert, 1863-1947. San Bernardino County Museum Association Quarterly, 42(3):83-84.
- Vredenburg, Larry M., 1996a. Early mines of the southern Clark Mountains, northern Mescal Range, and Ivanpah Mountains. San Bernardino County Museum Association Quarterly, 43(1):67-72.
- Vredenburg, Larry M., 1996b. Later mining history in the Mescal Range, Ivanpah Mountains and south Clark Mountain. San Bernardino County Museum Association Quarterly, 43(1):73-76.
- Vredenburg, Larry M. 1996c; Later Mining History of the Mescal Range, Ivanpah Mountains and south Clark Mountain. SBSMA Quarterly v. 43, n. 1. See also at http://vredenburg.org/mining_history/pages/clark_mescal_mtns_mining_later.html, accessed Dec. 5, 2015).
- Vredenburg, Larry M., 1996d, Early Mines of Southern Clark Mountain, the Northern Mescal Range and the Ivanpah Mountains, in Robert E. Reynolds and Jennifer Reynolds eds. Punctuated Chaos, in the Northeastern Mojave Desert, San Bernardino County Museum Association Quarterly Vol. 43 nos. 1 and 2, pp. 67-72,
- Vredenburg, Larry M., 1996d; Early Mines of Southern Clark Mountain, Northern Mescal Range and Ivanpah Mountains; http://vredenburg.org/mining_history/pages/clark_mescal_mtns_mining_early.html, Dec. 5, 2016
- Vredenburg, Larry M., 2017, Geology and Mineralization of Old Dad Mountains, in ECSZ Does It Revisiting the Eastern California Shear Zone, Robert E. Reynolds, editor, California State University Desert Studies Center, 2017 Desert Symposium Field Guide and Proceedings, p. 120-124.
- Vredenburg, L. M., G. L. Shumway and R. D. Hartill, 1981. Desert Fever, an overview of mining in the California desert. Canoga Park, Living West Press: 324 p.
- Walker, J.D., Burchfiel, B.C., and Davis, G.A., 1995, New age controls on initiation and timing of foreland belt thrusting in the Clark Mountains, Southern California: Geological Society of America Bulletin, v. 107, p. 742-750.
- Walker, R. T., 1928, Mineralized volcanic explosion pipes: Eng. and Min. Jour., v. 126, p. 895-898, 939- 982, 976-984.
- Walcott, C. D., 1908, Cambrian sections of the Cordilleran area: Smithsonian Misc. Coll., v. 53, no. 5, p. 167-230.
- Walcott, C. D., 1908, Cambrian geology and paleontology; no. 1, Nomenclature of some Cambrian Cordilleran formations: Smithsonian Misc. Collections., vol. 53, pp. 1-12.
- Walker, G. E., Lovering, T. G., and Stephens, H. G., 1956, Radioactive deposits in California: California Div. Mines Special Rept. 49, 3B pp.
- Ward, L. F., 1901, Geology of the Little Colorado Valley: Am. Jour. Sci., 4th ser., vol. 12, pp. 401-413.
- Wheeler, H. E., 1943, Lower and middle Cambrian stratigraphy in the Great Basin area: Geol. Soc. America Bull. 54, p. 1781-1822. (Tapeats Sandstone).
- Wiebelt, F.J., 1949, Investigation of Carbonate King zinc mine (Crystal Cave group), San Bernardino County, California: US Bureau Mines Report of Investigation 4522: 1. (Carbonate King Mine).
- Wiebelt, F. J., 1949, Investigation of Mohawk lead-zinc mine, San Bernardino County, California: U.S. Bur. Mines R. I. No. 447B, 7 pp.
- Wilkerson, Gregg, 2013, The Kelso Dunes Mining Claim Validity Examination, in Raising Questions in the Central Mojave, ed. Robert E. Reynolds, California State University Desert Studies Center, 2013 Desert Symposium, April, 2013 p. 147-158
- Wilshire, Howard G., 2002a, Digital Version of "Open-File Report 92-179, Geologic map of the Cow Cove Quadrangle, San Bernardino County, California", GIS database by David R. Bedford and Teresa Coleman, Open File Report 92-179 Version 1.0.
- Wilshire, Howard G., 2002b, Digital Version of "Open-File Report 92-181, Geologic map of the Indian Springs Quadrangle, San Bernardino County, California", GIS database by David R. Bedford and Teresa Coleman, Open File Report 92-181 Version 1.0.
- Wilshire, Howard G., 2002c, Digital Version of "Open-File Report 92-182, Geologic map of the Marl Mountain Quadrangle, San Bernardino County, California", GIS

- database by David R. Bedford and Teresa Coleman, Open File Report 92-182 Version 1.0.
- Wilshire, Howard G., 2002d, Digital Version of "Open-File Report 92-183, Geologic map of the Granite Springs Quadrangle, San Bernardino County, California", GIS database by David R. Bedford and Teresa Coleman, Open File Report 92-183 Version 1.0.
- Wilshire, H.G., Frisken, J.G., Jachens, R.C., Prose, D.V., Rumsey, C.M., and McMahan, A.B., 1987, Mineral resources of the Cinder Cones Wilderness Study Area, San Bernardino County, California: U.S. Geological Survey Bulletin 1712-B, 13 p.
- Wilson, E.D., Moore, R.T., and Cooper, J.R., 1969, Geologic map of Arizona: Arizona Bureau of Mines, scale 1:500,000.
- Wilusz, John P., 2002b, The colorful history of the California/ Nevada State Boundary Part 2., Professional Surveyor, February, 2002.
- Wilusz, John P., 2002a, The colorful history of the California/ Nevada State Boundary Part 1., Professional Surveyor, January 2002
- Wise, W.S., 1989. The mineralogy of the Mohawk Mine, San Bernardino County, California. San Bernardino County Museum Association Quarterly, 37(1):1-31.
- Wise, W.S., 1996. The Blue Bell claims and the Mohawk Mine: two prolific mineral localities in San Bernardino County, California. San Bernardino County Museum Association Quarterly, 43(1,2):91-94.
- Worl, R.G., Van Alstine, R.E., and Shawe, D.R., 1973, Fluorine, in Brobst, D.A., and Pratt, W.P., eds., United States mineral resources: U.S. Geological Survey Professional Paper 820, p. 223-235.
- Wright, L. A., R. M. Stewart, T. E. Gay Jr., and G. C. Hazenbush, 1953, Mines and mineral deposits of San Bernardino County, California. California Division of Mines, 49 (1,2), pp 49-259. 103-106. (Carbonate King Mine).
- Wright, Lauren A., Richard M. Stewart, Thomas E. Gay Jr., and George Hazenbush, 1953, Mines and mineral resources of San Bernardino County, California: California Journal of Mines and Geology: 49(1-2):1-192
- Wright, L A., 1954, Geology of the Alexander Hills area, Inyo and San Bernardino Counties: California Div. Mines Bull. 170, Map Sheet 17.
- Wooden, J.L., and Miller, D.M., 1990, Chronologic and isotopic framework for Early Proterozoic crustal evolution in the eastern Mojave Desert region, southeastern California: Journal of Geophysical Research, v. 95, no. B12, p. 20,133-20,146.
- Young, E.D., 1989, Petrology of biotite-cordierite-garnet gneiss of the McCullough Range, Nevada II. P- T-aH₂O path and growth of cordierite during late stages of low-P granulite-grade metamorphism: Journal of Petrology, v. 30, pt. 1, p. 61-78.
- Young, E.D., Anderson, J.L., Clarke, H.S., and Thomas, W.M., 1989, Petrology of biotite-cordierite-garnet gneiss of the McCullough Range, Nevada I. Evidence for Proterozoic low-pressure fluid-absent granulitegrade metamorphism in the southern Cordillera: Journal of Petrology, v. 30, pt. 1, p. 39-60.
- Young, E.D., Wooden, J.L., Shieh, Y.-N., and Farber, D., 1992, Geochemical evolution of Jurassic diorites from the Bristol Lake region, California, U.S.A. and the role of assimilation: Contributions to Mineralogy and Petrology, v. 110, p. 68-86.
- Zimmerman, Martin, 2009, "California metal mine regains luster," Los Angeles Times, 14 October 2009

Abstracts from proceedings: the 2018 Desert Symposium

David M. Miller, compiler

¹USGS 345 Middlefield Road, Menlo Park CA 94025; dmiller@usgs.gov

Early Miocene extension in the central Mojave; where do we go from here?

Ernie Anderson

P.O. 347, Kernville, CA 93238, geologisternie@gmail.com

Tectonic reconstructions of Neogene extension in the Cordillera depend on measurements that are accurate along chosen transects. Large errors in magnitude, timing, or kinematics in one area impose severe constraints on surrounding areas. Also, whether or not strain is integrated between widely separated areas where data are available is critical to accurate province-wide reconstructions. For the central Mojave metamorphic core complex (CMMCC), recent field studies have led to major revisions of the timing, magnitude, and cause of extension (Anderson, 2017), and integration with extension in the lower Colorado River is highly unlikely (Anderson and others, 2013). Some of these revisions, summarized below, are based on reconnaissance field studies, opening opportunities for much-needed detailed mapping and analytical studies also noted below.

Revising the extension paradigm

Among metamorphic core complexes in the Cordillera, the CMMCC is conspicuously small and isolated, yet previous workers suggested 40–60 km of Neogene extension associated with it based on 1) syn-extension deposition and steep tilting of upper-plate rocks of the 23–19 Ma Pickhandle Formation, 2) a localized gently dipping fault contact between Miocene plutonic rocks that were mylonitized at mid-crust depths and shallow rocks of the Pickhandle Formation, and 3) shear reorientation and mylonitization of steep Miocene dikes and pre-Tertiary lower-plate rocks and structures into parallelism with the Waterman Hills detachment fault (WHDF). Regarding 1: Pickhandle strata display no systematic up-section decrease in dip and thus do not record major syndepositional tilting. Most tilting shows no first-order relation to normal faulting. Tilting followed deposition and is, therefore, younger than previously reported. Most resulted from folding rather than faulting. Regarding 2: Only the upper part of the pluton is mylonitic and those fabrics record stretch rather than shear, raising the prospect that the mylonitization was more dependent on the thermal state of the pluton than on either shear strain or depth. Regarding 3: There exists little or no evidence that Miocene dikes are transposed by shear into parallelism with the WHDF, and many mylonites in the core complex are spatially, and presumably genetically, related to pre-Tertiary plutons and do not record Neogene

deformation. Based on these revisions, tectonic models of extreme detachment-related extension need replacement.

Geologic mapping in the Hinkley Hills shows a progressive SE to NW increase in fertility of Miocene plutonism ranging from a few narrow dikes through many broad dikes to exclusively dikes. Farther to the northwest, the pluton shows a shift from common porphyritic rocks to equigranular granitoids. In the adjacent Waterman Hills, the pluton grades, in the same direction, from dikes, including common aplites and pegmatites, to massive granitoids mostly lacking in aplites and pegmatites. In both structural blocks, the gradations reflect a NE-increase in depth of exposure of the pluton, which translates to tilting to the SE. Based on variations in the abundance of dikes and the absence of screens of pre-Tertiary rocks in the massive NW parts of the pluton, the emplacement mode is interpreted as dilatant and, although the entire CMMCC is viewed as having experienced SW–NE syn-plutonic spreading, spreading, like uplift, apparently increased from SE to NW.

Post-Pickhandle sedimentation in the SE Waterman Hills and Mitchel Range includes the 18.8 Ma Peach Springs Tuff, the 18.8–12.5 Ma Barstow formation, and interstratified and overlying exotic-clast conglomerate. The stratigraphic range of exotic-clast conglomerate, generally lacking in locally derived clasts, from middle Pickhandle to post Barstow illustrates 1) a distant enduring highland source terrain 2) a proximal coeval lowland basin, and 3) youthful uplift of local ranges.

In the southeastern CMMCC, pre-Pickhandle rocks are not found between the Pickhandle rocks and the WHP, even in areas closest to the supposed breakaway fault. Near the breakaway in the northern Hinkley Hills, it is extremely unlikely that pre-Pickhandle rocks could have been eliminated by low-angle shear. More likely, the thick Pickhandle rocks there, and in the Waterman Hills, formed the co-genetic lid of the pluton. If so, the upper highly mylonitized part of the pluton must have developed within 2–3 km of the surface, and exposure of the mylonitic parts of the pluton does not record extreme exhumation from the middle crust by a detachment fault as previous workers have assumed. Much, or possibly most, tilting in the Pickhandle could record late-stage growth of the directly underlying pluton, and total SW–NE extension equates to spreading during emplacement of the WHP. The amount of spreading could approach 15 km.

The eastern California shear zone (ECSZ) and regional N–S shortening

The ECSZ in the CMMCC is represented mainly by four northwest-striking right-slip faults widely interpreted as deformation distributed inboard of the North American plate boundary. From west to east, they are the Lockhart–Lenwood, Hinkley Hills (Mt. General), Harper Lake, and Calico faults. Cumulative right-sense offset is estimated at 16.4 km (Miller, 2017). Strike slip faulting associated with the ECSZ in the Mojave structural block could have initiated as early as 12 Ma but more likely 11–10 Ma (Miller, 2017). Study of dextral faults of the eastern California shear zone in the CMMCC is enhanced by the absence of large block rotations or large-displacement sinistral faults as exist elsewhere in the Mojave block. Also, the dextral faults slice through strong and persistent older steep NE-trending structural trends that serve as reliable strain markers. For example, cumulative dextral offset of structural markers on northwest-striking faults in the Mitchel Range is about 0.8 km across the 2.8 km-wide range block. In addition, lower-plate structures along the Harper Lake fault show strong clockwise rotation. Despite these advantages, identifying structures uniquely associated with the ECSZ in the CMMCC is complicated by recent studies showing that much uplift of the ranges accompanied dextral faulting. Bartley et al. (1990) suggested, on the basis of widely distributed folds, that late Cenozoic N–S shortening in the central Mojave region was neither related to extension nor spatially restricted to restraining bends in post-extension transpressional faults on the ECSZ. Instead, they suggested it is part of regional N–S shortening. Many folds involving Pickhandle and younger strata in the CMMCC area, including the large Waterman Mine syncline, are consistent with regional N–S shortening in the same time frame as displacement on faults of the ECSZ. A tectonic model of plate-boundary shear embedded in a region of N–S shortening best characterizes the ECSZ in the CMMCC. Recent studies reflect progress in understanding the transpressional aspect of the dextral system and lay the groundwork for recognizing the interplay between 1) range uplift and dextral faulting, 2) regional N–S shortening and dextral faulting, and 3) range uplift and “detachment faulting”, all of which post-dates major magmatism that records major crustal spreading.

If the Harper Lake fault is an expression of plate-boundary strain, as is generally assumed, its 135° strike is conservatively efficient and should neither be transpressional nor transtensional. Unlike the southern Calico Mountains where post-Barstow Formation shortening resulted from a left step in the dextral Calico fault (Singleton and Gans, 2008), clockwise bending of lower-plate foliation and north-south contraction exhibited in south-tilted and folded Miocene strata (including the Barstow Formation) along the Harper Lake fault suggest transpressional dextral shear within a broader tectonic framework of regional N–S contraction.

Suggestions for detailed study

- (1) Strike-slip-restored stratigraphic sections of thick Pickhandle strata align along a NE transect from the Hinkley Hills through the Waterman Hills to the Calico Hills. To determine whether there is a basis for structurally restoring these separate sections closer to one another than they currently are (by closing the basins in large-extension restoration), would require detailed stratigraphic sections and bracketing age data. Such details and data are not currently available.
- (2) The strength of mylonitic fabric in the Waterman Hills pluton (WHP) decreases from SE to NW, presumably in correlation with greater depth. But the correlation could, instead, be with age if younger plutonism in the NW somehow produced stretching of older parts of the pluton in the SE. To test any correlation with age, simply requires ages from the NW, central, and SE parts. To test the correlation with depth, the NW, central, and SE parts of the WHP could be quantitatively sampled for features that should also vary with depth such as 1. volume percent of aplite and pegmatite dikes, 2. coarseness of crystallization, and 3. porphyritic characteristics. These could be compared with the strength of mylonitic fabric. Reconnaissance study of these features suggests deeper parts in the NW, but measurements are needed.
- (3) It has been suggested (Glazner and Bartley, 1991) that the source of potassium that produced extensive metasomatic replacement in flows and shallow intrusive rocks in the upper plate directly above the Waterman Hills detachment fault was from widespread chloritization along steep fractures in the underlying Waterman Hills pluton. Recent reconnaissance suggests an inadequate volume of chlorite in those fractures, but quantitative data are needed.
- (4) On the basis of geochemical data from widespread samples of the WHP representing an approach to the WHDF, Glazner and Bartley (1991) noted that as much as 70% of rock volume had been lost during mylonitization and chloritization. More recent chemical analysis of only 30 m across the leached zone directly beneath the WHDF in the Waterman Window (WW) shows strong localized geochemical shifts mostly similar to those of the earlier study. The leaching, together with the preponderance of steep fractures in rocks above and below the detachment fault in the WW, is consistent with removal of large amounts of rock in an open system leading to collapse. Both studies lead to a model of up-flow across the WHDF. More data are needed to better define the volumes and chemical characteristics of the fluids involved in the alteration process and make estimates of the extent to which those processes, as opposed to tectonic processes, led to the development of the WHDF.

(5) Metamorphic core complexes represent uplift; deep rocks rest structurally against shallow rocks. In the CMMCC, mylonitic early Miocene granitoids have been inferred as uplifted from the middle crust. Even if the mylonite formed at a shallower level, the pluton was uplifted from its emplacement depth. But, upper-plate conglomerates that are apparently composed of detritus derived from sources outside the CMMCC occupy several stratigraphic intervals from the middle of the Pickhandle Formation to above the Barstow Formation, suggesting an enduring depocenter spanning the interval of uplift. How is this possible unless: 1) uplift was greater outside the complex than within it? or 2) uplift is very young and occurred mainly during regional N–S shortening and dextral faulting? or 3) some process other than low-angle shear is responsible for juxtaposing deep rocks against shallow rocks? A quantitative analysis of clast populations from conglomerates spanning the supposed uplift history and a search for their source areas is needed to help understand the history and distribution of uplift.

References cited

- Anderson, R.E., 2017, Major revision of the timing, style, magnitude, and cause of early Miocene extension in the central Mojave metamorphic core complex and subsequent role of the eastern California shear zone: *in* Reynolds, R.E., ed., ECSZ does it, Revisiting the eastern California shear zone: Desert Symposium, California State University, Fullerton, p. 60-70.
- Anderson, R.E., Beard, L.S., Mankinen, E.A., and Hillhouse, J.W., 2013, Analysis of Neogene deformation between Beaver, Utah and Barstow, California: Suggestions for altering the extensional paradigm: *in* Anderson, R.E. ed, Neogene deformation between Central Utah and the Mojave Desert, Geological Society of America Special Paper 499, p. 1-67.
- Bartley, J.M., Glazner, A.F., and Schermer, E.R., 1990, North-south contraction of the Mojave block and strike-slip tectonics in southern California: *Science*, v. 248, p. 1398-1401.
- Glazner, A.F., and Bartley, J.M., 1991, Volume loss, fluid flow and state of strain in extensional mylonites from the central Mojave Desert, California: *Journal of Structural Geology*, v. 13, p. 587-594.
- Miller, D.M., 2017, The late Cenozoic eastern California shear zone after 25 years of study: *in* Reynolds, R.E., ed., Revisiting the eastern California shear zone: Desert Studies Symposium, California State University, Fullerton, p.45-54.
- Singleton, J.S., and Gans, P.B., 2008, Structural and stratigraphic evolution of the Calico Mountains: Implications for early Miocene extension and Neogene transpression in the central Mojave Desert, California: *Geosphere*, v. 4, no. 3, p. 459-479.

Mammal diversity and tectonic history of the Basin and Range

Catherine Badgley¹ and Tara M. Smiley²

¹ *Department of Ecology and Evolutionary Biology, University of Michigan, Ann Arbor, MI 48109*

² *Department of Integrative Biology, Oregon State University, Corvallis, OR 97331*

Over the past 36 million years, a high plateau stretching from British Columbia to northern Mexico was pulled apart into the mountain ranges and desert basins of the present-day Basin and Range. As part of an interdisciplinary research group of biodiversity and earth scientists, we are investigating the effects of these major landscape changes on mammal diversity over time. Three aspects of this tectonic history could influence the number and ecological diversity of mammals over time. (1) The increase in surface area could stimulate an increase in species richness. (2) Changes in topographic barriers could open or close routes for dispersal of new species into the region. (3) The changing configuration of elevational gradients during the transformation of a large, high plateau into many small mountain ranges could stimulate the formation of new species and attract more species to the increased habitat heterogeneity across the region.

We are testing these factors with the fossil record of the Basin and Range. The Mojave region is noteworthy as having experienced high areal expansion over the last 20 million years and an increase in mammal diversity when the extension rate was greatest, around 15 million years ago. Mammal diversity rose in step with increasing relief. Integrating tectonic, climatic, and mammalian history for the Mojave region offers new insights about the effects of landscape history on diversification of mammals.

Silver production from the Silver King Vein, Calico, California: A forensic geology estimate

Joy Berry

Department of Geological Sciences, California State University San Bernardino, 5500 University Parkway, San Bernardino, California 92407-2318, USA. Advisor: Dr. Erik Melchiorre

The Calico District has long been regarded as a historically important contributor of silver in California, with an official reported total of 13–20 million troy ounces of silver removed from the mines. However, these reported values for the entire district are inconsistent with reported ore grades and volumes of material mined from just one of the main deposits, the King Vein. Underground mine mapping with laser range-finders was conducted under supervision of the mine rescue squad and county search and rescue to produce accurate stope maps along the King Vein. Silver ore grade maps for these stopes were made from fire-assay and portable XRF analysis of ore remnants in pillars and stope borders. It is assumed that remnant ore represents a minimum ore grade, not a maximum. The resulting volume and grade estimates provide a more accurate picture of the minimum amount of silver

removed from the King Vein. This research suggests that at least 26 million troy ounces of silver were produced from this single vein alone. Assuming a 20% milling loss, this still indicates that the King Vein yielded at least 21 million troy ounces of silver. This estimated production of the King Vein exceeds the high-end historical estimate for the whole district, even without contributions from the Red Jacket, Oriental, and Bismarck veins. This suggests that, at best, the privately-held companies at Calico kept poor records. But given the remote location of this early district, the proximity to Mexico, and elevated black-market silver prices, it may indicate an intentional and systematic effort by these companies to defraud the government of tax revenue.

Incision and reoccupation of a Miocene paleovalley in the northern Marble Mountains, California

David C. Buesch

USGS Menlo Park Office, dbuesch@usgs.gov

Lease and others (2009) propose a Miocene paleovalley in the northern Marble Mountains, California, that consisted of a valley incised into a volcanic terrain of basalt to dacite lava flows and tuffaceous sedimentary rocks with (1) the Peach Spring Tuff (PST) and Lost Marble gravel (LMg) as valley fill deposits, (2) PST deposited directly on nearby volcanic topographic highlands, and (3) a northern edge of the paleovalley, but are these correct? Recent examination indicates valley-fill deposits do form a mesa capped by a very shallowly dipping sequence of pre-LMg basalt flows overlain by 12–20 m of LMg and 20–33 m of PST, both LMg and PST deposits thicken to the north, and the elevation of the basal PST is 1080–1100 m. The PST has a basal nonwelded and vitric facies that grades upward into moderately welded and vitric facies (total thickness of vitric rocks is 2–4 m), and most of the deposit is densely welded and crystallized facies (with minor amounts of lithophysae) that grades upward to moderately to partially welded and crystallized facies, and compaction foliation is approximately parallel to the base of the deposit. The LMg is very poorly exposed, and typically is covered by PST talus with minor amounts of clasts from the LMg as float. Where exposed, it is poorly indurated and typically poorly sorted with clasts up to ~16 cm in a fine-to-medium-grained volcanic sandstone matrix. Clasts vary in abundance of basalt, andesite, dacite, and rhyolite, but most clasts are vitric to incipiently crystallized, mini-vesiculated (<1 mm diameter), sparsely porphyritic dacite. A series of highland exposures are 4–6 km east of the mesa and consist of 6–10 m of PST deposited on basalt lava flows (with no interstratified LMg). The PST has an intact section of 1–2 m thick basal vitric facies overlain by densely to moderately welded and crystallized facies, and it thickens to the north. The PST and basalt dip about 6–15° N to NNE, compaction foliation in the PST is consistent across the exposures, and the elevation of the basal PST is about 830–915 m. Orientations of the

eastern deposits were initially controlled by the pre-PST topography, and current orientation might have been slightly modified by down-to-the-east tilting of the eastern side of the Marble Mountains. These two areas define a moderately constrained southern edge of the paleovalley that trends $260^\circ \pm 10^\circ$ (WSW) but the north edge is not constrained, and valley might have had a relief of as little as 100 m.

About 0.5 km north of the mesa with thick PST and LMg paleovalley deposits is an elongate (0.4x3 km) W-WNW trending series of exposed PST rocks (with no LMg) that were deposited on a variety of pre-LMg volcanic rocks, and elevations of the basal PST rocks vary from 915–1000 m. Buesch (unpublished data, 1987; 1991) and Lease and others (2009) interpreted these PST deposits as onlap of the pre-PST volcanic rock highlands. However, this interpretation is not correct because the depositional base of the paleovalley deposits on the mesa would be topographically above the onlap highland deposits. Furthermore, the difference in elevation cannot be explained by folding nor dip-slip faulting because the pre-PST section has shallowly dipping (2–15°) deposits with only a few minor faults having and mostly strike-slip separation. These northern PST rock deposits consist of two types of sedimentary breccia of crystallized PST that record the re-incision of the paleovalley. (1) The monomictic “jumble” breccia is 20–45 m thick, dips 25–45° (based on bottom and top contacts), has no basal vitric facies, a very poorly preserved sequence of variously welded and crystallized rocks (with some mixing of different facies), blocks up to 5 m across, and variously oriented compaction foliation from block to block (implying rotation of the blocks) with many block-block contacts and locally preserved 2–40 cm thick seams of sand to pebbly sand breccia matrix. These deposits are interpreted as collapse (or topple) avalanche breccia formed during cliff retreat along the widening edge of an incised valley that occupied a similar position as the original paleovalley. (2) The “rubble” breccia forms 1–5 m thick deposits, has average dips of 15–25° (based on bottom and top contacts), no basal vitric rocks, and can have up to 15 percent non-PST clasts. Compared to the jumble breccia, the rubble breccia has smaller blocks (less than 2 m), a mixture of blocks with different welded and crystallization facies, and blocks with compaction foliation approximately parallel to bedding. Rubble breccia deposits are interpreted as colluvial to alluvial fan deposits consisting mostly of re-deposited PST clasts and formed along the margins of a younger re-incised paleovalley. Locally, there are one to two differently dipping, PST rubble breccia deposits that likely represent fans associated with steeper stream gradients compared to younger (Pliocene to early Quaternary) stream gradients and fan profiles. The jumble and rubble breccia deposits record a sequence of re-incised valleys that occupied the position of the initial valley.

References:

- Buesch, D.C., 1991, Changes in Depositional Environments Resulting From the Emplacement of Large-Volume Ignimbrite: *in* Smith, G.A., and Fisher, R.V., eds., "Sedimentation in Volcanic Terranes": SEPM (Society for Sedimentary Geology) Special Publication No. 45, p. 139-153.
- Lease, R.L, McQuarrie, Nadine, Oskin, Michael, and Leier, Andrew, 2009, Quantifying Dextral Shear on the Bristol-Granite Mountains Fault Zone: Successful Geologic Prediction from Kinematic Compatibility of the Eastern California Shear Zone: *The Journal of Geology*, v. 117, p. 37-53.

~3.7 Ma Black Mountains basalt flows geochemically correlated to boreholes in Superior Basin, western Fort Irwin, California

David C. Buesch
USGS Menlo Park Office, dbuesch@usgs.gov

Three boreholes in Superior Basin (SB) in the southwestern sector of the Fort Irwin National Training Center, California, penetrated porphyritic olivine basalt flows that have been geochemically correlated to basalt flows in the Black Mountains basalt field. The three boreholes were drilled during 2009–2010; however, the basin has 37 pre-2009 boreholes, and 17 are monitored for depth to water, but none were logged in a way that enabled identification of basalt flows, so a refined distribution of the basalt is not possible. The source area for the basalt in the boreholes is not known, but the two closest exposed basalt fields are Black Mountain (BM; ~3.7 Ma, revised from Oskin and Iriondo, 2004) about 8-25 km southwest of borehole SBTW, and Goldstone Mesa (GM; 16 Ma, Schermer et al., 1996) about 18-24 km northeast of SBTW. Conventional XRF data (WD-XRF) on powdered whole-rock samples from these two fields (5 from BM, and 13 from GM) indicate they are geochemically distinct on bivariate plots of oxides, elements, and elemental ratios. A portable XRF (p-XRF) was used to analyze hand specimens and powdered samples of BM and powdered samples of SB. BM WD-XRF and p-XRF data are similar, and plot in 3 sub-clusters. The five SB samples are very similar to one BM sample, so it is likely that at least one flow from the BM volcanic field traveled > 8 km northeastward to an ~3.7 Ma paleo-Superior Basin. In boreholes SBTW and SBMW (which are only 55 m apart), the top of the basalt is at 61.9 m depth, it is 3.0 m thick, and is interbedded with sandstone and conglomerate. In borehole SBMC, the top of the basalt is at 72.8 m depth, it is >12.8 m thick (the borehole terminated in basalt), and it is overlain by sandstone and conglomerate. Borehole SBMC is 1,114 m west of SBTW and the land surface elevation for both is 926.9 m, so there is a 10.7 m difference in elevation of the top of the basalt between these boreholes. The lower elevation of the basalt in borehole SBMC compared to SBTW suggests apparent slip on a buried down-to-the-west fault, or a westward structural tilting. The basalts in boreholes were not in

screened intervals in the wells, and do not have measured hydrogeologic properties. However, because basalt flows (1) are crystallized rock with cooling joint fracture systems, (2) have long runout, and (3) are continuous from surface exposures (which are possible water recharge sites) to deposits in sedimentary basins, they might exert an important control on the recharge and storage properties of groundwater in the Superior Basin.

Integrating geologic and geophysical data into a geologic framework model of two groundwater basins at Fort Irwin National Training Center in the Mojave Desert, California

Geoff Cromwell, Lyndsay Ball, David Buesch, David Miller, Jill Densmore-Judy
U.S. Geological Survey, gcromwell@usgs.gov

A preliminary three-dimensional (3D) geologic framework model has been constructed for two groundwater basins (Superior and Goldstone) at the Fort Irwin National Training Center as part of a broader study to evaluate groundwater availability. The 3D geologic framework model was developed from a suite of geologic and geophysical data including geologic maps, cross sections, geophysical logs, drillers logs, and drill cuttings from wells, gravity-derived depth-to-basement models, and resistivity models from airborne electromagnetic (AEM) surveys. Inclusion of both geologic and geophysical data allowed for the development of a more robust framework model, but the integration of such a range of data types was not without challenges, especially in such a geologically complex area. We evaluated the subsurface extent of five lithostratigraphic units, each with their own geologic and geophysical characteristics: 1) Mesozoic metamorphic and plutonic crystalline basement; 2) tuffaceous and volcanoclastic Miocene deposits; 3) Miocene mafic-felsic lava flows and domes; 4) young, post-Miocene basalt lava flows; and 5) late Pliocene-Quaternary sediments. The overall approach to defining the extent of each unit was to calibrate interpretive AEM resistivity zones to known geologic data and concepts. This integration process resulted in a detailed 3D geologic framework model that quantifies the complex subsurface geology of Superior and Goldstone basins.

Biodiversity of amphibians and reptiles at the Camp Cady Wildlife Area, Mojave Desert, California and comparisons with other desert locations

Kristy L. Cummings*, Shellie R. Puffer, Jeffrey E. Lovich, and Kathie Meyer-Wilkins
U. S. Geological Survey, Southwest Biological Science Center, 2255 North Gemini Dr., Flagstaff, AZ 86001, USA (KLC, SRP, JEL); 19233 Stratford Way, Apple Valley, CA 92308, USA (KMW)

We examined the biodiversity of amphibian and reptile species living in and near constructed ponds in the riparian area at the Camp Cady Wildlife Area (CCWA) in

the Mojave Desert of San Bernardino County, California based on field work from 1998–1999, 2015–2016, literature review, and searches for museum specimens using VertNet.org. A total of 11 species (201 captures), including two frogs and toads, one turtle, three snakes, and five lizards were captured at terrestrial drift fences with pitfall traps encircling two ponds (0.5 hectares) on the property in 1999. Three additional species, the Pacific treefrog (*Pseudacris regilla*), the desert spiny lizard (*Sceloporus magister*), and Great Basin gophersnake (*Pituophis catenifer deserticola*) were reported in 1978 from a ranch 1.6 km away from CCWA for a total of 15 species in the local area. The southwestern pond turtle (*Actinemys pallida*) was commonly observed at CCWA from 1998–1999 and documented as a breeding population. However, the species was extirpated at CCWA sometime after 2014 when the last individuals were photographed and none have been detected since then despite significant efforts to do so. Biodiversity of amphibians and reptiles at CCWA is relatively low compared with sites elsewhere in the Mojave Desert with more elevational diversity. The number of native species documented at CCWA (14, not including *L. catesbeianus*) accounts for approximately 21 percent of the native reptile and amphibian species reported from Stewart (1994) in the entire Mojave Desert, including peripheral species. Our smaller sample likely represents a group of easily detected species, and is biased toward those found in or near water. The herpetofauna inhabiting CCWA is notable for including riparian obligates like the western toad (*Anaxyrus boreas*), *P. regilla* and *A. pallida* that are otherwise absent from large portions of the Mojave Desert. Other species are typical of those that are expected in the low-elevation creosote scrub-dominated ecosystem in the area.

Quaternary record of Mojave River discharge determined from detrital ^{10}Be pebble exposure ages

Andrew J. Cyr and David M. Miller

US Geological Survey, 345 Middlefield Road, Menlo Park, CA 94025

The Mojave River, which extends from the high-elevation plateau of the San Bernardino Mountains northward and eastward to Silver Lake Playa, is the largest drainage basin in the Mojave Desert region, and the sedimentary deposits and geomorphic surfaces preserved along its course preserve a record of both regional tectonic activity and paleoenvironmental conditions. Sedimentologic and geomorphic observations of fine grained sediment along its course indicate that the Mojave River has carried enough discharge to sustain lakes at various stages of the Quaternary. If this is the case then there must also be a record of higher discharge in the coarser (sand and larger) grain sizes preserved in Mojave River sedimentary deposits.

We recently used cosmogenic beryllium-10 (^{10}Be) concentrations in quartzite pebbles collected from a fluvial strath terrace of the Mojave River, ~40 km

east of Barstow, CA, to measure the residence time of pebble-sized sediment in the Mojave River system. These quartzite pebbles are sourced exclusively from Miocene conglomerates in the San Bernardino Mountains or from older Mojave River deposits, and so the concentration of ^{10}Be in each pebble should record the total time spent by that pebble in transport and storage along the course of the Mojave River. We observed three different age populations of pebbles, $30.71^{+6.06}_{-4.76}$ ka, $70.53^{+8.65}_{-7.79}$ ka, and $129.83^{+19.48}_{-23.37}$ ka, and argued that these were representative of periods of exceptionally high Mojave River discharge.

We have repeated this experiment using pebbles from an older Mojave River alluvial surface in order to extend our existing record of Mojave River paleodischarge further back in time. We collected an additional ten rounded to well rounded, equidimensional to somewhat elongated, quartzite pebble clasts from a probable mid-Pleistocene-aged alluvial surface of the ancestral Mojave River on the western side of Iron Mountain, ~12 km north of Helendale, CA. Although the pebbles were collected from a degraded desert pavement, the degree of desert varnish development indicates that they are unlikely to have been recently exhumed from within the alluvial deposit, which would result in apparent ages that are younger than the true age of the alluvial surface. In addition to potentially constraining the specific timing of mid-Pleistocene large discharge events, these pebble ages will also place direct numeric age limits on the abandonment age of the alluvial surface, which has previously only been inferred from paleomagnetic data from boreholes in the Victorville Basin (Cox et al., 2003, *GSA Special Papers* n. 368, p. 1-42).

We have also sampled buried Mojave River sediments that may correlate with a late-Pleistocene alluvial surface of the ancestral Mojave River. Recent surficial geologic mapping in Hinkley Valley, on the northeastern side of Iron Mountain, has documented a late-Pleistocene Mojave River alluvial surface; however, unlike the mid-Pleistocene surface from which we collected quartzite pebbles, this younger surface is composed primarily of granular and smaller sized sediment. Detailed examination of sediment recovered from well cores in Hinkley Valley has identified similar sediments, likely sourced from the ancestral Mojave River, at depths of up to ~30 m. We collected samples of this probable Mojave River in 3 of these sediment cores for ^{26}Al and ^{10}Be analyses in order to determine the depositional ages. These analyses will provide the first numeric age control of the Mojave River in the central part of the drainage basin and, in addition to improving the temporal resolution of sediment transporting events in the Mojave River Basin, allow for a more refined interpretation of the tectonic controls on the evolution of the Mojave River course.

The Cerutti Mastodon site: evidence for hominins in southern California 130,000 years ago.

Thomas A Deméré¹ and Steven R. Holen²

¹San Diego Natural History Museum; ²Center for American Paleolithic Research

The Cerutti Mastodon (CM) site was discovered and excavated along State Route 54 in San Diego over a 5-month period during the winter of 1992–93 and yielded the partial remains of a single American mastodon (*Mammuth americanum*) in association with evidence indicating that hominins used hammers and anvils to break the limb bones and molars. The bone assemblage and associated cobbles are contained within a fine-grain silt/sand in a low-energy overbank depositional setting. The taphonomic evidence for human agency is diverse and includes bone impact features (e.g., cone flakes, bulbs of percussion, and a large arcuate impact notch with associated negative flake scars); stone impact and usewear features (e.g., negative flake scars, Hertzian initiations, deep cracks and angular fractures); bone, tusk, and stone distribution patterns (e.g., femoral diaphysis fragments clustered around a single large cobble, detached femoral heads positioned side-by-side, and vertically oriented tusk); differential bone breakage (e.g., intact fragile ribs vs. sharply broken heavy limb bones); and bone, molar, and stone refits (e.g., 80-cm displacement of 5 pieces of a partial femoral diaphysis, 3-meter displacement of 3 pieces of single molar, 3-meter displacement of 7 pieces of a single large cobble). Significantly, most CM bones and stones were enclosed within crusts of pedogenic carbonate that establish a “chain of evidence” showing that breakage and positioning of objects at the site occurred many thousands of years ago, and, as we contend, before burial of the site. No knapped stones or butchery-marked bones were recovered at the CM site, which we propose was a bone-processing site occupied for a very short period of time for a very limited set of activities (expedient stone hammers and anvils used to break mastodon bones for marrow extraction and/or raw materials). Evidence from experimental archaeology supports these interpretations, as does evidence of human breakage of proboscidean limb bones on several continents and at several younger Pleistocene sites in North America. Alternative hypotheses (e.g., debris flow, plunge pool, alluvial fan, trampling, carnivore scavenging, and damage by heavy equipment) do not account for the multiple lines of evidence preserved at the CM site. We discuss possible dispersal routes into North America 130,000 years ago that humans could have used. We also discuss the various species of the genus *Homo* that potentially could have arrived in the Americas during the deglaciation event marking the transition from MIS 6 to MIS 5. Future work should include multidisciplinary efforts to explore geologic deposits of this age for additional evidence of human activity.

Evaluating groundwater discharge and water quality at springs, Fort Irwin National Training Center, San Bernardino County, California

Jill N. Densmore

U.S. Geological Survey, jdensmore@usgs.gov

The U.S. Army at Fort Irwin National Training Center (NTC) currently (2017) obtains all of its potable water supply from three groundwater basins within the base boundaries. The U.S. Geological Survey (USGS) has been studying water resources, including long-term availability and groundwater quality, in these developed basins. Due to NTC's growth and increasing water demand, however, water-resource evaluations expanded in 2010 to include 10 mostly austere surrounding groundwater basins and nearby springs/seeps where hydrogeologic data are quite limited. The Army's objective is to ensure sustainable water resources for base operations in perpetuity. One important environmental concern NTC-wide, however, is the response at numerous springs/seeps to warfare training and increased groundwater development. In 2014, NTC personnel requested the USGS to evaluate the discharge, water quality, and the connectivity of springs to local aquifer systems. This poster describes the preliminary findings from discharge and water-quality data collected for this evaluation. Additionally, traditional methods used for measuring discharge and groundwater/surface water interaction, although informative, were inadequate since several of these springs discharge over diffuse areas. An alternative approach relies on using evapotranspiration (ET) based on plant species, which has been successfully demonstrated in nearby areas (Death Valley and Ash Meadows). Bitter Spring is selected as a demonstration site to prove the method and eventually provide estimates of discharge at other areally smaller springs. Water-quality data indicate that some of the springs are fed primarily by precipitation, not by groundwater directly from the local aquifer system, such as at Bitter Spring.

Trace element concentrations in alluvium of the Mojave River floodplain

Krishangi Groover and John Izbicki

U.S. Geological Survey, kgroover@usgs.gov

Drill cuttings and cores from 14 monitoring well sites, between 0 and 800 feet (ft) below land surface (BLS), located in the floodplain aquifer along the Mojave River, southern California, were analyzed using portable X-ray fluorescence (pXRF) for concentrations of twenty-seven elements including arsenic, chromium, and uranium. Alluvium composing the floodplain aquifer was primarily eroded from the San Bernardino and San Gabriel Mountains, with smaller admixtures from local sources, and subsequently deposited by the Mojave River. The mix of alluvium eroded from the various sources has changed over recent geologic time, and these changes in source terrain are reflected in the

trace-element composition of alluvium encountered by wells. The median concentration of arsenic in shallow floodplain alluvium, less than 20 feet below land surface, was 2.8 milligrams per kilogram (mg/kg). This value is only slightly higher than the median concentration of arsenic in surficial Mojave River alluvium of 2.2 mg/kg, and reflects geologically younger alluvium eroded from similar source terrains. In contrast, the median arsenic concentration in deeper floodplain alluvium, between 20 and 200 ft BLS, was 6.4 mg/kg—consistent with older alluvium eroded from different, higher-arsenic source terrains. The median arsenic concentration of deeper alluvium, 20 to 200 ft BLS in Mojave Valley downgradient from Barstow was 3 mg/kg, and similar to the concentration in surficial and shallow alluvium. This difference reflects the comparatively geologically recent arrival of the Mojave River in Mojave Valley, after erosion through alluvial fans near Barstow. The highest median arsenic concentration encountered by the wells, about 18 mg/kg, was in partly-consolidated deposits eroded from volcanic and hydrothermal rocks near Barstow underlying the floodplain aquifer at depths between 200 and 600 ft BLS. The distribution of chromium was similar to arsenic, with a median concentration of 28 mg/kg in deeper floodplain alluvium, between 20 and 200 ft BLS, compared to the median concentration of 7.6 mg/kg in shallower deposits and surficial alluvium. Unlike arsenic, chromium concentrations did not change along the length of the floodplain aquifer downgradient from Barstow. This suggests that the source of chromium in Mojave River alluvium—mafic rock in the San Gabriel Mountains—was no longer contributing alluvium when the river eroded through alluvial fans near Barstow and reached Mojave Valley. Uranium was not typically detected, except below 200 ft BLS in regional deposits at sites upgradient of Barstow.

Modeling land-surface deformation with UAV photogrammetry in Bicycle and Red Pass Basins, Fort Irwin National Training Center, California

Elizabeth K. Haddon, Jill N. Densmore, Josip D. Adams, J. Luke Blair, and David M. Miller
U.S. Geological Survey, ehaddon@usgs.gov

Accurate assessment of ongoing land subsidence and ground failures requires periodic imaging of the ground surface and reconstruction of topographic changes over multiple timescales. The U.S. Geological Survey monitors active land-surface deformation of playas occupying Red Pass and Bicycle Basins in the Mojave Desert to evaluate the influence of tectonic stress, fault barriers to groundwater flow, and declining groundwater levels due to pumping in nearby wells. Interferometric Synthetic Aperture Radar (InSAR) analyses and land surveys in Bicycle Basin show near-vertical change up to ~400 mm for the 1993–2015 duration at temporally and spatially variable rates. Limits on the spatial resolution of InSAR

are in excess of a few meters, however, and insufficient for the detailed study of gradually evolving fissures, desiccation cracks, and sink-like depressions. Here, we test the utility of photogrammetric surveys using unmanned aerial vehicles (UAV) for repeat monitoring of decimeter changes at a low cost relative to Light Detection and Ranging (LiDAR) methods. We use Agisoft's Structure-from-Motion (SfM) algorithm to gain depth information from sequences of overlapping (> 60%) photographs collected via 3DR Solo* quadcopters equipped with Ricoh GRII* cameras. Our four-day aerial survey of Bicycle Lake playa involved two-tiered flights at altitudes of 122 and 183 m. Flying grid patterns at these altitudes with the camera positioned at ~10 degrees off-nadir resulted in a ground sampling distance between ~3 and 5 cm. We constrained the geometry of the derived 3D model with post-processed locations for 35 Propeller AeroPoints* distributed about the playa (with stated horizontal and vertical accuracy of ~2 and 5 cm, respectively). Our approach to imaging Red Pass Lake playa involved an abbreviated, one-day survey with both gridded and orbital flight patterns at a steady altitude of 183 m and off-nadir look angles at ~10 and 30-degrees, respectively. Ground control spanning Red Pass Lake playa involved a relatively sparse arrangement of 10 points. The root-mean-square error (RMSE) of our digital surface model for Red Pass Lake playa is ~50 cm, which is relatively high compared with an estimated accuracy of ~20 cm for Bicycle Lake playa. The number and distribution of ground control points largely influences the difference in total error at these sites. Future photogrammetric collections at Bicycle Lake and Red Pass Lake playas will provide the opportunity to refine our approach and allow for change detection through differencing of datasets in the vertical or land-surface normal directions. Our custom SfM-built topographic models are also compatible with recently available, high-resolution lidar topography (vertical accuracy of ~12 cm) collected December of 2014. Taken together, these topographic datasets provide the opportunity to evaluate physical processes over multiple timescales and predict the future response of desert basins to changing climatic conditions.

* For descriptive purposes only and does not imply endorsement by the U.S. Government.

Fire frequency and C₄ vegetation expansion in the Barstow Formation

Anna Harkness¹, Katharine Loughney², Catherine Badgley³

¹Dept. of Earth and Environmental Sciences, University of Michigan, Ann Arbor, MI, 48109, annahark@umich.edu;

²Dept. of Earth and Environmental Sciences, University of Michigan, Ann Arbor, MI, 48109; ³Dept. of Ecology and Evolutionary Biology, University of Michigan, Ann Arbor, MI, 48109

The spread of C₄ grassland ecosystems in western North America occurred between ~8 and 3 Ma. Studies of

ungulate enamel, soil organic matter, and phytoliths from the middle Miocene Barstow Formation in the Mojave Desert of southern California have demonstrated a small but marked presence of C₄ vegetation between ~14 to 13 Ma prior to the expansion of C₄ grasslands in the late Miocene. An increase in fire frequency has been shown to promote the expansion of C₄ grasslands and has been suggested as the possible driver behind the increase of C₄ vegetation in the Barstow Formation during the middle Miocene. In our study we analyzed microscopic charcoal from sediment samples spanning the Barstow Formation in the Mud Hills in order to determine whether the frequency of fire changed throughout the formation and to investigate the relationship between increased fire and the expansion of C₄ vegetation.

We analyzed charcoal morphology to estimate the fuel source and counted charcoal grains to document changes in the charcoal-accumulation rate over time. The charcoal-accumulation rates were then analyzed to distinguish between a background charcoal-accumulation rate and peak charcoal-accumulation rates in order to identify large fire events. We found an increase in fire activity from 13.04 Ma to 12.86 Ma in the Barstow Formation with a clear peak fire event at 13.04 Ma. Enriched values of $\delta^{13}\text{C}$ from soil organic matter and phytoliths from this interval indicate the presence of C₄ grasses and dry, open-canopy habitats at this time. The peak in charcoal-accumulation rates coincides with climatic cooling and drying in southern California and increasingly open-canopy habitats in the Barstow Formation. Furthermore, we found that the majority of charcoal particles analyzed are indicative of a wood fuel source, which suggests that upper-canopy plants were being burned during this time period. Our data suggest that increased fire frequency contributed to the opening of vegetation from forest to wooded grassland, which then promoted the expansion of C₄ plants in the environment.

Comparison of heteromyid rodents from the Sespe Formation of Orange County with Mojave Desert local faunas

Jared R. Heuck and James F. Parham
California State University, Fullerton

Paleontological mitigation in Laguna Canyon, Orange County, has provided a sample of intact heteromyid teeth from two localities of the uppermost Sespe Formation. The identification of Miocene heteromyid rodents *Proheteromys sulculus*, *Mookomys altifluminis*, *Paratrogomys* sp., and *Trogomys rupinimenthae*, among others, led to the initial interpretation of the Sespe at Laguna Canyon as late Arikareean to Hemingfordian. The age of this unit is important because of the report of toothed mysticetes (aetiocetids and llanocetids) in the overlying Vaqueros Formation that are otherwise restricted to the Oligocene.

This study in progress reexamines, illustrates, and describes the heteromyid rodents from the Sespe and compares them to several recently described local faunas from the Mojave Desert of southern California. In doing so we can provide a better-justified age for the uppermost Sespe Formation at Laguna Canyon, as well as a maximum age for the toothed mysticetes from the overlying Vaqueros Formation.

Use of a summative scale for decision-making at a Cr(VI) contamination site

John A. Izbicki and Krishangi Groover
U.S. Geological Survey, jaizbicki@usgs.gov

Decision making at groundwater contamination sites is often controversial, with stakeholders commonly having different views on the source, and extent, of contamination—even after years of study. Summative scales that integrate different types of data to provide a framework for visualization, and discussion can be useful for decision-making at such sites. In this example, the extent of Cr(VI) contamination released from a natural-gas compressor station in the Mojave Desert between 1952 and 1964 remains uncertain; in part, because Cr(VI) occurs naturally in alkaline, oxic groundwater at different concentrations within different geologic, hydrologic, and geochemical settings; and concern that there may have been multiple releases of Cr(VI) at different locations in the study area.

Even after installation of more than 600 monitoring wells, and collection and analyses of more than 22,000 samples for Cr(VI), attempts to estimate background Cr(VI) concentrations and define plume margins have not reached consensus among stakeholders. Depending on the stakeholder, estimates of plume extent range from 3 miles to as much as 10 miles downgradient from the source; by either measure, this is believed to be the largest mapped Cr(VI) contamination plume in the world. To help reach consensus, a summative scale consisting of multiple items (formulated as questions requiring yes/no answers) is to be developed—a score of 1 for an item in the scale represents data consistent with release from the source, and a score of -1 represents data inconsistent with release from the source. Items within the scale include: 1) the source of water, evaluated on the basis of d18O and δD data; 2) the age of water, relative to the timing of the contaminant release, evaluated on the basis of chlorofluorocarbon, sulfur hexafluoride, tritium, helium-3/helium-4, and carbon-14 data; 3) geologic source and chromium concentrations of aquifer materials at the well screen, evaluated on the basis of lithology, depositional provenance, x-ray fluorescence, sequential extraction, mineralogic data, and 87/86Sr data; 4) occurrence of Cr(VI) in alkaline oxic groundwater, evaluated on the basis of pH and Cr(VI) concentrations; and 5) source and geochemical history of chromium, evaluated on the basis of $\delta^{52}\text{Cr}$ data. Scores for items in

the scale are to be summed for each of more than 100 wells sampled within the plume, near plume margins, and at distance upgradient, downgradient, and cross-gradient from the mapped plume. Water from wells having higher magnitude negative scores are believed to be more representative of background, while water from wells having higher magnitude positive scores are believed to be more representative of groundwater affected by anthropogenic sources. As the study proceeds and consensus builds, items within the scale can be weighted on the basis of geologic, hydrologic, or geochemical knowledge to allow the summative scale to be refined. Although the summative scale provides a framework for visualization, discussion, and decision-making, final interpretation of Cr(VI) background concentrations and plume extent is to be process-oriented. Geochemical processes affecting Cr(VI) concentrations, and age-dating information are to be evaluated with respect to understanding of groundwater movement since contaminant release to be developed on the basis of updates to a USGS groundwater flow model and particle-tracking analyses.

Motion camera surveillance for Mohave ground squirrel on mitigation parcels in the west Mojave Desert

Edward L. LaRue, Jr., M.S.

Circle Mountain Biological Consultants, Inc., Wrightwood, CA, ed.larue@verizon.net

California Department of Fish and Wildlife (CDFW) is in its initial stages of determining how mitigation parcels are longitudinally monitored to determine the presence of target species, including the State-listed, threatened Mohave ground squirrel (*Xerospermophilus mohavensis*) (MGS).

Between April 15 and June 2, 2017, the author established 65 motion camera stations on 2.5 square miles of mitigation lands addressed in the Cuddeback-Kramer Preserve Management Plan with the expressed intent of monitoring the occurrence of MGS on the three parcels.

Rather than day-to-day site visits over a five-day period, the author developed and implemented a methodology that allowed camera stations to function over a 2.5-month period, with visits at eight to ten day intervals, and with prolonged bait availability to MGS with limited availability to common ravens.

A total of 18 animal taxa was photographed in 460,960 images, including the following numbers of images (in descending order of occurrence): 43,751 rodents (mainly kangaroo rats and pocket mice); 6,041 common ravens; 3,949 black-tailed hares; 3,873 antelope ground squirrels; 2,063 kit foxes; 205 bird species (mostly horned larks and sparrow species); 114 domestic dogs; 57 LeConte's thrashers; 46 American badgers; 32 desert tortoises; 25 Botta pocket gophers; 19 coyotes; 13 turkey vultures; 9 loggerhead shrikes; 6 bobcats; and 2 MGS, which was the target species. There were also 399,353 "empty images,"

or 86.6% of the total, where no animal images were in the photographs.

The results will be compared with subsequent years to determine how species densities and distributions change over time. Determining means of reducing the number of "empty images" is important going forward. These new bait presentation methodologies will help CDFW determine how future camera monitoring on mitigation parcels may best be implemented.

High school student research at the Raymond Alf Museum of Paleontology: Filling the gap in alpha level paleontology for the Barstow Formation

Don Lofgren¹, Andrew Farke¹, and Gabe Santos¹

¹ *Raymond M. Alf Museum of Paleontology, Claremont, California 91711*

The Alf Museum is located on the campus of The Webb Schools, a private college-prep high school in Claremont, California. The museum was the creation of Raymond Alf, who taught at Webb for nearly 50 years and amassed a large collection of fossils with the help of Webb students. The tradition of having Webb students collect fossils on trips continues today, and these expeditions are now named "peccary trips" in reference to a new species of peccary found by a Webb student in the Barstow Formation in 1936. However, the focus is now on research as Webb students have the opportunity to take advanced courses in paleontology where they can study specimens from the collections or those found on recent peccary trips. Much of this research is alpha level paleontological analysis of specimens from the Barstow Formation. A host of museums, including the Alf Museum and American Museum of Natural History (AMNH), made significant collections at Barstow, but only a small percentage of this material was described and illustrated in publications (crews financed by Childs Frick recovered thousands of mammal specimens at Barstow between 1923–1952 that were later donated to the AMNH). Using the AMNH and RAM collections, study of a specific taxonomic group of vertebrate, invertebrate, or trace fossils (tracks) is assigned to a Webb student and they review the literature on the topic, and then measure, photograph, describe, and analyze their specimens (i.e. alpha level paleontology). Review of Barstow Formation proboscideans, peccaries, anchitherine horses, weasels, amphicyonids, tortoises, gastropods, and selected mammal tracks are some examples of recently completed student projects, all of which were published in a Desert Research Symposium volume. In addition to the important work of describing and illustrating unreported but significant specimens, new information is learned, like biostratigraphic and paleogeographic range extensions and discovery of new taxa in existing collections. Thus, Webb students have the unique opportunity to make a contribution to scientific knowledge, as well as to develop critical thinking and precise analytical skills.

Reconstructing environmental change in the Barstow Formation, Mojave Desert, California, through the Middle Miocene Climatic Optimum

Katharine M. Loughney¹, Michael T. Hren², and Selena Y. Smith¹

¹Department of Earth and Environmental Sciences, University of Michigan, Ann Arbor, MI, 48109; ²Center for Integrative Geosciences, University of Connecticut, Storrs, CT, 06269, loughney@umich.edu

The Barstow Formation of southern California is a terrestrial sequence that preserves a diverse Miocene mammalian fauna through a major interval of climate change. During the Middle Miocene Climatic Optimum (MMCO) between 17 and 14 Ma, moderate to high atmospheric CO₂ caused global temperatures to rise 2 to 4°C. After 14 Ma, cooling coincided with drying in the western interior. In order to establish the climatic and environmental context for high mammal diversity in the Mojave region during the middle Miocene, we used a multi-proxy approach to reconstruct paleoenvironments through the Barstow Formation. We combined carbon- and hydrogen-isotopic analysis from plant-derived biomarkers and soil organic matter with analysis of phytoliths (plant silica) to reconstruct hydrologic conditions, vegetation composition, and habitat structure before, during, and after the MMCO.

Results from isotopic analyses indicate that environments in the Barstow Basin were dry prior to the onset of the MMCO. Isotopic results indicate increased moisture availability between ~16 and 14 Ma, consistent with increased or year-round precipitation during the MMCO. Phytolith assemblages are dominated by forest indicators during this interval. After 14 Ma, a shift to drier, open-canopy habitats is represented by enrichment in carbon and hydrogen isotopes. Phytolith assemblages have varying proportions of grass and forest indicator morphotypes, representing lateral vegetation heterogeneity and mosaic habitats. Dry, wooded grasslands formed in the Barstow Basin after the end of the MMCO, as climate cooled and precipitation became more seasonal.

The southwestern pond turtle (*Actinemys pallida*) in the Mojave River of California: past, present and future

Jeffrey E. Lovich¹, Robert Fisher², Shellie R. Puffer¹, Kristy Cummings¹, Sarah Greely³ and Morgan Ford¹

¹U.S. Geological Survey, Southwest Biological Science Center, 2255 North Gemini Drive, MS-9394, Flagstaff, AZ 86005; ²U.S. Geological Survey, Western Ecological Research Center, 4165 Spruance Road Suite 200, San Diego, CA 92101; ³Living Desert Zoo and Gardens, 47900 Portola Ave, Palm Desert, CA 92260; [jeffrey_lovich@usgs.gov]

Two species of the turtle genus *Actinemys* currently range along the Pacific versant of the United States with relict populations in interior drainages of the Great Basin and Mojave deserts, as well as scattered oases in Baja California, Mexico. The genus was more widely

distributed from the Miocene to the Pleistocene as shown by the fossil record. Fossil evidence from California suggests that the southwestern pond turtle (*Actinemys pallida*) made it as far into the Mojave Desert as the Salt Creek region near Death Valley during the pluvial period. As the interior of North America transitioned to a warmer, drier climate about 10,000 years ago, the turtle's range contracted toward the coast, isolating the Mojave River population. Uplift of the San Bernardino Mountains in southern California occurred within the last 2–3 million years further isolating Mojave River turtles from coastal populations to the south. Genetic affinities of turtles in the lower reaches of the river at Afton Canyon are unknown, but evidence suggests that turtles at the Camp Cady Wildlife Area may have been augmented from coastal southern California populations. Published literature suggests that turtles were “not rare” in ponds along the intermittent, endorheic Mojave River in the early 1900s. Museum specimens (n=7) were collected from various localities along the river from 1937–1987. Ecological research on the lower Mojave River occurred in 1998 and 1999 documenting only 35 turtles with an estimated population size of less than 50 adults. Data on body size distribution, sex ratio, clutch size, egg size, nesting season, and nesting migrations differed little from data for populations elsewhere in the range of the species and the congener *A. marmorata*. Sporadic sightings of turtles document their continued presence along the lower Mojave River until 2014 at Camp Cady, after which they appear to have been extirpated for unknown reasons. Several photo-documented sightings and captures occurred in Afton Canyon through 2017, but the population is much smaller than what was documented in the 1990s. Small populations persist in portions of the upper river. Threats to the continued survival of the Afton Canyon population include floods, drought, and off-highway vehicle activity through the ponds and wetlands that support turtles.

Geologic framework of groundwater basins of western Fort Irwin, California

D.M. Miller¹, D.C. Buesch¹, V.E. Langenheim¹, L.B. Ball², P.A. Bedrosian², and G. Cromwell³

¹USGS 345 Middlefield Road, Menlo Park CA 94025; dmiller@usgs.gov; ²USGS Federal Center, Denver CO 80225; ³USGS 3130 Skyway Drive, Santa Maria CA 93455

Fort Irwin, the U.S. Army training ground for desert combat, occupies an extensive mountainous high-elevation area of the north-central Mojave Desert. Its operation vitally depends on water availability, and three basins have been developed for water resources. Western expansion of the base about a decade ago, along with generally increasing military use, created a need to explore three western basins. We conducted geologic mapping and geochemical studies of surface rocks and borehole samples. The geologic data were combined with inverted gravity data to model depth to crystalline basement,

incorporated airborne electromagnetic surveys, and all were used to develop 3D models that specifically calibrate resistivity with geologic strata. A new lidar database for Fort Irwin allowed us to better locate youthful faults.

The three sedimentary and groundwater basins (called the Nelson, Goldstone, and Superior basins) each consist of Mesozoic basement rocks overlain by Early Miocene volcanic strata. The volcanic strata are marginal to a large high volcanic plateau in the northwest. The volcanic strata are overlain by sandstone and conglomerate that is presumed to be Miocene to Pliocene in age. The relief on the Mesozoic basement rocks and the lack of Paleogene sedimentary rocks suggests that basin fill accumulated on Tertiary erosional topography. By the Late Miocene, the basins became structural in origin, each as part of the Eastern California Shear Zone faulting, but with distinctive differences. Nelson basin straddles the left-lateral Nelson fault, and comprises several east-elongate sub-basins partitioned by folds and faults. Goldstone basin corresponds to areas of localized extension alongside releasing bends in right-lateral faults in close vicinity to intersecting, left-lateral faults. Superior basin lies in a sag between south- and north-facing pediments cut into granitic rocks, and contains volcanic rocks overlying pediments in its eastern part. The sag appears to be an active syncline within the right-lateral fault system and has evidence for Pliocene development. Basalt encountered in wells is geochemically similar to the ~3.7 Ma Black Mountain basalt exposed to the southwest. The basalt evidently flowed northeastward into an existing lowland, after which it likely was warped down to the west, based on elevations of basalt encountered in boreholes. In addition to the warping, the basalt is buried by 62-73 m of sediment at the boreholes, indicating continued basin sagging. Modern playas string along the east-west line of the fold axis.

Groundwater resources are found within strata of Early Miocene, Pliocene, and Quaternary age in the exploratory boreholes of the three western basins of Fort Irwin. Recognition of groundwater in pre-Quaternary deposits expands the targets for water exploration beyond those of previous models and increases the importance of detailed geophysical study that excels at identifying the older strata.

First report of fossil plants from the Box Springs Mountains, Riverside, CA

Jess Miller-Camp, Andy Sanders, Lido Delgadillo, Jeremiah George

Dept. of Earth Sciences, University of California, Riverside,
jess.miller-camp@ucr.edu

We report here on the first fossils recovered from the Box Springs Mountains in Riverside, CA. The specimens consist of a small number of leaves, twigs, and their impressions, and a possible catkin. They were found and recovered by from a small lens of sedimentary rock in Poarch Rd. on the southwestern slopes of the region. The

lens was exposed during grading in August 2011 and contained completely within the road. Recent surveys of the area have failed to find other sedimentary deposits, meaning this one was either highly localized or is the remnant of a much wider deposit that has been eroded away. Nearby gullies crossing the lens' depth expose no buried sedimentary layers, making the latter explanation highly unlikely. The habitat restrictions of the species in the sample provide additional support for the former.

Three species can be identified among the specimens: *Quercus berberidifolia*, California scrub oak, for which there is one leaf and its counterslab; *Platanus racemosa*, California sycamore, for which there are two leaves and the counterslab of one; and *Salix lasiolepis*, arroyo willow, for which there is one leaf and its counterslab. Additional leaves may be identifiable to species after preparation, though much of the material is too fragmentary to assign to lower taxonomic levels.

Quercus berberidifolia are the most common scrub oak in Southern California. Today, they range from Northern California to Northern Baja California along the Coast Ranges, Transverse Ranges, Peninsular Ranges, and the Sierra Nevada's western foothills. They thrive in mid-elevations of 330–5900 ft within chaparral and coastal sage scrub environments, and are most commonly found on moderate to steep slopes composed of sedimentary rock and Mesozoic granites. Relatively few are present in the valleys of the Peninsular Ranges today. The closest living individuals to the fossil site are three clones in the eastern-facing Two Trees Canyon on the north side of the Box Springs. Unpublished data shows that these individuals began growing in the Pleistocene. There is, however, a published Pleistocene age for individuals of a species with similar habitat restrictions, *Q. palmeri*, growing in the Jurupa Mountains. Both oaks were part of a vegetation community that was more extensive in Southern California in the Pleistocene, with only remnants remaining now.

Platanus racemosa ranges from central California to Northern Baja California along the South Coast Ranges, Transverse Ranges, Peninsular Ranges, Sierra Nevada's western foothills, and the Central Valley. They thrive in low to high elevations within evergreen forest, chaparral, valley grasslands, and wetland-riparian environments. They can be found in a wide range of slopes (gentle to steep) composed of sands, clays, and bedrock. They reside along stream banks and floodplains within the valleys as well as within mountain canyons reaching up to 3000 ft elevation.

The native *Salix lasiolepis* occurs across much of the American West and can be found along nearly all of California's ranges and valleys. They thrive in low to high elevations up to 7000 feet within evergreen forest, foothill woodland, chaparral, valley grassland, and wetland-riparian environments. They most commonly reside on shores, marshes, meadows, springs, and bluffs composed of a variety of soils. Fossil riparian plant communities

consisting of both *S. lasiolepis* and *P. racemosa* have occurred in the Southwest for at least 20 million years.

Multiple lines of evidence support that the lens containing these fossils was deposited in a gully. The extremely localized nature of the lens with no evidence of past erosion over a wide area is one. The sandstone itself contains grains larger than one would expect from wind deposition. *P. racemosa* and *S. lasiolepis* are both constrained to gullies in the area today, and *Q. berberidifolia* is locally confined to them. The whole of the flora requires wetter environments than are found on open hillsides. Additionally, one rock contains a mass of twigs that appear to have been gathered together by flowing water.

Slope deposits of sandstone in eastern Riverside and nearby parts of San Bernardino counties have yielded fossils that are Late Pleistocene in age, while soil deposits within the valleys are Holocene. We are tentatively considering these plants to be from the Late Pleistocene based on: 1) the tight habitat and geographic restrictions of the identified species within Southern California in the modern age relative to the Pleistocene, 2) the location of the lens on a southeast-facing slope, which is more sensitive to increased aridity than other slopes, and 3) their containment within sandstone rather than soil. Carbon dating analyses are forthcoming.

How long can desert tortoises, *Gopherus agassizii*, hide in their burrows from climate change?

Jenna L. Norris¹, Jeffrey E. Lovich², Rafael A. Lara Reséndiz³ and Shellie R. Puffer²

¹Department of Geology, Northern Arizona University, Flagstaff, Arizona 86011-4099; ²U. S. Geological Survey, Southwest Biological Science Center, 2255 North Gemini Dr., Flagstaff, AZ 86001, USA; ³Department of Ecology and Evolutionary Biology, University of California, Santa Cruz, California 95064 (RALR)

Multiple studies modeling the effects of global climate change have concluded that during the 21st century the southwestern United States will be disproportionately subjected to trends in rising temperatures and increased aridity, leading to the potential for increased drought duration and frequency. Southwestern ecosystems will invariably respond in different ways to the increased aridity, but many desert species are already struggling to survive in the harsh desert conditions where climate change is predicted to have its most severe impact. Numerous studies have concluded that the distribution and concentration of particularly sensitive species, such as the desert tortoise *Gopherus agassizii*, will be both directly and indirectly impacted by the warming temperatures and decreased precipitation predicted to occur over the course of the next century. Contrary to popular belief, desert tortoises are not well adapted to modern desert conditions, but are rather exapted specialists already surviving on the edge of their abilities to endure arid conditions. If the warming trend continues and precipitation levels

simultaneously lower or become more variable, studies have shown that *G. agassizii* can only endure droughts for so long before they perish. Additionally, decreased precipitation is directly correlated with decreased annual food plant production, further restricting tortoises' access to an already limited food source. Finally, *G. agassizii* have environmental sex determination and some studies suggest warming temperatures might limit natural production of male hatchlings in turtles. In response to increasingly harsh conditions, *G. agassizii* may be able to shift their distributions northward or to higher elevations, or otherwise become extirpated. However, multiple studies show animals may not be able to respond quickly enough. One study cites that in order for species to adapt to the rate of changing climates, evolution would have to occur at a rate that is >10,000 faster than what is normal. Even if this accelerated rate of evolution was achieved, habitat fragmentation limits the ability of *G. agassizii* to track climatic niches. Our study site was near the southern boundary of Joshua Tree National Park in the Sonoran Desert of California. We collected temperatures every 15 minutes under current conditions using data loggers simulating tortoise shells. Data loggers were placed in burrows and rock shelters from May–July, a time period when tortoises are surface active at the site. We evaluated the percent of time the data loggers recorded temperatures that were above the critical thermal maximum (CTM = 41.3 °C; temperatures that are lethal for tortoises) under current climatic conditions. We then added 4 °C to all of the temperature recordings based on estimates for temperature increases due to climate change in the next 60–90 years in the southwest United States. Again, we measured the time above CTM. As expected, tortoise activity was reduced under a warming climate scenario. Tortoises spend up to 98% of their annual activity cycle below ground and inactive due to the harsh environment at the desert surface. Future climatic conditions that further restrict hours available to tortoises for above ground activity will have a potentially major impact on survival rates. It is feasible that as hours of activity are reduced, tortoises may not be able to meet all of their crucial biological needs, potentially pushing them past a tipping point for survival.

Preliminary geologic map of the Mesquite Springs Fault Zone

G. Phelps

U.S. Geological Survey, gphelps@usgs.gov

We recently completed geologic mapping of the Mesquite Springs Fault Zone, an east-trending fault zone within the Eastern California Shear Zone. It is one of several approximately east-trending faults, including the Manix, Cady, Broadwell Mesa, and Cave Mountain, that form a discontinuous link between the northwest trending Calico and Bristol–Granite Mountains Fault Zones. It is a ~20 km zone of east-northeast to west-northwest striking

left-lateral faults exposed along the northern edge of the Mesquite Hills near Crucero, CA. Splays at the western end of the fault zone project both northwestward towards the Manix Fault and southwestward into the northernmost Cady Mountains. Faults at the eastern end of the Mesquite Springs Fault Zone step south and cut the very northernmost Bristol Mountains, beyond which they cannot be traced through the Quaternary sediments.

The Mesquite Hills themselves occupy the central part of the fault zone and form a row of east-trending hills with up to ~350 m of relief and are perpendicular to the local northward drainage from the Cady and Bristol mountains. Uplift and folding along the fault zone, including gently folded Miocene volcanoclastic sediments exposed at the northwestern end, indicate transpressional tectonics along the fault zone. Crosscutting relationships among the fault strands indicate that the earliest movement along the fault zone was west-northwest, followed by younger east-northeast movement. The Quaternary geomorphic surfaces that abut faulted topography in the Mesquite Hills are typically Late Pleistocene in age, indicating the greatest movement within the fault zone, partitioned into both left-lateral motion and uplift, occurred 30–80 ka. Lack of clear piercing points leaves uncertain the total amount of slip along the fault zone, however outcrops of similar igneous rocks are separated across the fault by 5 km. Evidence of more recent movement has not been found, although younger scarps may be obscured by eolian deposits, which are widespread throughout the Mesquite Hills area. Spring seeps occur along the fault at the northwestern edge of the Mesquite Hills, locally supporting increased vegetation and trapping of eolian sediment. Quaternary spring deposits also occur along the fault zone, with evidence of wetlands occurring thousands to tens of thousands of years ago, the latter coinciding with the period of greatest activity along the fault.

These new observations of the timing of slip on the Mesquite Springs Fault Zone, combined with planned geophysical data collection on the western end, and newly acquired high-resolution topographic data (LiDAR and SfM DEMs) that cover both ends of the fault zone, are being used to determine whether the Mesquite Springs Fault Zone and Manix Fault are two parts of the same fault system and, if so, whether they merge with the NW-striking Calico and Bristol–Granite Mountains Fault Zones to the west and east, respectively. This connection would significantly increase the rupture length of a potential earthquake, as well as have broader implications for how slip is distributed across the Eastern California Shear Zone.

Birds not in flight: using camera traps at desert tortoise (*Gopherus agassizii*) burrows to study avian behavior at a wind farm

Shellie R. Puffer^{1*}, Laura A. Tennant¹, Mickey Agha², David Delaney³, Jeffrey E. Lovich^{1*}, Leo J. Fleckenstein⁴, Jessica Briggs⁵, Terence R. Arundel¹, Amanda L. Smith⁶, Andrew Walde⁷, Joshua R. Ennen⁸
¹U.S. Geological Survey, Southwest Biological Science Center, 2255 North Gemini Drive, MS-9394, Flagstaff, Arizona 86001, USA; ²Department of Wildlife, Fish, and Conservation Biology, University of California, Davis, One Shields Avenue, Davis, California, 95616, USA; ³U.S. Army Construction Engineering Research Laboratory, P.O. Box 9005, Champaign, Illinois 61826-9005, USA; ⁴Department of Forestry, University of Kentucky, Lexington, Kentucky 40546, USA; ⁵Colorado State University, Fort Collins, Colorado 80523, USA; ⁶The Sonoran Institute, 100 North Stone Avenue, Suite 400, Tucson, Arizona 85701, USA; ⁷Walde Research and Environmental Consulting, Atascadero, California, USA; ⁸Tennessee Aquarium Conservation Institute, 175 Baylor School Rd, Chattanooga, Tennessee 37405, USA. *Corresponding authors: e-mails: mpuffer@usgs.gov; jeffrey_lovich@usgs.gov

Wind energy facilities are dangerous landscapes for many bird species. The increase in construction of wind farms worldwide in recent years is a significant concern of bird conservation efforts. However, it can be difficult and time-consuming to study birds in a wind farm. Visual surveys and sweeps for carcasses have been used in the past, both of which can be subject to detection biases. Thermal and infrared imaging focused on the swept areas of turbine rotors can yield information about bird behavior and mortality, but generally do not allow species determination since focal areas are greater than 30 m from the cameras. We implemented a novel ground-based technique using camera traps installed at the burrows of desert tortoises (*Gopherus agassizii*) at a wind farm near Palm Springs, California to study and quantify avian species presence, behavior, and use. Birds utilize these burrows for nesting, resources (e.g. food and nesting material), hibernacula, and as a thermal refugia. We observed a total of 12 avian species in the photos taken by our camera traps. Mortality from turbine strikes has been documented in the literature for 10 of these species, although all of the species are considered vulnerable. We collected over 13,000 photos from 1 June–14 November 2013. When an individual bird triggered the same camera within a five-minute period, these photographs exhibited high temporal correlation and were considered to be a single ‘event’. There were a total of 1,968 ‘events’ distributed across 45 tortoise burrows. We observed birds using the burrows to collect nesting material and food, displaying hunting and defensive behaviors, dust bathing, and entering and/or exiting the burrows. Bird counts increased with the minimum estimated age of desert tortoise burrows, possibly indicative of older burrows being known resources to individual birds. Estimated bird counts at burrows exhibited a non-linear relationship with distance from wind turbines. As distance from wind

turbines increased, estimated bird counts increased at 0 to \leq 150 m from turbines, decreased at >150 to \leq 300 m, and decreased further at $>$ 300 m. This indicates a distance threshold of around 150 m from wind turbines in which avian presence actually increases at desert tortoise burrows, in contrast to expectations of avoidance. Passive observation of avian use and behavior at wind farms through ground-based camera trapping allows for species identification, determination of activity patterns and behavior, and habitat preference, all of which can provide useful knowledge for wildlife managers.

Pleistocene lakes and paleohydrologic environments of the Tecopa Basin: constraints on the drainage integration of the Amargosa River

Marith Reheis, John Caskey, and Jordon Bright
retired mreheis@usgs.gov

The Tecopa basin served as the terminus of the Amargosa River during much of the Quaternary. Its stratigraphy, sedimentology, chronology, and diagenesis have long been studied to investigate paleoclimate. We use shoreline deposits and strandlines to reconstruct lake level and ostracodes preserved in lake and groundwater-discharge deposits to interpret depositional and hydrochemical environments. These two lines of evidence shed light on the history of the Amargosa River, both its upstream integration past Eagle Mountain and downstream integration into Death Valley.

We can document only 8 lakes that had enough fetch to construct distinct shorelines; nearshore deposits of three of these lakes lack significant beach gravel and were likely quite shallow. The oldest shallow lake (L1) coincided with deposition of the 2.01-Ma Huckleberry Ridge tephra and overlying lower Glass Mountain tephra. Deposits of this lake crop out only in the southeastern part of the basin, east of Tecopa Hot Springs. The second lake (L2) rose just prior to deposition of a 1.25-Ma tephra (previously correlated with the older Huckleberry Ridge). Ostracodes in these two deposits are mostly incompatible with alkaline Amargosa River water; the lakes were probably sustained by spring discharge sourced mainly from the regional carbonate aquifer. A third shallow lake (L3) may have formed around 1 Ma, as its nearshore sands are bracketed by two upper Glass Mountain tephra. The fourth lake (L4) exhibits limited deposits of beach gravel and just predates the 0.76-Ma Bishop ash, which locally bears oscillation ripples. This lake probably records the first incursion of the Amargosa River; ostracodes in this and younger lakes tolerate its alkaline water. The next lake (L5) is bracketed by the Bishop and Lava Creek ash beds. The first apparently long-lived lake (L6, the “Lava Creek Lake”), as suggested by thickness of lake sediment, preceded and coincided with deposition of the 0.63-Ma Lava Creek ash. A later lake (L7), which we term the “High Lake”, is recorded by thick deposits of beach gravel and sand as well as deltaic deposits that lie \sim 12-15 m stratigraphically higher than the Lava Creek ash. This

lake may have an age of \sim 600-500 ka based on deposition rates and U-series analysis by J. B. Paces (U.S. Geol. Surv., written commun., 2013).

We infer a long hiatus between High Lake and a much younger, slightly lower lake (L8), hypothesized as being early OIS 6 in age based on geomorphic relations in the area of Greenwater fan. Lava Creek Lake and High Lake deposits in this area are deformed and faulted, and High Lake deposits are locally overlain by many meters of calcareous and oxidized distal-fan and groundwater-discharge deposits that are also faulted. These oxidized deposits are in turn overlain by beach gravel and sand that appear to have been rapidly worked into channels incised in older units during the youngest lake cycle. This younger lake (L8) led to incision of the Sperry Hills threshold, creating the Amargosa River canyon and river flow into Lake Manly by early OIS-6 time (supported by the appearance of an alkaline-tolerant ostracode indicator species in the Death Valley core). A lower and somewhat younger lake (L9?) likely resided in the Tecopa basin during a stillstand at the level of Proterozoic bedrock in the upper Amargosa Canyon, which would have greatly slowed the rate of river incision.

Gravels and strandlines representing the Lava Creek Lake and High Lake are present from the north end of the basin to the south end. Differences in elevation of these gravels indicate as much as 23 m [510–487 m] of displacement up to the north for deposits of the Lava Creek Lake and 18 m [526–508 m] for those of the High Lake, all or nearly all due to displacement along a NE-trending monoclinical fold that transects the northern part of the basin.

The Island of California: is there a scientific explanation for the 17th-century myth?

Jenny E. Ross
Truckee, CA, jennyross.com

After the first pioneering Spanish investigations of the Gulf of California and lower Colorado River by explorers Francisco de Ulloa in 1539 and Hernando de Alarcón in 1540, Baja California was correctly shown on maps as a peninsula for the remainder of the 16th century. But beginning in the early 17th century, cartographers abruptly began depicting ‘California’—encompassing both lower (Baja California) and upper California (the U.S. state of California)—as an island. The notion that California was an enormous island lying next to the west coast of North America was widely adopted as true, and was persistently reflected in European cartography throughout the 1600s. Moreover, despite observations by later explorers during the 18th century that refuted this misguided concept, the error proved difficult to eradicate. The issue was finally settled beyond dispute when Juan Bautista de Anza traveled on land from present-day Arizona to the west coast of California for the first time in 1774.

The myth of California as an island remains one of the most notorious cartographic errors in history. Why this major misconception began holding sway over European cartography and the public imagination in the early 17th century after the truth had already been determined in the mid-16th century has been a baffling mystery for four hundred years. Historians have proposed complex speculative theories grounded on the assumption that the reasons for the error lie in various political and sociological dynamics of the time. Such interpretations discount and explain away the reported observations of early explorers as fantasy, ignorance, or propaganda. But no factually well-supported explanation for the depiction of California as an island has been offered that fully accounts for the specific timing and details of the famous misunderstanding. Importantly, no study has considered whether there might be a scientific explanation.

I propose that observations by Spanish explorers during early 17th-century expeditions to the lower Colorado River and delta region and along the U.S. west coast reflected the occurrence of severe widespread flooding, and resulted in revision of the correct 16th-century European cartographic understanding of those areas and the incorrect depiction of California as an island. When considered in combination with historical records, multi-proxy paleoclimate data from ice cores, tree rings, speleothems, coral, lake sediments, and river flood deposits suggest that in the early 17th century: (a) the climate was exceedingly wet in the U.S. southwest; (b) severe flooding occurred along the lower Colorado River; (c) Lake Cahuilla, a very large intermittent Pleistocene-to-Holocene Salton Basin lake with a highstand overflow path to the Colorado River delta, existed and was probably overflowing; and (d) large river systems along the coast of northern California and southern Oregon were likely inundating the surrounding land and greatly expanding their deltas. I suggest the climate forcing that caused these extreme hydrological consequences probably resulted from multiple large explosive volcanic eruptions in the Southern Hemisphere with global effects that occurred from the late 16th century through the beginning of the 17th century, and El Niño events identified by ENSO reconstruction and supported by modeling of post-eruption hydroclimate.

Collectively, paleoclimate data, hydrological evidence, and historical accounts indicate the 1602-1603 expedition of Sebastian Vizcaino along the U.S. west coast by ship and the 1604-1605 expedition of Juan de Onate to the lower Colorado River and delta by land happened during exceedingly wet climate conditions and extreme flooding that followed the major eruption of Peru's Huaynaputina volcano (VEI 6) in 1600 and other large explosive eruptions in the late 16th century (including Kelud in 1586, Billy Mitchell in 1587 (approximate), Raung in 1593 and 1597, and Nevado del Ruiz in 1595). Contemporaneous records of the Onate and Vizcaino expeditions describing the conditions actually observed

by those men correspond closely with documentation of major flooding along the lower Colorado and Gila Rivers, in the Colorado River delta region, and in coastal river systems of northern California and southern Oregon during the potentially analogous "Noachian Deluge" and "Great Flood" of 1861-62 following the 1861 eruption of Dubbi volcano. Although California was not actually an island in the early 17th century, it may reasonably have seemed to be in the eyes of explorers who attempted to reconnoiter key regions during that time.

Pre-development water-levels in the Centro area of the Mojave River groundwater basin

Whitney A. Seymour and John A. Izbicki
U.S. Geological Survey, wseymour@usgs.gov

Groundwater pumping in excess of recharge, between the onset of large-scale agricultural pumping in the early 1950s and the adjudication of the basin in 1998, resulted in water-level declines in excess of 50 feet in the Centro area of the Mojave River groundwater basin, about 80 miles northeast of Los Angeles. Present-day hydrologic conditions do not reflect predevelopment conditions in the aquifer with respect to groundwater recharge, discharge, or movement—especially in areas where formerly saturated, highly-permeable alluvium is now unsaturated as a result of water-level declines. Regional groundwater models including the Centro area were developed in 1971 and 2001 to evaluate groundwater conditions at those times. Pre-development (steady-state) water-level maps were prepared to support calibration of those models. A revised, finer-scale pre-development map for the Centro area was developed using data from a U.S. Geological Survey (USGS) report published in 1929, a California Department of Water Resources report published in 1934, and data available in the USGS online database, NWIS-Web, and previously unpublished USGS data. When combined with gravity data collected as part of this study, the map shows thickness of pre-development saturated alluvial deposits and can be used to increase knowledge of pre-development groundwater recharge, movement, and discharge in support of an external consultant update to the 2001 USGS regional groundwater flow model for the Centro area. In addition to supporting the groundwater flow model development, the map also shows 1) areas of different groundwater recharge processes to be investigated using noble gases and other environmental tracer data, 2) areas of groundwater discharge near Harper (dry) Lake, and 3) areas of formerly saturated highly-permeable Mojave River alluvium to be investigated using geophysical techniques.

Initial report of fossil wood from the Alverson formation, Anza-Borrego Desert State Park, California

Tom Spinks

Paleontology Volunteer, Anza-Borrego Desert State Park, 200 Palm Canyon Drive, Borrego Springs, CA 92004, tispinks217@gmail.com

Mid-Miocene volcanism in the southeastern California is related to regional, Basin and Range extensional tectonics. The Volcanic Hills (VH) in Anza-Borrego Desert State Park record this event as occurring from around 15 to 20 million years ago (Ruisaard, 1979). Local vegetation, mostly stem material from trees and shrubs, is preserved in fine grained sediments. Preliminary evaluation of the mineralogical and taxonomic characteristics of the VH fossil wood specimens shows they are distinctly different from the later Pliocene wood fossils from the Arroyo Diablo Formation that overlies the Volcanic Hills deposits (Fourt, 1979). The VH fossil woods have been sorted into several groups based on anatomical features. The features suggest taxonomic relationship to the Fabaceae and Rhamnaceae plant families, neither of which is represented in the late Pliocene Palm Spring flora (Remeika, 2006). A set of comparables is being developed based on Axelrod's (1940) work, as well as a work plan that outlines the remaining work needed to complete the study.

References

- Axelrod, D.I. 1939. A Miocene Flora from the Western Border of the Mohave Desert. Carnegie Institute of Washington Publication 516:1-129.
- Remeika, P. 2006. Ancestral woodlands of the Colorado River delta plain. Pp. 75-87 in (eds. G.T. Jefferson and L. Lindsay) *The Fossil Treasures of the Anza-Borrego Desert*. Sunbelt Publications, San Diego, California.
- Fourt, R. 1979. Post-batholithic Geology of the Volcanic Hills and Vicinity, San Diego County, California. MS Thesis, San Diego State University, California 66 p.
- Ruisaard, C. 1979. Stratigraphy of the Miocene Alverson Formation, Imperial County, California. MS Thesis, San Diego State University, 137 p.

The Las Vegas Formation

Kathleen B. Springer¹, Jeffrey S. Pigati¹, Craig R. Manker², and Shannon A. Mahan³

¹U.S. Geological Survey, Geologic Division, Denver Federal Center, Denver, CO 80225; ²Department of Geological Sciences, California State Polytechnic University, Pomona, CA 91768 USA; ³U.S. Geological Survey, Denver Federal Center, Box 25046, MS-974, Denver CO 80225 USA

The Las Vegas Formation was established half a century ago to designate the distinctive, light-colored, fine-grained, fossil-bearing sedimentary deposits exposed in and around the Las Vegas Valley, Nevada (USA). Coeval with that designation, the sediments were subdivided into informal units with stratigraphic and chronologic frameworks that have persisted in the literature to the present. Usage of the Las Vegas Formation name has

been hampered due to the lack of a robust definition and characterization of the entire lithostratigraphic sequence, its geographic distribution, and chronology. In this study, we have reevaluated and described deposits attributed to the Las Vegas Formation with detailed stratigraphy, sedimentology, and field relations. A large suite of both radiocarbon and luminescence ages facilitates revision and temporal expansion of the geochronology. In all, we characterize 17 informal geologic units within the formation, each dating to a unique period of geologic time, with stratigraphically ascending members X, A, B, D, and E and attendant beds in members B, D, and E. The age of the Las Vegas Formation spans at least the middle Pleistocene to early Holocene (~573 ka–8.53 ka) and is related to past groundwater discharge in the Las Vegas Valley. The contextual information derived from this new framework is dually noteworthy, given that the sediments entomb one of the most significant Pleistocene vertebrate faunas in the American Southwest, the Tule Springs local fauna, and represent a paleohydrologic system that responded dynamically to abrupt changes in climate throughout the late Quaternary. Characterizing the nature of these important deposits will facilitate studies of similar deposits associated with desert wetland ecosystems elsewhere in the southwestern U.S.

Ecological diversity of mammalian faunas of the Mojave Desert and the Great Plains, in relation to landscape history

Bian Wang^{1,3}, Catherine Badgley^{2,3}

¹ Department of Earth and Environmental Sciences, University of Michigan, Ann Arbor, MI; ² Department of Ecology and Evolutionary Biology, University of Michigan, Ann Arbor, MI; ³ University of Michigan Museum of Paleontology, Ann Arbor, MI

Disentangling individual ecological and evolutionary factors that shape the observed species-richness patterns remains a major challenge in ecology and evolutionary biology. Here, we analyze the ecological diversity of extant and fossil North American mammals to investigate the effect of landscape history (i.e. topography and climate) and associated environmental filtering processes on mammalian biodiversity and biogeography. In modern ecosystems, physiographically complex areas support a higher number of mammal species than adjacent areas with low relief, but little is known about the difference in ecological functions represented by mammalian faunas in such areas. We hypothesize that a greater number of mammal species are found in topographically and climatically complex regions because greater environmental heterogeneity accommodates more ecologically diverse species.

Our current research investigates the trends in two functional traits of extant North American mammals, body size and dietary habit, along environmental gradients, as well as the effect of the climate space on the geographic ranges of mammal species. Our data show

that the observed overall species richness pattern is the result of multiple diversity gradients that exist across North America. Future work will focus on comparing the diet and body size of fossil ungulate mammals from the Mojave Desert and the central Great Plains during the mid-Miocene climatic optimum (17 – 14 million years ago). The Mojave Desert is part of the Basin and Range province that underwent substantial tectonic changes during the Miocene, while the Great Plains has remained tectonically quiescent. These two regions were topographically and climatically distinct in the middle Miocene, and presumably supported different levels of ecological diversity of mammals. We will analyze the stable-isotope composition of mammalian tooth enamel and compare the morphological variability and body mass of ungulate mammals from middle Miocene fossil assemblages of the Mojave Desert and the central Great Plains.



Playa: Flooded dry lake north of Mt. General. View to the south. March 7, 2005.
D. M. Miller photograph.

